

https://dspace.org/

Contribution of novel biomarkers to adverse cardiac remodelling and myocardial dysfunction in a rodent model of pressure overload

Mkhize, Siluleko

2025

University of the Witwatersrand, Johannesburg

https://hdl.handle.net/10539/50025

Mkhize, Siluleko. (2025). Contribution of novel biomarkers to adverse cardiac remodelling and myocardial dysfunction in a rodent model of pressure overload [PhD thesis, University of the Witwatersrand, Johannesburg]. WIReDSpace. https://hdl.handle.net/10539/50025

Downloaded from a DSpace repository. https://dspace.org/

Contribution of novel biomarkers to adverse cardiac remodelling and myocardial dysfunction in a rodent model of pressure overload



UNIVERSITY OF THE
WITWATERSRAND,
JOHANNESBURG

Siluleko Mkhize

A thesis submitted to the Faculty of Health Sciences, University of the Witwatersrand, Johannesburg, South Africa in fulfilment of requirements for the degree of Doctor of Philosophy

July 2025

Declaration

I, **Siluleko Advice Mkhize**, declare that this thesis is my own, unaided work. It is being submitted for the degree of **Doctor of Philosophy (PhD: Physiology)** in the Faculty of Health Sciences, University of the Witwatersrand, Johannesburg, South Africa. The work contained in this thesis has not been submitted before for any degree or examination at any other University.

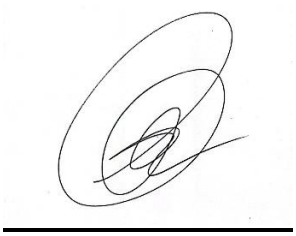

Siluleko Advice Mkhize

Date: **22 July 2025**



Frederic Michel



Ashmeetha Manilall



Sule Gunter

Whatever you are doing, that which makes you feel the most alive…that is where God is

~ St Ignatius of Loyola

To **Itumeleng V. Mahloko**, thank you for being a guiding light in my life, gently steering me closer to faith. Your presence has been a constant source of strength, grounding me through life's twists and turns. You've made this journey more meaningful, and for that, I am eternally grateful.

Your memory will not fade;

A tapestry of light, your life has made.

With Mary's hand and Christ above,

I thank you for the gift of love.

Born 29 July 2002 – Passed 24/25 November 2024

Acknowledgements

First and foremost, I extend my deepest gratitude to my supervisors, **Professors Frederic Michel, Sulé Gunter, and Dr. Ashmeetha Manilall**. Your unwavering guidance, expertise, and encouragement have been instrumental in shaping both my academic journey and personal growth. Your mentorship has been invaluable, and I am truly fortunate to have had the opportunity to learn from each of you.

I would also like to express heartfelt thanks to **Professors Aletta Millen and Sooraj Baijnath** for your unwavering support throughout this project. Your insights, kindness, and dedication have been a constant source of motivation, and I am immensely grateful for the role you've played in helping me reach this milestone.

A special thank you goes out to all the students in our lab at IMPRI. Your camaraderie, collaboration, and the many beautiful conversations we shared have made this journey far more enriching. The sense of community we built kept me grounded and motivated, even during the most challenging moments.

"My angels"—**Adalayne Ramsamy, Sanelisiwe Xhakaza, and Radhini Veerapen**—you have been my lifeline. In more ways than one, you've stood by my side, offering unwavering friendship and emotional support. You kept me sane through the toughest times, and I could not have made it this far without you. Thank you from the bottom of my heart.

I wholeheartedly thank my family for their love, and encouragement throughout this journey, which has been my greatest source of strength.

Conference presentations

1. ***14th International Symposium on Mechanisms of Vasodilatation (MOVD) (26 – 29 November 2021)**

   Quercetin Improves Endothelium-Mediated Responses in Mesenteric and Renal Arteries of Female Sprague Dawley Rats.

2. ***Cardiometabolic Health & Diabetes Africa Congress (22 - 25 February 2022):** 2nd best oral presentation

   Quercetin Improves Endothelium-Mediated Responses in Mesenteric and Renal Arteries of Female Sprague Dawley Rats.

3. ***School of Physiology Research day (13 September 2023):** Best oral presentation

   Quercetin Improves Endothelium-Mediated Responses in Mesenteric and Renal Arteries of Female Sprague Dawley Rats.

4. ***Southern African Hypertension Society 2nd NextGen Spring School 2023:** 2nd best oral presentation

   Quercetin Improves Endothelium-Mediated Responses in Mesenteric and Renal Arteries of Female Sprague Dawley Rats.

5. **American Journal of hypertension Summer School, Loyola University, Chicago, Illinois USA (25 – 29 July2024).** Involvement of microRNAs-146a-5p, -155-5p, and -29b-5p in cardiac remodelling and dysfunction in spontaneously hypertensive rats.

6. **Southern African Hypertension Society Biennial Congress (16 – 18 August 2024).** Involvement of pentraxin-3 in the development of hypertension but not left ventricular hypertrophy in male spontaneously hypertensive rats.

7. **50th conference anniversary of the Physiological Society of Southern Africa (PSSA) (25 – 28 August 2024):** 3rd best oral presentation in the Cyril Wyndham competition.

   Involvement of microRNAs-146a-5p, -155-5p, and -29b-5p in cardiac remodelling and dysfunction in spontaneously hypertensive rats.

8. **Faculty of Health Sciences Biennial Research Day (05 September 2024).**

   Involvement of pentraxin-3 in the development of hypertension but not left ventricular hypertrophy in male spontaneously hypertensive rats.

9. **30th Meeting of the International Society of Hypertension 2024 (19 – 22 September 2024).**

   Involvement of microRNAs-146a-5p, -155-5p, and -29b-5p in cardiac remodelling and dysfunction in spontaneously hypertensive rats.

**denotes scholarly works that, while not central to the core argument of this thesis, were produced as part of the broader academic training undertaken during my PhD*

Research outputs emanating from this work

(a) Conference proceedings

1. ***Mkhize, S. A.**, & Michel, F. S. (2021). **(ABSTRACT).** Quercetin Improves Endothelium-Mediated Responses in Mesenteric and Renal Arteries of Female Sprague Dawley Rats. *Journal of Cardiovascular Pharmacology, 78(Suppl 6), S88–S101.* https://doi.org/10.1097/FJC.0000000000001184
2. **Mkhize, S.A.**, Manilall, A., Gunter, S., Mokotedi, L., Millen, A.M.E., Nthlane, R.A., & Michel, F.S. (2024). **(ABSTRACT).** Involvement of microRNAs-146a-5p, -155-5p, and -29b-5p in cardiac remodelling and dysfunction in spontaneously hypertensive rats. *Journal of Hypertension, 42(Suppl 3): e32-e33.* https://doi.org/10.1097/01.hjh.0001062736.94728.1b

(b) Published articles

3. **Mkhize, S. A.**, Manilall, A., Mokotedi, L., Gunter, S., & Michel, F. S. (2024). Involvement of pentraxin-3 in the development of hypertension but not left ventricular hypertrophy in male spontaneously hypertensive rats. *Physiological Reports, 12(20), e70086.* https://doi.org/10.14814/phy2.70086
4. ***Mkhize, S.A.**, Nthlane, R.A., Xhakaza, S.P., Verhaert, P.D., Baijnath, S., Millen, A.M.E, & Michel, F.S. (2024). Decreased blood pressure with acute administration of quercetin in L-NAME-induced hypertensive rats. *Basic & Clinical Pharmacology & Toxicology. 2024;1-14.* https://doi:10.1111/bcpt. 14113
5. **Mkhize, S. A.**, Gunter, S., Manilall, A., Mokotedi, L., Mosoma, K. L., Nthlane, R., Millen, A. M. E., & Michel, F. S. (2025). Involvement of microRNA-146a-5p, but not -

155-5p and -29b-5p, in left ventricular remodeling and dysfunction in spontaneously hypertensive rats. *American Journal of Physiology - Heart and Circulatory Physiology*, *328*(4), H885–H899. https://doi.org/10.1152/ajpheart.00696.2024

(c) Manuscript under peer review

6. **Mkhize, S.A.**, Gunter, S., Manilall, A., Mosoma, K.L, Nthlane, R.A., & Michel, F.S. (2024). Runt-related transcription factor 1 modulates cardiac structural changes through mechanisms related to cell survival in male spontaneously hypertensive rats. *The Federation of American Societies for Experimental Biology.*

**denotes scholarly outputs that, while not central to the core argument of this thesis, were produced as part of the broader academic training undertaken during my PhD*

Abstract

Background: Hypertension drives the development of concentric left ventricular hypertrophy (LVH) and adverse cardiac remodelling. Concentric LVH is characterised by an increase in wall thickness relative to chamber size. La Place's law posits that concentric LVH initially serves as an adaptive response to maintain optimal wall tension. Over time, the sustained pressure overload causes maladaptive remodelling, leading to a transition towards an eccentrically-remodelled phenotype marked by chamber dilation and thinning of the ventricular walls. This maladaptive remodelling involves complex molecular mechanisms, including novel biomarkers such as pentraxin-3 (PTX-3), microRNAs (miRNAs), and transcription factors, which may play important roles in these pathological changes. However, their functional roles and contribution to hypertensive cardiac remodelling and dysfunction remains elusive.

Aim: In the present thesis, we elucidated the functional role of three novel biomarkers; namely, PTX-3, specific miRNAs, and the runt related transcription factor 1 (*RUNX-1*), in the development of hypertensive cardiac pathology. Specifically, we assessed the contribution of PTX-3 in the hypertrophic myocardium, and evaluated whether PTX-3 is amenable to modulation using two anti-hypertensive therapies with differential effects on the development of concentric LVH. Additionally, we sought to determine the patterns of expression and functional roles of three miRNAs of interest in the development of LVH, fibrosis, and overall myocardial function. Finally, we examined the role of *RUNX-1* during the transition towards an eccentrically-remodelled phenotype, and explored its putative involvement in fibrotic and apoptotic mechanisms.

Methods: Spontaneously hypertensive rats (SHRs) and normotensive Wistar Kyoto rats (WKY), were utilised to investigate hypertensive cardiac pathology at different stages. To determine the role of PTX-3 in the development of LVH, 3-month-old SHRs received either 20 mg/kg/day

hydralazine (SHR+H, n=6), 40 mg/kg/day captopril (SHR+C, n=6), or plain gelatine cubes (untreated SHR, n=7) for four months. Measurements were conducted at 7-months-old when LVH was established. To investigate the role of miR-146a-5p, miR-155-5p, and miR-29b-5p in the development of LVH and cardiac dysfunction, seven-month-old SHR (n=7 male, n=10 female), and normotensive WKY (n=7 male, n=9 female) were used. Lastly, to investigate the role of expression of *RUNX-1* and its putative involvement in fibrotic and apoptotic mechanisms, 3-month-old rats (n=9 SHR, and n=9 WKY) and 12-month-old rats (n=9 SHR, and n=9 WKY) were used. Different sets of rats were used for each sub-study. Blood pressure (BP) was measured via tail-cuff plethysmography. Cardiac geometry and function were assessed through M-mode and Doppler transthoracic echocardiography. Circulating levels of inflammatory markers, mRNA, and miRNA expressions were quantified using enzyme-linked immunosorbent assays (ELISA) and RT-PCR, respectively. Left ventricular (LV) collagen deposition, cardiomyocyte size, macrophage infiltration, and cardiomyocyte nuclei density were determined histologically.

Results: At 7 months, circulating PTX-3 levels were elevated in untreated SHR compared to WKY; mean difference [95% CI], −0.51 [−0.87 to −0.15, P = 0.004], correlating positively with increased systolic blood pressure (SBP) (r = 0.722; P= 0.0001) but showing no independent associations with indices of concentric LVH: LVPWTd (r = 0.372; P = 0.097), normalized heart mass (r = 0.216; P = 0.565) and normalized LV mass (r = 0.343; P = 0.109). Treatment with captopril and hydralazine reduced circulating levels of PTX-3; mean difference [95% CI], 0.58 [0.20 to 0.96, P = 0.002] and 0.68 [0.30 to 1.06, P = 0.0004], with captopril exhibiting a more pronounced effect in reversing LVH (P = 0.011 for RWT). Despite these changes in plasma PTX-3, its LV cardiomyocyte mRNA expression remained similar across groups (all P > 0.05). Concurrently, miR-146a-5p expression was elevated in the hypertrophic myocardium of SHR (P

< 0.0001), correlating with SBP (r = 0.7; P = 0.0004), normalised LV mass (r = 0.5; P = 0.011), RWT (r = 0.5; P = 0.029), collagen fraction area (r = 0.4; P = 0.027), and diastolic dysfunction (r = -0.5; P = 0.027 for e'). Myocardial macrophage infiltration was greater in SHR compared with WKY (P < 0.0001) but similar between male and female rats (P = 0.159). Perivascular collagen deposition was also greater in SHR compared with WKY (P <0.05) but similar between male and female rats (P = 0.280). When disaggregated by sex to delineate sexually dimorphic features, sample clustering was observed in the principal component analysis biplot and a permutational multivariate analysis of variance (PERMANOVA) test revealed highly significant sex-specific differences in PCA scores (Pillai's Trace = 0.72, P < 0.001). In moderation analyses illustrating the relationship between circulating concentrations of VCAM-1 and myocardial macrophage infiltration while considering the moderating effects of miR-146a-5p and SBP, the two-way interaction term between VCAM-1 and miR-146a-5p was highly significant (β = -0.0038, SE = 0.0002, P < 0.001), indicating a strong negative association with myocardial macrophage infiltration. In contrast, the two-way interaction term between VCAM-1 and SBP did not reach statistical significance (β = 0.00001769, SE = 0.0000204, P = 0.386), indicating that the combined effect of VCAM-1 and SBP does not significantly influence macrophage infiltration. The Wald chi-squared test result with two degrees of freedom (χ^2 = 299.8, P < 0.001) showed that the slopes of the interaction effects differ significantly from each other. At 3 months, SHRs exhibited greater normalised heart mass (P = 0.049), increased LV mass (P = 0.003), and elevated cardiomyocyte nuclei number (P = 0.001). By 12 months, SHRs showed reduced PWTd (P = 0.005), lower RWT (P = 0.012), and enlarged LVIDd (P = 0.007). Diastolic function parameters at 12 months included elevated E/e′ ratio (P = 0.020), reduced a' velocity (P = 0.027), and decreased e′/a′ ratio (P = 0.006). Molecular analyses revealed increased MMP-9 expression (P = 0.033), reduced Bax expression (P

= 0.019), reduced cleaved PARP-1 (P = 0.002), a trend toward a lower Bax/Bcl-2 ratio (P = 0.062), and elevated cleaved caspase-3 (P = 0.065). RUNX-1 expression declined with age (P = 0.0002) but increased with hypertension (P = 0.001). RUNX-1 expression correlated positively with normalised LV mass (r = 0.54, P < 0.0001), RWT (r = 0.54, P = 0.002), and Bax/Bcl-2 ratio (r = 0.44, P = 0.010), and negatively with LVIDd (r = -0.57, P = 0.001) and MMP9 expression (r = -0.48, P = 0.013).

Conclusions: Our study provides novel mechanistic insights into the molecular underpinnings of hypertensive cardiac remodelling. While PTX-3 likely reflects the localised inflammatory milieu associated with hypertension, it may not be directly involved in the development of LVH in SHR. Transcriptionally, miR-146a-5p appears to play a significant role in hypertension-induced LV remodelling. Specifically, miR-146a-5p emerged as a key counter-mechanism, modulating VCAM-1-mediated transendothelial macrophage infiltration into the hypertrophic myocardium, inflammation, and oxidative stress by enhancing IκBa and SOD2 expression. RUNX-1 expression was positively associated with markers of concentric cardiac remodeling. Over time, RUNX-1 expression progressively declined, coinciding with a transition from concentric to eccentric remodeling in SHR. This temporal decrease in RUNX-1 expression appears to be linked to the shift in remodeling phenotype observed in SHR. Consequently, modulating RUNX-1 activity could represent a therapeutic strategy to prevent the transition from compensated hypertrophy to heart failure. While our findings provide valuable insights into the expression patterns and potential roles of PTX-3, RUNX-1, and specific miRNAs in hypertensive cardiac remodeling, they remain associative in nature. Future studies employing targeted molecular interventions are necessary to establish definitive mechanistic and functional roles for these potential biomarkers.

Preface

This thesis represents the culmination of my academic journey, driven by a profound curiosity about the intricate molecular processes involved in hypertensive cardiac pathology. As someone deeply passionate about cardiovascular physiology, the opportunity to explore novel biomarkers in the context of cardiac remodelling has been both challenging and rewarding. Through my research, I aimed to investigate how hypertension leads to the development of left ventricular hypertrophy (LVH) and adverse cardiac remodelling, and the role that novel molecular regulators such as pentraxin-3 (PTX-3), microRNAs (miRNAs), and the transcription factor RUNX-1 play in these processes.

Structurally, this thesis is divided into five chapters. **Chapter 1** lays the foundation with a comprehensive introduction and review of the current literature, setting the context for the research and identifying key knowledge gaps. The core empirical work is presented in Chapters 2 through 4, each featuring individual manuscripts that align with the overall aims of the project. **Chapter 2** features the investigation of the role of PTX-3 in the hypertrophic myocardium and evaluates its modulation through two antihypertensive therapies—captopril and hydralazine—highlighting the differential impacts of these treatments on the development of LVH. **Chapter 3** examines the expression patterns and functional roles of three miRNAs (miR-146a-5p, miR-155-5p, and miR-29b-5p) in cardiac hypertrophy, fibrosis, and function. **Chapter 4** focuses on the gene expression of the transcription factor RUNX-1, its associations with fibrotic and apoptotic processes, and its involvement in the transition from compensated LVH to eccentric remodelling. Finally, **Chapter 5** summarises the key findings through an overarching discussion. This chapter also addresses the study's limitations and offers directions for future research, highlighting avenues for further exploration of the identified biomarkers.

Table of Contents

Declaration i

Acknowledgements iii

Conference presentations iv

Research outputs emanating from this work vi

Abstract viii

Preface xi

List of abbreviations and symbols xx

List of figures xxiii

List of tables xxvii

Chapter 1 1

1.1 Background 2

1.1.1 Novel biomarkers in cardiovascular disease 3

1.1.2 Hypertension: Prevalence, and Pages' revised mosaic theory 5

1.2 Literature review 7

1.2.1 Progression from hypertension to concentric, and eccentric left ventricular hypertrophy 7

1.2.2 Molecular mechanisms involved in the development of heart failure 9

1.2.3 The role of pentraxin-3: A novel biomarker of inflammatory cardiovascular disease 12

1.2.4 Contribution of runt-related transcription factor (RUNX-1) 14

1.2.5 Non-coding RNAs as novel biomarkers: Their targets genes and contribution to the pathogenesis of left ventricular hypertrophy and myocardial dysfunction 15

1.2.6 Biogenesis of microRNAs: Canonical pathway 18

1.3 Problem statement 24

1.4 Aim 26

1.5 Objectives 26

Chapter 2 27

Involvement of pentraxin-3 in the development of hypertension but not left ventricular hypertrophy in male spontaneously hypertensive rats 28

Abstract 29

2.1 Introduction 30

2.2 Methods 32

2.2.1 Animals and housing 32

2.2.2 Study design 32

2.2.3 Non-invasive blood pressure measurement 34

2.2.4 Urine collection 34

2.2.5 Transthoracic echocardiography 34

2.2.6 Blood and tissue sampling 35

2.2.7 Circulating levels of inflammatory markers and urinary creatinine 36

2.2.8 Total RNA extraction and cDNA synthesis 36
2.2.9 Relative mRNA expression of pentraxin-3 in LV tissue 37
2.2.10 Total collagen content from LV tissue 37
2.2.11 Cardiomyocyte width from LV tissue 38
2.2.12 Statistical analyses 38
2.3 Results 38
2.3.1 Haemodynamic and gravimetric parameters 38
2.3.2 LV geometry and systolic function 41
2.3.3 Total collagen content and cardiomyocyte width 43
2.3.4 Circulating inflammatory markers 46
2.3.5 Circulating pentraxin-3 concentration and LV mRNA expression 47
2.3.6 Associations between circulating levels of pentraxin-3 with indices of left ventricular hypertrophy, inflammatory markers, kidney function, and collagen content 48
2.4 Discussion 50
2.5 Limitations 54
2.6 Conclusion 54
Chapter 3 56
Involvement of microRNA-146a-5p, but not -155-5p and -29b-5p, in cardiac remodelling and dysfunction in spontaneously hypertensive rats 57
Abstract 58

New and noteworthy 59

3.1 Introduction 60

3.2 Methods 63

3.2.1 Animals and housing 63

3.2.2 Study design 63

3.2.3 Non-invasive blood pressure measurement 64

3.2.4 Transthoracic echocardiography 64

3.2.5 Blood and tissue sampling 65

3.2.6 Circulating plasma levels of inflammatory markers 65

3.2.7 Myocardial macrophage infiltration 66

3.2.8 Perivascular and myocardial collagen content 66

3.2.9 Total RNA isolation 67

3.2.10 Expression of target genes 67

3.2.11 MicroRNA expression 68

3.2.12 Statistical analyses 69

3.3 Results 71

3.3.1 Systolic and diastolic blood pressure 71

3.3.2 Body and organ masses 71

3.3.3 Left ventricular geometry, diastolic and systolic function 73

3.3.4 LV tissue-specific expression of MicroRNAs 76

3.3.5 Circulating concentrations of inflammatory markers 78

3.3.6 Macrophage infiltration, perivascular and myocardial fibrosis in left ventricular tissue 80

3.3.7 Gene expression in left ventricular tissue 84

3.3.8 Associations between microRNAs and haemodynamic, gravimetric, echocardiographic, and molecular parameters 86

3.3.9 Sexually dimorphic features 88

3.3.10 Moderation effects of miR-146a-5p and systolic blood pressure 90

3.4 Discussion 91

3.5 Limitations 98

3.6 Conclusion 99

Chapter 4 101

Runt-related transcription factor 1 modulates cardiac structural changes through mechanisms related to cell survival in male spontaneously hypertensive rats 102

Abstract 103

4.1 Introduction 105

4.2 Methods 108

4.2.1 Animals and housing 108

4.2.2 Study design 108

4.2.3 Transthoracic echocardiography 109

4.2.4 LV tissue sampling 110

4.2.5 Total collagen content, macrophage infiltration, and cardiomyocyte nuclei density in LV tissue 110

4.2.6 Total RNA isolation 111

4.2.7 Expression of target genes 111

4.2.8 Immunoblotting 112

4.2.9 Statistical analyses 113

4.3 Results 114

4.3.1 Gravimetric parameters 114

4.3.2 Systolic and diastolic blood pressure 116

4.3.3 LV geometry and histological assessment of the left ventricle 116

4.3.4 Echocardiographic parameters showing left ventricular diastolic and systolic function 120

4.3.5 Gene expression of apoptotic and fibrotic markers, RUNX1 transcription factor, cardiomyocyte nuclei density, and collagen fraction area in LV tissue 122

4.3.6 Gene expression of apoptotic and fibrotic markers in LV tissue 123

4.3.7 Protein expression of the apoptotic markers including cleaved poly(ADP-Ribose) polymerase 1 (cPARP1), and cleaved caspase-3 (cCaspase-3) in LV tissue 125

4.3.8 Associations between mRNA expression of RUNX-1 with indices of LV remodelling, systolic and diastolic function, and gene expression in LV tissue 127

4.4 Discussion 129

4.5 Limitations 136

4.6 Conclusions 137

Chapter 5 138

5.1 Summary of findings, limitations, and future research directions 139

5.2 Pentraxin-3 140

5.2.1 Summary of findings 140

5.3 MicroRNAs 141

5.3.1 Summary of findings 141

5.4 RUNX-1 144

5.4.1 Summary of findings 144

5.5 Limitations 145

5.6 Future research directions 147

5.7 Conclusions 147

References 149

Appendix 1: Ethics application for 3- and 12-month-old male WKYs and SHRs 201

Appendix 2: Ethics application for 7-month-old male and female WKY and SHR 202

Appendix 3: Turnitin Report 203

List of abbreviations and symbols

SHR	Spontaneously Hypertensive Rats
WKY	Wistar Kyoto Rats
Bcl2	B-cell lymphoma 2
Bax	B-cell lymphoma 2 associated protein X
CM	Cardiomyocyte
Col1a	Collagen type 1a
Col3a	Collagen type 3a
LOX1	Lysyl Oxidase 1
RUNX-1	Runt-related Transcription Factor 1
AZL-M	Azilsartan Medoxomil
CSQ-tg	Calsequestrin-transgenic
TAC	Transverse Aortic Constriction
KO	Knockout
ANG-2	Angiotensin II
Iso	Isoproterenol
DOCA	Deoxycorticosterone Acetate
SD	Standard Deviation or Sprague-Dawley (context-specific)
p-AMPK	Phosphorylated AMP-activated Protein Kinase
DCM	Dilated Cardiomyopathy
EF	Ejection Fraction
CDCs	Cardiosphere-Derived Cells
STAT-3	Signal Transducer and Activator of Transcription 3

TGF-β1	Transforming Growth Factor Beta 1
hiPSC-CMs	Human Induced Pluripotent Stem Cell-Derived Cardiomyocytes
PTX-3	Pentraxin-3
CRP	C-Reactive Protein
TNF-α	Tumour Necrosis Factor Alpha
IL-6	Interleukin-6
IL-1β	Interleukin-1β
VCAM-1	Vascular Cell Adhesion Molecule-1
Cr	Creatinine
RAAS	Renin Angiotensin Aldosterone System
eGFR	Estimated Glomerular Filtration Rate
HPRT1	Hypoxanthine Guanine Phosphoribosyl Transferase
LV	Left Ventricle
SBP	Systolic Blood Pressure
DBP	Diastolic Blood Pressure
miR	microRNA
miR-146a-5p	microRNA-146a-5p
miR-155-5p	microRNA-155-5p
miR-29b-5p	microRNA-29b-5p
SnU6	Small Nuclear RNA U6
miR-16-5p	microRNA-16-5p
miR-191-5p	microRNA-191-5p
SV	Stroke Volume

endFS	Endocardial Fractional Shortening
midFS	Midwall Fractional Shortening
RWT	Relative Wall Thickness
e’	Early Peak Tissue Lengthening Velocity
a’	Late Peak Tissue Lengthening Velocity
E	Maximum Early Mitral Inflow Velocity
A	Maximum Late Mitral Inflow Velocity
E/A	Early to Late Diastolic Filling Velocity Ratio
E/e’	Early Diastolic Mitral Inflow to Tissue Lengthening Velocity
LVH	Left Ventricular Hypertrophy
LVIDd	Left Ventricular Internal Diameter in Diastole
LVIDs	Left Ventricular Internal Diameter in Systole
IVSTs	Interventricular Septal Thickness in Systole
IVSTd	Interventricular Septal Thickness in Diastole
LVPWTs	Left Ventricular Posterior Wall Thickness in Systole
PWTd	Posterior Wall Thickness in Diastole
PWTs	Posterior Wall Thickness in Systole

List of figures

Figure 1.1 Involvement of miRNAs in maturation, regeneration/repair and disease onset/progression (Image created with biorender.com)……..……...17

Figure 1.2 Schematic illustration of miRNA biogenesis via the canonical pathway (Image created with biorender.com)…….…….19

Figure 2.1A A diagrammatic illustration of the study design….……..33

Figure 2.1B A diagrammatic illustration of the sequence and timeline of the experimental procedures……..……33

Figures 2.2A and 2.2B A graphical representation of the haemodynamic parameters, systolic blood pressure (A), and diastolic blood pressure (B) in normotensive WKYs, untreated SHRs, and SHRs treated with either hydralazine or captopril…….…….40

Figures 2.3A and 2.3B A graph illustrating indices of left ventricular hypertrophy; left ventricular posterior wall thickness (LVPWT) in diastole (A), and relative wall thickness (B) in normotensive WKYs, untreated SHRs, and SHRs treated with either hydralazine or captopril…….……43

Figure 2.4 A graph depicting the collagen fraction area, expressed as a percentage of the total LV section, along with representative micrographs of normotensive WKYs, untreated SHRs, and SHRs treated with either hydralazine or captopril…….44

Figure 2.5 A graph depicting cardiomyocyte width, along with representative micrographs of normotensive WKYs, untreated SHRs, and SHRs treated with either hydralazine or captopril…….……45

Figures 6A, 6B, and 6C A graph illustrating the circulating concentrations of inflammatory markers including C-Reactive Protein (A), Tumour Necrosis Factor alpha (B), and Vascular Cell Adhesion Molecule-1 (C) in normotensive WKYs, untreated SHRs, and SHRs treated with either hydralazine or captopril……..……...46

Figures 2.7A and 2.7B A graph illustrating circulating levels of the inflammatory marker; pentraxin-3 (A), and LV tissue-specific relative mRNA expression of *pentraxin-3* (relative to *HPRT1* as endogenous control, B) in normotensive WKYs, untreated SHRs, and SHRs treated with either hydralazine or captopril……..…….47

Figure 2.8 A graph plot illustrating the relationship between circulating levels of pentraxin-3 with systolic blood pressure, indices of left ventricular hypertrophy, inflammatory markers, kidney function, and collagen fraction area in normotensive WKYs, untreated SHRs, and SHRs treated with either hydralazine or captopril. Open circles represent the point estimate (r, correlation coefficient). Horizontal lines bisecting the open circles represent the lower and upper limits of the 95% confidence interval (CI)……..……...49

Figures 3.1A-C A violin plot illustrating heart tissue-specific expression of MicroRNAs relative to miR-191-5p as endogenous control including miR-146a-5p (A), miR-155-5p (B), and miR-29b-5p (C)…….…….77

Figures 3.2A-D Circulating concentrations of the pro-inflammatory markers C-reactive protein (CRP, A), interleukin-6 (IL-6, B), tumour necrosis factor-α (TNF-α, C), and vascular cell adhesion molecule-1 (VCAM-1, D) in male and female normotensive WKY and SHRs……..……79

Figure 3.3A Representative micrographs illustrating myocardial macrophage infiltration in H&E-stained left ventricular tissue sections from male and female WKYs and SHRs (scale bar = 50 μm)……..……...81

Figure 3.3B Representative micrographs illustrating coronary perivascular fibrosis in sirius red-stained left ventricular tissue sections from male and female WKYs and SHRs (scale bar = 50 μm)……..……...82

Figure 3.3C Representative micrographs illustrating myocardial interstitial fibrosis in sirius red-stained left ventricular tissue sections from male and female WKYs and SHRs (scale bar = 50 μm)……..……...83

Figure 3.4 A volcano plot depicting associations between the three microRNAs (miR-146a-5p, miR-155-5p, and miR-29b-5p) and cardiovascular parameters, gene expression in left ventricular tissue, and circulating concentrations of inflammatory markers…….87

Figures 3.5A-5B An eigenvalue scree plot (A) depicting principal component analysis (PCA)……..……...89

Figure 3.6 An interaction plot illustrating the relationship between circulating concentrations of VCAM-1 and percent myocardial macrophages, while considering the moderating effects of

miR-146a-5p levels (coloured lines) and SBP levels (line types: solid, dashed, and dotted)……...90

Figures 4.1A-D A graph illustrating indices of left ventricular remodelling including left ventricular mass normalised to body mass (1A), left ventricular posterior wall thickness in diastole (1B), left ventricular internal diameter in diastole (1C), and relative wall thickness (1D) in 3- and 12-month-old normotensive WKYs and SHRs……...118

Figure 4.2 A graph illustrating gene expression of runt related transcription factor 1 in left ventricular tissue of 3- and 12-month-old normotensive WKY and SHR……..…….121

Figures 4.3A-D Protein expression of the apoptotic markers including cleaved poly(ADP-Ribose) polymerase 1 (cPARP1, 43kDa), and cleaved caspase-3 (cCaspase-3, 17kDa) in LV tissue of 3- and 12-month-old normotensive WKYs and SHRs……..125

Figure 4.4 A volcano plot illustrating the associations between mRNA expression of runt-related transcription factor 1 with cardiovascular parameters, and gene expression in left ventricular tissue……127

List of tables

Table 1.1 MiR-146a modulates the development of left ventricular hypertrophy and myocardial dysfunction in pressure overload……..……..23

Table 2.1 Gravimetric analyses and kidney function in normotensive WKYs, untreated SHRs, and SHRs treated with either hydralazine or captopril……...…….41

Table 3.1 Haemodynamic parameters, body and organ masses of male and female WKY and SHRs…….……72

Table 3.2 Echocardiographic parameters showing left ventricular geometry, diastolic, and systolic function in male and female normotensive WKY and SHR…….75

Table 3.3 Gene expression in the left ventricular tissue of male and female WKYs and SHRs…….85

Table 4.1 Gravimetric parameters showing body and organ masses in 3- and 12-month-old normotensive WKY and WKY…….....114

Table 4.2 Echocardiographic parameters showing left ventricular geometry, diastolic, and systolic function in 3- and 12-month-old normotensive WKY and SHR……...…….117

Table 4.3 Echocardiographic parameters showing left ventricular diastolic and systolic function in 3- and 12-month-old normotensive WKYs and SHRs……120

Table 4.4 Relative gene expression of molecular markers including apoptotic and fibrotic genes in 3- and 12-month-old normotensive WKY and SHR……123

Chapter 1

1.1 Background

Heart failure is defined as the heart's inability to pump blood effectively to meet the body's metabolic demands or doing so at abnormally high cardiac filling pressures (Nabeebaccus et al., 2016). Clinically, heart failure is characterised by dysfunction in either left ventricular systolic (contractile) or diastolic (relaxation) functions (Nabeebaccus et al., 2016). Heart failure manifests in two modalities: heart failure with reduced ejection fraction (HFrEF) and heart failure with preserved ejection fraction (HFpEF). HFrEF is marked by systolic dysfunction, with an ejection fraction of less than 40%. In contrast, HFpEF is characterised by diastolic dysfunction and elevated cardiac filling pressures, with a normal ejection fraction (EF≥50%). Additionally, heart failure with mid-range ejection fraction (HFmrEF) has been described and features an ejection fraction between 40% and 50% (Andronic AA, 2016).

According to the Framingham and Rotterdam heart studies, over 50% of all heart failure cases are HFpEF. HFrEF is also increasingly prevalent, with mortality rates of 45-60% (Framingham heart study) and 41% (Rotterdam heart study), over five years following diagnosis (Mosterd et al., 2001). While these studies predominantly focus on ischaemic causes of heart failure, such as ischaemic heart disease arising from myocardial infarctions, a different pattern emerges in Sub-Saharan Africa, where hypertension is the primary cause of heart failure (hypertensive heart disease) (Cappuccio & Miller, 2016). Moreover, in our South African context, the incidence of heart failure has been inadequately studied. To the best of our knowledge, no population-based studies have assessed the incidence of heart failure in South Africa (Jessen et al., 2023); and most research is hospital-based which may not be reliable considering the state of our healthcare system. Various studies suggest that heart failure predominantly affects older adults in South Africa, typically between their third and fifth decades of life, with a varying sex predilection (Hitzeroth et

al., 2020). Indeed, the Heart of Soweto study (Sliwa et al., 2008), the largest ongoing investigation of confirmed heart failure cases in South Africa, identifies hypertensive heart disease as the leading cause of heart failure.

Over the past decade, heart failure has become the focus of extensive research, significantly enhancing our understanding of its underlying pathophysiology (Kemp et al., 2014). Despite these advances, treatment options remain limited owing to the shortcomings in identifying alternative therapeutic targets (Braunwald, 2015). These limitations are, in part, attributable to the complex phenotypic heterogeneity of heart failure and the multiplicity of its underlying aetiologies (Kemp et al., 2014). Therefore, classifying heart failure based on its pathophysiological manifestations may offer a unique window of opportunity for targeted therapeutic interventions (Samak et al., 2016). To this end, echocardiography is the mainstay for clinical diagnosis, distinguishing between preserved and reduced ejection fraction (Drazner, Rame, & Marino, 2004). Notably, recent work points to the contribution of novel biomarkers as diagnostic, prognostic, and therapeutic targets in heart failure (Ibrahim & Januzzi, 2018).

1.1.1 Novel biomarkers in cardiovascular disease

According to the National Institute of Health (NIH) Biomarkers Definitions Working Group, a biomarker is defined as a characteristic that is objectively measured and evaluated as an indicator of normal biological processes, pathogenic processes, or pharmacologic responses to a therapeutic intervention (Ahmad et al., 2023; Strimbu & Tavel, 2010). Novel biomarkers are emerging biological indicators that provide insights into previously unexplored or less understood aspects of disease processes (McDermott et al., 2013). Unlike traditional biomarkers, which have long been used to detect known disease states, novel biomarkers are often discovered through advancements in genomic, proteomic, and metabolomic technologies, allowing researchers to uncover unique

molecular signatures associated with specific diseases (Qiu et al., 2023). These biomarkers can include proteins, genes, metabolites, or other molecules that offer new avenues for early disease detection, risk assessment, and understanding of the underlying mechanisms (Bodaghi et al., 2023). Their development is particularly valuable in chronic diseases like cardiovascular disease (CVD), where early detection and targeted interventions can greatly improve patient outcomes.

In cardiovascular research and clinical setting, novel biomarkers have the potential to transform disease diagnosis, prognosis, and treatment strategies. For instance, markers like high-sensitivity troponins and natriuretic peptides such as B-type natriuretic peptide (BNP) and N-terminal pro B-type natriuretic peptide (NT-ProBNP), have enabled more accurate detection of myocardial injury and heart failure (Wang et al., 2020), but newer biomarkers such as galectin-3, soluble suppression of tumourigenicity 2, and various microRNAs are helping to further elucidate the complex pathways involved in inflammation, fibrosis, and endothelial dysfunction (Piek et al., 2018). These insights allow for the identification of high-risk individuals, the monitoring of disease progression, and the assessment of therapeutic efficacy more precisely (Alowais et al., 2023). As research continues to validate these novel biomarkers, they may become essential tools in predictive modelling and personalised medicine approaches in cardiovascular care (DeGroat et al., 2024), facilitating more tailored and effective treatment strategies based on individual risk profiles and molecular characteristics.

Despite the promise of novel biomarkers in cardiovascular research, significant gaps remain in our understanding of their clinical utility and predictive power across diverse patient populations, especially in the setting of cardiovascular disease. Many emerging biomarkers show potential in early studies, but their roles in specific cardiovascular conditions such as HFpEF, HFrEF, or in

patients with essential hypertension are not yet fully understood (Ibrahim et al., 2016). Additionally, while novel biomarkers have demonstrated associations with cardiovascular function in controlled research settings, there is limited evidence on their performance (Vlachopoulos et al., 2015). This gap in knowledge underscores the need for further research to explore the efficacy and stability of biomarkers across heterogeneous populations and clinical settings. Addressing these gaps would not only expand our understanding of the pathophysiological mechanisms underlying these diseases but also improve cardiovascular disease management. Therefore, advancing research in this area is essential to unlocking the full potential of novel biomarkers and establishing evidence-based protocols in the setting of cardiovascular disease, including hypertension and heart failure.

1.1.2 Hypertension: Prevalence, and Pages' revised mosaic theory

Hypertension is recognised as a traditional risk factor for the pathogenesis of heart failure (Mihl C, 2008; Samak et al., 2016). The first wave of the South African National Health and Nutrition Examination Survey (SANHANES-1) (Kandala et al., 2021), a nationwide sentinel study conducted in 2012, revealed that one-in-three South African adults aged 15 years and older were living with hypertension. The 2016 South African Demographic and Health Survey (Kandala et al., 2021) estimated the prevalence of hypertension at 46% for females and 44% for males. Despite this high prevalence, late detection and lack of adherence contribute to poor blood pressure control among hypertensive patients in South Africa (Fina Lubaki et al., 2009). Additionally, access to quality healthcare is limited, resulting in a significant number of undiagnosed, and therefore untreated cases. Consequently, long-standing uncontrolled hypertension often develops into hypertensive heart disease (Iyer et al., 2010).

The aetiology of hypertension is complex and multifactorial, involving genetic, environmental, and lifestyle factors that contribute to changes in blood vessel tone and fluid volume regulation (Harrison et al., 2021). Traditionally, hypertension was understood through the lens of individual factors, such as cardiac output or peripheral vascular resistance, but this approach has evolved significantly with the introduction of the mosaic theory (Magder, 2018). Initially proposed by Irvine Page and Floyd L. Loop in 1963, the mosaic theory posited that hypertension results from an interaction between genetic predisposition, neurohumoral factors, vascular changes, renal function, and environmental influences (Harrison et al., 2021). Over time, this theory has been revised to accommodate advances in molecular biology and our understanding of the intricate physiological processes governing blood pressure.

The revised mosaic theory of hypertension expands on this foundational concept by integrating newer insights into immune system involvement, endothelial dysfunction, and neurogenic factors, emphasising the complex interdependence among these physiological systems (Hengel et al., 2022). The revised mosaic theory helps us understand that concentric and eccentric LVH are not isolated phenomena, but rather stages along a continuum of cardiac adaptation and maladaptation driven by a complex network of hemodynamic, neurohormonal, immune, and endothelial factors. According to the revised theory, hypertension arises not solely from isolated mechanisms but from a "mosaic" of interlinked factors that act synergistically to disrupt normal blood pressure regulation. For example, chronic inflammation—triggered by immune cells in response to environmental and lifestyle stressors—can lead to endothelial dysfunction (Pacinella et al., 2022), where the blood vessels lose their ability to dilate properly. This, in turn, increases peripheral resistance and blood pressure. Similarly, neurogenic factors such as sympathetic nervous system overactivity contribute to hypertension by promoting vasoconstriction (Charkoudian & Rabbitts,

2009). Together, these interrelated pathways form a multifaceted, dynamic system, underscoring the importance of a holistic approach in both understanding and managing hypertension. The revised mosaic theory thus not only informs multi-targeted treatment strategies but also helps explain how chronic hypertension can lead to structural heart changes, such as concentric and eccentric left ventricular hypertrophy (LVH), highlighting the importance of novel biomarkers in monitoring these pathological developments.

1.2 Literature review

1.2.1 Progression from hypertension to concentric, and eccentric left ventricular hypertrophy

The development of heart failure secondary to hypertension is marked by adverse cardiac remodelling and progressive impairment of myocardial function, both diastolic and systolic (Mihl C, 2008). According to LaPlace's law, one key structural adaptation to myocardial injury, such as increased wall stress in response to hypertension-induced haemodynamic pressure overload, is the development of LVH (Ertl & Frantz, 2012). Chronic hypertension prompts physiological and structural adaptations in the heart that initially lead to concentric LVH (Azevedo et al., 2016; Bytyci & Bajraktari, 2015; Mann & Bristow, 2005). This remodelling is characterised by thickening of the myocardium (an increase in wall thickness relative to chamber size) due to the parallel replication and arrangement of cardiomyocytes. According to LaPlace's law, concentric LVH serves as a compensatory mechanism to offset against the increased wall stress during haemodynamic pressure overload (Lee et al., 2013).

Indeed, we and others have previously shown that concentric LVH is initially beneficial as it offsets against wall stress in response to haemodynamic pressure overload (Bernardo et al., 2012;

Mkhize et al., 2024). However, with sustained hypertension, this hypertrophic response becomes maladaptive (Bernardo et al., 2012). The maladaptive process in hypertension is complex and involves the activation of various mechanisms, including neurohormonal adaptations in the renin-angiotensin-aldosterone system (RAAS) (Millen et al., 2018), the sympathetic nervous system (Charkoudian & Rabbitts, 2009; Winter et al., 2018), and inflammation (Adamo et al., 2020). Chronic hypertension primarily drives the transition from a concentrically remodelled myocardium to an eccentrically remodelled phenotype. The shift from concentric to eccentric LVH occurs when collagen cross-links, which stabilise cardiomyocytes in their three-dimensional configuration, disintegrate, leading to side-to-side cardiomyocyte slippage and lengthening (Mann & Bristow, 2005). The development of hypertension-induced eccentric LVH involves cardiomyocyte apoptosis (Akins et al., 2024; Condorelli et al., 1999; Li & Jia, 2022; Li et al., 1997), which predisposes the heart to reactive fibrosis (Schipke et al., 2017).

Cardiac fibrosis is characterised by excessive accumulation of extracellular matrix components, primarily collagen type I, within the heart. This process results in the formation of fibrotic scar tissue (Ni et al., 2021), compromising the structural and functional integrity of the myocardium. The development of cardiac fibrosis is driven by the differentiation of cardiac fibroblasts into myofibroblasts (Schipke et al., 2017), which are highly secretory cells that produce an extracellular matrix predominantly composed of collagen. Initially, this response aims to maintain tissue integrity. However, excessive production of fibrotic tissue in the heart disrupts the coordination of excitation-contraction coupling (Schwinger, 2021), along with the heart's elastic properties and the contractile function of the left ventricle. Myocardial fibrosis is believed to precede diastolic dysfunction (Masiha et al., 2013). Excessive cardiac fibrosis can increase the stiffness of the left ventricle, leading to reduced ventricular compliance and impaired relaxation (Manilall et al.,

2021). As cardiac fibrosis progresses, left ventricular diastolic dysfunction emerges as an early manifestation of heart failure, making it (Andronic AA, 2016) one of the strongest predictors of cardiovascular events in hypertensive patients and a significant contributor to the progression to heart failure (Masenga & Kirabo, 2023). Fibrosis also plays a critical role in the pathophysiology of systolic dysfunction (McDermott et al., 2013). Increased fibrosis, coupled with the loss of cardiomyocytes through apoptosis and/or necrosis, reduces myocardial contractility (Roostalu et al., 2021). Mechanistically, continuous collagen deposition disrupts the normal architecture of cardiac tissue, stiffens the heart, impairs systolic function, and leads to conduction abnormalities, including arrhythmias (Rusnati et al., 2004; Usui et al., 2012; Wu et al., 2019).

There is ongoing controversy in the literature regarding whether concentric and eccentric LVH represent sequential stages along a single pathological continuum or distinct, parallel phenotypes with different underlying mechanisms. Some studies support a progression model (Drazner, Rame, & Marino, 2004), where sustained pressure overload and maladaptive remodeling lead from concentric to eccentric LVH and ultimately to heart failure. Others argue that these phenotypes may arise independently, influenced by genetic predisposition, comorbidities, or differential activation of molecular pathways. This distinction has important implications for prognosis and therapeutic strategies, and remains an area of active investigation.

1.2.2 Molecular mechanisms involved in the development of heart failure

1.2.2.1 Renin Angiotensin Aldosterone System

Several mechanisms contribute to the progression of heart failure, including neurohormonal adaptations in the renin-angiotensin-aldosterone system (RAAS) and the sympathetic nervous system (Hartupee & Mann, 2017). Initially protective, the activation of these neurohormonal systems becomes maladaptive with sustained hypertension (Manolis et al., 2023). The severity of

left ventricular dysfunction in heart failure patients is closely linked to neurohormonal activation. The RAAS plays a crucial role in the disease progression, promoting cardiac remodelling through cell death and reactive fibrosis (Kemp et al., 2014). RAAS blockade, achieved via use of angiotensin converting enzyme inhibitors such as captopril, has shown benefits for patients with chronic systolic heart failure (Chen et al., 2008; Ernsberger et al., 2007). Additionally, excessive adrenergic activation contributes to the transition to heart failure (Chan, 2011). Studies with transgenic animal models indicate that reduced adrenergic activation protects against cardiac dilation and heart failure under pressure overload conditions (Perez, 2021). In this regard, β-adrenergic receptor blockade is also effective in preventing the progression from cardiac hypertrophy to heart failure in hypertensive conditions (Perez, 2021).

Of note, spontaneously hypertensive rats (SHRs), a well-established hypertensive rodent model of genetic origins that closely recapitulates the milieu associated with essential hypertension and its consequences in humans (Lerman et al., 2019), demonstrate an increased susceptibility to adrenergic-induced cardiac dilation and contractile dysfunction (Lymperopoulos et al., 2013). Use of SHRs enables a controlled investigation of hypertension-related mechanisms and the effects of potential interventions, providing valuable insights into hypertensive pathology and treatment responses relevant to human health (Lerman et al., 2019). In clinical practice, the recommended treatment strategy for patients with HFrEF includes a combination of an angiotensin-converting enzyme inhibitor, a β-blocker, and a mineralocorticoid receptor antagonist (Malgie et al., 2023). Despite the beneficial effects of this regimen, the mortality rate amongst HFrEF patients remains high, indicating that other neurohumoral systems, beyond the sympathetic nervous system and RAAS, are involved. These additional systems are likely associated with non-traditional risk factors such as inflammation (Narayan et al., 2023). However, the role of the inflammatory

response in SHRs remains incompletely understood, with limited insights into how inflammation contributes to hypertension development and related cardiovascular remodelling in this model.

1.2.2.2 Inflammation

In the hypertrophic myocardium, untreated haemodynamic pressure overload leads to further tissue injury and triggers the inflammatory response (Mann & Bristow, 2005). This pro-inflammatory state has long been implicated in myocardial fibrosis and diastolic dysfunction in both human studies and animal models of pressure overload (Samak et al., 2016). Initially, the innate immune system provides short-term adaptation to tissue injury. However, with time, it becomes maladaptive, leading to chronic inflammation (Adamo et al., 2020). Activation of the innate immune system occurs through cytosolic and transmembrane Pattern Recognition Receptors (PRRs) that identify molecular motifs from endogenous materials released by dying or distressed cells, known as Damage-Associated Molecular Patterns (DAMPs) (Mann & Bristow, 2005; Soller et al., 2016; Sun et al., 2012). DAMPs activate PRRs, initiating signalling cascades that regulate the expression of genes encoding pro-inflammatory mediators like interleukins (IL-1β, -6, and -8), tumour necrosis factor (TNF-α), and the acute phase proteins (C-reactive protein; CRP, and pentraxin-3; PTX-3). Indeed, multiple studies support the role of cytokines and chemokines in the pathogenesis of diastolic dysfunction (Kocyigit et al., 2014; Levick et al., 2010; Unlu et al., 2013; Usui et al., 2012; Yavuzer et al., 2016). Notably, infusion of TNF-α in rat peritoneal cavities at concentrations commensurate to those observed in human heart failure led to time-dependent changes in cardiac dimensions and function (En-Wei Wang, 2017).

Impaired diastolic function has been observed in cross-sectional studies involving patients with adverse inflammatory profiles (Metra & Teerlink, 2017; Peterlin et al., 2020; Valentova et al., 2016). Inflammatory cytokines such as IL-1β and IL-6 seem to mediate hypertrophic remodelling

and myocardial fibrosis by activating myofibroblasts (Beaumont et al., 2017). These activated myofibroblasts differentiate and take on a different profile that is physiologically distinct from their precursors. In brief, they secrete collagens type I and type III (encoded for by the Col1a and Col3a genes, respectively), which are then further cross-linked by lysyl oxidase (LOX, encoded for by the LOX1 gene), an enzyme that strengthens collagen fibers by forming covalent bonds between them, resulting in a stiffer, more resilient scaffold that is resistant to degradation by matrix metalloproteinases (MMPs-1 and -9) (Beaumont et al., 2017; Nabeebaccus et al., 2016; Soller et al., 2016; Tan et al., 2012). This altered ECM composition affects cardiomyocytes, causing the ECM to become stiffer and less compliant. Consequently, the stiffened extracellular matrix limits the heart's ability to expand and contract efficiently, contributing to impaired cardiac function, which are hallmarks of cardiac remodelling in hypertensive heart disease and heart failure. Additionally, the inflammation-induced overexpression of tissue inhibitors of matrix metalloproteinases (TIMMPs) exacerbates insult to the fibrosed and inflamed myocardium by inhibiting collagen degradation through inactivation of MMPs (Ibrahim & Januzzi, 2018; Soller et al., 2016).

1.2.3 The role of pentraxin-3: A novel biomarker of inflammatory cardiovascular disease

Inflammation is one of the molecular pathways activated during hypertension and may significantly influence the development of concentric LVH (Salles et al., 2007). Pentraxin-3 (PTX-3), an acute-phase protein released in response to the activation of the innate immune system (Bottazzi et al., 2016), has garnered attention for its potential role in cardiovascular pathology. PTX-3 acts as a local inflammatory mediator and is involved in tissue repair and remodelling (Magrini et al., 2016). In hypertensive patients, elevated circulating PTX-3 levels have been observed, which negatively correlate with flow-mediated dilation, an index of endothelial function

(Alp et al., 2019; Parlak, Aydogan, et al., 2012). Endothelial dysfunction occurs when the endothelium, the inner lining of blood vessels, loses its normal ability to regulate vascular tone, maintain blood flow, and respond to physiological stimuli (Sandoo et al., 2010). However, the exact role of PTX-3 in endothelial dysfunction and vascular remodelling remains controversial.

In vitro studies present conflicting results regarding the effects of PTX-3 on the vasculature. Some studies suggest that PTX-3 modulates angiogenesis (Presta et al., 2018), impairs the regenerative response in vessels (Doni et al., 2019), and influences the progression of atherogenesis (Doni et al., 2019). Similarly, research on the role of PTX-3 in concentric LVH due to increased afterload also yields contradictory findings. In a murine model of pressure overload induced by transverse aortic constriction (TAC), the absence of PTX-3 expression attenuated LV hypertrophic changes, while overexpression of PTX-3 exacerbated these changes (Suzuki et al., 2013). Conversely, administering recombinant PTX-3 protein in SHR with heart failure improved LV remodelling and systolic dysfunction associated with hypertension (Chen, Zhuang, et al., 2021). Anti-hypertensive therapies, including ACE inhibitors such as enalapril, have been shown to reduce plasma levels of pentraxin-3 (PTX-3) in hypertensive patients (Buda et al., 2017; Morii et al., 2012; Parlak, Iyisoy, et al., 2012; Unlu et al., 2013), consistent with findings in SHRs with heart failure (Chen, Zhuang, et al., 2021). Further, the lack of consensus in these studies is further complicated by the use of supraphysiological concentrations of PTX-3, leaving a gap in understanding the effects of physiological levels of PTX-3, whether circulating or myocardial, on the development of concentric LVH in hypertension. This discrepancy underscores the need for further research to clarify the role of PTX-3 in hypertensive cardiac pathology.

1.2.4 Contribution of runt-related transcription factor (RUNX-1)

The RUNX superfamily of transcription factors, including RUNX-1, RUNX-2, and RUNX-3, encode DNA-binding alpha subunits that form heterodimeric transcription factors with core binding factor (Martin et al., 2022). These RUNX proteins can act as both activators and repressors of target genes in various physiological and pathological contexts (Riddell et al., 2020). Although RUNX-1 is often associated with leukemic translocations and has been extensively studied in haematological malignancies, its role in the heart has been less explored. This is partly because RUNX-1 is minimally expressed in the adult heart, despite its presence in neonatal cardiomyocytes (McCarroll et al., 2018). Recent evidence, however, suggests that RUNX-1 is reactivated in cardiomyocytes located in the border zone adjacent to the infarct zone in myocardial infarction patients and experimental animal models (McCarroll et al., 2018; Riddell et al., 2020). However, it remains uncertain whether RUNX-1 activation post-myocardial infarction serves merely as a marker of myocardial injury or if it actively contributes to adverse cardiac remodelling.

To address this question, RUNX-1 activity in cardiomyocytes plays a pivotal role in cardiac remodelling and function post-myocardial infarction. In a murine model, RUNX-1 inhibition enhanced sarcoplasmic reticulum calcium absorption via phospholamban, protecting against adverse remodelling and preserving left ventricular systolic function (McCarroll et al., 2018; Riddell et al., 2020). These findings position RUNX-1 as a potential therapeutic target to prevent progression to systolic dysfunction and associated mortality. Beyond ischemic pathology, RUNX-1 upregulation has also been observed in pressure overload models (Zhang et al., 2021), suggesting a broader role in cardiac conditions, though its involvement in hypertension and diastolic dysfunction remains unexplored.

Consequently, the studies (McCarroll et al., 2018; Riddell et al., 2020) concluded that RUNX-1 reactivation post-myocardial infarction plays a crucial role in excitation-contraction coupling and adverse cardiac remodelling. This makes RUNX-1 a potential therapeutic target for reducing the progression from adverse remodelling to systolic dysfunction, which is associated with increased cardiovascular mortality despite improved therapies (Koth et al., 2020; Martin et al., 2022; Suzuki et al., 2023). Interestingly, the involvement of RUNX-1 in hypertension and LVH, particularly in models of impaired diastolic function, remains unexplored. Notably, RUNX-1 upregulation is not limited to ischaemic pathology; it has also been observed in animal models of pressure overload achieved via transverse aortic constriction (Riddell et al., 2020). This suggests that RUNX-1 may have a broader role in cardiac pathologies beyond myocardial infarction.

1.2.5 Non-coding RNAs as novel biomarkers: Their target genes and contribution to the pathogenesis of left ventricular hypertrophy and myocardial dysfunction

While considerable progress has been made in understanding the inflammatory mechanisms underlying heart failure, our comprehension of the upstream gene regulatory pathways governing the phenotypic expression of cardiac remodelling and dysfunction remains incomplete (Schirone et al., 2017). In this regard, recent research has shed light on the unique contribution of non-coding RNAs (ncRNAs) in this context (Ratti et al., 2020). NcRNAs are RNA molecules that are transcribed from DNA but do not encode proteins (Schirone et al., 2017). They play crucial regulatory roles in various cellular processes, including gene expression, epigenetic regulation, and post-transcriptional modifications (Thornburg et al., 2020). While this thesis focuses on microRNAs (miRNAs), it is important to acknowledge the contributions of other ncRNAs, such as small interfering RNAs (siRNAs), which share functional similarities with miRNAs in gene silencing pathways. For the purposes of this research, we specifically chose to study miRNAs due

to their well-established roles in cardiovascular pathophysiology and their potential as therapeutic targets. MiRNAs are short ncRNAs, approximately 22 nucleotides long, which post-transcriptionally regulate gene and protein expression by inhibiting the translation of messenger RNA (mRNA) or inducing its degradation (Novak et al., 2014). Differential patterns of expression of miRNAs have been associated with various pathophysiological mechanisms of heart failure, including myocardial fibrosis, intra-cardiac activation of RAAS components, myocardial sarco-endoplasmic reticulum-mediated calcium sequestration (SERCA), endothelial dysfunction and inflammation (Nabeebaccus et al., 2016; Samak et al., 2016). Consequently, the ability of miRNAs to modulate the expression of target genes represents an endogenous source of gene therapy and a potential therapeutic target in heart failure (Song & Zhang, 2024). For instance, a pioneering trial (Taubel et al., 2021) employing antisense therapy to target miR-132 demonstrated improvements in ejection fraction, reductions in plasma levels of circulating N-terminal pro-B-type Natriuretic Peptide (NT-ProBNP) and profibrotic markers, as well as increased QRS complex duration, suggesting intraventricular conduction delay. Aberrant expression of miRNAs has been implicated in the development of concentric left ventricular hypertrophy (LVH), with specific roles suggested for miR-146a-5p, miR-29b-5p, and miR-155-5p in regulating gene expression linked to myocardial remodeling and dysfunction (Oh et al., 2018; Silva & da Costa Martins, 2022; Thum et al., 2008; Zhang et al., 2014). Furthermore, previous studies have reported sexual dimorphism in arterial blood pressure and cardiovascular outcomes in SHRs, suggesting that sex-specific differences may influence the expression and diagnostic utility of non-coding RNAs as biomarkers in hypertensive cardiac remodeling (Al-Gburi et al., 2017; Reckelhoff, 2001; Reckelhoff et al., 1998; Reckelhoff et al., 2000; Reckelhoff et al., 1999). Indeed, miRNAs may exert broad

regulatory effects on downstream signalling pathways in a sex-specific manner, as demonstrated in previous studies (Wallace et al., 2015; Wei et al., 2013).

The expression of ncRNAs, including miRNAs, is significantly altered in various cardiac diseases, representing a form of adaptive regulation within the body (Lu et al., 2022). From the initial discovery of abnormal miRNA expressions to the exploration of newer ncRNAs, such as long non-coding RNAs (lncRNAs) and circular RNAs (circRNAs), research on ncRNAs in heart failure has rapidly expanded (Singh et al., 2023). RNA-targeted therapies present novel opportunities for drug discovery, leveraging chemically modified oligonucleotides and novel target-binding motifs (Crooke et al., 2018). Compared to traditional chemistry-based drugs or antibodies, RNA-based drugs offer conceptual and practical advantages (Damase et al., 2021). However, challenges such as the regulation of ncRNAs, off-target effects, and potential toxicity must be addressed before clinical application (Hueso et al., 2021). **Figure 1.1** provides a schematic diagram showing the involvement of miRNAs in maturation, regeneration/repair and disease onset/progression, providing a concise overview of the properties of miRNAs and their mode of action. MiRNAs play a crucial role in the maturation of the fetal heart by regulating gene expression pathways essential for cardiac development. In the adult heart, they are also involved in regenerative and repair mechanisms, helping to modulate cellular responses following myocardial injury or disease.

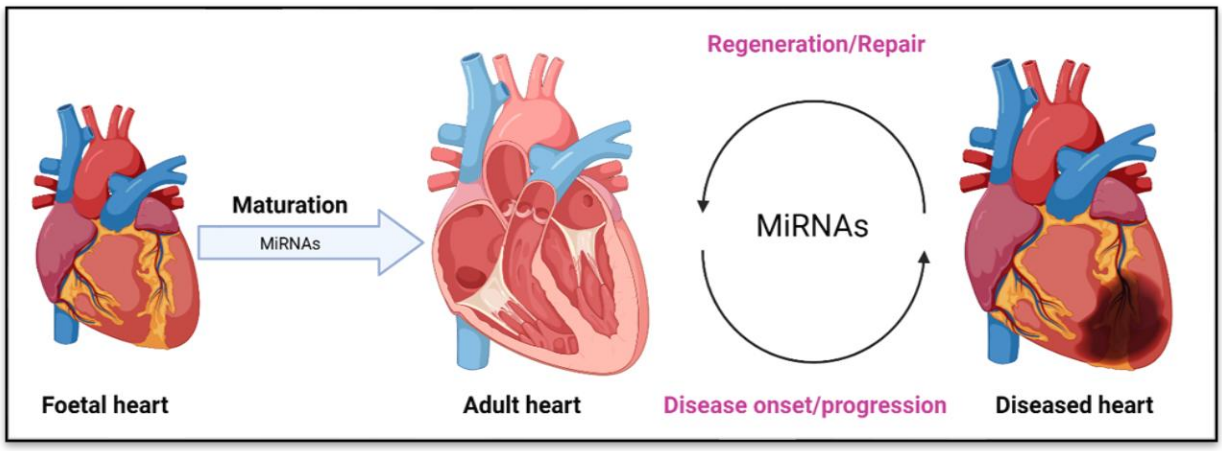

Figure 1.1: Involvement of miRNAs in maturation, regeneration/repair and disease onset/progression (Image created with biorender.com).

1.2.6 Biogenesis of microRNAs: Canonical pathway

The biogenesis and mechanism of action of miRNAs have been extensively reviewed (O'Brien et al., 2018) as understanding in this field has evolved over the years. Despite variations in biogenesis within the miRNA family, they all culminate in the formation of a functional ribonucleoprotein complex known as the RNA-induced silencing complex (RISC) (Carthew & Sontheimer, 2009). Typically, miRNAs originate from the transcription of their primary miRNA (pri-miRNA) by RNA polymerase II or III, which is then cleaved by RNase III Drosha and the RNA-binding protein DiGeorge critical region-8 (DGCR8) to produce precursor molecules (pre-miRNA) (Jin et al., 2020). Subsequently, the pre-miRNAs are transported into the cytoplasm via the Exportin5/RanGTP complex (Wang et al., 2011), where RNase III Dicer1 further processes them to generate mature miRNA duplexes (Johanson et al., 2013). These duplexes are then loaded onto Argonaute family proteins (AGO1-4) and unwound to form single miRNA guide strands utilised by the RISC for targeted mRNA silencing (Carthew & Sontheimer, 2009; Johanson et al., 2013; O'Brien et al., 2018). **Figure 1.2** presents a simplified schematic of miRNA biogenesis.

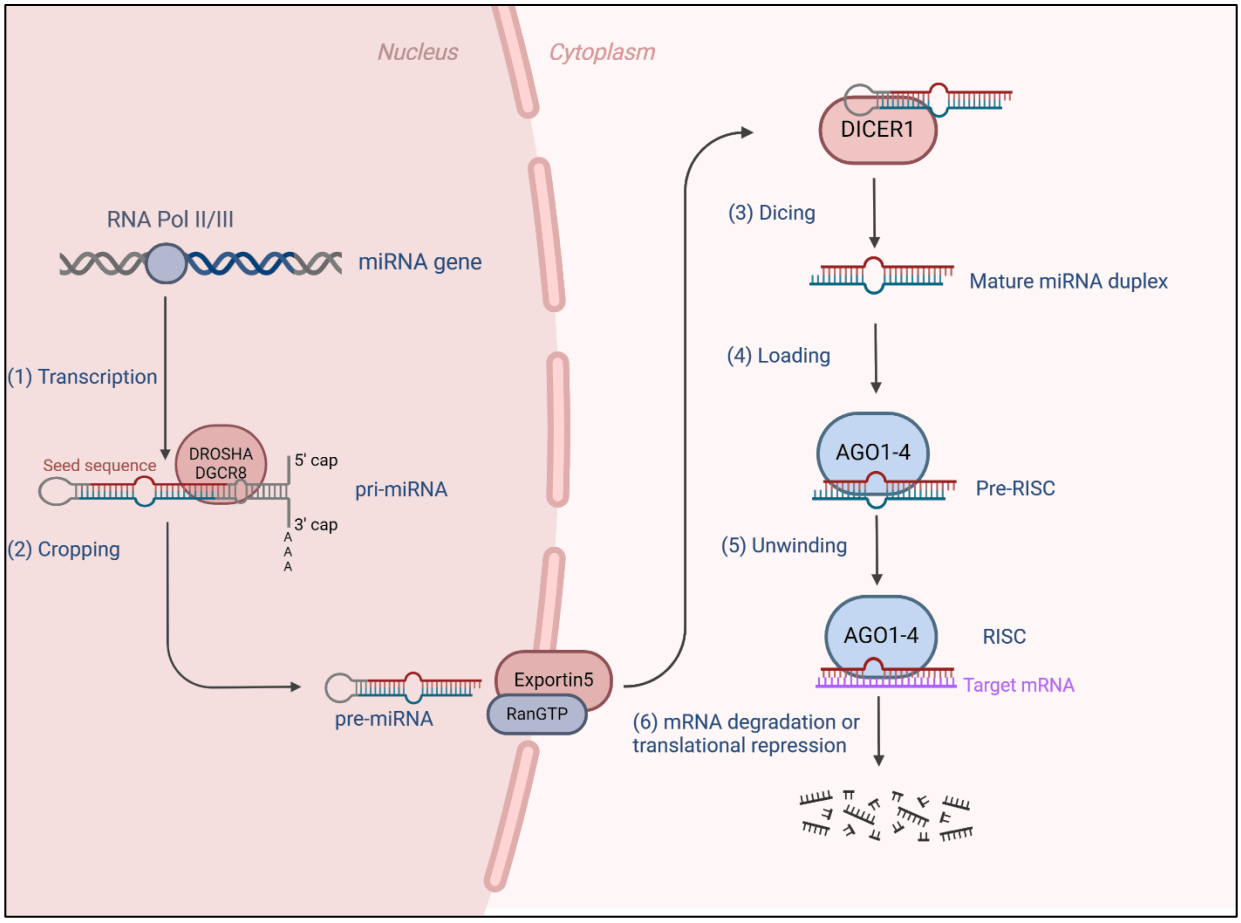

Figure 1.2: Schematic illustration of miRNA biogenesis via the canonical pathway (Image created with biorender.com).

MiRNA biogenesis involves a multi-step process beginning with (1) the transcription of primary miRNA (pri-miRNA) by RNA polymerase II or III. (2) The pri-miRNA is then cropped by the RNase III enzyme Drosha and RNA-binding protein DiGeorge critical region-8 (DGCR8), forming precursor miRNA (pre-miRNA). (3) These pre-miRNAs are exported to the cytoplasm via the Exportin5/RanGTP complex, where (4) RNase III enzyme Dicer1 processes them into mature miRNA duplexes. (5) The duplexes are loaded onto Argonaute proteins (AGO1-4), forming the Pre-RISC complex, and are subsequently (6) unwound to produce a single-stranded

miRNA guide. This guide strand directs the RISC to target mRNAs, silencing gene expression at the post-transcriptional level.

In cardiovascular research, miRNAs have emerged as critical regulators of gene expression, influencing key pathological processes such as cardiac remodelling and dysfunction. While extensive studies have explored the roles of miRNAs in hypertension, this thesis specifically focuses on their contributions to cardiac remodelling and/or dysfunction, with the ultimate aim of identifying miRNAs that could help predict patients at risk of developing heart failure. Despite the known significance of miRNAs, the contributions and expression patterns of specific ones, including miR-146a-5p, miR-155-5p, and miR-29b-5p, in the spontaneously hypertensive rat (SHR) model remain largely unexplored. Furthermore, while ncRNAs broadly, such as siRNAs and other subclasses, play roles in hypertensive cardiac remodelling, their sex-specific mechanisms in male and female SHR have yet to be well characterised. To address these gaps, we selected miR-146a-5p, miR-155-5p, and miR-29b-5p based on a comprehensive literature review highlighting their relevance to pathological processes driving cardiac remodelling in hypertension. MiR-146a-5p was identified for its role in mediating inflammation, fibrosis, and endothelial dysfunction (Gilyazova et al., 2023; Oh et al., 2018). MiR-155-5p was chosen for its involvement in vascular remodelling, endothelial nitric oxide synthase (eNOS) regulation, and oxidative stress (Malmhall et al., 2020). Lastly, miR-29b-5p was prioritised due to its association with cardiomyocyte proliferation, hypertrophy, and fibrosis (Zhang et al., 2014). While other miRNAs also contribute to these processes, we focused on these three due to their potential relevance to hypertensive cardiac pathology. Given that SHR is a genetic model of hypertension, we hypothesize that the selected miRNAs may play significant roles in driving adverse cardiac remodeling and dysfunction. **Table 1.1** summarises various studies investigating the role of miR-

146a-5p in cardiac hypertrophy and dysfunction. Decreased miR-146a levels were associated with LVH in a severe heart failure mouse model, with treatment using an angiotensin II receptor blocker restoring these levels (Kaneko et al., 2017). Evidence suggests that reduced miR-146a-5p levels offer protection against pressure overload-induced cardiac hypertrophy and dysfunction (Heggermont et al., 2017), and have cardioprotective effects *in vivo*, whereas overexpression impairs cardiac function (Oh et al., 2018). This contradiction highlights the complexity of miR-146a regulation and underscores the need for further research to clarify its context-dependent effects in hypertensive heart disease. In a rat model of unilaterally nephrectomised + deoxycorticosterone acetate (DOCA) with 1% salt SD rats, decreased miR-146a was linked to a heightened pro-inflammation state, cardiac fibrosis, and hypertrophy, with the anti-diabetic agent, metformin treatment, restoring its levels (Amara et al., 2019). Increased miR-146a-5p expression has been associated with reduced myocardial fibrosis in pigs and pediatric patients with dilated cardiomyopathy (Kenta Hirai et al., 2020). There is a temporal asymmetry in the expression of miR-155 and miR-146a during macrophage activation, which establishes a dynamic feedback network where miR-155 promotes and miR-146a suppresses NF-κB activity allowing fine-tuned regulation of the inflammatory response (Mann et al., 2017). A correlation between miR-146a-5p levels and left ventricular tract obstruction in hypertrophic cardiomyopathy has also been identified (Ntelios et al., 2021). Furthermore, extracellular vesicles derived from adipose tissue stem cells with reduced miR-146a levels were found to be more effective in lowering hypertrophic and inflammatory markers in stimulated cardiomyocytes (Constantin et al., 2022). The findings surrounding miR-146a-5p and its role in cardiac remodelling and dysfunction are complex and, at times, contrasting, highlighting the need for further research.

Table 1.1 MiR-146a modulates the development of left ventricular hypertrophy and myocardial dysfunction in pressure overload.

Author	Model	Intervention	Findings
(Kaneko et al., 2017)	CSQ-tg mouse, a severe heart failure model	Azilsartan medoxomil (AZL-M), an angiotensin II type 1 receptor blocker	Decreased miR-146a expression in model with LVH. AZL-M restored miR-146a expression. Atrial weight, an index of congestion, was correlated with miR-146a in CSQ-tg mice treated with vehicle and AZL-M.
(Heggermont et al., 2017)	TAC & KO (Pressure overload)	ANG-2 & Iso	Decreased miR-146a protected against cardiac hypertrophy and dysfunction.
(Oh et al., 2018)	Isolated cardiomyocytes from TAC mice co-cultured with fibroblasts (Pressure overload)	MiR-146a inhibition (AntagomiR) & forced expression using a mimic	Decreased miR-146a was cardioprotective *in vivo*. Overexpression impairs cardiac function *in vivo*.
(Amara et al., 2019)	Unilaterally nephrectomised + DOCA with 1% salt SD rats (Pressure & volume overload)	Low & High dose metformin	Decreased miR-146a and increased miR-155 in model. Metformin restored miR-146a and miR-155. Although metformin could not reverse the heart index at organ level, it could increase p-AMPK and reverse fibrosis at molecular level.
(Kenta Hirai et al., 2020)	Pigs and pediatric patients with DCM and reduced EF	Intracoronary infusion with CDCs	Increased CDCex-derived miR-146a-5p expression was associated with reduced myocardial fibrosis.

Author	Model	Intervention	Findings
(Ntelios et al., 2021)	Patients with hypertrophic cardiomyopathy	N/A	Positive correlation between miR-146a with the rs2910164 SNP.
(Pfeffer et al., 2023)	Postpartum patients and postpartum prone CM mice with a cardiomyocyte restricted STAT3-deficiency	N/A	Increased miR-146a in model. PPCM mice developed LVH, a high mRNA expression of the hypertrophic markers.
(Mann et al., 2017)	MiR-146a-deficient mice (macrophage specific miR-155-deficient)	N/A	MiR-155-deficient macrophages exhibit a suboptimal inflammatory response
(Constantin et al., 2022)	Cardiomyocytes (hiPSC-CMs)	ANG-2 and TGF-β1	CM secretome exhibited decreased miR-146a.

Abbreviations: Azilsartan Medoxomil, AZL-M**;** Calsequestrin-transgenic, (CSQ)-tg; Transverse Aortic Constriction, TAC; Knockout, KO; Angiotensin II, ANG-2; Isoproterenol, Iso; Deoxycorticosterone Acetate, DOCA; Sprague-Dawley, SD; Phosphorylated AMP-activated Protein Kinase, p-AMPK; Interventricular Septal Thickness in Diastole, IVSTd; Posterior Wall Thickness in Diastole, PWTd; Dilated Cardiomyopathy, DCM; Ejection Fraction, EF; Cardiosphere-Derived Cells, CDCs; Cardiomyocyte, CM; Signal Transducer and Activator of Transcription 3, STAT-3; Transforming Growth Factor Beta 1, TGF-β1; and Human Induced Pluripotent Stem Cell-Derived Cardiomyocytes, hiPSC-CMs.

In addition to miR-146a-5p, two others—miR-29b-5p, and miR-155-5p have also been recognised for their significant roles in the development of LVH in response to pressure overload (Barringhaus & Zamore, 2009; Hu et al., 2022; Malmhall et al., 2020; Mann et al., 2017; Wu et al., 2022; Zhang et al., 2014). Under conditions of increased afterload, such as transverse aortic constriction (TAC) and angiotensin-II administration in combination with isoproterenol, miR-146a is upregulated, which impairs myocardial calcium sequestration and suppresses pro-inflammatory NFκB signalling (Mann et al., 2017). Conversely, miR-29b-5p and miR-155-5p show sex-specific expression patterns; miR-155-5p was downregulated in sex-matched healthy volunteers and positively correlated with LV mass index (Ikitimur et al., 2015), while miR-29b-5p was upregulated in females after pressure overload (Zhang et al., 2023). These findings suggest that these miRNAs play crucial, sex-specific roles in cardiac function and the development of concentric LVH and myocardial dysfunction.

1.3 Problem statement

Adverse cardiac remodelling and myocardial dysfunction are critical consequences of cardiovascular disease, such as hypertension. These conditions represent significant contributors to morbidity and mortality worldwide. Although the mechanisms of hypertension have been extensively studied, the specific roles of key molecular pathways and biomarkers driving the progression from compensatory LVH to heart failure remain poorly understood. This knowledge gap highlights the need for further exploration of potential biomarkers and their associations with hypertensive cardiac pathology. Emerging evidence suggests that PTX-3, the RUNX-1 transcription factor, and specific miRNAs may play pivotal roles in these processes. However, their precise contributions to cardiac remodelling and dysfunction, particularly in models of essential hypertension such as SHRs, are not well-characterised.

PTX-3, an acute-phase protein released during innate immune activation, has been implicated in cardiovascular pathology. Elevated PTX-3 levels in hypertensive patients correlate with endothelial dysfunction and vascular remodelling. However, its role in concentric LVH development remains contentious, with studies reporting both protective and detrimental effects. For instance, PTX-3 deficiency attenuates LV hypertrophy in pressure overload models, whereas recombinant PTX-3 ameliorates LV remodeling in SHRs with heart failure. These conflicting findings underscore the need for an improved understanding of the role of PTX-3 in hypertensive cardiac remodelling at physiological levels.

The RUNX superfamily of transcription factors, including RUNX-1, also plays a critical role in cardiac remodelling. RUNX-1 expression, minimal in the adult heart, is reactivated under pathological conditions such as myocardial infarction and pressure overload. Studies have shown that RUNX-1 deficiency protects against adverse remodelling by enhancing sarcoplasmic reticulum-mediated calcium sequestration, yet its role in hypertensive LVH and diastolic dysfunction remains largely unexplored.

MiRNAs, including miR-146a-5p, miR-29b-5p, and miR-155-5p, are key regulators of gene expression in cardiac pathology. In pressure overload conditions such as aortic stenosis and hypertension, aberrant expression of these miRNAs correlates with LVH and myocardial dysfunction (Rasoulinejad et al., 2021; Seok et al., 2014; Zhang et al., 2014). For instance, miR-146a-5p is upregulated and linked to increased left ventricular wall thickness, impaired calcium sequestration, and suppressed pro-inflammatory signalling. Furthermore, miR-29b-5p and miR-155-5p exhibit sex-specific expression patterns that may influence cardiac function. Despite these insights, the expression patterns and relative contributions of these miRNAs, together with PTX-3 and RUNX-1 in hypertensive cardiac pathology remain underexplored, particularly in the SHR model which closely mimics human essential hypertension. While other biomarkers exist, these were prioritised due to their novelty and translational potential.

1.4 Aim

The present study aims to explore time-dependent changes of myocardial dimensions and function in the progression from hypertension to heart failure, and determine the expression of candidate biomarkers, in a spontaneously hypertensive rat model.

1.5 Objectives

- To determine the role of circulating PTX-3 concentration or LV relative mRNA expression of PTX-3 in the development of concentric LVH in SHR using two anti-hypertensive therapies with differential effects on the development of concentric hypertrophy,
- To determine the patterns of expression and involvement of miR-146a-5p, -155-5p, and -29b-5p in male and female SHR with established concentric LVH,
- To determine the expression and role of RUNX-1 in cardiac remodelling in spontaneously hypertensive rats (SHR), with a focus on its relationship to structural changes and its putative involvement in anti-fibrotic and anti-apoptotic mechanisms.

Chapter 2

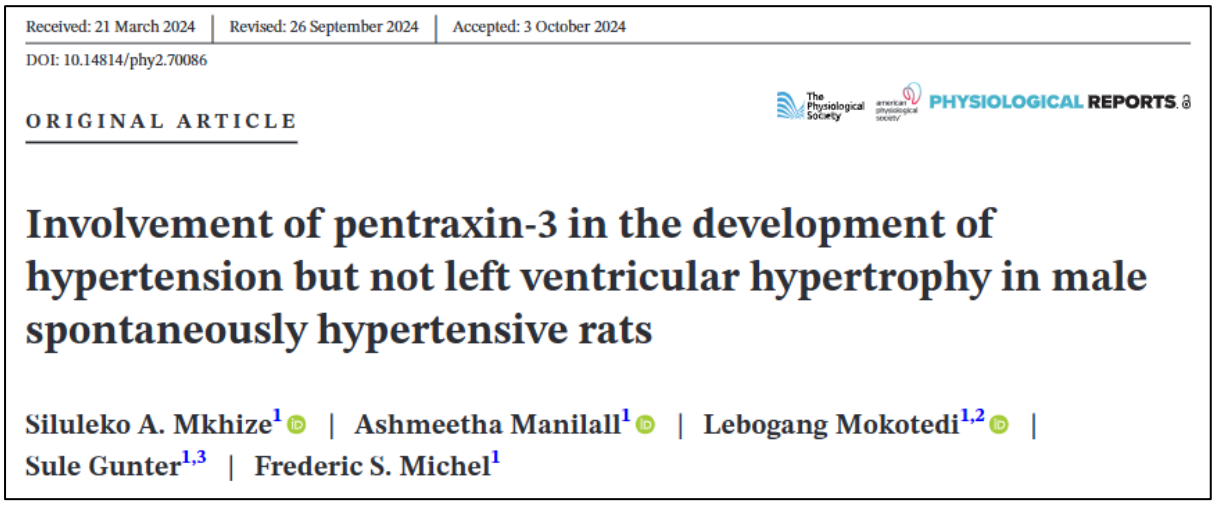

Received: 21 March 2024 | Revised: 26 September 2024 | Accepted: 3 October 2024

DOI: 10.14814/phy2.70086

ORIGINAL ARTICLE

PHYSIOLOGICAL REPORTS

Involvement of pentraxin-3 in the development of hypertension but not left ventricular hypertrophy in male spontaneously hypertensive rats

Siluleko A. Mkhize[1] | Ashmeetha Manilall[1] | Lebogang Mokotedi[1,2] | Sule Gunter[1,3] | Frederic S. Michel[1]

The work presented in this chapter has been published in the journal "Physiological Reports"

Mkhize, S. A., Manilall, A., Mokotedi, L., Gunter, S., & Michel, F. S. (2024). Involvement of pentraxin-3 in the development of hypertension but not left ventricular hypertrophy in male spontaneously hypertensive rats. *Physiological reports*, *12*(20), e70086. https://doi.org/10.14814/phy2.70086

Involvement of pentraxin-3 in the development of hypertension but not left ventricular hypertrophy in male spontaneously hypertensive rats

Authors: Siluleko A Mkhize[1], Ashmeetha Manilall[1], Lebogang Mokotedi[1,2], Sule Gunter[1,3], and Frederic S Michel[1]

Affiliations: [1]Integrated Molecular Physiology Research Initiative, School of Physiology, Faculty of Health Sciences, University of the Witwatersrand, Johannesburg, South Africa

[2]Department of Physiology, School of Medicine, Sefako Makgatho Health Sciences University

[3]Department of Health Sciences and Medicine, Bond University, Gold Coast, Queensland, Australia

Running head: Pentraxin-3 and left ventricular hypertrophy

Corresponding author: Siluleko A Mkhize (Email: siluleko.mkhize@wits.ac.za)

Abstract

Background: Hypertension drives the development of concentric left ventricular hypertrophy (LVH). However, the relative contribution of pentraxin-3 (PTX-3), a novel marker for inflammatory cardiovascular disease, in the hypertrophic response to pressure overload has not been adequately elucidated. **Aim:** We investigated the role of PTX-3 in the development of LVH in spontaneously hypertensive rats (SHR), untreated and treated with either captopril (an ACE inhibitor) or hydralazine (a non-specific vasodilator). **Methods:** Three-month-old SHR received either 20 mg/kg/day hydralazine (SHR+H, n=6), 40 mg/kg/day captopril (SHR+C, n=6), or plain gelatine cubes (untreated SHR, n=7) orally for 4 months. Wistar Kyoto rats (WKY, n=7) were used as the normotensive controls. Blood pressure (BP) was measured using the tail-cuff method. Cardiac geometry and function were determined using M-mode echocardiography. Circulating concentrations of inflammatory markers were measured in plasma by ELISA. LV fibrosis and cardiomyocyte width were assessed by histology. Relative mRNA expression of *PTX-3* was determined in the LV by RT-PCR. **Results:** Untreated SHR exhibited greater systolic BP and relative wall thickness (RWT) compared to WKY. Captopril and hydralazine normalised BP but only captopril reversed RWT in SHR. Circulating PTX-3 and VCAM-1 levels were elevated in untreated SHR and reduced with captopril and hydralazine. Circulating PTX-3 was positively associated with systolic BP but lacked independent relations with indices of LVH. LV relative mRNA expression of *PTX-3* was similar between the groups. **Conclusion:** PTX-3 may not be involved in the development of LVH in SHR, but plausibly reflects the localised inflammatory milieu associated with hypertension.

Keywords: Hypertension, inflammation, left ventricular hypertrophy, vascular cell adhesion molecule-1, pentraxin-3

2.1 Introduction

In the setting of hypertension, the development of concentric left ventricular hypertrophy (LVH) has been subject to profound interest, grounded in the principles of La Place's law (Lorell & Carabello, 2000). As the heart contends with heightened afterload, the left ventricle (LV) undergoes a dynamic process of adaptation in order to maintain optimal wall stress (Lorell & Carabello, 2000). In addition to La Place's law, the interplay of molecular pathways in the development of concentric LVH is intricate and complex (Samak et al., 2016). In this regard, the use of an angiotensin-converting enzyme (ACE) inhibitor, that decreases the systemic and tissue activation of the renin-angiotensin-aldosterone system (RAAS), has been shown to have a greater beneficial effect on the development of concentric LVH beyond its anti-hypertensive effect (Chen et al., 2020). Conversely, hydralazine, a non-specific vasodilator that may activate the sympathetic nervous system, presents with nuanced results on the development of concentric LVH in hypertensive models. While lowering blood pressure (BP), hydralazine may lack efficacy in attenuating the development of concentric LVH (Katholi & Couri, 2011). Taken together, these data demonstrate the importance of targeting the molecular pathways in addition to the control of hypertension in order to reduce concentric LVH.

Amongst other molecular pathways activated during hypertension, inflammation may significantly influence the development of concentric LVH (Masiha et al., 2013). Pentraxin-3 (PTX-3), an acute-phase protein released in response to the activation of the innate immune system (Inoue et al., 2012), has gained attention for its potential role in cardiovascular pathology (Ristagno et al., 2019). PTX-3 is a member of the pentraxin superfamily of proteins, which also includes the well-known C-reactive protein (CRP). PTX-3 is a long pentraxin, structurally and functionally distinct from short pentraxins like CRP and serum amyloid P (SAP) (Li et al., 2024). In particular, PTX-3, which functions as a local inflammatory mediator, has been shown to contribute to tissue repair and remodelling (Doni et al., 2015; Ristagno et

al., 2019). In hypertensive patients, circulating PTX-3 concentration is increased and negatively correlates with flow-mediated dilatation, an index of endothelial function (Alp et al., 2019). However, the role of PTX-3 in the development of endothelial dysfunction and vascular remodelling remains controversial (Carrizzo et al., 2015; Zlibut et al., 2019). The discrepant data are mirrored by *in vitro* studies wherein PTX-3 has been shown to have differing effects on the vasculature by modulating angiogenesis (Camozzi et al., 2006; Leali et al., 2012; Rusnati et al., 2004), impairing regenerative response in vessels (O'Neill et al., 2016), and influencing the progression of athrogenesis (Gustin et al., 2008; Liu et al., 2014). In respect of concentric LVH in response to increased afterload, results are also controversial.

In a murine model of pressure overload achieved by transverse aortic constriction, LV hypertrophic changes, assessed as heart mass normalised to body mass and interventricular septal thickness, were attenuated by a deficiency in the expression of *PTX-3* while an overexpression increased these changes (Suzuki et al., 2013). In contrast, the administration of recombinant PTX-3 protein in spontaneously hypertensive rats (SHR) with heart failure ameliorated the LV remodelling and systolic dysfunction associated with hypertension (Chen, Zhuang, et al., 2021). In addition to the lack of consensus, both studies used supraphysiological concentration of PTX-3 leaving a gap on the effect of physiological level of PTX-3 (circulating or myocardial) on the development of concentric LVH in hypertension.

Understanding the precise roles and regulatory mechanisms of PTX-3 may lay the foundations for novel interventions aimed at mitigating inflammation-driven cardiac and vascular damage. In this regard, studies elucidating the context-specific functions of PTX-3 and exploring its crosstalk with other inflammatory mediators in the setting of hypertension are lacking. We therefore aimed to determine the role of circulating PTX-3 concentration or LV relative mRNA expression of *PTX-3* in the development of concentric LVH in SHR using two anti-hypertensive therapies with differential effects on the development of concentric hypertrophy.

2.2 Methods

2.2.1 Animals and housing

The present study was approved by the Animal Research Ethics Committee of the University of the Witwatersrand (**clearance number:** 2021/03/03C), conducted in accordance with the National Institutes of Health Guide for the Care and Use of Laboratory Animals, and conforms to the Animal Research: Reporting of *In vivo* Experiments (ARRIVE) guidelines (Percie du Sert, Hurst, et al., 2020). The animals were housed individually under conditions of controlled ambient temperature with a light-dark cycle of 12-hours with *ad libitum* access to drinking water and standard laboratory animal chow (Labchef, Johannesburg, South Africa).

2.2.2 Study design

Twenty-six (n=26), 3-month-old male rats consisting of spontaneously hypertensive rats (SHR, n=19, RRID: RGD_10043828) and normotensive Wistar-Kyoto rats (WKY, n=7, RRID: RGD_61119) were sourced and housed at the Wits Research Animal Facility (WRAF). In SHR, the hypertrophic response to pressure overload is sexually dimorphic (Al-Gburi et al., 2017). It is for this reason that we utilised male rats in the present study. For a period of two weeks, the rats were allowed to acclimatise to the housing environment and habituated to consumption of plain gelatine cubes. Thereafter, the SHR were randomly assigned to three groups. The first group (SHR, n=7) received plain gelatine cubes. The second group (SHR + H, n=6) received hydralazine at a dose of 20 mg/kg/day in a gelatine cube (Li et al., 2020). The third group (SHR + C, n=6) received captopril at a dose of 40mg/kg/day in a gelatine cube (Ernsberger et al., 2007). The normotensive WKY (n=7) also received plain gelatine cubes. **Figure 2.1A** shows a diagrammatic illustration of the study design. The selected doses have been previously shown to elicit antihypertensive effects in SHR. The antihypertensive therapies or the plain gelatine cubes were given for 4 months. To ensure complete oral uptake of the drugs, bovril was added to improve palatability of the gelatine cubes. The gelatine cubes were eaten immediately by the

rats. In the literature, a sample size of six to eight rats per group was adequate to show statistical differences in this model (Wilson et al., 2017). **Figure 2.1B** shows a diagrammatic illustration of the sequence and timeline of the experimental procedures.

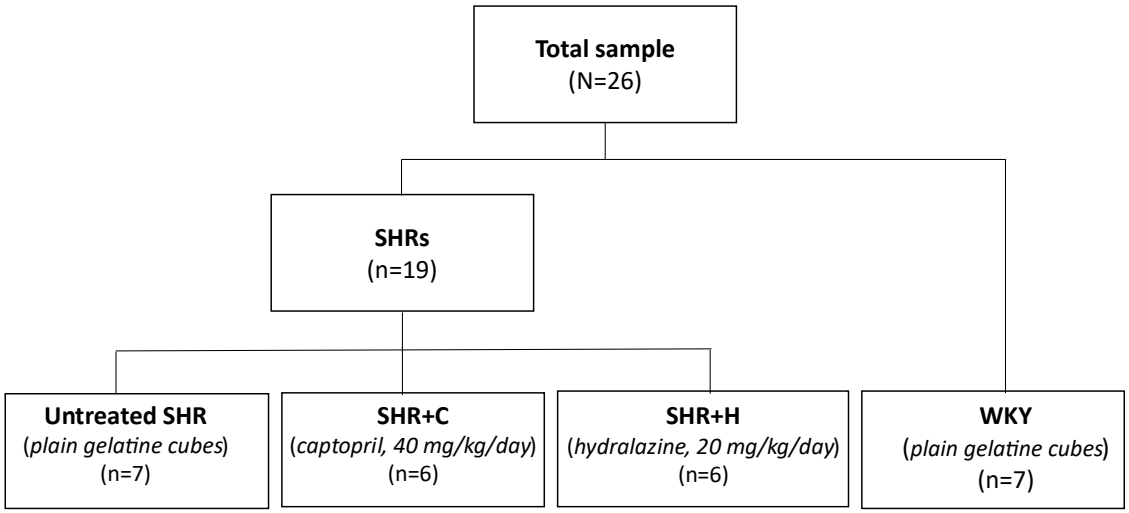

Figure 2.1A: A diagrammatic illustration of the study design.

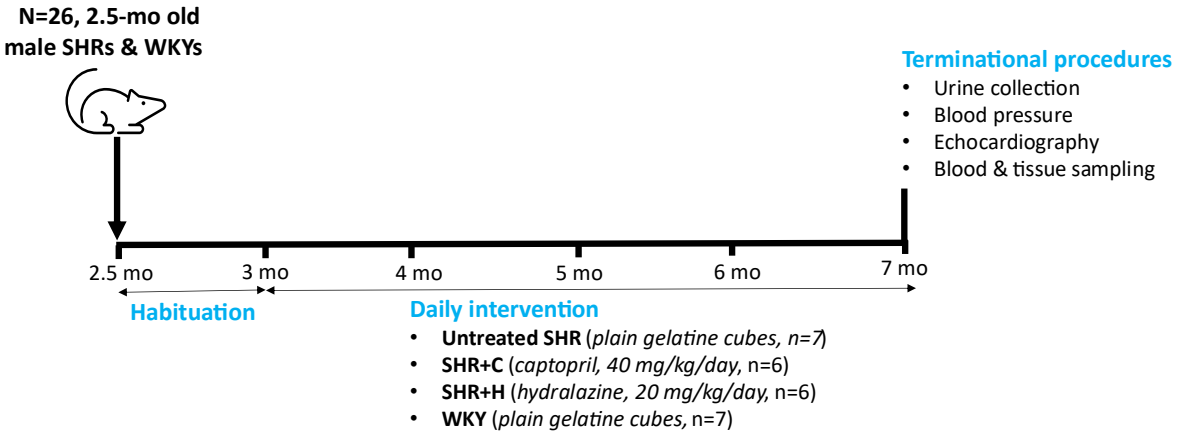

Figure 2.1B: A diagrammatic illustration of the sequence and timeline of the experimental procedures.

2.2.3 Non-invasive blood pressure measurement

For each animal, BP measurement was performed once a week for the last four weeks prior to termination. BP was measured using a tail-cuff technique (Mokotedi et al., 2019) which employs non-invasive BP (NIBP) amplifiers (Biopac systems, Santa Barbara, USA). A built-in pump automatically inflates the tail cuff to occlude the vessel in the tail of a rat and then slowly deflates when the inflation point is reached, providing a linear drop in pressure. Amplifiers have two analog outputs for pressure and pulse waveforms, and a plus gain adjustment to amplify or attenuate the pulse signal. To obtain BP, a conscious rat was placed in a restrainer with a cuff attached to a heated tail. Rats were habituated before the first measurement to enable them to adapt to the restrainer and BP measurement. In our study, we opted for the tail-cuff method over more invasive techniques like telemetry to minimise stress and discomfort to the animals, ensuring their welfare while still obtaining reliable BP measurements. This decision aligns with ethical considerations and enhances the feasibility of conducting comprehensive cardiovascular assessments in our experimental model.

2.2.4 Urine collection

At the end of the treatment period, rats were individually placed in metabolic cages and fasted overnight for no more than 12 hours (from 7 PM to 7 AM). The following morning, urine samples were collected, and the volume (V_{urine}) was measured. The samples were then centrifuged at 1500 rpm for 5 minutes and stored at -80°C for further analyses.

2.2.5 Transthoracic echocardiography

At termination of the study, the rats were anaesthetised using isoflurane (5% induction, and maintained at a constant concentration of 1–2.5% delivered by 100% O_2 mask inhalation). Subsequent to anaesthesia, M-mode echocardiographic parameters were assessed on anaesthetised rats. M-mode offers superior temporal resolution, allowing for accurate

assessment of dynamic changes in cardiac structure and function during the cardiac cycle. As such, M-mode imaging provides clear visualisation of key parameters such as wall thickness, chamber dimensions, and myocardial motion, which are essential for characterising cardiac remodelling and dysfunction (McNamara et al., 2024). A long-axis parasternal view of the LV was obtained using a non-invasive high-resolution (paediatric-10MHz) ultrasound probe coupled to an echocardiogram (Siemens, Acuson SC2000, Diagnostic ultrasound system; Siemens Medical Solutions, USA, Inc.). LV dimensions were measured, including LV internal diameter in systole (LVIDs), left ventricular internal diameter in diastole (LVIDd), interventricular septal thickness in systole (IVSTs), interventricular septal thickness in diastole (IVSTd), LV posterior wall thickness in systole (LVPWTs), and LV posterior wall thickness in diastole (LVPWTd). Thereafter, indices of systolic function were computed using LV dimensions. First, endocardial fractional shortening (endFS) was calculated as endFS = (LVIDd – LVIDs)/LVIDd × 100. Second, midwall fractional shortening (midFS) was calculated as, midFS = [(LVIDd + PWTd) - (LVIDs + PWTs)] / [(LVIDd + PWTd)] x 100. LV relative wall thickness (RWT) was calculated as RWT = (2xPWTd) / LVIDd. Lastly, systolic wall stress was computed as wall stress = [(SBP)*(LVIDs/2)] / 2PWTs. Echocardiographic assessment was conducted by a trained sonographer who was blinded to the experimental groups. Assessments were conducted in accordance with the American Society of Echocardiography guidelines (McNamara et al., 2024).

2.2.6 Blood and tissue sampling

Following echocardiography, a thoracotomy was performed, and the rats were exsanguinated by cardiac puncture. Blood was collected into sterile EDTA tubes (plasma), centrifuged, and stored at -80°C for further analysis. The heart and kidneys were removed, weighed, and stored in an RNA stabilising reagent, RNAlater (Ambion, Sigma Aldrich, Germany), for tissue

storage to maintain the integrity of the RNA within the post-mortem samples for reliable gene expression analysis.

2.2.7 Circulating levels of inflammatory markers and urinary creatinine

Plasma concentrations of the inflammatory markers including C-reactive protein (CRP), tumour necrosis factor alpha (TNF-α), and pentraxin-3 (PTX-3), vascular cell adhesion molecule-1 (VCAM-1), in plasma; and creatinine (Cr) in plasma and urine were determined by solid phase sandwich enzyme-linked immunosorbent assay (ELISA) (Elab Science Biotechnologies, Co Ltd, Wuhan, China). The lower detectable limits for TNF-α, CRP, PTX-3, VCAM-1, and Cr were 78 pg/ml, 0.3 ng/ml, 0.16 ng/ml, 12.5 pg/ml, and 1.25 µg/ml, respectively. Additionally, both inter-assay and intra-assay coefficients of variation were below 10% for all kits used. PTX-3 was included as a specific marker of local vascular inflammation in the context of hypertension (Adamo et al., 2020), while CRP and TNF-α were included to determine whether local inflammatory changes summated into a systemic pro-inflammatory state. Urine and plasma Cr concentrations were used to assess kidney function by computing the estimated glomerular filtration rate as eGFR = $(Cr_{urine} * V_{urine}) / Cr_{plasma}$.

2.2.8 Total RNA extraction and cDNA synthesis

Total RNA was extracted from LV tissue using an Illustra™ RNAspin Mini Isolation kit (GE Healthcare, Buckinghamshire, United Kingdom) according to manufacturer's instructions. The presence and quantity of RNA was confirmed using a Nanodrop OneC spectrophotometer (Thermo Fisher Scientific, Waltham, USA). The RNA was then reverse-transcribed to cDNA using SuperScript™ IV VILO™ cDNA synthesis master mix (Thermo Fisher Scientific, Life Technologies, Carlsbad, USA), according to manufacturer's instructions. The presence of cDNA was again confirmed using a Nanodrop OneC spectrophotometer (Thermo Fisher Scientific, Waltham, USA). The cDNA constructs were stored at -20°C for further analyses.

2.2.9 Relative mRNA expression of pentraxin-3 in LV tissue

Comparative gene expression RT-PCR was performed in duplex reactions using the cDNA templates (~1 µl), pre-designed Taqman™ probe mixes for the reference gene Hypoxanthine Guanine Phosphoribosyl Transferase-1 *(HPRT1)* (0.25 µl, Taqman assay ID: Rn01527838_g1, Thermo Fisher Scientific, Life Technologies, Carlsbad, USA), the gene of interest (0.5 µl, Taqman gene expression assay) and Taqman Fast Advanced PCR Master Mix (5 µl) in a final volume of 10 µl. The relative expression of the gene of interest was computed using the $2^{-\Delta\Delta Ct}$ method. Reporting of data complied with the conventions as set out in the Minimum Information for Publication of Quantitative Real-Time PCR Experiments (MIQE) guidelines (Johnson et al., 2014).

2.2.10 Total collagen content from LV tissue

LV tissue samples preserved in 10% buffered formalin were processed for standard paraffin embedding. Thin sections, 5µm in thickness, were cut from the paraffin-embedded tissues using a microtome, followed by deparaffinisation and rehydration (Mokotedi et al., 2020). The sections were then stained for 60 minutes at room temperature with a 0.1% sirius red solution dissolved in saturated picric acid. After staining, the slides were rinsed with acidified water, dehydrated, and mounted with Digital Picture Exchange (DPX) mounting medium. The tissue sections were examined using a Zeiss Axioscope 2 Plus microscope with a Zeiss AxioCam (Zeiss, Peabody, MA, USA, RRID: SCR_023747). Visualisation was conducted under bright-field with a 10x objective lens (oil magnification x100). Using ImageJ software (RRID: SCR_003070), the collagen fraction area was calculated for each tissue section by dividing the collagen-occupied area by the total tissue area (Mokotedi et al., 2020).

2.2.11 Cardiomyocyte width from LV tissue

Haematoxylin and Eosin (H&E) staining was used to measure LV cardiomyocyte width at the level of the nucleus. First, the tissue samples were deparaffinised in xylene and then rehydrated through graded ethanol concentrations. After this, the samples were stained with Harris' haematoxylin and eosin solutions, followed by dehydration in ethanol and xylene, and mounted with DPX mountant. A single evaluator who was blinded to the experimental groups examined the slides using a DVM6 digital microscope (Leica Biosystems, Vista, CA, USA), with a max. FOV of 12.55 mm and a magnification range of 46x to 675x. LV cardiomyocyte width was measured using the straight-line tool. Each sample was measured three times, and the average width (µm) was recorded.

2.2.12 Statistical analyses

Statistical analysis was performed using GraphPad Prism version 10.0.0 for Windows (GraphPad Software, Boston, Massachusetts USA, www.graphpad.com). Normality was confirmed using a Shapiro-Wilk test. Normally distributed data is expressed as arithmetic mean ± SD. Group differences were ascertained using one-way analysis of variance (ANOVA) test followed by a Tukey's *post hoc* test to correct for multiple comparisons. Associations between circulating PTX-3 and indices of LVH were determined from linear regression analyses, with and without controlling for the confounding effect of systolic BP. Statistical significance was considered at $P<0.05$, *a priori*.

2.3 Results

2.3.1 Haemodynamic and gravimetric parameters

Untreated SHR exhibited significantly greater systolic BP compared to WKY ($P<0.0001$). SHR treated with either hydralazine or captopril experienced a decrease in SBP by ~0.79 folds

compared to untreated SHR (P<0.0001). The diastolic BP was similar between all the groups (P>0.05) (**Figures 2.2A and 2.2B**). WKY were significantly heavier than treated SHR (all P<0.001). The hearts of untreated SHR (P=0.015) and SHR treated with hydralazine (P=0.040), but not captopril (P=0.756), were significantly heavier compared to the hearts of WKY. The LV was significantly heavier in untreated SHR compared to WKY (P=0.004). When normalised to body mass, the hearts of the three different SHR groups were significantly heavier than those of WKY (all P<0.0001). SHR treated with hydralazine had significantly heavier normalised heart mass compared to SHRs treated with captopril (P=0.029). When normalised to body mass, the LV of the three different SHR groups were significantly heavier than those of WKY (all P<0.0001). Kidney mass (absolute and normalised to body mass) and eGFR were similar amongst all the groups (all P>0.05, **Table 2.1**).

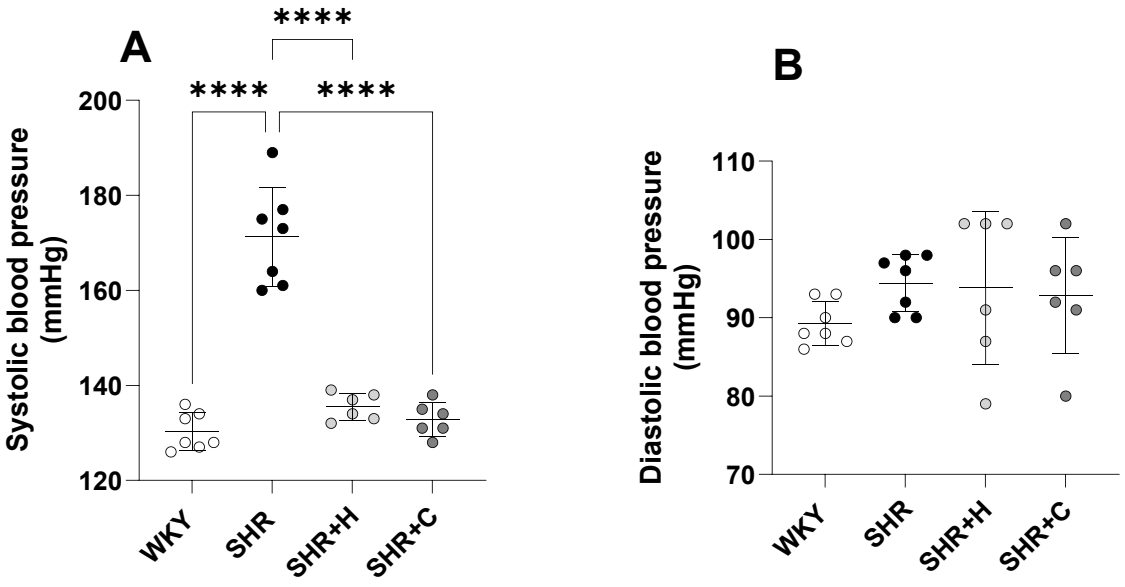

Figures 2.2A and 2.2B: A graphical representation of the haemodynamic parameters, systolic blood pressure (A), and diastolic blood pressure (B) in normotensive WKYs, untreated SHRs, and SHRs treated with either hydralazine or captopril.

Data expressed as mean ± SD

1-way ANOVA with Tukey *post hoc* test

****P<0.0001

Table 2.1: Gravimetric analyses and kidney function in normotensive WKYs, untreated SHRs, and SHRs treated with either hydralazine or captopril.

	WKY **n=7**	**SHR** **n=7**	**SHR + H** **n=6**	**SHR + C** **n=6**
Body mass (g)	389 ± 15	360 ± 69	336 ± 25**	336 ± 23**
Heart mass (g)	1.28 ± 0.08	1.50 ± 0.16*	1.48 ± 0.07*	1.35 ± 0.15
Heart (g/100g)	0.33 ± 0.02	0.42 ± 0.03***	0.44 ± 0.02***	0.40 ± 0.02***$
LV mass (g)	0.85 ± 0.10	1.12 ± 0.17**	1.04 ± 0.09	1.01 ± 0.12
LV (g/100g)	0.22 ± 0.03	0.31 ± 0.03***	0.31 ± 0.02***	0.30 ± 0.01***
Kidney mass (g)	1.39 ± 0.09	1.32 ± 0.16	1.27 ± 0.11	1.23 ± 0.07
Kidney (g/100g)	0.36 ± 0.01	0.37 ± 0.04	0.38 ± 0.03	0.31 ± 0.15
eGFR (ml/min)	0.46 ± 0.21	0.29 ± 0.17	0.38 ± 0.29	0.31 ± 0.19

Abbreviations: WKY, Wistar Kyoto rats; SHR, spontaneously hypertensive rats; H, hydralazine; C, captopril; LV, left ventricle; and eGFR, estimated glomerular filtration rate

Data expressed as mean ± SD

Organ masses were normalised to body mass and expressed as g/100g

1-way ANOVA with Tukey *post hoc* test

***P<0.0001, **P<0.001, *P<0.05 vs WKY

$P<0.05 vs SHR + H

2.3.2 LV geometry and systolic function

All indices of LV geometry were similar among the groups (all P>0.05). Despite hydralazine or captopril having lowered BP in the treated SHR, the midwall fractional shortening was significantly decreased when compared to WKY (P=0.043 for hydralazine) and (P=0.018 for captopril). Endocardial fractional shortening and systolic wall stress were similar between the groups (all P>0.05, **Table 2.2**).

Untreated SHR exhibited significantly greater LV posterior wall thickness in diastole compared to WKY (P=0.023), which was neither regressed by captopril (P=0.074) nor hydralazine (P>0.05, **Figure 2.3A**). Relative wall thickness was greater in untreated SHR compared to WKY (P=0.011) and regressed with captopril (P=0.011) but not hydralazine (P>0.05, **Figure 2.3B**).

Table 2.2: Echocardiographic parameters showing left ventricular geometry and systolic function in normotensive WKYs, untreated SHRs, and SHRs treated with either hydralazine or captopril.

	WKY n=7	**SHR n=7**	**SHR + H n=6**	**SHR + C n=6**
LV geometry				
LVIDs (cm)	0.35 ± 0.09	0.34 ± 0.15	0.29 ± 0.13	0.39 ± 0.18
LVIDd (cm)	0.68 ± 0.06	0.61 ± 0.08	0.67 ± 0.13	0.73 ± 0.11
IVSTs (cm)	0.38 ± 0.09	0.37 ± 0.07	0.30 ± 0.12	0.38 ± 0.05
IVSTd (cm)	0.27 ± 0.08	0.30 ± 0.09	0.23 ± 0.08	0.28 ± 0.07
LVPWTs (cm)	0.28 ± 0.09	0.34 ± 0.04	0.34 ± 0.09	0.26 ± 0.08
Systolic function				
endFS (%)	43 ± 12	45 ± 4	35 ± 13	30 ± 5
midFS (%)	30 ± 5	23 ± 3	18 ± 9*	17 ± 7*

Wall stress (kdynes.cm^{-2})	50 ± 24	57 ± 20	43 ± 31	65 ± 17

Abbreviations: WKY, Wistar Kyoto rats; SHR, spontaneously hypertensive rats; H, hydralazine; C, captopril; LVIDs, left ventricular internal diameter in systole; LVIDd, left ventricular internal diameter in diastole; IVSTs, interventricular septal thickness in systole; IVSTd, interventricular septal thickness in diastole; LVPWTs, left ventricular posterior wall thickness in systole; endFS, endocardial fractional shortening; and midFS, midwall fractional shortening

Data expressed as mean ± SD

1-way ANOVA with Tukey *post hoc* test

*P<0.05 vs WKY

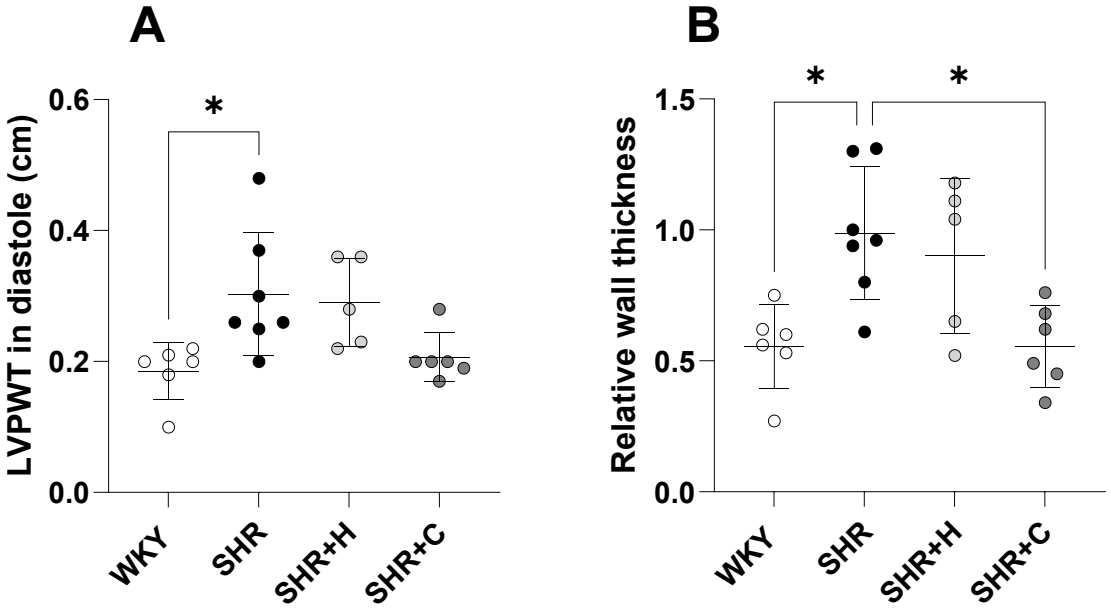

Figures 2.3A and 2.3B: A graph illustrating indices of left ventricular hypertrophy; left ventricular posterior wall thickness (LVPWT) in diastole (A), and relative wall thickness (B) in normotensive WKYs, untreated SHRs, and SHRs treated with either hydralazine or captopril.

Data expressed as mean ± SD

1-way ANOVA with Tukey *post hoc* test

****P<0.0001, **P<0.001, and *P<0.05

2.3.3 Total collagen content and cardiomyocyte width

Figure 2.4 shows the collagen fraction area, expressed as a percentage of the total section, along with representative micrographs for each experimental group. The collagen fraction area was significantly higher in SHR compared to WKY (P=0.021), but neither captopril (P=0.063) nor hydralazine (P=0.573) treatment reduced it. Cardiomyocyte width in SHR was similar to that of WKY (P=0.197). SHR treated with hydralazine had a significantly greater cardiomyocyte width compared to WKY (P=0.0002) and untreated SHR (P=0.024), while captopril treatment reduced cardiomyocyte width significantly (P=0.001) (**Figure 2.5**).

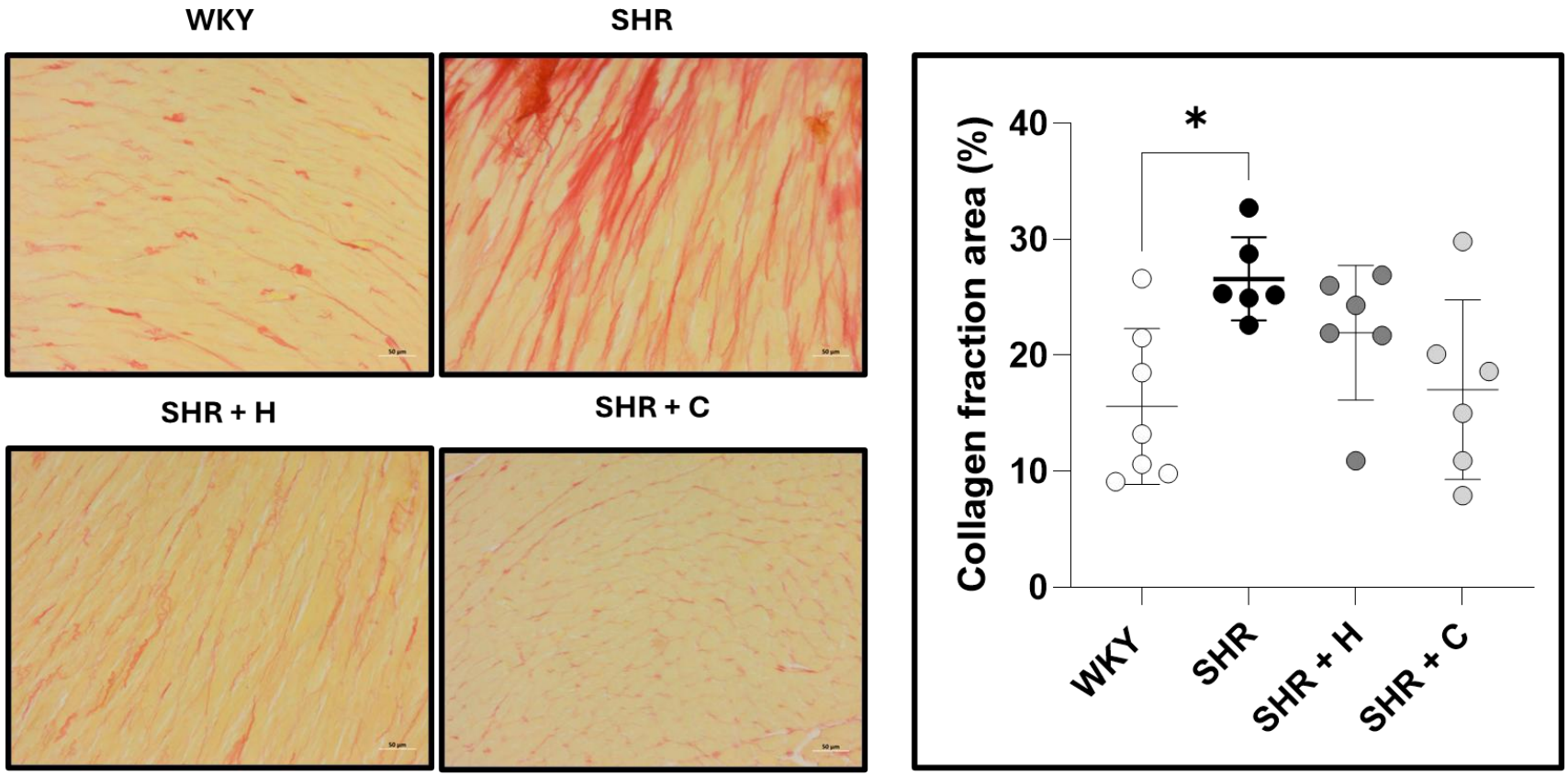

Figure 2.4: A graph depicting the collagen fraction area, expressed as a percentage of the total LV section, along with representative micrographs of normotensive WKYs, untreated SHRs, and SHRs treated with either hydralazine or captopril.

Data expressed as mean ± SD; 1-way ANOVA with Tukey *post hoc* test

*P<0.05

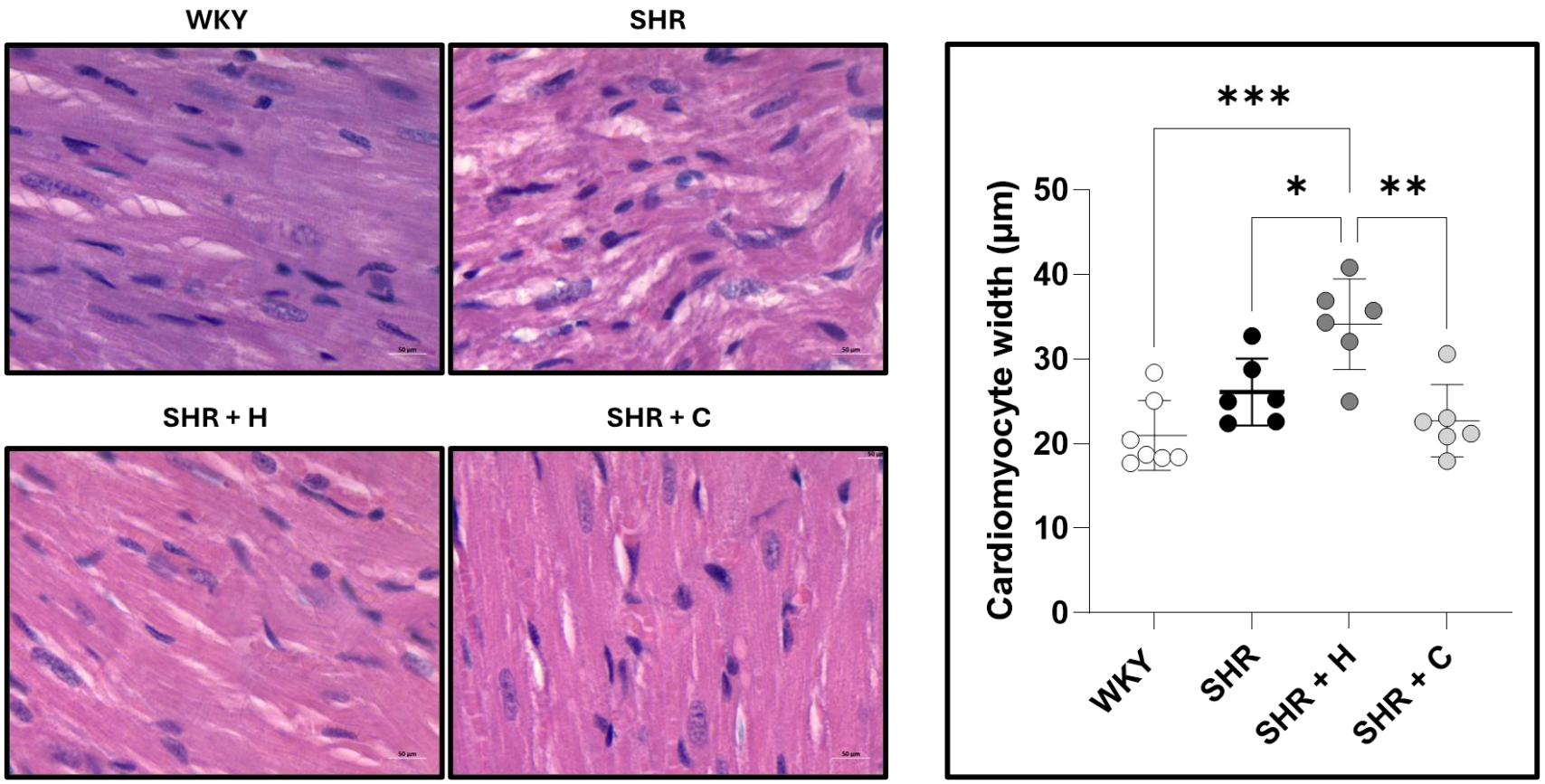

Figure 2.5: A graph depicting cardiomyocyte width, along with representative micrographs of normotensive WKYs, untreated SHRs, and SHRs treated with either hydralazine or captopril.

Data expressed as mean ± SD; 1-way ANOVA with Tukey *post hoc* test

*P<0.05, **P<0.001, and ***P<0.0001

2.3.4 Circulating inflammatory markers

The circulating levels of the inflammatory markers, including CRP and TNF-α concentrations were similar amongst the four different experimental groups (all P>0.05, **Figures 2.6A** and **2.6B**). Circulating concentrations of VCAM-1 were significantly greater in SHR compared to WKY (P<0.0001), and decreased significantly upon treatment with captopril (P=0.002), and hydralazine (P=0.019, **Figure 2.6C**).

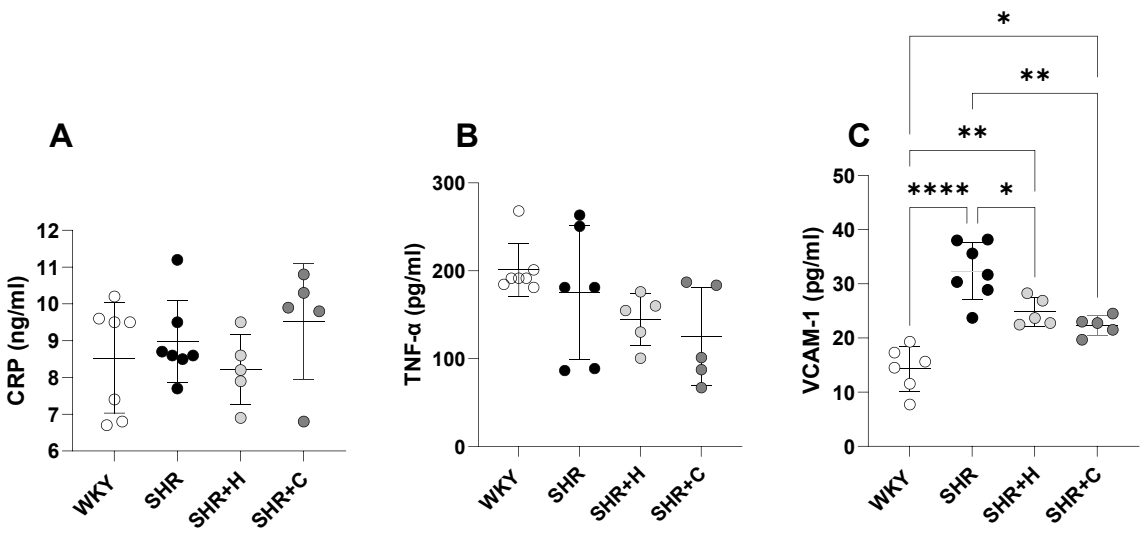

Figures 6A, 6B, and 6C: A graph illustrating the circulating concentrations of inflammatory markers including C-Reactive Protein (A), Tumour Necrosis Factor alpha (B), and Vascular Cell Adhesion Molecule-1 (C) in normotensive WKYs, untreated SHRs, and SHRs treated with either hydralazine or captopril.

Data expressed as mean ± SD

1-way ANOVA with Tukey *post hoc* test

****P<0.0001, **P<0.001, and *P<0.05

2.3.5 Circulating pentraxin-3 concentration and LV mRNA expression

Figures 2.7A and 2.7B show the circulating concentration of the inflammatory marker; pentraxin-3 (**A**), and LV mRNA expression of pentraxin-3 (relative to the endogenous reference control gene; *HPRT1*, **B**) in normotensive WKY, untreated SHR, and SHR treated with either hydralazine or captopril. The circulating levels of pentraxin-3 were significantly higher in untreated SHRs compared to WKY; mean difference [95% CI], -0.51 [-0.87 to -0.15, P=0.004], and were decreased by hydralazine; 0.68 [0.30 to 1.06, P=0.0004], and captopril; 0,58 [0.20 to 0.96, P=0.002]. However, the LV relative mRNA expression of *PTX-3* was not different among the groups (all P>0.05).

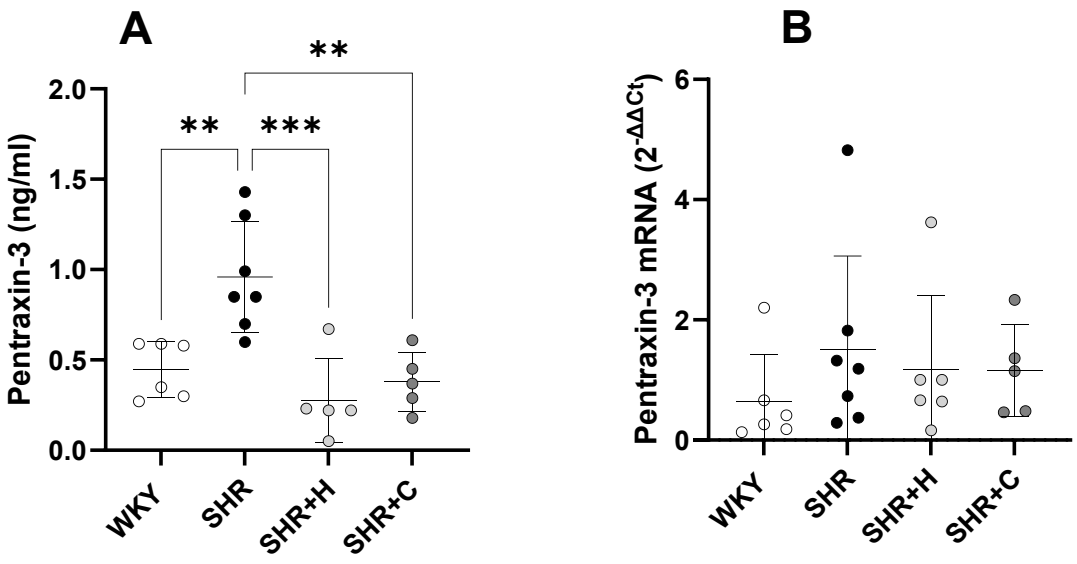

Figures 2.7A and 2.7B: A graph illustrating circulating levels of the inflammatory marker; pentraxin-3 (A), and LV tissue-specific relative mRNA expression of *pentraxin-3* (relative to *HPRT1* as endogenous control, B) in normotensive WKYs, untreated SHRs, and SHRs treated with either hydralazine or captopril.

Data expressed as mean ± SD

1-way ANOVA with Tukey *post hoc* test

****P<0.0001, **P<0.001

2.3.6 Associations between circulating levels of pentraxin-3 with indices of left ventricular hypertrophy, inflammatory markers, kidney function, and collagen content

Figure 2.8: A forest plot illustrating the relationship between circulating concentrations of pentraxin-3 with systolic blood pressure, indices of left ventricular hypertrophy, inflammatory markers, kidney function, and collagen fraction area in normotensive WKYs, untreated SHRs, and SHRs treated with either hydralazine or captopril. Open circles represent the point estimate (r, correlation coefficient). Horizontal lines bisecting the open circles represent the lower and upper limits of the 95% confidence interval (CI). Circulating concentration of pentraxin-3 was positively and significantly associated with systolic BP (r=0.722; P=0.0001), VCAM-1 (r=0.545; P=0.009), relative wall thickness (r=0.562; P=0.008), but not with systolic wall stress (r=-0.191; P=0.408). However, in multivariable linear regression analyses adjusting for the confounding effect of SBP, relative wall thickness, β coefficient [95% CI]: 0.248 [-0.227 to 0.724, P= 0.286] and VCAM-1, β coefficient [95% CI]: -0.004 [-0.028 to 0.020, P=0.714] were no longer associated with circulating concentrations of pentraxin-3. Circulating concentrations of pentraxin-3 were also not associated with CRP (r=-0.013; P=0.954), nor with TNF-α (r=0.076; P=0.738). No associations between the circulating concentrations of pentraxin-3 and LVPWTd (r=0.372; P=0.097), normalised heart mass (r=0.216; P=0.565) or normalised LV masses (r=0.343; P=0.109) were observed. Lastly, no associations were observed between pentraxin-3 and eGFR (r=-0.187; P=0.382) and collagen fraction area (r=-0.006; P=0.998). Circulating concentrations of VCAM-1 was positively and significantly associated with systolic BP (r=0.755; P<0.0001).

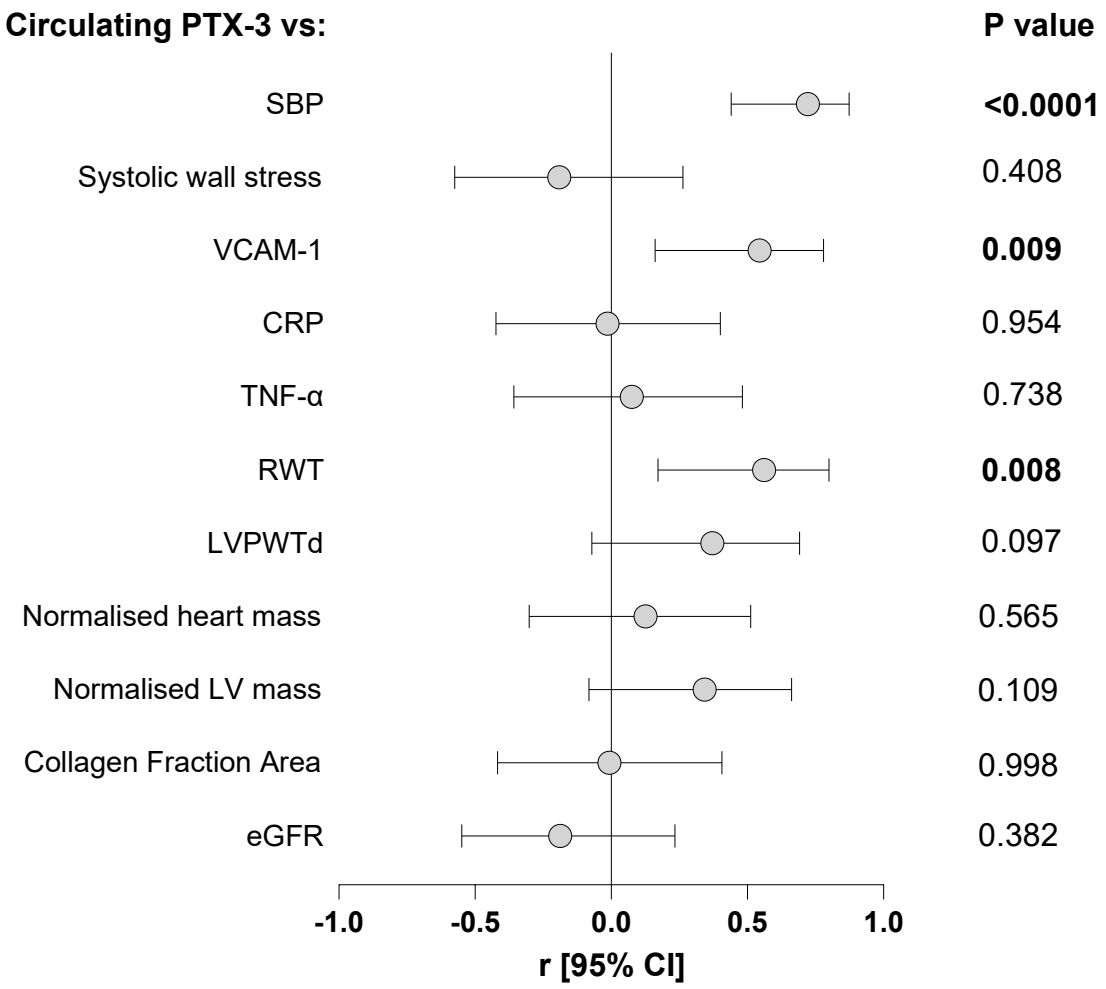

Figure 2.8: A graph plot illustrating the relationship between circulating levels of pentraxin-3 with systolic blood pressure, indices of left ventricular hypertrophy, inflammatory markers, kidney function, and collagen fraction area in normotensive WKYs, untreated SHRs, and SHRs treated with either hydralazine or captopril. Open circles represent the point estimate (r, correlation coefficient). Horizontal lines bisecting the open circles represent the lower and upper limits of the 95% confidence interval (CI).

2.4 Discussion

The current study shows that hypertension present in SHR subsided upon treatment with hydralazine or captopril. Furthermore, treatment with captopril but not with hydralazine resulted in the regression of concentric LVH indexed by relative wall thickness and cardiomyocyte width. We also showed that circulating PTX-3 and VCAM-1 concentrations were elevated with hypertension. In addition, circulating PTX-3 and VCAM-1 concentrations were positively associated with SBP. However, circulating PTX-3 concentration was not independently associated with indices of concentric LVH. Finally, LV relative mRNA expression of *PTX-3* was not different between the experimental groups. Therefore, the current study highlights the role of circulating and LV-specific expression of PTX-3 in the development of hypertension-induced concentric LV remodelling.

Hypertension is one of the main risk factors for the development of concentric LVH (Lorell & Carabello, 2000). Despite some discordant results (Wu et al., 2019), circulating PTX-3 concentration has been shown to be elevated in patients with hypertension (Carrizzo et al., 2015; Damiani et al., 2015; Yano et al., 2010; Yavuzer et al., 2016). Moreover, except in one study involving hypertensive patients with obesity (Karamfilova et al., 2022), circulating PTX-3 concentration was associated with systolic and diastolic BP (Chen, Liu, et al., 2021; Kizilgul et al., 2017; Parlak, Aydogan, et al., 2012). Finally, anti-hypertensive therapies, including ACE inhibitors such as enalapril, have been shown to decrease plasma levels of PTX-3 in hypertensive patients (Buda et al., 2017; Morii et al., 2012; Parlak, Iyisoy, et al., 2012; Unlu et al., 2013). Similar to what has been shown in SHR with heart failure (Chen, Zhuang, et al., 2021), the present study showed a greater circulating PTX-3 concentration with hypertension. In addition, the use of anti-hypertensive therapies with different modes of action restored the circulating PTX-3 concentration to normal levels resulting in a positive relationship between systolic BP and circulating PTX-3 concentration.

Despite the absence of direct measurements of endothelial function, the greater circulating concentrations of VCAM-1 in SHR as well as its association between VCAM-1 concentrations and SBP in the present study support the role of endothelial activation in the development of hypertension (McCarron et al., 1994; Usui et al., 2012; Y. Liu et al., 1996). Moreover, captopril is known to protect against endothelial dysfunction in humans and SHRs (Chen et al., 2008). Hydralazine, a non-specific vasodilator, has also been shown to ameliorate endothelial dysfunction (Knowles et al., 2004). In line with the previous results, the present study showed that both captopril and hydralazine, despite having different modes of action, reduce the circulating VCAM-1 concentrations in SHR suggesting amelioration of the endothelial dysfunction with both anti-hypertensive therapies. PTX-3, a pro-inflammatory mediator released during tissue injury, may be involved in endothelial activation, an important mechanism in the establishment of hypertension (Carrizzo et al., 2015). In the present study, the concentrations of circulating PTX-3 were associated with those of VCAM-1. In addition, PTX-3 was no longer associated with SBP following adjustments for VCAM-1. Taken together, the present study suggests that PTX-3 is involved, at least as a mediator, in response to endothelial activation and the establishment of hypertension in SHR.

While the differences in CRP or TNF-α did not reach statistical significance, the trends in CRP or TNF-α concentrations across groups were similar to those of PTX-3 and VCAM-1. Significant differences in CRP or TNF-α concentrations may have been recorded with a larger sample size. However, a systemic pro-inflammatory status in SHR was not confirmed in the present study, since only circulating PTX-3 and VCAM-1 concentrations were increased. Nonetheless, our findings confirm those of previous studies reporting that PTX-3 is a more sensitive marker of endothelial dysfunction compared to CRP (Yano et al., 2010). Unlike CRP, which is predominantly produced in the liver, PTX-3 is produced locally at the site of inflammation by various cell types including endothelial cells, immune cells, fibroblasts, and

renal epithelial cells (Li et al., 2024; Luo et al., 2023; Nauta et al., 2005). This local production positions PTX-3 as a more specific marker of tissue-specific inflammatory responses compared to the systemic marker, CRP. Indeed, unlike CRP, which is produced in the liver, PTX-3 is reported to be produced directly within the blood vessels/site of injury following endothelial activation, making it a more accurate marker of localised inflammation and tissue repair (Carrizzo et al., 2015; Kanbay et al., 2015; Knoflach et al., 2012; Kocyigit et al., 2014; Zlibut et al., 2019). However, to delineate a potential mechanism behind the differences in circulating PTX-3, the present study lacks evidence regarding the specific source of circulating PTX-3. Given that eGFR remained unchanged in SHR, showing no evidence of impaired kidney function, but rather suggesting an enhanced autoregulatory capacity to insulate glomeruli from barotrauma (Bidani & Griffin, 2004). For this reason, it is unlikely that circulating PTX-3 was produced by renal epithelial cells.

As a consequence of hypertension, the heart adapts in order to neutralise the afterload by increasing the LV wall thickness (Lorell & Carabello, 2000). In our study, LV mass (absolute and normalised to body mass), LVPWTd, and RWT were greater in SHR compared to WKY, indicating presence of LVH. Variations in the degree and pattern of hypertrophy may lead to differential impacts on wall thickness and overall LV mass. Concentric hypertrophy, as indexed by increased wall thickness without proportional chamber dilation, might be more readily detected through echocardiographic parameters such as LVPWTd and RWT as compared to gravimetric assessment using organ masses. In concert with previous studies (Fouad-Tarazi & Liebson, 1987; Levick et al., 2010; Mokotedi et al., 2019; Reddy et al., 1996), the present data demonstrate that only captopril successfully prevented the development of concentric LVH in SHR. Despite its BP-lowering effect, hydralazine had limited beneficial effect on the development of concentric LVH in SHR. Evidence has demonstrated the differential effects of these anti-hypertensive therapies on the development of LVH in pressure overload (Fouad-

Tarazi & Liebson, 1987). The regression of LVH by captopril may be attributed to blockade of the intra-cardiac renin angiotensin system (Reddy et al., 1996), whereas the limited effect of hydralazine on concentric LVH may be attributed to activation of the sympathetic nervous system (Fouad-Tarazi & Liebson, 1987; Levick et al., 2010). The concomitant activation of the sympathetic nervous system by hydralazine may condition LVH regression, albeit with opposing trophic effects that preclude regression. Therefore, the use of anti-hypertensive drugs with differential LV hypertrophic effects may then assist in understanding the molecular pathways involved in the development of concentric LVH.

Amongst other molecular pathways, inflammation may play a key role in the development of concentric LVH (Adamo et al., 2020). PTX-3, a mediator with chemoattractant properties released during tissue injury and repair, has been shown to be involved in the development of concentric LVH in pressure overload (Chen, Zhuang, et al., 2021; Suzuki et al., 2013). However, the role of increased physiological concentration of PTX-3 on the development of LVH in hypertension still requires elucidation. Using the differential effects of anti-hypertensive therapies in the present study, circulating PTX-3 concentration was associated only with relative wall thickness and not with any other indices of concentric LVH. However, this association disappeared after adjusting for the confounding effect of SBP, suggesting that circulating PTX-3 may not play a direct role in the development of LVH beyond its relationship with blood pressure. In this way, SBP appears to be a stronger determinant of LVH than PTX-3, indicating that the hypertrophic changes are more likely driven by the effects of elevated blood pressure rather than a direct effect of PTX-3. The absence of significant changes in systolic wall stress suggests that the hypertrophic response to haemodynamic pressure overload in SHR compensated sufficiently to prevent excessive wall stress. Further, systolic wall stress lacked associations with circulating concentration of PTX-3, indicating that PTX-3 did not modulate mechanical adaptation to pressure overload.

Some evidence shows that localised rather than systemic inflammation may contribute to the development of concentric LVH in SHR (Li et al., 2008). However, LV cardiac-specific *PTX-3* gene expression was not increased in SHR. The present study was performed when LVH was already established. Therefore, the present data do not unequivocally indicate that circulating or tissue PTX-3 was not involved prior to this stage in SHR as cardiac fibroblasts may be already activated in this advanced hypertensive state. However, the observation that captopril, an anti-hypertensive agent that decreases BP and ameliorates detrimental molecular pathways associated with hypertrophic remodelling in the myocardium, did not alter *PTX-3* gene expression, suggests that PTX-3 may not play a significant role in this context.

2.5 Limitations

The current study had limitations to consider. Although circulating plasma levels of PTX-3 associated with SBP, causality could not be ascertained. While there was no change in the relative mRNA expression of *PTX-3* in SHRs, which was not impacted by anti-hypertensive treatment with either captopril or hydralazine, we did not evaluate PTX-3 protein expression within heart tissue. It is plausible that diastolic function may be impaired. However, tissue and pulsed doppler imaging were not determined. Beyond eGFR, the present study may also benefit from extensive characterisation of renal structure from histological assessment to delineate a potential mechanism behind the differences in circulating PTX-3. Lastly, because the development of concentric LVH may be sexually dimorphic in SHR, future investigations using both sexes are warranted to further elucidate the functional role of PTX-3 in the development of concentric LVH.

2.6 Conclusion

Our study highlights the involvement of PTX-3 in the development of hypertension but not in the development of LVH using the differential effects of captopril and hydralazine in SHR.

Specifically, the administration of captopril reduced systolic BP, circulating VCAM-1 and PTX-3 levels, as well as effectively prevented the development of concentric LVH. While hydralazine similarly decreased systolic BP and improved circulating PTX-3 levels, it did not demonstrate any beneficial effects on the hypertrophic response. Consequently, circulating PTX-3 concentration was positively associated with SBP but not independently associated with indices of LVH. The lack of involvement of PTX-3 is confirmed with the similar LV relative mRNA expression of PTX-3 between the groups despite the different phenotype related to the development of LVH. The dissociation between circulating levels of PTX-3 and indices of concentric LVH poses significant clinical implications. Firstly, it challenges the conventional view of PTX-3 as a biomarker directly associated with the development or progression of LVH, particularly in hypertensive individuals. Secondly, it underscores the multifactorial nature of LVH pathogenesis, which highlights the need for a more comprehensive understanding of the underlying mechanisms involved. Lastly, this suggests that PTX-3 may not be the sole determinant of LVH in hypertensive patients and warrants further investigation into alternative biomarkers or pathways involved in the development of concentric LVH. Further investigations are warranted to elucidate the precise role of PTX-3 in mediating adverse cardiac remodelling under conditions of pressure overload. Such future studies may provide valuable insights into the mechanistic pathways involved and aid in the development of novel therapeutic strategies aimed at mitigating hypertensive cardiac complications to broaden our understanding of the inflammatory pathways involved.

Chapter 3

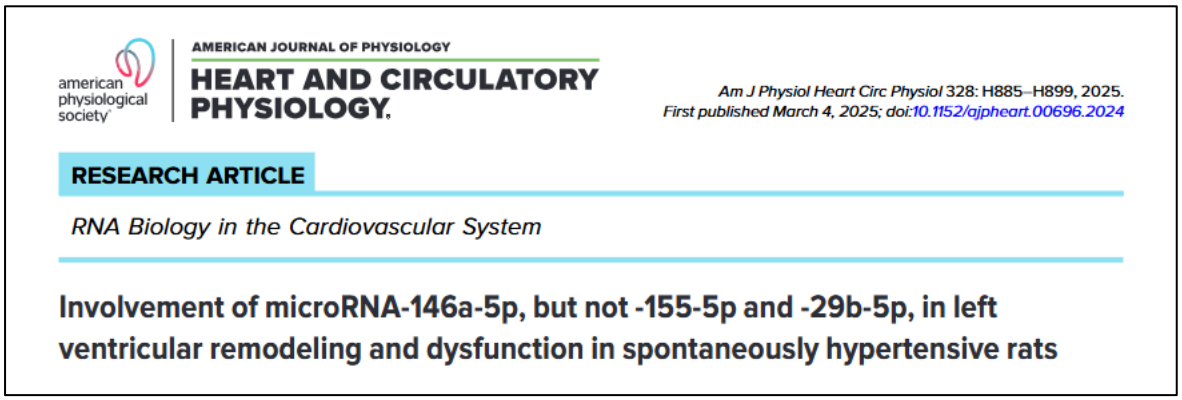

The work presented in this chapter has been published in the journal "**American Journal of Physiology – Heart and Circulatory Physiology**"

Mkhize, S. A., Gunter, S., Manilall, A., Mokotedi, L., Mosoma, K. L., Nthlane, R., Millen, A. M. E., & Michel, F. S. (2025). Involvement of microRNA-146a-5p, but not -155-5p and -29b-5p, in left ventricular remodeling and dysfunction in spontaneously hypertensive rats. *American journal of physiology. Heart and circulatory physiology*, *328*(4), H885–H899. https://doi.org/10.1152/ajpheart.00696.2024

Involvement of microRNA-146a-5p, but not -155-5p and -29b-5p, in cardiac remodelling and dysfunction in spontaneously hypertensive rats

Authors: Siluleko A Mkhize[1], Sulé Gunter[1,2], Ashmeetha Manilall[1], Lebogang Mokotedi[1,3], Kgotso L Mosoma[1], Aletta AM Millen[1], Refentshe Nthlane[1], and Frederic S Michel[1]

Affiliations: [1]Integrated Molecular Physiology Research Initiative, Department of Physiology, School of Biomedical Sciences, Faculty of Health Sciences, University of the Witwatersrand, 7 York Road, Parktown, 2193 Johannesburg, South Africa

[2]Department of Health Sciences and Medicine, Bond University, Gold Coast, Queensland, Australia

[3]Department of Physiology, School of Medicine, Sefako Makgatho Health Sciences University

Running title: MicroRNAs in hypertensive cardiac dysfunction

Corresponding author: Siluleko A Mkhize, University of the Witwatersrand, 7 York Road, Parktown, 2193 Johannesburg, South Africa. Tel: (+27) 717 2483; Email: siluleko.mkhize@wits.ac.za

Keywords: MicroRNAs, hypertension, cardiac dysfunction, fibrosis, inflammation

Abstract

Background: The contribution of microRNAs remain poorly understood in the context of hypertensive cardiac pathology. **Aim:** The role of miR-146a-5p, miR-155-5p, and miR-29b-5p in the development of cardiac hypertrophy and dysfunction was investigated in spontaneously hypertensive rats (SHR). **Methods:** Seven-month-old SHR (n=7 male, n=9 female), and normotensive Wistar Kyoto rats (WKY, n=7 male, n=9 female) underwent echocardiography. Plasma concentrations of inflammatory markers were measured by ELISA. Interstitial and perivascular collagen content was determined from sirius red-stained left ventricular (LV) tissue sections. Percentage macrophage infiltration was determined from H&E-stained LV tissue sections. LV tissue mRNA expressions of markers of cardiac remodelling and miRNA expressions were determined by RT-PCR. **Results:** LV posterior wall thickness in diastole (LVPWTd), RWT, E/e', perivascular and myocardial fibrosis, percent myocardial macrophages, circulating vascular cell adhesion molecule 1 (VCAM-1) concentration, and LV mRNA expression of *NFKBIA* and *SOD2* were greater in SHR. Midwall fractional shortening (MidFS), e', and a' were lower in SHR. LV mRNA expression of lysyl oxidase 1 (*LOX1)*, collagen type I to type III (*Col1a/Col3a)* ratio, and plasma circulating c-reactive protein (CRP), interleukin-6 (IL-6), and tumour necrosis factor alpha (TNF-α) were greater in females compared to males. No difference in miR-29b-5p expressionwas noted between the groups. MiR-155-5p expression was lower in female rats and was associated with absolute heart, and LV masses, and stroke volume. MiR-146a-5p expression was greater in SHR and associated with BP, circulating concentrations of VCAM-1, macrophage infiltration, myocardial fibrosis, normalised heart and LV masses, LV internal diameter in diastole (LVIDd), posterior wall thickness in diastole (PWTd), relative wall thickness (RWT), and late diastolic tissue lengthening velocity (a'). MiR-146a-5p was also independently associated with circulating VCAM-1 after adjustments for sysolic blood pressure (SBP). In addition, greater expression of

cardiac miRNA-146a annhiles the relationship between circulating VCAM-1 and macrophage infiltration. **Conclusion:** Changes in expression of miR-155-5p may be involved with a cardiac phenotype related to sexual dimorphism. Conversely, upregulation of miR-146a-5p expression may act as a counter-mechanism induced by myocardial inflammation in the setting of reactive fibrosis, established LV hypertrophy and impaired diastolic function.

New and noteworthy

We investigated the roles of microRNAs-146a-5p, -155-5p, and -29b-5p in the development of cardiac hypertrophy and dysfunction in SHRs. We showed that miR-146a-5p expression is upregulated in SHR and positively associated with indices of concentric LVH and diastolic dysfunction, potentially as a counter-mechanism in response to myocardial inflammation; whereas miR-155-5p is expressed in a manner consistent with sexual dimorphism. Our data may offer novel insights on the involvement of miRNAs in myocardial inflammation in hypertension-induced cardiac hypertrophy and dysfunction.

MiR-146a-5p as a counter-mechanism in endothelial activation and monocyte infiltration in hypertensive rats

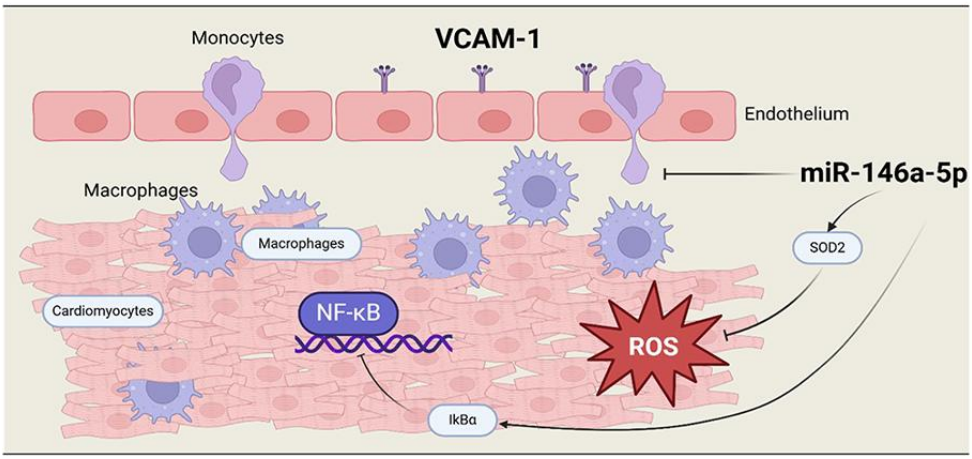

Upregulation of miR-146a-5p, as a potential counter-mechanism, may suppress inflammatory responses and oxidative stress via increased expression of the negative regulator of NF-κB signaling (IκBα) and SOD2 (superoxide dismutase 2)

AMERICAN JOURNAL OF PHYSIOLOGY
HEART AND CIRCULATORY PHYSIOLOGY. © 2025
american physiological society

3.1 Introduction

The mechanims involved in hypertension-induced cardiac remodelling and the associated dysfunctions remain an important area of research (Tomek & Bub, 2017). The progression from hypertension to heart failure is driven by multiple pathological mechanisms, resulting in marked phenotypic heterogeneity (Pfeffer et al., 2023). Nevertheless, it is well accepted that an increased afterload results in left ventricular hypertrophy (LVH), which is independently associated with the development of heart failure (Drazner, Rame, Marino, et al., 2004). In light with phenotypic heterogeneity, sex-differences have been observed in the development, progression, and manifestation of hypertension-induced heart failure (Reckelhoff, 2001; Tipton et al., 2014; Weinberg et al., 1999). In this regard, heart failure with preserved ejection fraction is more prevalent in women (Douglas et al., 1998; Lang et al., 2015; Pfeffer et al., 2023), whereas heart failure with reduced ejection fraction is more common in men (Lang et al., 2015). This sexual dimorphism extends beyond anatomical variances and encompasses diverse physiological, hormonal, and genetic factors that influence cardiac function and pathology (Reckelhoff et al., 1998; Reckelhoff et al., 2000; Reckelhoff et al., 1999). Although the underlying mechanisms have been described in the literature, less is known about the upstream translational regulation of genes involved in the molecular pathways that govern the phenotypic expression of cardiac remodelling and dysfunction.

Recent work points to the unique contribution of non-coding RNAs (ncRNAs) (Kenta Hirai et al., 2020; Sanchis-Gomar et al., 2021; Szczerba et al., 2020). Of the ncRNAs, microRNAs (miRNAs) have received particular attention, due to their involvement in various pathophysiological conditions. In fact, the 2024 Nobel Prize in Physiology or Medicine, awarded jointly to Victor Ambros and Gary Ruvkun, highlights the critical role of miRNAs in post-transcriptional gene regulation. MiRNAs are small ncRNAs, ~22 nucleotides long, that post-transcriptionally regulate gene and protein expression by binding to the 3' untranslated

region (UTR) of target mRNA, thereby modulating its translation (Taubel et al., 2021). In this regard, dysregulated miRNA expression patterns have been associated with various pathophysiological mechanisms in cardiac remodelling and dysfunction (Kaneko et al., 2017), including myocardial fibrosis (García et al., 2020) and inflammation (An et al., 2018; Heggermont et al., 2017).

In rodent models of of impaired cardiac function, miRNAs have been shown to regulate genes that modulate the development of concentric LVH and myocardial dysfunction (Szczerba et al., 2020). The aberrant expression of miRNAs has been linked to the development of concentric LVH (Oh et al., 2018; Silva & da Costa Martins, 2022; Thum et al., 2008; Zhang et al., 2014). In particular, miR-146a-5p (Oh et al., 2018), miR-29b-5p (Zhang et al., 2014), and miR-155-5p (Seok et al., 2014) may play a role in regulating gene expression, influencing the development of concentric LVH and myocardial dysfunction. Specifically, miR-146a-5p was upregulated after transverse aortic constriction (TAC) or angiotensin-II administration in combination with isoproterenol (Heggermont et al., 2017). In patients with aortic stenosis, miR-146a-5p was significantly upregulated and positively associated with increased LV wall thickness, an index of LVH (Heggermont et al., 2017).

In male mice subjected to TAC, miR-29b-5p was downregulated (García et al., 2020) but upregulated in female mice. In streptozotocin-induced diabetic cardiomyopathy, miR-146a-5p was also downregulated (Feng et al., 2017), with no indications of sexually dimorphic features. Conversely, miR-29-5p was upregulated in female rats after pressure overload, suggesting that miRNAs may have sex-specific effects on cardiac function (García et al., 2020). Studies have indicated that miR-155-5p may be upregulated in females with inflammatory conditions (Hu et al., 2022), whereas miR-146a-5p, which plays a role in inflammation and immune response, could also exhibit sex differences in its regulation (Gilyazova et al., 2023). However, these findings are context-dependent and seem to vary across tissues and disease states.

Taken together, these findings indicate that miR-146a-5p, miR-29b-5p, and miR-155-5p may be key regulators in cardiac remodelling and dysfunction. Yet, to the best of our knowledge, their contribution to hypertensive cardiac pathology remains poorly described. Spontaneously hypertensive rats (SHR) is a well-established genetic model that closely recapitulates the milieu associated with the development and consequences of human essential hypertension (Tipton et al., 2014). The SHR model may therefore be the most appropriate model to study the relative contribution of ncRNAs in adverse cardiac remodelling and dysfunction. To the best of our knowledge, the patterns of expression and relative contributions of miR-146a-5p, -155-5p, and -29b-5p remain unexplored in male and female SHR. We therefore investigated the patterns of expression and involvement of miR-146a-5p, -155-5p, and -29b-5p in male and female SHR with established concentric LVH.

3.2 Methods

3.2.1 Animals and housing

We obtained approval from the Animal Ethics Screening Committee of the University of the Witwatersrand, Johannesburg, South Africa (**Clearance number: 2021/03/03C**), and adhered to the National Institutes of Health Guide for the Care and Use of Laboratory Animals, as well as the Animal Research: Reporting of *In vivo* Experiments (ARRIVE) guidelines (Percie du Sert, Ahluwalia, et al., 2020). Animals were housed individually in controlled ambient temperature conditions with a 12-hour light-dark cycle, and provided *ad libitum* access to drinking water, and standard laboratory animal chow (Labchef, Johannesburg, South Africa). Coloured balls and tunnels were provided for environmental enrichment.

3.2.2 Study design

Seven-month-old spontaneously hypertensive rats (SHR, n=7 male, n=9 female, RRID: RGD_10043828), and normotensive Wistar-Kyoto rats (WKY, n=7 male and n=9 female, RRID: RGD_61119) were obtained from and housed at the Wits Research Animal Facility (WRAF). Both sexes were used in the present study because evidence of a sexual dimorphism in arterial blood pressure and adverse cardiovascular outcomes have been shown in SHR (Al-Gburi et al., 2017; Reckelhoff, 2001; Reckelhoff et al., 1998; Reckelhoff et al., 2000; Reckelhoff et al., 1999); however, we did not evaluate the oestrous cycle in female rats. For a period of two weeks, the rats were acclimatised to handling and the housing environment. Sample size estimation was determined based on previous studies (Al-Gburi et al., 2017; Reckelhoff, 2001; Reckelhoff et al., 1998; Reckelhoff et al., 2000; Reckelhoff et al., 1999). In brief, an *a priori* sample size calculation using a two-way Analysis of Variance, with an alpha of 0.05 and 80% power, indicated that a total of 32 rats (n=7-9 per group) would be adequate to detect statistical differences in this model (G*Power, version 3.1.9.2).

3.2.3 Non-invasive blood pressure measurement

Prior to termination, BP was measured in all rats. In brief, the tail-cuff technique was employed using non-invasive BP (NIBP) amplifiers (Biopac Systems Inc, Santa Barbara, USA, RRID:SCR_014829). To obtain BP readings, conscious rats were placed in a restrainer with the tail lassoed with a BP cuff and placed on a thermostatic blanket (adjusted to 37 °C) according to a previously described protocol (Mokotedi et al., 2020). Rats were habituated before the first measurement to enable them to adapt to the restrainer and BP measurement protocol. Measurements were taken at midday to avoid diurnal variations in BP.

3.2.4 Transthoracic echocardiography

Rats were anaesthetised with isoflurane (5% for induction, and thereafter maintained at 1–2.5% concentration via 100% O_2 mask inhalation). Under anaesthesia, echocardiography was performed using a non-invasive high-resolution (paediatric-10MHz) ultrasound probe connected to an echocardiogram (Siemens, Acuson SC2000, Diagnostic ultrasound system; Siemens Medical Solutions, USA, Inc.). In the parasternal long-axis view of the LV, LV dimensions, including LV internal diameter in systole (LVIDs), left ventricular internal diameter in diastole (LVIDd), interventricular septal thickness in systole (IVSTs), interventricular septal thickness in diastole (IVSTd), LV posterior wall thickness in systole (LVPWTs), and LV posterior wall thickness in diastole (LVPWTd), were measured from M-Mode echocardiography. Indices of LV systolic function were derived from the LV dimensions. Stroke volume was calculated using Teichholz method (Lang et al., 2015). Ejection fraction was computed as EF = [(LVEDV – LVESV) / LVEDV] × 100, where LVEDV and LVESV are the LV end diastolic volume and LV end systolic volume, respectively. Endocardial fractional shortening (endFS) was computed as endFS = (LVIDd – LVIDs) / LVIDd × 100. Midwall fractional shortening (midFS) was determined as midFS = [(LVIDd + PWTd) – (LVIDs +

PWTs)] / [(LVIDd + PWTd)] x 100. LV relative wall thickness (RWT) was calculated as RWT = (2xPWTd) / LVIDd (Lang et al., 2015).

LV diastolic function was evaluated via pulsed doppler imaging to ascertain mitral valve inflow patterns. In brief, in the apical 4-chamber view, early (E) and late (A) diastolic inflow velocities were recorded with the sample volume positioned at the tip of the mitral valve leaflet, and the E, A, and E/A ratio was calculated as indices of relaxation. Tissue doppler imaging (TDI) was used to assess peak myocardial tissue lengthening velocities during early (e') and late (a') diastole recorded at the level of the lateral mitral annulus in the apical four-chamber view. Data are expressed as e', an index of myocardial relaxation, e'/a', an index of myocardial stiffness, and E/e' representing LV filling pressure (Mokotedi et al., 2020).

Echocardiographic assessment was conducted by a trained sonographer who was blinded to the experimental groups. All assessments were conducted in accordance with the American Society of Echocardiography guidelines (Sahn et al., 1978).

3.2.5 Blood and tissue sampling

After echocardiography, a thoracotomy was performed, and rats were exsanguinated via cardiac puncture. Blood was collected into sterile EDTA tubes for plasma, centrifuged, and stored at -80°C for subsequent analysis. The organs were excised and weighed. LV tissue was divided and either preserved in 10% buffered formalin for histological analysis or in RNAlater® (Ambion, Sigma Aldrich, Germany), an RNA stabilising reagent, to ensure RNA integrity in post-mortem tissue samples for reliable gene expression analysis.

3.2.6 Circulating plasma levels of inflammatory markers

A cassette of plasma concentrations of the inflammatory markers including c-reactive protein (CRP), tumour necrosis factor-alpha (TNF-α), interleukin-6 (IL-6), and vascular cell adhesion molecule-1 (VCAM-1) were determined using commercially available solid phase sandwich

enzyme-linked immunosorbent assay (ELISA) kits (Elab Science Biotechnologies, Co Ltd, Wuhan, China). Each sample was run in duplicate, with TNF-α, IL-6, CRP, and VCAM-1 exhibiting lower detection limits of 78.13 pg/ml, 62.50 pg/ml, 0.31 ng/ml, and 12.5 pg/ml, respectively. All measurements had coefficients of variation <10%.

3.2.7 Myocardial macrophage infiltration

LV tissue samples that were preserved in 10% buffered formalin underwent standard procedures for embedding in paraffin. Thin (5µm) sections were prepared from the embedded tissues using a microtome, then subjected to deparaffinisation and rehydration (Mokotedi et al., 2020). Thereafter, the tissue sections were stained with haematoxylin and eosin (H&E) to visualise nuclei and cytoplasm, respectively. Following staining, the slides were rinsed in acidified water, dehydrated, and mounted using digital picture exchange (DPX) mounting medium. Examination of the tissue sections was performed using a Zeiss Axioscope 2 Plus microscope equipped with a Zeiss AxioCam (Zeiss, Peabody, MA, USA, RRID:SCR_023747). Macrophages were identified based on their distinct morphology, including round to oval shapes, abundant eosinophilic cytoplasm, and large, eccentrically placed nuclei.

3.2.8 Perivascular and myocardial collagen content

LV tissue sections were stained using a 0.1% sirius red solution dissolved in a saturated picric acid solution for 60 minutes at ambient temperature. Following staining, the slides were rinsed in acidified water, dehydrated, and mounted using digital picture exchange (DPX) mounting medium. Examination of the tissue sections was performed using a Zeiss Axioscope 2 Plus microscope equipped with a Zeiss AxioCam (Zeiss, Peabody, MA, USA, RRID:SCR_023747). The sections were visualised under bright-field using a 10x objective lens. Utilising ImageJ software (RRID:SCR_003070), myocardial collagen fraction area was determined for each tissue section by dividing the area occupied by collagen by the total tissue area (Mokotedi et

al., 2020). Perivascular collagen content of the coronary vessels was quantified as the total area stained with sirius red, and expressed as a percentage of the total tissue section.

3.2.9 Total RNA isolation

Total RNA was extracted from LV tissue using an Illustra™ RNAspin Mini Isolation kit (GE Healthcare, Buckinghamshire) according to manufacturer's instructions. The quality and quantity of RNA was confirmed using a Nanodrop OneC spectrophotometer (Thermo Fisher Scientific, Waltham, USA). The RNA was then reverse-transcribed using SuperScript™ IV VILO™ cDNA Synthesis Master Mix (Thermo Fisher Scientific, Waltham, USA). The quality and quantity (>1000ng/µL) of cDNA was again confirmed using a Nanodrop OneC spectrophotometer (Thermo Fisher Scientific, Waltham, USA). The cDNA products were stored at -20°C for further analyses.

3.2.10 Expression of target genes

Comparative gene expression RT-PCR was performed using the cDNA (~2 µg), pre-designed Taqman probe mixes for the reference gene hypoxanthine guanine phosphoribosyl transferase (*HPRT1*, 0.25 µl, Taqman assay ID: Rn01527838_g1, Thermo Fisher Scientific, Life Technologies, Carlsbad, USA), the gene of interest (0.5 µl, Taqman gene expression assay) and Taqman Fast Advanced PCR master mix (5 µl) in a final volume of 10 µl. Comparative gene expression of *Col1a* mRNA, which codes for Collagen type-I (Taqman assay ID: Rn01463848_m1), *Col3a* mRNA, which codes for Collagen type-III (Taqman assay ID: Rn01437681_m1), *LOX1* mRNA, which codes for lysyl oxidase 1 (Taqman assay ID: Rn01463024_g1), *NFKBIA* mRNA, which codes for the nuclear factor of kappa light polypeptide gene enhancer in B-cells inhibitor alpha (commonly abbreviated as IκBα, Taqman assay ID: Rn01473657_g1), *IL-1β* mRNA, which codes for inteleukin-1β (Taqman assay ID: Rn00676333_g1), *PTX-3* mRNA, which codes for pentraxin-3 (Taqman assay ID: Rn01769850_m1), *RUNX-1* mRNA, which codes for runt related transcription factor 1

(Taqman assay ID: Rn01645281_m1), and *SOD2* mRNA, which codes for superoxide dismutase 2 (Taqman assay ID: Rn00690588_g1) were all determined in duplex reactions with the endogenous control probe *HPRT1*, in duplicated plates. The relative expression of each gene of interest was calculated using the $2^{-\Delta\Delta Ct}$ method (Livak & Schmittgen, 2001).

3.2.11 MicroRNA expression

The cDNA templates were used for microRNA expression analyses by comparative expression RT-PCR. Here, three (3) candidate endogenous control probes, including small nuclear RNA (SnU6, Taqman assay ID: 002299), miR-16-5p (Taqman assay ID: rno481312_miR), and miR-191-5p (Taqman assay ID: rno480971_miR), were tested across a subset of samples that represented all experimental groups (7 per group, n=28 in total). The most suitable endogenous control was selected using RefFinder (RRID:SCR_000472). MiR-191-5p proved to be expressed with the least variability across all samples and between experimental groups, with a distinguishably low standard deviation in cycle threshold values, and was therefore considered as the most reliable reference gene for the remaining microRNA analyses.

Thereafter, commercially available microRNA Taqman probes were used to analyse microRNA expression, including miR-29b-5p (Taqman assay ID: rno481033_miR), -146a-5p (Taqman assay ID: rno481451), and -155-5p (Taqman Assay ID: rno480953_miR). Each well of a 96-well plate comprised a total volume of 20µL consisting of 5 µL of cDNA template, 10 µL of Taqman Fast Advanced Master Mix (2X), 1 µL Taqman Advanced microRNA Assay (20X) (Thermo Fisher Scientific, Waltham, USA) and 4 µL of RNase-free water. Each sample was assayed in duplicate reactions. The reaction plate was loaded into the StepONE Plus real-time PCR instrument (Thermo Fisher Scientific, Waltham, USA). The $2^{-\Delta\Delta Ct}$ method was used to calculate the microRNA expression relative to the expression of the endogenous reference control, miR-191-5p (Taqman assay ID: rno480971_miR) (Livak & Schmittgen, 2001). The miRNAs selected for our study were based on the literature, where we identified candidates

that were previously implicated in cardiovascular processes relevant to our research. Thereafter, *in silico* analysis using TargetScan (http://www.targetscan.org/vert_80/) and MiRDB (http://www.mirdb.org/) were conducted to identify their putative targets. TargetScan and miRDB are computational tools that predict putative miRNA targets by identifying conserved 8mer, 7mer, and 6mer sites matching the seed regions of miRNAs.

3.2.12 Statistical analyses

Statistical analyses were performed using the STATA software, version 16.1 (STATA Institute Inc., College Station, TX, USA). Visualisations were performed using GraphPad Prism version 10.3.1 for Windows (GraphPad Prism, Massachusetts, USA, RRID:SCR_002798). Data are expressed as arithmetic mean ± standard deviation (SD). Group differences were determined by two-way analysis of variance (2-way ANOVA) test with strain (WKY vs SHR) and sex (male vs female) as the main effects. Following the 2-way ANOVA, Tukey's *post-hoc* tests were conducted to correct for multiple comparisons. Bivariate correlations were determined using Pearson's correlation analyses and presented as a volcano plot. For dimensionality reduction, a principal component analysis (PCA) was conducted using the FactoMineR and factoextra packages in RStudio using the R programming language (R Core Team, 2024) accessed via the R Foundation for Statistical Computing, Vienna, Austria (https://www.R-project.org/). First, the data were standardised (mean=0, SD=1) to ensure comparability across variables. The PCA produced eigenvalues and proportions of variance for 35 components. A scree plot was generated to visualise the eigenvalues, and the contribution of variables to the principal components was assessed. As a visual heuristic, the scree plot determined that the first two principal components captured most of the variance in the dataset using the elbow method. A biplot was constructed to ascertain whether there was significant clustering in the PCA scores when disaggregated by sex. A permutational multivariate analysis of variance (PERMANOVA) test utilising the Euclidean method was performed to categorically examine

whether there were significant sex-specific differences in the PCA scores using the vegan package.

In multivariable analyses, interaction terms were created to assess whether the relationship between VCAM-1 and macrophage infiltration was moderated by miR-146a-5p and SBP. Prior to the analysis, data was filtered to include only rows with non-missing and finite values for VCAM-1, miR-146a-5p, and SBP. Thereafter, a multivariable linear regression model with three-way interaction terms was run. The final model included the main effects of VCAM-1, miR-146a-5p, and SBP, along with their two-way interaction terms and a Wald chi-squared test was performed to compare the coefficients of the slopes. To visualise the interaction effects, a prediction dataset was generated using a grid of VCAM-1 values ranging from its observed minimum to maximum. MiR-146a-5p and SBP were each set at their mean, as well as one standard deviation above and below the mean, capturing low, medium, and high levels of these variables. Predicted macrophage infiltration values were obtained using the fitted model, and results visualised using an interaction plot. Statistical significance was considered at $P<0.05$.

3.3 Results

3.3.1 Systolic and diastolic blood pressure

Systolic BP (**Table 3.1**) was significantly higher in SHR compared to WKY ($P<0.0001$). A significant interaction ($P<0.0003$) was noted for diastolic BP (**Table 3.1**). Diastolic BP was significantly higher in female SHR compared to the other three experimental groups (all $P<0.0001$).

3.3.2 Body and organ masses

WKY were significantly heavier than SHR ($P<0.0001$, **Table 3.1**). Male rats were significantly heavier compared to their female counterparts ($P<0.0001$). The heart and LV mass of SHRs were significantly greater than that of normotensive WKY rats ($P=0.008$ and $P=0.001$, respectively). Additionally, the heart and LV mass of male rats were significantly greater compared to those of female rats ($P<0.0001$ for both). Similarly, the kidney and liver mass of WKY rats were significantly greater than those of SHRs ($P=0.016$ and $P=0.034$, respectively). The kidney and liver mass of male rats were significantly greater than those of female rats ($P<0.0001$ for both). When normalised to body mass, the heart and LV mass of female rats were significantly greater than those of male rats ($P<0.0001$ for both). The liver mass normalised to body mass was significantly greater in female compared male rats ($P=0.003$) and in SHR compared to WKY ($P<0.0001$). The kidney mass normalised to body mass was not different between the different experimental groups ($P>0.05$).

Table 3.1: Haemodynamic parameters, body and organ masses of male and female WKY and SHRs.

	Male		Female		P value		
	WKY (n=7)	**SHR (n=7)**	**WKY (n=9)**	**SHR (n=9)**	**Strain**	**Sex**	**Interaction**
Haemodynamic							
SBP (mmHg)	130 ± 4	171 ± 11	126 ± 6	171 ± 5	**<0.0001**	0.401	0.331
DBP (mmHg)	89 ± 3	95 ± 4	89 ± 3	107 ± 6$^{\#\#\#\dagger⁋}$	<0.0001	0.001	**0.0003**
Gravimetric							
Body mass (g)	389 ± 15	355 ± 28	240 ± 23	202 ± 11	**<0.0001**	**<0.0001**	0.788
Heart mass (g)	1.28 ± 0.08	1.48 ± 0.15$^{\$¥}$	0.94 ± 0.10***	0.95 ± 0.09$^{\#\#\#\$}$	0.008	<0.0001	**0.022**
Heart mass (g/100g)	0.33 ± 0.02	0.41 ± 0.03	0.39 ± 0.03	0.47 ± 0.04	**<0.0001**	**<0.0001**	0.794
LV mass (g)	0.85 ± 0.10	1.11 ± 0.17$^{\$¥}$	0.67 ± 0.08*	0.68 ± 0.07$^{\#\#\#\$}$	0.001	<0.0001	**0.003**
LV mass (g/100g)	0.22 ± 0.02	0.31 ± 0.03	0.28 ± 0.03	0.34 ± 0.03	**<0.0001**	**0.0002**	0.119
Kidney mass (g)	1.39 ± 0.09	1.32 ± 0.15	0.87 ± 0.08	0.78 ± 0.04	**0.016**	**<0.0001**	0.698
Kidney mass (g/100g)	0.36 ± 0.01	0.37 ± 0.04	0.36 ± 0.02	0.38 ± 0.03	0.071	0.323	0.777
Liver mass (g)	9.97 ± 0.52	11.2 ± 1.33	6.94 ± 0.56	7.29 ± 1.12	**0.034**	**<0.0001**	0.232
Liver mass (g/100g)	2.56 ± 0.17	3.15 ± 0.35	2.89 ± 0.19	3.60 ± 0.49	**<0.0001**	**0.003**	0.646

Abbreviations: WKY, Wistar Kyoto rats; SHR, spontaneously hypertensive rats; SBP, systolic blood pressure; and DBP, diastolic blood pressure

Data expressed as mean ± SD. Organ masses are normalised to body mass and expressed as g/100g. 2-way ANOVA with Tukey *post hoc* test

***P<0.0001 in WKY (male vs female), $^{\#\#\#}$P<0.0001 in SHR (male vs female), $^{\$}$P<0.05 vs WKY male, $^{¥}$P<0.05 vs WKY female, †P<0.0001 vs WKY male, and $^{⁋}$P<0.0001 vs WKY female

3.3.3 Left ventricular geometry, diastolic and systolic function

The LVIDs and LVPWTs were similar among all the groups (all P>0.05, **Table 3.2**). The LVIDd of SHR was significantly reduced compared to that of WKY (P=0.010). In addititon, female rats had smaller LVIDd compared to male rats (P=0.013). Female rats had smaller IVSTs and IVSTd compared to male rats (P=0.007 and P=0.027, respectively). The RWT of SHR was significantly greater compared to WKY (P=0.0002), and exhibited that female rats had greater RWT compared to male rats (P=0.043). Lastly, the LVPWTd of SHR was significantly greater compared to that of WKY (P=0.0003), but tended to be greater in female compared to male rats (P=0.078). The e'/a' and E/A ratios were similar among the groups (all P>0.05, **Table 3.2**). The e' and a' were significantly lower in SHR compared to WKY (P=0.003 and P=0.0002, respectively). The E, A, and E/e' ratio were significantly greater in SHR compared to WKY (P=0.045, P=0.034 and P=0.011, respectively). No significant sex effect was noted for all indices of LV diastolic function (all P>0.05). The endFS was similar among all the groups (all P>0.05, **Table 3.2**). The midFS was greater in WKY compared to SHR (P=0.011). Female rats exhibited lower midFS compared to male rats (P=0.004). Ejection fraction was similar between the groups (P>0.05). Stroke volume was decreased in SHR compared to WKY (P=0.003) and also decreased in female rats compared to their male counterparts (P=0.033).

Table 3.2: Echocardiographic parameters showing left ventricular geometry, diastolic, and systolic function in male and female normotensive WKY and SHR.

	Male		Female		P value		
	WKY (n=7)	**SHR (n=7)**	**WKY (n=9)**	**SHR (n=9)**	**Strain**	**Sex**	**Interaction**
LV geometry							
LVIDs (cm)	0.35 ± 0.09	0.35 ± 0.14	0.29 ± 0.06	0.31 ± 0.07	0.787	0.225	0.922
LVIDd (cm)	0.68 ± 0.06	0.62 ± 0.08	0.61 ± 0.05	0.53 ± 0.09	**0.010**	**0.013**	0.930
IVSTs (cm)	0.38 ± 0.09	0.37 ± 0.07	0.29 ± 0.04	0.30 ± 0.06	0.961	**0.007**	0.708
IVSTd (cm)	0.27 ± 0.08	0.31 ± 0.11	0.21 ± 0.01	0.24 ± 0.06	0.210	**0.027**	0.867
LVPWTs (cm)	0.28 ± 0.09	0.34 ± 0.06	0.31 ± 0.03	0.35 ± 0.06	0.056	0.381	0.566
LVPWTd (cm)	0.19 ± 0.04	0.31 ± 0.09	0.24 ± 0.07	0.35 ± 0.06	**0.0003**	0.078	0.727
RWT	0.55 ± 0.16	1.03 ± 0.26	0.83 ± 0.26	1.14 ± 0.23	**0.0002**	**0.043**	0.375
LV diastolic function							
e’ (cm/s)	4.33 ± 1.03	3.29 ± 0.76	4.50 ± 1.64	3.00 ± 0.67	**0.003**	0.879	0.566
a’ (cm/s)	8.33 ± 2.58	3.57 ± 1.13	6.00 ± 3.52	3.60 ± 1.17	**0.0002**	0.170	0.160
e’/a’	0.54 ± 0.11	0.97 ± 0.28	1.15 ± 0.99	0.90 ± 0.31	0.636	0.177	0.088
E (cm/s)	60 ± 19	155 ± 142	56 ± 26	107 ± 89	**0.045**	0.462	0.530
A (cm/s)	26 ± 9	64 ± 45	27 ± 24	53 ± 48	**0.034**	0.740	0.706
E/A	2.43 ± 0.80	2.48 ± 0.98	2.79 ± 1.16	2.15 ± 1.07	0.458	0.970	0.387
E/e’	14 ± 5	46 ± 36	13 ± 5	35 ± 29	**0.011**	0.524	0.599

LV systolic function							
Stroke volume (ml)	0.57 ± 0.19	0.36 ± 0.15	0.42 ± 0.12	0.26 ± 0.13	**0.003**	**0.033**	0.663
Ejection fraction (%)	78 ± 11	82 ± 4	79 ± 8	69 ± 11	0.396	0.101	0.071
endFS (%)	43 ± 12	45 ± 4	43 ± 9	34 ± 8	0.311	0.112	0.143
midFS (%)	29 ± 5	23 ± 3	22 ± 8	17 ± 3	**0.011**	**0.004**	0.743

Abbreviations: WKY, Wistar Kyoto rats; SHR, spontaneously hypertensive rats; LVIDs, left ventricular internal diameter in systole; LVIDd, left ventricular internal diameter in diastole; IVSTs, interventricular septal thickness in systole; IVSTd, interventricular septal thickness in diastole; LVPWTs, left ventricular posterior wall thickness in systole; LVPWTd, left ventricular posterior wall thickness in diastole; RWT, relative wall thickness; e', early peak tissue lengthening velocity at lateral mitral annulus; a', late peak tissue lengthening velocity at lateral mitral annulus; e'/a', early to late peak tissue lengthening velocity ratio; E, maximum early mitral inflow velocity; A, maximum late mitral inflow velocity; E/A, early to late diastolic filling velocity ratio, E/e', early diastolic mitral inflow to tissue lengthening velocity at lateral mitral annulus; endFS, endocardial fractional shortening; and midFS, midwall fractional shortening

Data expressed as mean ± SD

2-way ANOVA with Tukey *post hoc* test

3.3.4 LV tissue-specific expression of MicroRNAs

LV tissue miR-146a-5p expression was greater in SHR compared to WKY ($P<0.0001$) but similar between male and female rats ($P=0.805$, **Figure 3.1A**). Conversely, LV tissue miR-155-5p expression was lower in female rats compared to male rats ($P=0.012$) but similar between WKY compared to SHR ($P=0.899$, **Figure 3.1B**). Lastly, LV tissue miR-29b-5p expression was not different between all the experimental groups (all $P>0.05$, **Figure 3.1C**).

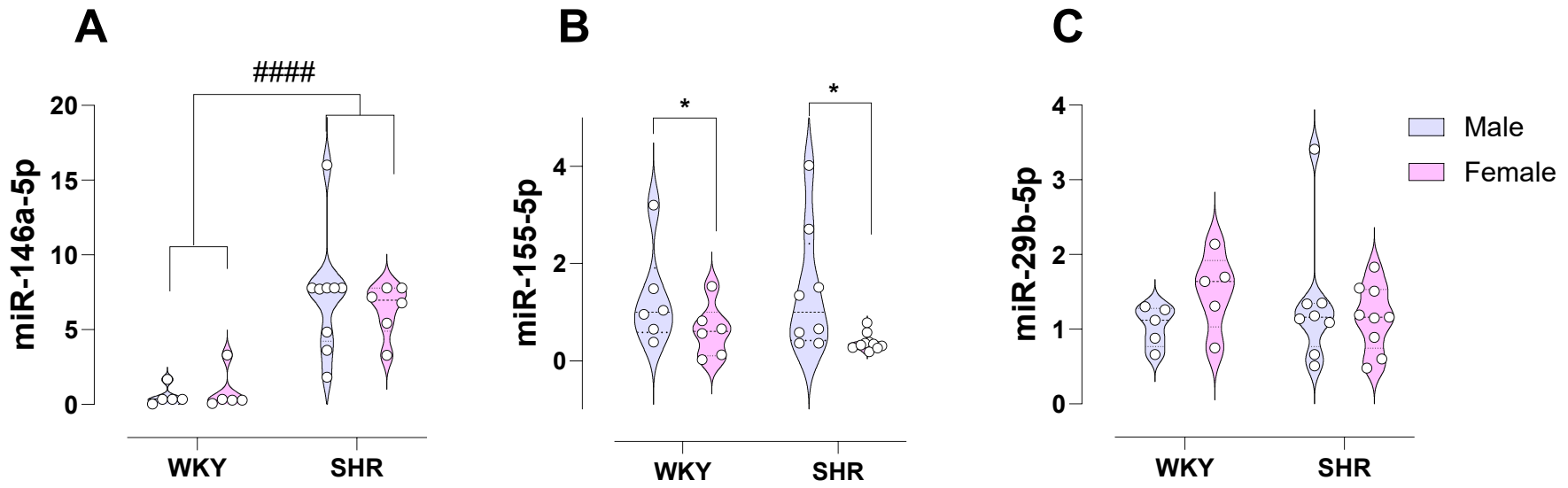

Figures 3.1A-C: A violin plot illustrating heart tissue-specific expression of MicroRNAs relative to miR-191-5p as endogenous control including miR-146a-5p (**A**), miR-155-5p (**B**), and miR-29b-5p (**C**).

2-way ANOVA with Tukey *post hoc* test

*P<0.05, and $^{\#\#\#\#}$P<0.0001

3.3.5 Circulating concentrations of inflammatory markers

The circulating concentration of CRP did not differ between WKY and SHR (P=0.559) but was greater in female compared to male rats (P=0.022, **Figure 3.2A**). The circulating concentrations of IL-6 (**Figure 3.2B**) and TNF-α (**Figure 3.2C**) were similar between WKY and SHR (P=0.599 and P=0.684, respectively) but were also greater in female compared to male rats (P=0.011 and P<0.0001, respectively). The circulating concentration of VCAM-1 was similar between male and female rats (P=0.082) but was greater in SHR compared to WKY (P<0.0001, **Figure 3.2D**).

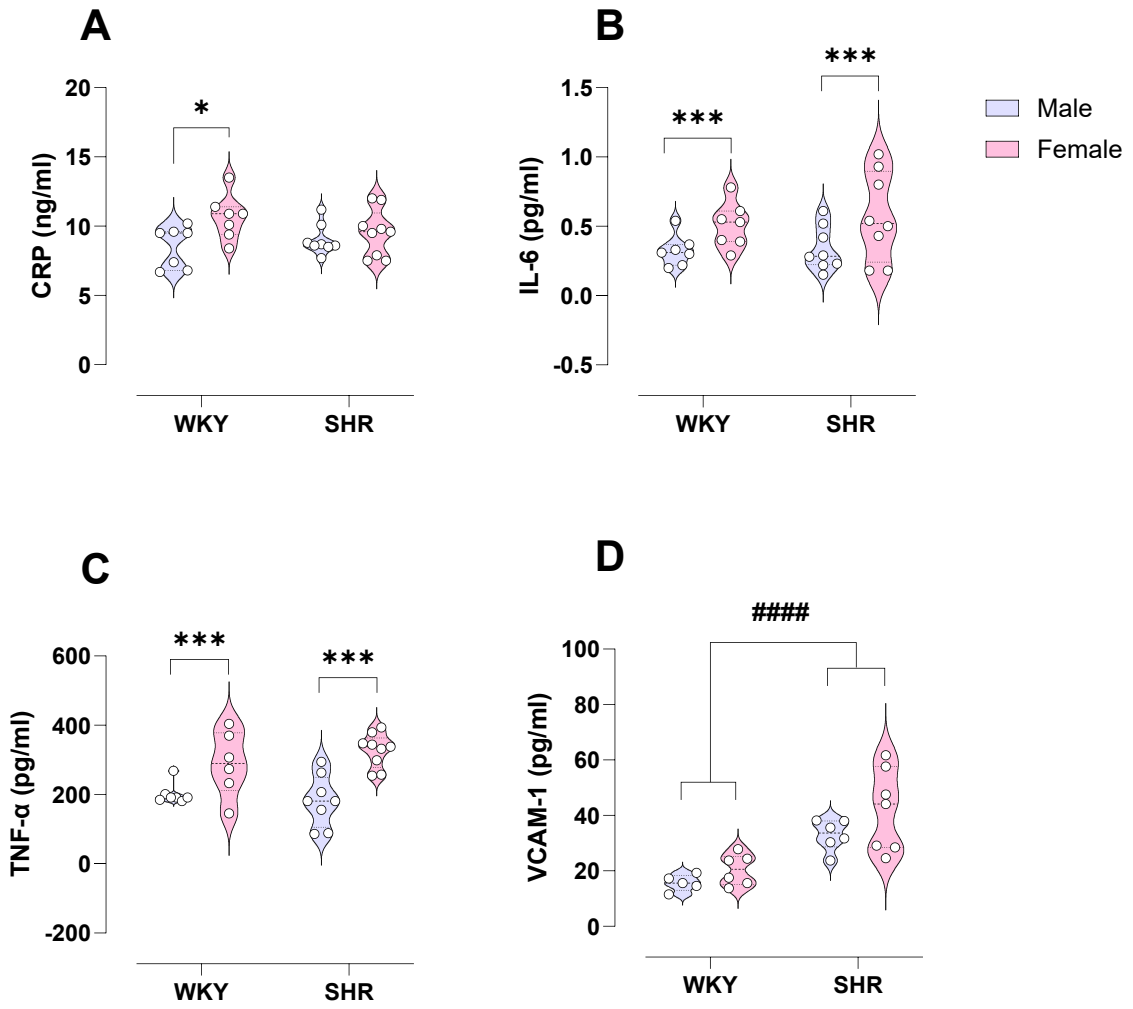

Figures 3.2A-D: Circulating concentrations of the pro-inflammatory markers C-reactive protein (CRP, **A**), interleukin-6 (IL-6, **B**), tumour necrosis factor-α (TNF-α**, C**), and vascular cell adhesion molecule-1 (VCAM-1, **D**) in male and female normotensive WKY and SHRs.

2-way ANOVA with Tukey *post hoc* test

*P<0.05, ***P<0.0001, and ####P<0.0001

3.3.6 Macrophage infiltration, perivascular and myocardial fibrosis in left ventricular tissue

Myocardial macrophage infiltration was greater in SHR compared to WKY ($P<0.0001$) but similar between male and female rats ($P=0.159$) (**Figure 3.3A**). Perivascular collagen deposition was also greater in SHR compared to WKY ($P<0.05$) but similar between male and female rats ($P=0.280$) (**Figure 3.3B**). Myocardial collagen content, expressed as a percentage of the total section was significantly greater in SHR compared to WKY ($P=0.016$) but similar between male and female rats ($P=0.659$) (**Figure 3.3C**).

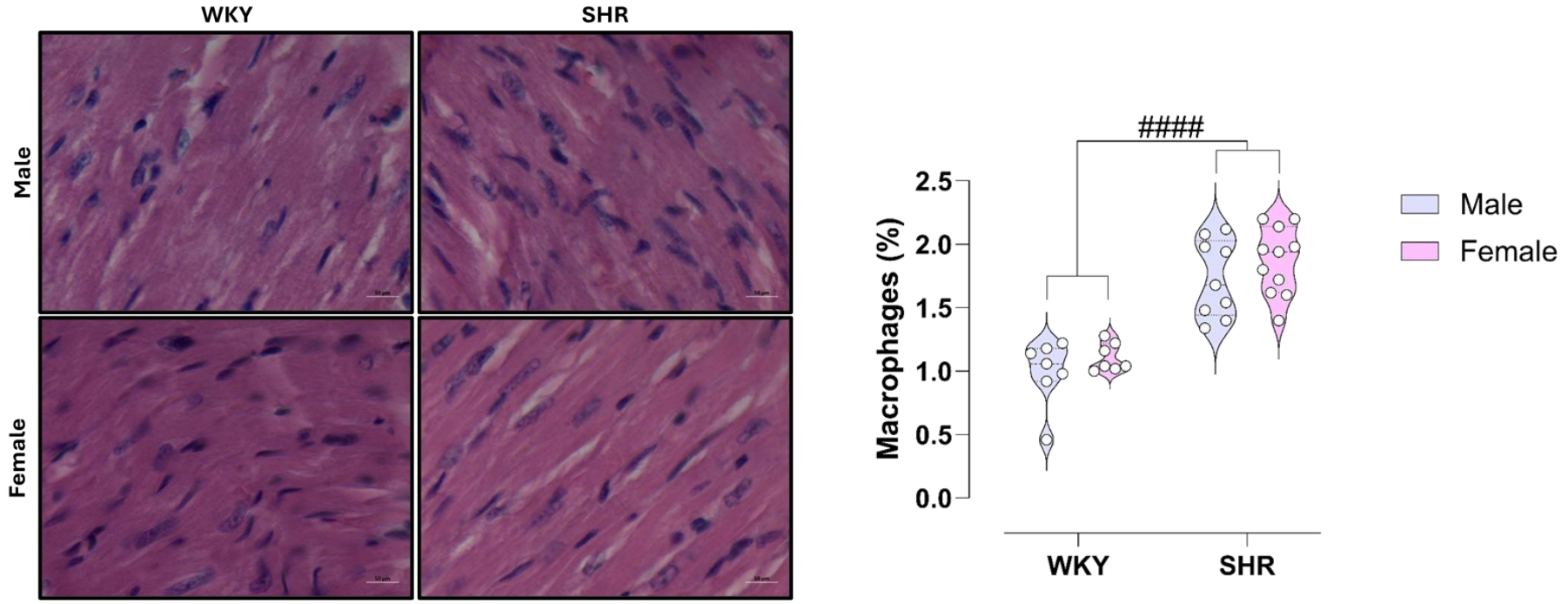

Figure 3.3A: Representative micrographs illustrating myocardial macrophage infiltration in H&E-stained left ventricular tissue sections from male and female WKYs and SHRs (scale bar = 50 μm).

2-way ANOVA with Tukey *post hoc* test

$^{\#\#\#\#}P<0.0001$

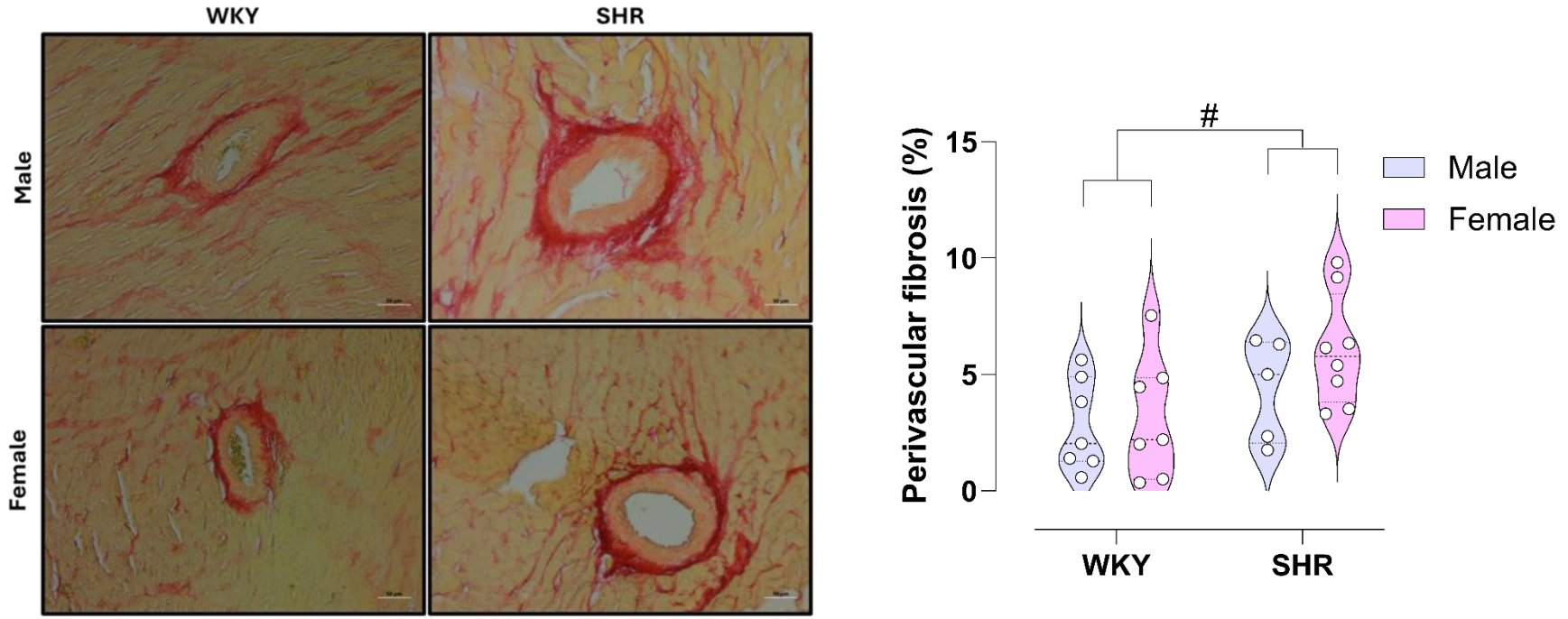

Figure 3.3B: Representative micrographs illustrating coronary perivascular fibrosis in sirius red-stained left ventricular tissue sections from male and female WKYs and SHRs (scale bar = 50 μm).

2-way ANOVA with Tukey *post hoc* test

$^{\#}P<0.05$

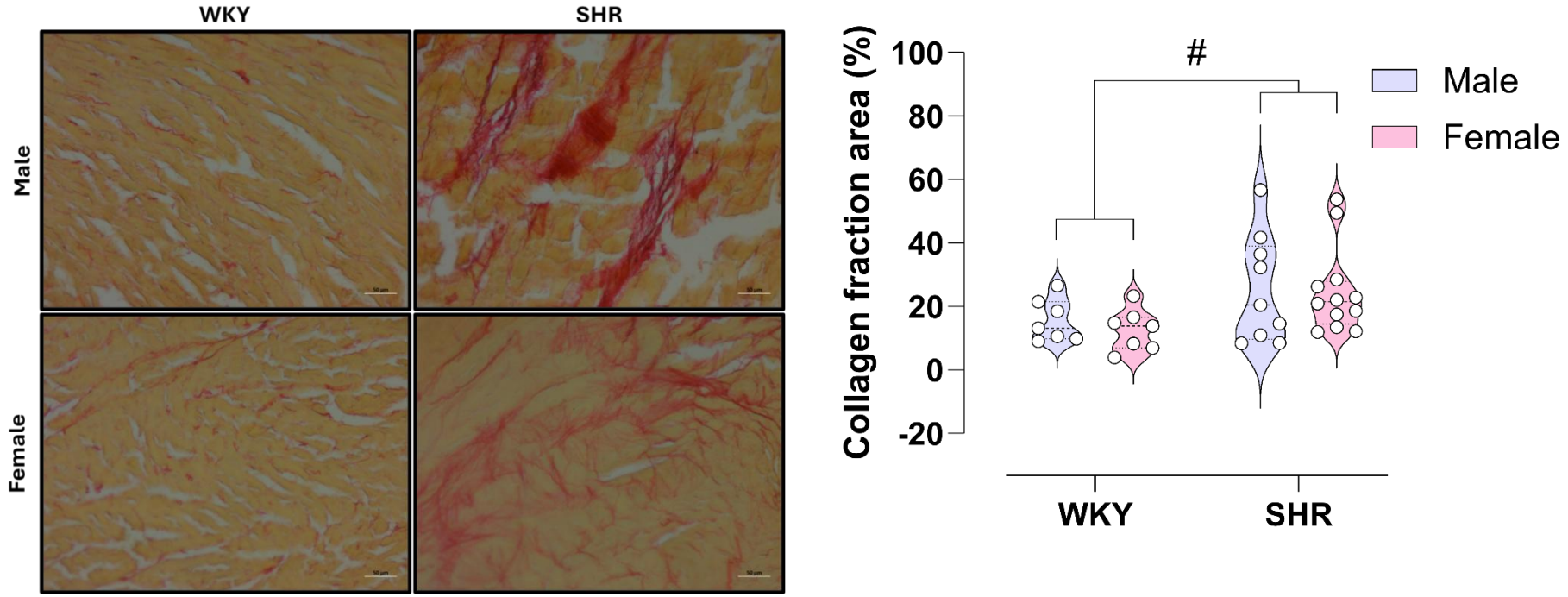

Figure 3.3C: Representative micrographs illustrating myocardial interstitial fibrosis in sirius red-stained left ventricular tissue sections from male and female WKYs and SHRs (scale bar = 50 µm).

2-way ANOVA with Tukey *post hoc* test

$^{\#}P<0.05$

3.3.7 Gene expression in left ventricular tissue

In the left ventricular tissue, gene expression levels were analysed across male and female WKY and SHR (**Table 3.3**). For *NFKBIA*, expression was higher in SHRs than WKYs (P=0.024), but no significant differences were observed for sex (P=0.634) or interaction effects (P=0.504). *IL-1β* showed no significant differences in strain (P=0.301), sex (P=0.849), or interaction (P=0.240). *PTX-3* expression was significantly higher in females compared to males (P=0.037) but showed no strain and interaction effects (P=0.484 and P=0.501, respectively). For fibrosis-related genes, *Col3a* showed no significant differences in strain (P=0.655), sex (P=0.941), or interaction (P=0.428). *Col1a* expression was significantly higher in females compared to males (P<0.0001), with no significant strain (P=0.235) or interaction (P=0.631) effects. Similarly, *Col1a/Col3a* ratio and *LOX1* were significantly higher in females than males (P=0.0094 and P=0.0006, respectively). *RUNX1*, related to apoptosis, was also significantly elevated in females (P=0.0002), with no significant strain (P=0.520) or interaction (P=0.893) effects. Finally, *SOD2*, related to oxidative stress, showed higher expression in SHRs compared to WKYs (P=0.001) but no significant differences by sex (P=0.628) or interaction (P=0.645).

Table 3.3: Gene expression in the left ventricular tissue of male and female WKYs and SHRs.

	Male		Female		P value		
	WKY (n=7)	**SHR (n=7)**	**WKY (n=9)**	**SHR (n=9)**	**Strain**	**Sex**	**Interaction**
Inflammation							
NFKBIA	1.04 ± 0.48	1.49 ± 0.49	1.07 ± 0.25	1.32 ± 0.41	**0.024**	0.634	0.504
IL-1β	1.37 ± 0.65	1.30 ± 0.29	0.88 ± 0.39	1.99 ± 2.31	0.301	0.849	0.240
PTX-3	1.43 ± 2.04	1.45 ± 1.52	2.39 ± 1.50	3.28 ± 1.94	0.484	**0.037**	0.501
Fibrosis							
Col1a	0.61 ± 0.69	0.91 ± 0.56	2.40 ± 1.68	3.10 ± 1.20	0.235	**<0.0001**	0.631
Col3a	1.04 ± 0.58	1.11 ± 0.43	1.18 ± 0.47	0.94 ± 0.40	0.655	0.941	0.428
Col1a/Col3a	1.04 ± 1.33	0.83 ± 0.62	2.07 ± 1.97	3.48 ± 2.12	0.365	**0.0094**	0.226
LOX1	0.63 ± 0.80	1.12 ± 0.90	2.62 ± 1.91	3.90 ± 2.21	0.159	**0.0006**	0.522
Apoptosis							
RUNX-1	0.59 ± 0.55	0.94 ± 0.64	3.48 ± 1.57	4.00 ± 2.64	0.520	**0.0002**	0.893
Oxidative stress							
SOD2	0.98 ± 0.09	1.16 ± 0.17	1.02 ± 0.06	1.16 ± 0.12	**0.001**	0.628	0.645

Abbreviations: WKY, Wistar Kyoto rats; SHR, spontaneously hypertensive rats; NFKBIA, nuclear factor of kappa light polypeptide gene enhancer in B-cells inhibitor alpha; IL-1β, interleukin-1β; PTX-3, pentaxin-3; Col1a, collagen type-I; Col3a, collagen type-III; LOX1, lysil oxidase 1; RUNX1, runt related transcription factor 1; and SOD2, superoxide dismutase 2

Data expressed as mean ± SD; 2-way ANOVA with Tukey *post hoc* test

3.3.8 Associations between microRNAs and haemodynamic, gravimetric, echocardiographic, and molecular parameters

Figure 3.4 shows a volcano plot depicting associations between the three microRNAs (miR-146a-5p, miR-155-5p, and miR-29b-5p) and cardiovascular parameters, gene expression in left ventricular tissue, and circulating concentrations of inflammatory markers. The x-axis displays the Pearson's correlation coefficients (r), while the y-axis shows the $-\log_{10}$(P-value). Points above the horizontal dashed line ($-\log_{10}$(p-value) =1.30, equivalent to P=0.05) indicate statistically significant correlations. Red markers highlight significant positive correlations, particularly involving miR-146a-5p (e.g., SBP, RWT, LVIDd, LVPWTd, VCAM-1, myocardial fibrosis, macrophage infiltration, and normalised liver mass, LV mass, and heart mass). Parameters associated with miR-155-5p (e.g., absolute LV mass, kidney mass, heart mass, and stroke volume) are also highlighted in red. The turquoise marker represents a significant negative correlation between miR-146a-5p and e' (cm/s). Although the expression of *NFKBIA* and *SOD2* were greater in SHR, their association with miR-146a-5p did not reach statistical significance (both P>0.05). In multivariable analyses, miR-146a-5p was persistently associated with circulating concentrations of VCAM-1 independent of the confounding effect of SBP; β [95% CI]: 0.468 [0.033 to 0.902], P=0.040.

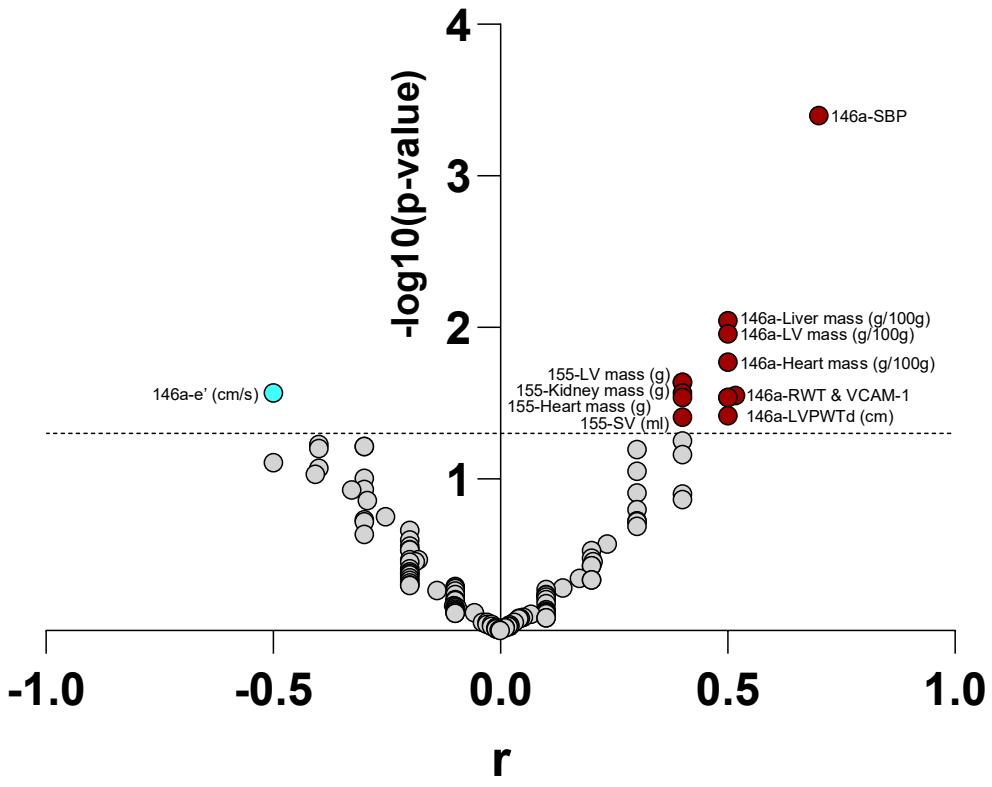

Figure 3.4: A volcano plot depicting associations between the three microRNAs (miR-146a-5p, miR-155-5p, and miR-29b-5p) and cardiovascular parameters, gene expression in left ventricular tissue, and circulating concentrations of inflammatory markers. The x-axis displays the Pearson's correlation coefficient (r), while the y-axis shows the -log10(p-value). Points above the horizontal dashed line (-log10(p-value) =1.30, equivalent to P=0.05) indicate statistically significant correlations. Red markers highlight significant positive correlations, particularly involving miR-146a-5p (e.g., SBP, RWT, LVPWTd, and normalised liver mass, LV mass, and heart mass). Parameters associated with miR-155-5p (e.g., absolute LV mass, kidney mass, heart mass, and SV) are also highlighted in red. The turquoise marker represents a significant negative correlation between miR-146a-5p and e' (cm/s).

3.3.9 Sexually dimorphic features

Figure 3.5A depicts the eigenvalue scree plot exhibiting principal components analysis (PCA). The first principal component (PC1) explains 25.7% of the total variance, indicating that it is the most important axis of variation in the dataset. The second principal component (PC2) explains 15.7% of the total variance. As such, including more components adds diminishing amounts of explained variance. For PC1, the most contributing variables include absolute kidney mass (4.67%), normalised heart mass (3.98%), and normalised left ventricular mass (3.24%). For PC2, important contributors include absolute heart (6.50%) and liver masses (7.12%). When disaggregated by sex, sample clustering was observed in the biplot (**Figure 3.5B)**, and a PERMANOVA test revealed highly significant sex-specific differences in PCA scores (Pillai's Trace=0.71596, $P<0.001$).

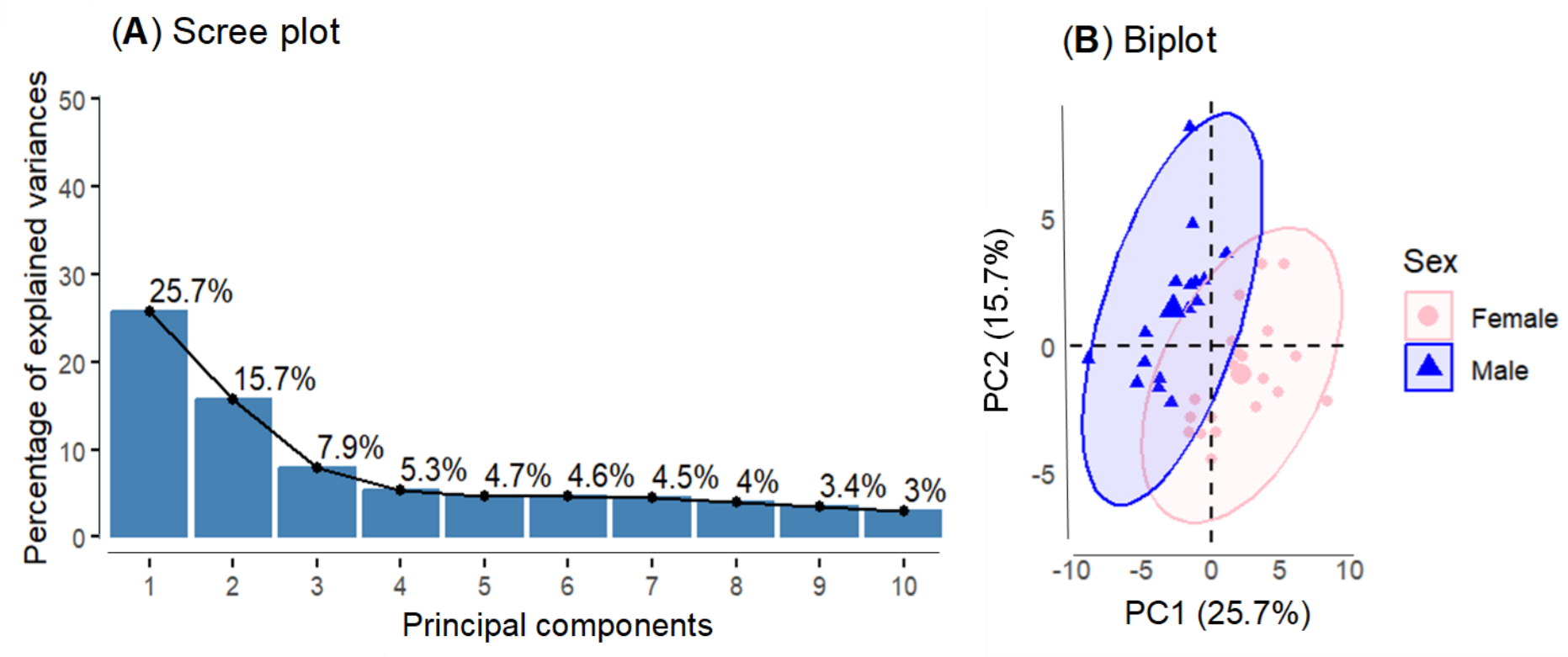

Figures 3.5A-5B: An eigenvalue scree plot (**A**) depicting principal component analysis (PCA). When disaggregated by sex, sample clustering was observed in the biplot (**B**), and a PERMANOVA test revealed highly significant sex-specific differences in PCA scores (Pillai's Trace = 0.71596, P<0.001). The ellipses (95% CI) represent the euclidean space within which the data points from each sex are expected to fall. Within each of the ellipses, the centroid reflects the mean location of sex in the euclidean space.

3.3.10 Moderation effects of miR-146a-5p and systolic blood pressure

The interaction plot (**Figure 3.6**) illustrates the relationship between circulating concentrations of VCAM-1 and myocardial macrophage infiltration, while considering the moderating effects of miR-146a-5p levels (coloured lines) and SBP levels (line types: solid, dashed, and dotted). The two-way interaction term between VCAM-1 and miR-146a-5p was highly significant (β=-0.0038, SE=0.0002, P<0.001), indicating a strong negative association with myocardial macrophage infiltration. In contrast, the two-way interaction term between VCAM-1 and SBP did not reach statistical significant (β=0.00001769, SE=0.0000204, P=0.386), indicating that the combined effect of VCAM-1 and SBP does not significantly influence macrophage infiltration. The Wald chi-squared test result with two degrees of freedom (^{2}=299.8, P<0.001) showed that the slopes of the interaction effects differ significantly from each other.

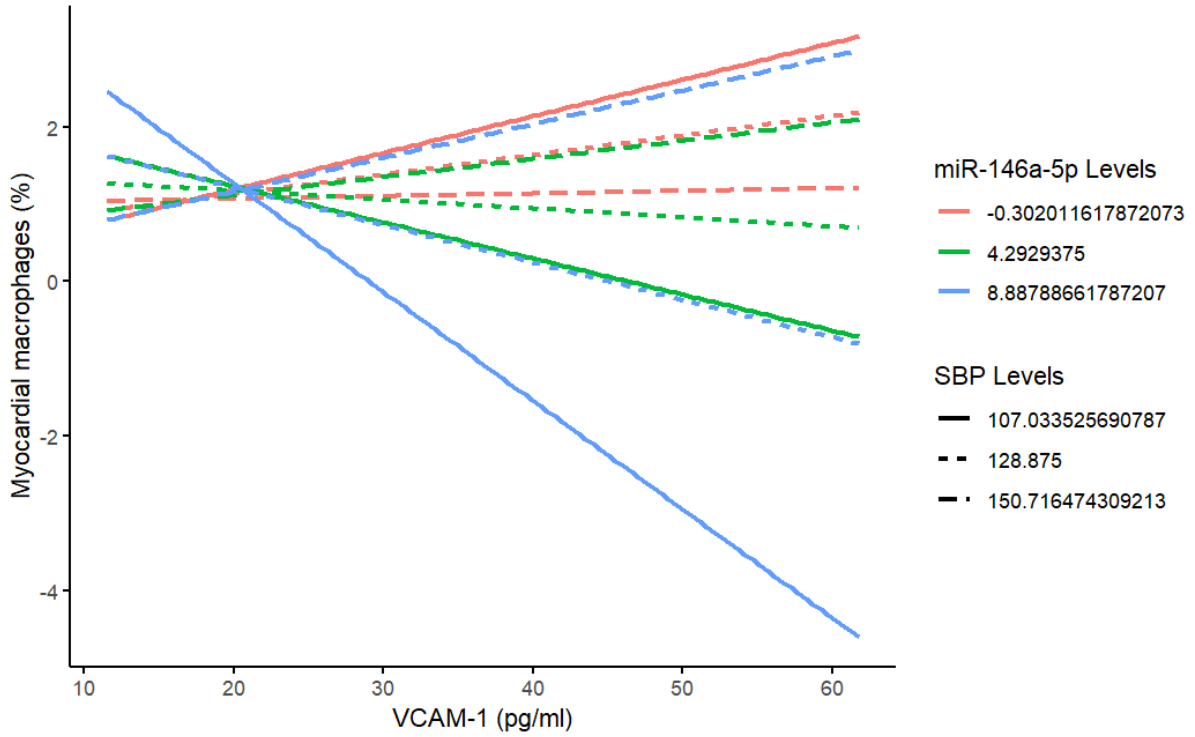

Figure 3.6: An interaction plot illustrating the relationship between circulating concentrations of VCAM-1 and percent myocardial macrophages, while considering the moderating effects of miR-146a-5p levels (coloured lines) and SBP levels (line types: solid, dashed, and dotted).

3.4 Discussion

In this study, we uncovered distinct patterns of miRNA regulation associated with hypertensive cardiac pathology in male and female SHR compared to normotensive WKY. Hypertensive rats had established concentric LVH, and impaired systolic and diastolic function as well as increased perivascular and interstitial cardiac fibrosis. In addition, hypertensive rats showed endothelial activation and vascular permeability indexed by the increased circulating concentrations of VCAM-1, transendothelial macrophage infiltration into cardiac tissue, and increased gene expression of the negative regulator of NF-κB signalling (*NFKBIA)* and oxidative stress (*SOD2)*. Female rats exhibited increased LV growth, increased relative mRNA expression of pro-fibrotic genes and a heightened pro-inflammatory state. We showed that cardiomyocyte expression of miR-146a-5p was upregulated in the hypertensive heart, while miR-155-5p expression was downregulated in female rats, irrespective of the strain. Cardiomycyte expression of miR-155-5p was positively associated with absolute heart, LV, kidney masses, and stroke volume. MiR-146a-5p was positively associated with circulating concentrations of VCAM-1 independently of increases in systolic blood pressure, and associated with indices of concentric LVH, diastolic function, and reactive fibrosis. In moderation analyses, increasing expression of miR-146a-5p appeared to reverse the relationship between VCAM-1 and macrophage infiltration, and the lack of a significant interaction effect between VCAM-1 and SBP suggests that VCAM-1 and SBP may not have a combined effect on macrophage infiltration. Our data may offer novel mechanistic insights into the role of ncRNAs in the development of hypertension-induced cardiac remodelling and sexual dimorphisms.

LVH is an adaptive response to chronic hypertension, triggered by pressure overload to counteract increased wall stress (Philippe, 2005; Tipton et al., 2014). The present study is consistent with previous reports (Hawlitschek et al., 2022b; Mkhize et al., 2024), showing that

7-month-old SHR had established concentric LVH, as evidenced by the increased RWT, LVPWTd, and normalised heart and LV masses. Although there is a paucity of literature, miRNAs have gained attention as potential mediators of LVH in pressure overload conditions, regulating cardiac remodelling and hypertrophic signalling pathways. One previous study reported that miR-155-5p and miR-29b-5p expression is reduced in the pressure overload-induced hypertrophic heart and silencing of these miRNAs may induce cardioprotective effects (Seok et al., 2014). In the present study, the cardiomyocyte expression of miR-29b-5p and miR-155-5p did not differ between SHR and WKY.

However, consistent with a study in a rodent model of pressure overload induced LVH (Heggermont et al., 2017), the present study showed upregulation of miR-146a-5p in the LV of SHR. In addition, miR-146a-5p exhibits the most robust and diverse associations with several key parameters related to LVH (RWT, LVPWTd and normalised heart and LV masses) and diastolic function (e') as well as an index of endothelial activation and vascular permeability (circulating VCAM-1 concentration), markers of cardiac inflammation (macrophage infiltration, SOD2 and IkBα), and histological assessment of myocardial fibrosis. The diverse and significant correlations of miR-146a-5p with these parameters suggests that miR-146a-5p may be involved in inflammatory signalling and oxidative stress related to structural remodelling. The E/e' ratio was increased in 7-month-old SHRs compared to WKYs, indicating increased filling pressures and the presence of diastolic impairment.

Previous studies investigating the role of miR-146a-5p in regulating cardiac remodelling and function in hypertensive states have reported inconsistent findings, where some have suggested a protective role for miR-146a-5p against cardiac hypertrophy and dysfunction (An et al., 2018; Feng et al., 2017; Heggermont et al., 2017; Oh et al., 2018), while others have reported that miR-146a-5p overexpression has adverse effects on cardiac function (Oh et al., 2018). The

differences observed when comparing to other models of experimentally-induced hypertension may be related to the inbred nature of the present model used where the upregulation of miR-146a-5p expresion in SHR may be inherited (Rapp, 2000).

One mechanism whereby miR-146a-5p has been suggested to be involved in the hypertrophic response, is through inflammation-induced fibrosis of the myocardium (Feng et al., 2017; Halkein et al., 2013). In high-grade inflammatory conditions, miR-146a-5p directly targets key adaptor molecules *IRAK1* and *TRAF6* involved in the TLR/NF-κB signalling (An et al., 2018). However, in the present study, the concentrations of pro-inflammatory markers were similar between SHR and WKY. Limited evidence exists to suggest that SHR is a model of low-grade systemic inflammation (Dinh et al., 2014). This suggests that the hypertension-induced cardiac remodeling and dysfunction in SHR may depend on localised rather than systemic inflammation. Indeed, recent evidence indicates that localised inflammation may contribute to the development of concentric LVH in SHR (Li et al., 2008), likely due to immune cell infiltration into myocardial tissue.

In the present study, the elevated circulating concentrations of VCAM-1 in SHRs suggest increased endothelial activation (McCarron et al., 1994; Usui et al., 2012), which is permissive to extravasation of monocytes into the myocardium (Schmitz et al., 2013). In this respect, VCAM-1 mediates monocyte adhesion to the endothelium and subsequent transendothelial migration into cardiac tissue (Medrano-Bosch et al., 2023), that may contribute to the observed increase in myocardial macrophage infiltration in SHRs. Interestingly, miR-146a-5p was still associated with VCAM-1 even when adjusted for SBP, suggesting that endothelial activation and vascular permeabilization may be a result of miRNA-146a-5p activation. Indeed, increasing expression levels of miR-146a-5p, but not SBP, appeared to reverse the expected relationship between VCAM-1 and macrophage infiltration. The infiltrating macrophages have

been shown to predominantly polarise toward the pro-inflammatory M1 phenotype (Luo et al., 2024), a process likely modulated by miR-146a-5p via regulation of the *NF-κB* pathway (R. Chen et al., 2024). MiR-146a-5p has been shown to target key components of the *NF-κB* pathway, including *NFKBIA*, which encodes the negative regulator IκBα (Cuenca-Zamora et al., 2024). In the present study, elevated *NFKBIA* expression in SHRs suggests a compensatory mechanism to counterbalance hyperactivated *NF-κB* signalling (Prescott et al., 2021). In line with the involvement of miR-146a-5p as a counter-mechasnism, we observed similar *IL-1β* expression in SHR compared to WKY. This may suggest a dampened macrophage-derived myocardial inflammation.

Oxidative stress is another key contributor to hypertensive cardiac remodelling (Rababa'h et al., 2018). The increased mRNA expression of *SOD2*, which encodes a key antioxidant enzyme, in the myocardium of SHRs reflects a compensatory response to heightened oxidative stress (Sam et al., 2005). In this regard, miR-146a-5p may modulate redox homeostasis (Dasgupta et al., 2015). The miR-146a-5p-mediated regulatory network on *SOD2* expression links it to redox imbalance (Zorov et al., 2014), as dysregulation may compromise antioxidant defences (Zong et al., 2024), which drive the apoptotic cascade. Apoptosis further contributes to myocardial remodelling by reducing cardiomyocyte density, promoting cardiomyocyte slippage, and enhancing extracellular matrix deposition to compensate for structural deficits (Bennett, 2002). This cascade ultimately drives the transition from compensated hypertrophy to maladaptive remodelling characterised by ventricular dilation and fibrosis.

Given the pleiotropic nature of miRNAs, it is not inconceivable that miR-146a-5p may influence many other pathological processes. In our study, while no significant differences were observed in collagen volume fraction between sexes, the gene expression analysis indicated higher levels of *Col1* and *Col3* genes in females. We postulate that post-transcriptional

regulation may potentially impact on mRNA stability (Nouaille et al., 2017), RNA binding proteins (Van Assche et al., 2015), collagen processing or its translational efficiency in SHRs (Tuller et al., 2010), leading to higher protein levels in the LV without changes in mRNA expression. However, these mechanistic insights could not be gleaned from the present investigation. Elevated blood pressure may drive both perivascular and interstitial fibrosis in SHRs, with the fibrosis following the myocardial wall stress gradient from perivascular regions encroaching into the interstitium (Diez et al., 2020). This gradient reflects higher wall stress adjacent to the vasculature due to increased pressure load, which perpetuates inflammation, and fibroblast activation (Torimoto et al., 2024). The interplay between miR-146a-5p-mediated inflammation and the mechanical stress environment underscores its critical role in hypertensive cardiac remodelling.

In addition to strain-specific expression, miRNAs may have broad effects on downstream signalling pathways in a sex-specific manner (Wallace et al., 2015; Wei et al., 2013). The observed clustering by sex in the PCA biplot indicates that males and females can be differentiated based on their physiological profiles, as captured by the contributing variables, reinforcing the idea that biological sex is a key determinant of variability in the measured parameters. In the present study miR-146a-5p and miR-29b-5p expression did not differ between the sexes. However, we showed a downregulation of miR-155-5p in female rats compared to their male counterparts. The sexual dimorphism in the regulation of miR-155-5p expression may be explained by its relative abundance on the 21q21 X chromosome (Malmhall et al., 2020) and the oestrogen-mediated regulation of its transcription and processing (Florijn et al., 2018). In this regard, given that miR-155-5p is located on the X chromosome, its reduced expression in female rats may be explained by X-chromosome inactivation, a process that silences one X chromosome in each cell to balance gene dosage between sexes (Loda et al., 2022). While some genes escape X-chromosome inactivation, others are tightly regulated,

potentially leading to lower miR-155-5p abundance in females. Taken together, the available evidence on the sex-specific differences in miRNA expression is discordant and warrants further exploration. The relationship between differential cardiomyocyte expression of miRNAs and echocardiographically-derived LV dimensions and function was investigated. We observed phenotypic differences indicative of sexual dimorphism, with female rats exhibiting greater normalised heart and LV masses and higher RWT, suggesting that they may have relatively larger hearts and other organs for their body size compared to male rats. One possible reason for the sexual dimorphism may be an adaptation to different physiological demands between male and female rats (St Pierre et al., 2022). For this reason, these phenotypic changes may be indicative of increased physiological growth in female rats attributable, in part, to the oestrogen-mediated trophic effects on the myocardium (Bhupathy et al., 2010).

Moreover, sex-specific differences in LV systolic function were observed, with female rats exhibiting lower stroke volume and midFS compared to male rats. We attributed these differences to the Frank-Starling effect, which describes the relationship between end diastolic volume and stroke volume as a major effect on decreased myocardial contractility (midFS) and cardiac output in female rats (Pfeffer et al., 1979). Moreover, the lower midFS and LVIDd in female rats contrasts with clinical findings suggesting women may have slightly higher midFS (Gerdts et al., 2001). These differences may stem from sex-based structural and haemodynamic factors, such as smaller heart size and the influence of oestrogen on myocardial function. Additionally, variations in myocardial stiffness, chamber compliance, and afterload could affect heart function and disease susceptibility, particularly in conditions like hypertension or heart failure, independent of the miRNAs tested in our study.

Additionally, sex as a biological variable may influence the pathogenesis of heart-related conditions at the molecular and cellular levels. In the present study, collagen deposition was

greater in female rats that also showed increased expression of circulating levels of pro-inflammatory markers (CRP, IL-6, and TNF-α), pro-fibrotic genes (*LOX1* mRNA and *Col1a/Col3a* ratio), *RUNX-1*, and *PTX-3*. Numerous lines of evidence have found that females exhibit higher circulating levels of pro-inflammatory cytokines, such as IL-6 and TNF-α, compared to males (Dela Justina et al., 2021; Sullivan et al., 2009). Another study investigated the impact of sex hormones on inflammation in SHR, revealing higher expression of pro-inflammatory markers in the kidneys of female rats (Tipton et al., 2014). However, further research is warranted to establish the direction of causaility between sex hormones, systemic inflammation and fibrotic remodelling in the context of hypertension.

In line with the sexual dimorphism related to the phenotype, the present study shows decreased relative expression of miR-155-5p in female rats that was associated with decreased stroke volume. The observed sexual dimorphism may, at least in part, be attributable to the translational regulation by miR-155-5p of genes involved in these pathways. In this regard, alongside Mann et al. (Mann et al., 2017), the decreased expression of miR-155-5p may explain the increased circulating levels of pro-inflammatory markers in female rats. Specifically, miR-155-5p is known to promote inflammation by targeting negative regulators of the NF-κB pathway, thereby sustaining its activation (Mann et al., 2017). In the present study, miR-155-5p was found to be downregulated in female rats, which may paradoxically lead to disinhibition of the NF-κB pathway. This is because miR-155-5p also plays a role in fine-tuning inflammatory responses by contributing to feedback regulation. Its reduced expression in female rats could impair this regulatory balance, allowing unchecked NF-κB activation and contributing to an enhanced pro-inflammatory state in female rats. Pro-inflammatory markers and immune cell infiltration into the myocardium may lead to activation of cardiac fibroblasts, and excessive deposition of extracellular matrix components (*Col1a*), and increased collagen

cross linking (*LOX1*) (Theall & Alcaide, 2022). MiR-155-5p may clarify the cross-talk between inflammation, myocardial fibrosis, and impairment of cardiac function.

3.5 Limitations

Our study focused on miR-146a-5p, miR-155-5p, and miR-29b-5p, potentially overlooking other microRNAs that could contribute to cardiac dysfunction. The mechanisms underlying the observed alterations in miRNA expression profiles and their downstream effects remain incompletely understood, necessitating further mechanistic studies. Notably, miR-146a-5p may be expressed by various cell types, including cardiac fibroblasts and infiltrating macrophages, therefore our measurement of global LV miRNA levels does not allow us to attribute its expression specifically to cardiomyocytes. As such, while the observed changes in miR-146a-5p levels are associated with the pathology, the specific cellular source of this miRNA remains unclear. Moreover, while our study highlights sex-specific differences in miRNA regulation and cardiac outcomes, the oestrous cycle was not evaluated in female rats. Potentially, evaluating the oestrous cycle may add granularity when investigating sex-specific differences between the two strains. Also, because of the pleiotropic nature of miRNAs, our study may benefit from assays confirming base complimentarity with our target genes. Whether the overexpression of miR-146a-5p in the present study is a cause or a consequence could not be determined. In this regard, rescue experiments involving cardiac-specific silencing or overexpression of miR-146a-5p in SHR may provide crucial information about the upstream regulation of the expression of genes related to the hypertensive and hypertrophic phenotype in SHR. Lastly, the relevance of our preclinical findings require validation in human cohorts to translate these observations into meaningful mechanistic insights in hypertensive patients.

3.6 Conclusion

The current study sheds light on the intricate role of miRNAs, particularly miR-146a-5p, miR-155-5p, in the pathogenesis of hypertensive cardiac dysfunction. The relative expression of miR-146a-5p was upregulated in response to pressure overload and was associated with markers of LVH, diastolic dysfunction, and reactive fibrosis. Specifically, miR-146a-5p emerged as a key counter-mechanism, mitigating VCAM-1-mediated transendothelial macrophage infiltration into the myocardium, inflammation and oxidative stress by enhancing IκBα and SOD2 expression. Conversely, miR-155-5-p was under-expressed in female rats, consistent with a cardiac phenotype characteristic of sexual dimorphism. By elucidating sex-specific differences in miRNA expression profiles and their associations with cardiac phenotypes in SHR, our data may offer novel insights into the molecular mechanisms underlying hypertensive heart disease. However, further research is warranted to fully elucidate the mechanistic pathways involved and validate our findings in human populations. Ultimately, a deeper understanding of these miRNA-mediated regulatory networks may pave the way for the development of targeted therapeutic strategies to mitigate cardiovascular complications associated with hypertension.

DISCLOSURES

The authors declare that no perceived or potential competing interests exist.

ACKNOWLEDGEMENTS

The authors would like to thank the staff from the Wits Research Animal Facility for their technical assistance.

GRANTS

This work was supported by the South African National Research Foundation (NRF) grants awarded to SAM (**MND210430598430**) and FM (**CSRP170502229389**).

DATA AVAILABILITY

The data presented in this manuscript is available upon reasable request to the corresponding author.

AUTHOR CONTRIBUTIONS

SAM, AM, and FM conceived and designed the study. SAM, FM, SG, KLM, RAN, LM, and AM performed experiments, analysed data, and interpreted results of experiments. SAM, AM, and FM prepared figures, and drafted manuscript. All authors edited, revised, and approved final iteration of manuscript.

Chapter 4

At the time of submission of the present thesis for examination, the work presented in this chapter was under peer review for publication in the journal "**Federation of American Societies of Experimental Biology**"

Impact factor: 5.8

Runt-related transcription factor 1 modulates cardiac structural changes through mechanisms related to cell survival in male spontaneously hypertensive rats

Authors: Siluleko A Mkhize[1], Sulé Gunter[1,2], Ashmeetha Manilall[1], Kgotso Mosoma[1], Refentshe Nthlane[1], Yigael Powrie[1], Ncumisa Madolo[3], Sylvester Omoruyi[3], and Frederic S Michel[1]

Affiliations: [1]Integrated Molecular Physiology Research Initiative, [2]Department of Physiology, [3]Department of Anatomical Sciences, School of Biomedical Sciences, Faculty of Health Sciences, University of the Witwatersrand, 7 York Road, Parktown, 2193 Johannesburg, South Africa

[2]Department of Health Sciences and Medicine, Bond University, Gold Coast, Queensland, Australia

Running title: RUNX1 and cardiac remodelling

Corresponding author: Siluleko A Mkhize, University of the Witwatersrand, 7 York Road, Parktown, 2193 Johannesburg, South Africa. Tel: (+27) 717 2483; Email: siluleko.mkhize@wits.ac.za

Keywords: RUNX1, Eccentric Remodelling, Hypertension, Apoptosis, Fibrosis

Abstract

Background: Runt-related transcription factor 1 (RUNX-1) is a key transcription factor involved in gene regulation. **Aim:** This study explored its role in the transition from concentric left ventricular hypertrophy (LVH) to cardiac dilation in spontaneously hypertensive rats (SHRs), a model of hypertensive heart disease. **Methods:** Thirty-six (n=36) male WKY and SHRs aged 3 or 12 months (n=9 per group) were studied. Blood pressure was measured using the tail-cuff method, and echocardiographic assessment of cardiac structure and function was performed under anaesthesia. Relative mRNA expression of fibrotic, apoptotic, and RUNX-1 genes was assessed in the left ventricle (LV) via RT-PCR, while apoptotic protein markers were evaluated by Western blot. **Results:** Structurally, SHRs exhibited greater normalised heart (P=0.049) and LV mass (P=0.003), and increased cardiomyocyte nuclei number (P=0.001) at 3 months. By 12 months, they showed reduced posterior wall thickness in diastole (PWTd) (P=0.005), lower relative wall thickness (RWT) (P=0.012), and enlarged LV internal diameter in diastole (LVIDd) (P=0.007), consistent with progression toward eccentric remodeling and early cardiac dilation. Diastolic dysfunction was also evident at 12 months, as indicated by elevated E/e′ ratio (P=0.020), reduced late diastolic tissue lengthening velocity (a′) (P=0.027), and decreased e′/a′ ratio (P=0.006). At the molecular level, 12-month-old SHRs exhibited significantly elevated expression of matrix metalloproteinase 9 (MMP-9) (P=0.033). Apoptotic signaling was dysregulated, with reduced Bax (P=0.019) and cleaved PARP-1 (P=0.002), a trend toward a lower Bax/Bcl-2 ratio (P=0.062), and elevated cleaved caspase-3 (P=0.065), suggesting partial or incomplete apoptosis. RUNX-1 expression declined with age (P=0.0002) but increased with hypertension (P=0.001), suggesting reactivation of the foetal gene program. Notably, RUNX-1 expression correlated positively with normalised LV mass (r=0.54, P<0.0001), RWT (r=0.54, P=0.002), and Bax/Bcl-2 ratio (r=0.44, P=0.010), and negatively with LVIDd (r=-0.57, P=0.001) and MMP9 expression (r=-0.48, P=0.013). These associations

remained after adjusting for SBP, indicating RUNX-1 involvement in structural remodeling independent of haemodynamic stress. **Conclusion:** In summary, 12-month-old SHRs displayed maladaptive fibrotic remodeling, diastolic dysfunction, and early cardiac dilation. RUNX-1 emerged as a modulator of hypertrophic and fibrotic remodeling rather than a direct regulator of myocardial performance, underscoring its potential role in early cardiac adaptation to hypertension.

4.1 Introduction

Hypertension-induced concentric left ventricular hypertrophy (LVH) is characterised by an increase in wall thickness relative to chamber size, which initially serves as an adaptive response to maintain optimal wall tension (Lorell & Carabello, 2000; Philippe, 2005; Samak et al., 2016). However, over time, the sustained pressure causes maladaptive remodelling, leading to a transition towards an eccentrically-remodelled phenotype marked by chamber dilation and thinning of the ventricular walls (Katholi & Couri, 2011; Lorell & Carabello, 2000; Wilson et al., 2017). This progressive remodelling is associated with the development of heart failure, with both systolic and diastolic dysfunction becoming evident as the heart loses its ability to contract and relax efficiently during diastole (Anderson et al., 2018; Nauta et al., 2005). The chronic stress and injury imposed on cardiomyocytes by prolonged hypertension also trigger the reactivation of the foetal gene program (Vigil-Garcia et al., 2021), a hallmark of maladaptive cardiac remodelling. This reactivation leads to changes in gene expression that further compromise cardiac function, promoting fibrosis (Ni et al., 2021), apoptosis (Li & Jia, 2022), and impaired myocardial performance (Ni et al., 2021; Xu et al., 2023). Therefore, there is a need to explore the role and contribution of transcription factors in gene regulation in order to enhance our understanding of the pathophysiological mechanisms underlying hypertension-induced cardiac remodelling and dysfunction.

Transcription factors are proteins that bind to specific DNA sequences to regulate the expression of target genes, controlling key cellular processes such as growth, differentiation, and survival (Mitsis et al., 2020). Runt-related transcription factor 1 (*RUNX-1*) is a member of the RUNX superfamily of proteins which typically functions by dimerising with core-binding factor β (CBFβ) to form a transcriptionally active heterodimer that can activate or repress specific target genes (McCarroll et al., 2018; Qi et al., 2023; Riddell et al., 2020). In the murine model of pressure overload achieved by transverse aortic constriction (TAC), inhibition of

RUNX-1 led to remission of cardiac enlargement (Qi et al., 2023), improved ejection fraction, and endocardial fractional shortening (Qi et al., 2023). Rescue experiments also indicated that *RUNX-1* promotes cardiac hypertrophy in a p53-dependent manner (Zhang et al., 2021). Lastly, *RUNX-1*, located at the promoter region of the transforming growth factor-β1 receptor (TGFBR1) was shown to regulate TGFβ expression, potentially modulating myocardial fibrosis (Xu et al., 2023). Additionally, *RUNX-1* expression is amenable to modulation by various regulatory factors, including STAT3 (Suzuki et al., 2023), RNA interference (Martin et al., 2023), protein phosphatases (McCarroll et al., 2018), and several microRNAs such as miR-101 (Li et al., 2019), miR-199a-3p (Liu et al., 2022), and miR-18-5p (Li & Jia, 2022). These modulators can influence downstream targets that are critical in cardiac function and remodelling. For instance, changes in *RUNX-1* activity may alter Sarcoplasmic/Endoplasmic Reticulum Ca^{2+}-ATPase (SERCA)-mediated Ca^{2+} sequestration and phospholamban expression, which are active processes contributing to myocardial contractility (Li et al., 2019; McCarroll et al., 2018; Riddell et al., 2020). Moreover, modulation of *RUNX-1* can affect the TGF-β/Smad signalling pathway, helping to limit fibrosis, promote cell survival, and ultimately preserve heart function (Liu et al., 2023; Qi et al., 2023).

To the best of our knowledge, no studies have explored the role of *RUNX-1* in spontaneously hypertensive rats (SHRs), a well-established rodent model of pressure overload. Most of the evidence has been gleaned from murine models of myocardial infarction (MI) achieved by coronary ligation of the left anterior descending artery (H. Chen et al., 2024; Li et al., 2019; Martin et al., 2022; McCarroll et al., 2018). However, MI leads to an eccentric phenotype almost immediately (McCarroll et al., 2018). Whereas cardiac remodelling due to pressure overload begins with concentric hypertrophy, which gradually shifts to an eccentric phenotype (Samak et al., 2016), revealing time-dependent changes in the development of myocardial dysfunction. Therefore, we hypothesised that *RUNX-1* might be involved in the shift from

compensatory left ventricular (LV) hypertrophy to maladaptive remodelling, potentially serving as a critical regulator in the progression toward heart failure in both MI and pressure-overload conditions. In the present study, we investigated the expression and role of *RUNX-1* in cardiac remodelling in spontaneously hypertensive rats (SHR), with a focus on its relationship to structural changes and its putative involvement in anti-fibrotic and anti-apoptotic mechanisms.

4.2 Methods

4.2.1 Animals and housing

We received approval from the Animal Ethics Screening Committee at the University of the Witwatersrand, Johannesburg, South Africa (**Clearance number**: AREC22-08-009B), and followed both the National Institutes of Health Guide for the Care and Use of Laboratory Animals and the ARRIVE (Animal Research: Reporting of *In Vivo* Experiments) guidelines (Percie du Sert, Ahluwalia, et al., 2020). The animals were housed individually in a controlled environment with a 12-hour light-dark cycle, had unrestricted access to drinking water and standard laboratory chow (Labchef, Johannesburg, South Africa), and were provided with coloured balls and tunnels for environmental enrichment.

4.2.2 Study design

Male spontaneously hypertensive rats (SHR, n=18, RRID: RGD_10043828) and normotensive Wistar-Kyoto rats (WKY, n=18, RRID: RGD_61119), both at 3 and 12 months of age, were obtained from and housed at the Wits Research Animal Facility (WRAF). The rats were acclimated to handling and their housing environment for two weeks prior to the study. An *a priori* sample size calculation using a two-way Analysis of Variance, with an alpha of 0.05 and 80% power, indicated that a total of 36 rats (9 per group) would be adequate to detect statistical differences in this model (G*Power, version 3.1.9.2) (Charan & Biswas, 2013).

4.2.3 Non-invasive blood pressure measurement

Before termination, blood pressure (BP) was measured in all rats using the tail-cuff technique with non-invasive BP amplifiers (Biopac Systems Inc, Santa Barbara, USA, RRID: SCR_014829). Conscious rats were placed in a restrainer with the cuff attached to a heated tail, following a standard protocol (Mokotedi et al., 2020). To ensure accuracy, rats were habituated

to the restrainer and BP measurement process before the initial readings. Measurements were conducted at midday to minimise diurnal variations in BP.

4.2.3 Transthoracic echocardiography

Rats were anaesthetised with isoflurane (5% for induction and 1–2.5% for maintenance) via a 100% oxygen mask. During anaesthesia, echocardiography was performed using a high-resolution (10 MHz) ultrasound probe connected to an echocardiogram (Siemens Acuson SC2000, Siemens Medical Solutions, USA, Inc.). LV dimensions were measured in the parasternal long-axis view using M-Mode echocardiography. These measurements included LV internal diameter in systole (LVIDs), LV internal diameter in diastole (LVIDd), interventricular septal thickness in systole (IVSTs), interventricular septal thickness in diastole (IVSTd), LV posterior wall thickness in systole (LVPWTs), and LV posterior wall thickness in diastole (LVPWTd). From these, indices of LV systolic function were derived: endocardial fractional shortening (endFS) was determined as (LVIDd – LVIDs) / LVIDd × 100; midwall fractional shortening (midFS) was calculated as [(LVIDd + PWTd) - (LVIDs + PWTs)] / (LVIDd + PWTd) × 100; and LV relative wall thickness (RWT) was computed as (2 × PWTd) / LVIDd. Teichholz method was used to estimate LV end diastolic volume (LVEDV) from the formular LVEDV (ml) = $[7/(2.4 + LVIDd)] \times [LVIDd]^3$ and LV end systolic volume from the formular LVESV (ml) = $[7/(2.4 + LVIDs)] \times [LVIDs]^3$. Stroke volume was then computed as stroke volume (ml) = LVEDV – LVESV. Ejection fraction was computed as ejection fraction (%) = [(LVEDV – LVESV) / LVEDV] × 100.

LV diastolic function was assessed with pulsed doppler imaging to evaluate mitral valve inflow patterns. In the apical 4-chamber view, early (E) and late (A) diastolic inflow velocities were recorded at the tip of the mitral valve leaflet, and the E/A ratio was calculated as an index of relaxation. Tissue doppler imaging (TDI) was used to measure peak myocardial tissue lengthening velocities during early (e') and late (a') diastole at the lateral mitral annulus level.

Data were expressed as e', indicating myocardial relaxation; e'/a', indicating myocardial stiffness; and E/e', representing LV filling pressure.

All echocardiographic assessments were performed by a single trained observer who was blinded to the experimental groups. Echocardiographic assessment adhered guidelines as outlined by the American Society of Echocardiography (Lang et al., 2015).

4.2.4 LV tissue sampling

Following echocardiography, a thoracotomy was performed. The organs were then removed and weighed. LV tissue was processed in two ways: it was either preserved in 10% buffered formalin for histological analysis or placed in RNAlater® (Ambion, Sigma Aldrich, Germany), an RNA stabilising reagent, to maintain RNA integrity for reliable gene expression analysis.

4.2.5 Total collagen content, macrophage infiltration, and cardiomyocyte nuclei density in LV tissue

LV tissue was preserved in 10% buffered formalin for histological analysis. Total collagen content was assessed from histological analysis of the LV. In brief, LV tissue that was preserved in 10% buffered formalin was embedded in paraffin. Thin (5 µm) sections were cut using a microtome, then deparaffinised and rehydrated. The sections were stained with a 0.1% Sirius Red solution (Schipke et al., 2017) in saturated picric acid for 60 minutes at room temperature, rinsed in acidified water, dehydrated, and mounted with Digital Picture Exchange (DPX) medium. Collagen content was analysed using a Zeiss Axioscope 2 Plus microscope with a 10x objective lens and Zeiss AxioCam (Zeiss, Peabody, MA, USA, RRID: SCR_023747). Collagen fraction area was quantified with ImageJ software (RRID: SCR_003070) by dividing the collagen area by the total tissue area. Haematoxylin and Eosin (H&E) staining was performed to quantify LV cardiomyocyte nuclei per unit area (CM nuclei/mm^2) and macrophage infiltration. Macrophages were recognized by their characteristic appearance, including a

rounded to oval morphology, eosinophilic cytoplasm, and conspicuous nuclei positioned off-centre. A blinded evaluator examined the slides using a DVM6 digital microscope (Leica Biosystems, Vista, CA, USA) with a maximum FOV of 12.55 mm and a magnification range of 46x to 675x. The LV total collagen content, cardiomyocyte nuclei per unit area, and macrophage infiltration were measured three times, with the average value recorded.

4.2.6 Total RNA isolation

Total RNA was extracted from LV tissue that had been preserved in RNAlater® (Ambion, Sigma Aldrich, Germany) using an Illustra™ RNAspin Mini Isolation kit (GE Healthcare, Buckinghamshire) according to manufacturer's instructions. RNAlater® is an RNA stabilising reagent that maintains RNA integrity for reliable gene expression analysis. Subsequent to total RNA extraction, the quality and quantity of RNA was confirmed using a Nanodrop OneC spectrophotometer (Thermo Fisher Scientific, Waltham, USA). The RNA was then reverse-transcribed using SuperScript™ IV VILO™ cDNA Synthesis Master Mix (Thermo Fisher Scientific, Waltham, USA). The quality and quantity (>1000ng/µL) of cDNA was again confirmed using a Nanodrop OneC spectrophotometer (Thermo Fisher Scientific, Waltham, USA). The cDNA products were stored at -20°C until further analyses.

4.2.7 Expression of target genes

Comparative gene expression was measured using RT-PCR with cDNA templates (~2 µg). The procedure involved pre-designed Taqman probe mixes: 0.25 µl for the reference gene hypoxanthine guanine phosphoribosyl transferase 1 (*HPRT1*, Taqman assay ID: Rn01527838_g1, Thermo Fisher Scientific, Life Technologies, Carlsbad, USA), 0.5 µl for the gene of interest (Taqman gene expression assay), and 5 µl of Taqman Fast Advanced PCR master mix, resulting in a final volume of 10 µl. Gene expression was assessed for *Col1a* mRNA (collagen type-I), *Col3a* mRNA (collagen type-III), *LOX1* mRNA (lysyl oxidase 1),

MMP9 mRNA (matrix metalloproteinase 9), *Bax*, *Bcl-2*, and *RUNX-1* mRNA (which code for B-cell lymphoma 2 associated protein X, B-cell lymphoma 2, and runt-related transcription factor 1) using duplex reactions with the endogenous control *HPRT1* in duplicate plates. The relative expression of each gene was calculated using the $2^{-\Delta\Delta Ct}$ method (Livak & Schmittgen, 2001).

4.2.8 Immunoblotting

Western blot analysis was conducted in LV tissue that had been preserved in RNAlater. In brief, the LV tissue was homogenised using a radioimmunoprecipitation assay (RIPA) lysis buffer composed of 50 mM Tris-HCl (maintained at pH 7.4–8.0), 150 mM NaCl, 1% Triton X-100, 0.5% sodium deoxycholate, and 0.1% sodium dodecyl sulphate (SDS). Presence of proteins in the lysate was determined using a BCA assay. To prevent protein degradation and dephosphorylation, protease and phosphatase inhibitors were freshly added. After cell lysis, the protein lysate was resolved by SDS-PAGE using either 10% or 15% gels, depending on the target protein's molecular weight, and transferred onto a Hybond ECL membrane (Amersham Biosciences). To confirm equal protein loading and efficient transfer, the membrane was briefly stained with Ponceau S solution prior to blocking. The membrane was blocked with 5% low-fat milk in PBS containing 0.1% Tween-20 (PBST) and incubated overnight at 4 °C with a primary antibody targeting poly(ADP-ribose) polymerase-1 (PARP1) (Santa Cruz Biotechnology, sc-7150), caspase-3, and β-actin (St. Louis, MO, USA) as a loading control. Following three PBST washes, the membrane was treated with HRP-conjugated secondary antibodies (1:5000, Bio-Rad) for 1 hour at room temperature. Protein bands were visualized using a chemiluminescent detection system (Thermo Fisher Scientific, Hudson, NH, USA). Densitometric analysis was performed using ImageJ software to quantify the intensity of protein bands.

4.2.9 Statistical analyses

Statistical analyses were performed in GraphPad Prism version 10.5.0 for Windows (GraphPad Prism, Massachusetts, USA, RRID: SCR_002798). The Kolmogorov-Smirnov test with a Dallal-Wilkinson-Lilliefors P value and visual inspection using quantile-quantile (Q-Q) plots, indicated that all variables followed and exhibited the expected quantiles of a Gaussian distribution. Data are expressed as arithmetic mean ± standard deviation (SD). Group differences were determined by two-way analysis of variance (2-way ANOVA) test with strain (WKY vs SHR) and time (3 months vs 12 months) as the main effects. When a significant interaction effect was observed, a Tukey's *post-hoc* test was conducted. Bivariate correlations were determined using Pearson's correlation analyses and presented as a volcano plot. For the correlation analyses, a large effect size ($r = 0.5$) was anticipated. Power analysis indicated that with the sample size of n=36 rats, the study achieves 98% power, demonstrating sufficient sensitivity to detect meaningful correlations (G*Power, version 3.1.9.2). Variables that were significant in the bivariate analyses were subjected to multivariable linear regression analyses to adjust for the confounding effect of SBP and presented as β [95% CI]. Statistical significance was considered at $P<0.05$

4.3 Results

4.3.1 Gravimetric parameters

Table 4.1 shows the gravimetric parameters including body and organ masses of 3- and 12-month-old normotensive WKYs and SHRs. WKYs were significantly heavier than SHRs at both 3 and 12 months ($P=0.001$). Regardless of strain, 12-month-old rats were heavier than 3-month-old rats ($P<0.0001$) and had greater absolute heart, LV, and kidney masses (all $P<0.0001$). When indexed to body mass, SHRs exhibited significantly greater heart ($P=0.049$), and kidney masses compared to WKYs ($P<0.0001$). A significant interaction was observed for absolute liver mass ($P=0.002$). At 3 months, there was no difference in liver mass between WKYs and SHRs ($P>0.05$), but at 12 months, SHRs had a significantly heavier liver compared to WKYs ($P=0.0003$). Regardless of strain, liver mass in 12-month-old rats was greater than in 3-month-old rats ($P<0.001$). When indexed to body mass, the interaction remained ($P=0.001$), with SHRs having a greater indexed liver mass than WKYs at both 3 months ($P=0.039$) and 12 months ($P<0.0001$). Additionally, both 3-month-old WKYs and SHRs had greater indexed liver mass compared to 12-month-old WKYs (both $P<0.0001$).

Table 4.1: Gravimetric parameters showing body and organ masses in 3- and 12-month-old normotensive WKY and SHR.

	3 Months		12 Months		P value		
	WKY (n=9)	**SHR (n=9)**	**WKY (n=9)**	**SHR (n=9)**	**Time**	**Strain**	**Interaction**
Gravimetric							
Body mass (g)	291 ± 27	266 ± 22	443 ± 37	405 ± 16	**<0.0001**	**0.0014**	0.4758
Heart mass (g)	1.07 ± 0.14	1.12 ± 0.20	1.53 ± 0.14	1.48 ± 0.07	**<0.0001**	0.9092	0.2979
Heart mass (g/100g)	0.37 ± 0.07	0.42 ± 0.06	0.35 ± 0.05	0.37 ± 0.02	**0.0320**	**0.0489**	0.3869
LV mass (g)	0.81 ± 0.09	0.86 ± 0.14	1.11 ± 0.08	1.16 ± 0.07	**<0.0001**	0.1466	0.9738
Kidney mass (g)	0.95 ± 0.07	0.96 ± 0.12	1.34 ± 0.13	1.40 ± 0.11	**<0.0001**	0.3496	0.5411
Kidney mass (g/100g)	0.33 ± 0.01	0.36 ± 0.03	0.30 ± 0.01	0.34 ± 0.02	**0.0024**	**<0.0001**	0.4929
Liver mass (g)	9.69 ± 0.45^{c}	9.62 ± 0.83^{c}	11.55 ± 0.99^{b}	13.72 ± 1.44^{a}	**<0.0001**	**0.0034**	**0.0020**
Liver mass (g/100g)	3.35 ± 0.26^{b}	3.62 ± 0.12^{a}	2.61 ± 0.11^{c}	3.38 ± 0.27$^{a, b}$	**<0.0001**	**<0.0001**	**0.0010**

Abbreviations: WKY, Wistar Kyoto rats; and SHR, spontaneously hypertensive rats; and LV, left ventricle

Data expressed as mean ± SD

Organ masses were normalised to body mass and expressed as g/100g

2-way ANOVA with Tukey *post hoc* test. On compact letter display, comparisons that do not share the same letter are statistically significant.

4.3.2 Systolic and diastolic blood pressure

Table 4.2 shows the haemodynamic parameters including systolic and diastolic blood pressure of 3- and 12-month-old normotensive WKY and SHR. We observed a significant interaction for SBP ($P<0.0001$). SHRs had significantly higher SBP compared to WKYs at both 3 months ($P<0.0001$) and 12 months ($P<0.0001$). While the SBP of WKYs remained unchanged between 3 and 12 months ($P=0.619$), SHRs showed a significant increase in SBP over the same period ($P<0.0001$). DBP was also higher in SHRs than in WKYs at both 3 and 12 months (both $P<0.0001$). Regardless of strain, 12-month-old rats had a higher DBP compared to 3-month-old rats ($P=0.029$).

4.3.3 LV geometry and histological assessment of the left ventricle

Table 4.2 shows the haemodynamic parameters including left ventricular geometry, and histological assessment of the left ventricle tissue of 3- and 12-month-old normotensive WKY and SHR. The LVIDs was larger in SHRs than in WKYs ($P=0.002$). Regardless of strain, 12-month-old rats had a greater LVIDs compared to 3-month-old rats ($P=0.001$). No other significant differences were observed in LV geometry indices between SHRs and WKYs (all $P>0.05$) or between the two age groups (all $P>0.05$). We observed a significant interaction for cardiomyocyte nuclei density ($P=0.0006$). Cardiomyocyte nuclei density was significantly greater in 3-month-old SHRs compared to all experimental groups (all $P<0.05$). Myocardial tissue collagen content was similar between all experimental groups (all $P>0.05$).

Figures 4.1A-2D illustrate the indices of left ventricular remodelling in 3- and 12-month-old normotensive WKY and SHR. At both time points, the normalised LV mass of SHRs was significantly greater than that of WKYs ($P=0.003$). However, 3-month-old rats had a heavier normalised LV mass compared to 12-month-old rats ($P=0.015$). At 12 months, the LVPWTd was lower in SHRs compared to WKYs ($P=0.005$). LVIDd exhibited a significant interaction effect ($P=0.035$); wherein, LVIDd was greater in 12-month-old SHRs compared to all other

groups ($P<0.0001$). RWT was lower in 12-month-old SHRs compared to WKYs ($P=0.014$), and overall, the RWT of 12-month-old rats was lower than that of 3-month-old rats, regardless of strain.

Table 4.2: Echocardiographic parameters showing left ventricular geometry, diastolic, and systolic function in 3- and 12-month-old normotensive WKY and SHR.

	3 Months		12 Months		P value		
	WKY (n=9)	**SHR (n=9)**	**WKY (n=9)**	**SHR (n=9)**	**Time**	**Strain**	**Interaction**
Haemodynamic							
SBP (mmHg)	122 ± 6[c]	148 ± 12[b]	127 ± 6[c]	186 ± 7[a]	**<0.0001**	**<0.0001**	**<0.0001**
DBP (mmHg)	87 ± 15	110 ± 5	94 ± 11	119 ± 6	**0.0299**	**<0.0001**	0.0788
LV geometry							
LVIDs (mm)	2.29 ± 0.52	3.06 ± 0.69	3.14 ± 0.99	4.22 ± 0.62	**0.0010**	**0.0022**	0.5764
IVSTs (mm)	3.44 ± 0.81	3.49 ± 0.45	3.59 ± 0.70	3.64 ± 0.76	0.5585	0.8494	0.9943
IVSTd (mm)	2.14 ± 0.98	2.38 ± 0.53	2.44 ± 0.55	2.71 ± 0.88	0.2412	0.3461	0.9453
LVPWTs (mm)	2.94 ± 0.44	2.94 ± 0.46	2.83 ± 0.64	2.74 ± 0.53	0.4402	0.8230	0.8117
Histology							
CM nuclei/mm^2	60.4 ± 12.7[b]	68.9 ± 14.4[a]	61.6 ± 9.5[b]	53.8 ± 8.4[b]	**0.0161**	0.1479	**0.0006**
Collagen content (%)	0.65 ± 0.76	1.88 ± 1.58	1.55 ± 1.65	1.56 ± 1.28	0.1303	0.5227	0.5468

Abbreviations: WKY, Wistar Kyoto rats; SHR, spontaneously hypertensive rats; SBP, systolic blood pressure; DBP, diastolic blood pressure; LV, left ventricle; LVIDs, left ventricular internal diameter in systole; IVSTs, interventricular septal thickness in systole; IVSTd, interventricular septal thickness in diastole; LVPWTs, left ventricular posterior wall thickness in systole; and CM, cardiomyocyte.

Data expressed as mean ± SD, 2-way ANOVA with Tukey *post hoc* test. On compact letter display, comparisons that do not share the same letter are statistically significant.

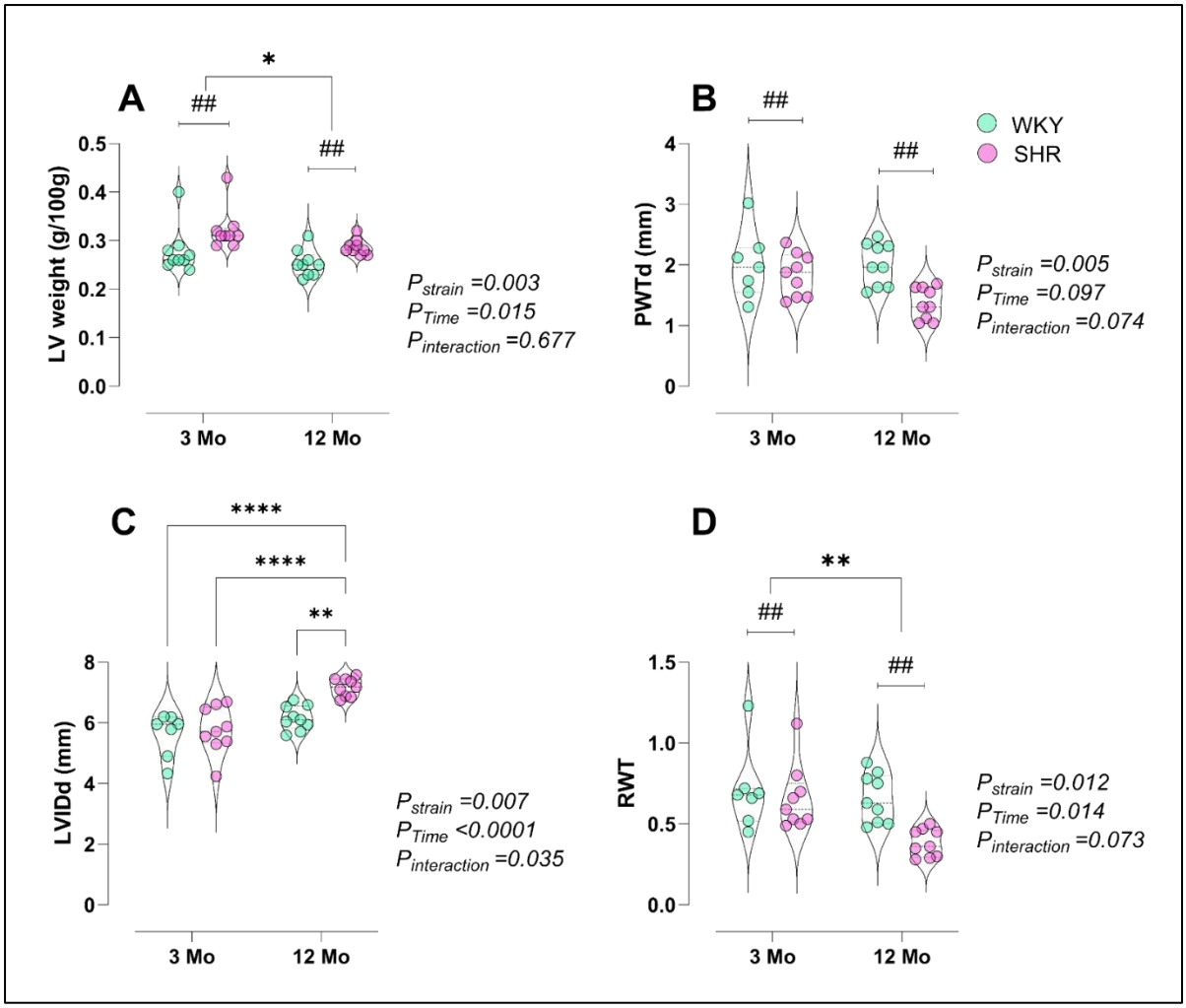

Figures 4.1A-D: A graph illustrating indices of left ventricular remodelling including left ventricular mass normalised to body mass (**1A**), left ventricular posterior wall thickness in diastole (**1B**), left ventricular internal diameter in diastole (**1C**), and relative wall thickness (**1D**) in 3- and 12-month-old normotensive WKYs and SHRs. Data expressed as mean ± SD. 2-way ANOVA with Tukey *post hoc* test. $^{\#\#}$P<0.001 WKY vs SHR. *P<0.05, **P<0.001, and ****P<0.0001 3 Mo vs 12 Mo

4.3.4 Echocardiographic parameters showing left ventricular diastolic and systolic function

Table 4.3 shows the echocardiographic parameters showing left ventricular diastolic and systolic function in 3- and 12-month-old normotensive WKYs and SHRs. A significant interaction effect was noted found for a' (P=0.027), e'/a' (P=0.005), and E/e' (P=0.020). Specifically, in SHRs, a' was higher at 12 months than at 3 months (P=0.004), and at 12 months, a' was higher in SHRs compared to WKYs (P=0.025). The e'/a' ratio was lower in SHRs at 12 months compared to 3 months (P=0.012), and at 12 months, it was lower in SHRs compared to WKYs (P=0.007). The E/e' ratio was greater in SHRs at 12 months compared to 3 months (P=0.031), and it was also greater in SHRs compared to WKYs at 12 months (P=0.046). Regardless of strain, 12-month-old rats had significantly higher E values than 3-month-old rats (P=0.049). SHRs had lower A values than WKYs (P=0.047). The e' and E/A were similar between the groups (all P>0.05). In SHR, endFS (P=0.001) and midFS (P<0.0001) were lower compared to WKY. Irrespective of strain, 12-month-old rats had greater stroke volume (P=0.006), but lower ejection fraction (P=0.031**)** compared to 3-month-old rats.

Table 4.3: Echocardiographic parameters showing left ventricular diastolic and systolic function in 3- and 12-month-old normotensive WKYs and SHRs.

	3 Months		12 Months		P value		
	WKY (n=9)	**SHR (n=9)**	**WKY (n=9)**	**SHR (n=9)**	**Time**	**Strain**	**Interaction**
Diastolic function							
e' (m/s)	0.05 ± 0.01	0.06 ± 0.01	0.05 ± 0.02	0.06 ± 0.01	0.3769	0.2818	0.9212
a' (m/s)	0.04 ± 0.01[a, b]	0.03 ± 0.01[b]	0.04 ± 0.01[b]	0.05 ± 0.02[a]	**0.0232**	0.1708	**0.0266**
e'/a'	1.43 ± 0.52[a, b]	1.68 ± 0.28[a]	1.71 ± 0.48[a]	1.05 ± 0.35[b]	0.2648	0.1744	**0.0056**
E (m/s)	0.77 ± 0.18	0.70 ± 0.11	0.93 ± 0.19	0.80 ± 0.19	**0.0490**	0.1414	0.6338
A (m/s)	0.62 ± 0.15	0.44 ± 0.15	0.66 ± 0.20	0.56 ± 0.19	0.2445	**0.0471**	0.5860
E/A	1.28 ± 0.33	1.70 ± 0.43	1.45 ± 0.20	1.69 ± 0.96	0.7321	0.1527	0.7031
E/e'	15.43 ± 3.39[a, b]	12.84 ± 2.75[b]	13.23 ± 3.55[b]	19.08 ± 6.68[a]	0.2489	0.3480	**0.0202**
Systolic function							
endFS (%)	58 ± 6	47 ± 8	56 ± 13	31 ± 11	0.1943	**0.0009**	0.4238
midFS (%)	30 ± 2	21 ± 3	30 ± 9	15 ± 6	0.2062	**<0.0001**	0.1679
Stroke volume (ml)	128 ± 39	128 ± 37	148 ± 43	189 ± 32	**0.0064**	0.1391	0.1486
Ejection fraction (%)	87 ± 4	77 ± 9	77 ± 17	70 ± 10	**0.0306**	0.0670	0.6217

Abbreviations: WKY, Wistar Kyoto rats; SHR, spontaneously hypertensive rats; e', early peak tissue lengthening velocity at lateral mitral annulus; a', late peak tissue lengthening velocity at lateral mitral annulus; e'/a', early to late peak tissue lengthening velocity ratio; E, maximum early mitral inflow velocity; A, maximum late mitral inflow velocity; E/A, early to late diastolic filling velocity ratio; E/e', early diastolic mitral inflow to tissue lengthening velocity at lateral mitral annulus; endFS, endocardial fractional shortening; and midFS, midwall fractional shortening.
Data expressed as mean ± SD, 2-way ANOVA with Tukey *post hoc* test. On compact letter display, comparisons that do not share the same letter are statistically significant.

4.3.5 Gene expression of apoptotic and fibrotic markers, RUNX1 transcription factor, cardiomyocyte nuclei density, and collagen fraction area in LV tissue

At 3 and 12 months, *RUNX1* expression was significantly higher in SHRs compared to WKYs (P=0.001). Irrespective of strain, 3-month-old rats exhibited higher *RUNX1* expression than 12-month-old rats (P=0.0002). Lastly, *RUNX1* expression lacked a significant interaction (P=0.578).

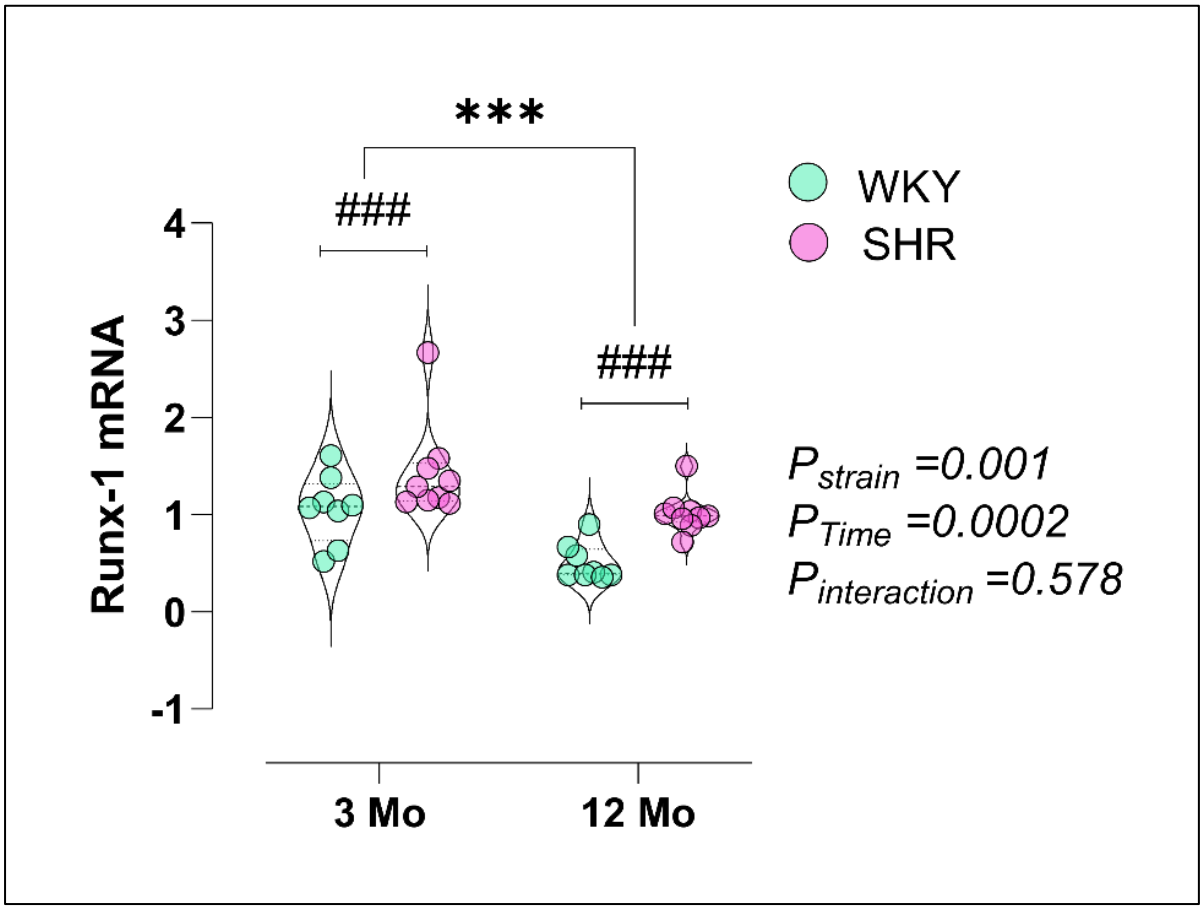

Figure 4.2: A graph illustrating gene expression of runt related transcription factor 1 in left ventricular tissue of 3- and 12-month-old normotensive WKY and SHR. Data expressed as mean ± SD. 2-way ANOVA with Tukey *post hoc* test. ###P<0.0001 in WKY vs SHR. **P<0.0001 in 3 Mo vs 12 Mo

4.3.6 Gene expression of apoptotic and fibrotic markers in LV tissue

Table 4.4 shows the relative gene expression of molecular markers including apoptotic and fibrotic genes in 3- and 12-month-old normotensive WKY and SHR. A significant interaction was observed for *Bax* expression (P=0.019). At 12 months, *Bax* expression was lower in SHRs compared to all other experimental groups (all P<0.05). *Bcl-2* (P=0.417) expression and the *Bax/Bcl-2* ratio (P=0.111) showed no significant differences between the groups. The interaction was also not statistically significant for *Bcl-2* (P=0.871) and *Bax/Bcl-2* (P=0.088) ratio. Similarly, the expression levels of *Col1a, Col3a, LOX1* were comparable across all experimental groups (all P>0.05). The *Col1a/Col3a* ratio was significantly higher in SHRs than in WKYs (P=0.003) but did not show a significant interaction (P=0.099). *MMP9* expression showed a significant interaction (P=0.033), wherein, *MMP9* was greater in 12-month-old SHRs compared to 3-month-old WKYs and SHRs (all P<0.05).

Table 4.4: Relative gene expression of molecular markers including apoptotic and fibrotic genes in 3- and 12-month-old normotensive WKY and SHR.

	3 Months		12 Months		P value		
	WKY (n=9)	**SHR (n=9)**	**WKY (n=9)**	**SHR (n=9)**	**Time**	**Strain**	**Interaction**
Apoptotic markers (mRNA)							
Bax	1.03 ± 0.23^{a}	1.07 ± 0.19^{a}	1.01 ± 0.12^{a}	0.70 ± 0.27^{b}	**0.0105**	0.0710	**0.0193**
Bcl2	1.03 ± 0.24	1.06 ± 0.20	0.95 ± 0.11	1.00 ± 0.07	0.2256	0.4171	0.8708
Bax/Bcl2 ratio	1.02 ± 0.18	1.03 ± 0.23	1.00 ± 0.10	0.75 ± 0.32	0.0619	0.1106	0.0879
Fibrotic markers (mRNA)							
Col1a	1.10 ± 0.48	1.12 ± 0.35	0.97 ± 0.10	1.01 ± 0.15	0.2416	0.7534	0.9204
Col3a	1.05 ± 0.31	0.96 ± 0.30	0.74 ± 0.43	1.02 ± 0.20	0.2616	0.3815	0.1084
Col1a/Col3a ratio	0.98 ± 0.21	1.17 ± 0.12	1.01 ± 0.12	1.63 ± 0.67	0.0613	**0.0025**	0.0985
LOX-1	1.07 ± 0.38	1.01 ± 0.24	1.03 ± 0.15	1.00 ± 0.08	0.7837	0.6220	0.8898
MMP-9	0.77 ± 0.40^{b}	0.57 ± 0.27^{b}	$0.98 \pm 0.49^{a,b}$	1.46 ± 0.31^{a}	**0.0010**	0.3290	**0.0325**

Abbreviations: WKY, Wistar Kyoto rats; SHR, spontaneously hypertensive rats; Bcl2, B-cell lymphoma 2; Bax, B-cell lymphoma 2 associated protein X; Col1a, collagen type 1a; Col3a, collagen type 3a, LOX1, lysil oxidase 1; and MMP9, matrix metalloproteinase 9. Data expressed as mean ± SD. 2-way ANOVA with Tukey *post hoc* test. On compact letter display, comparisons that do not share the same letter are statistically significant.

4.3.7 Protein expression of the apoptotic markers including cleaved poly(ADP-Ribose) polymerase 1 (cPARP1), and cleaved caspase-3 (cCaspase-3) in LV tissue

Figures 4.3A-D depict immunoblotting of cPARP1 (**3A**) and cCaspase-3 (**3B**) in LV tissue. cPARP1 expression exhibited a significant interaction effect (P=0.002); wherein, cPARP1 was decreased in 12-mo-old SHRs compared to 12-mo-old WKYs (P=0.003) (**3C**). cCaspase-3 expression showed a significant time effect (P=0.049) wherein cCaspase-3 was increased in 12-mo-old rats compared to 3-months-old rats, irrespective of the strain. Neither strain effect (P=0.065) nor interaction (P=0.075) was observed for cCaspase-3 expression (**3D**).

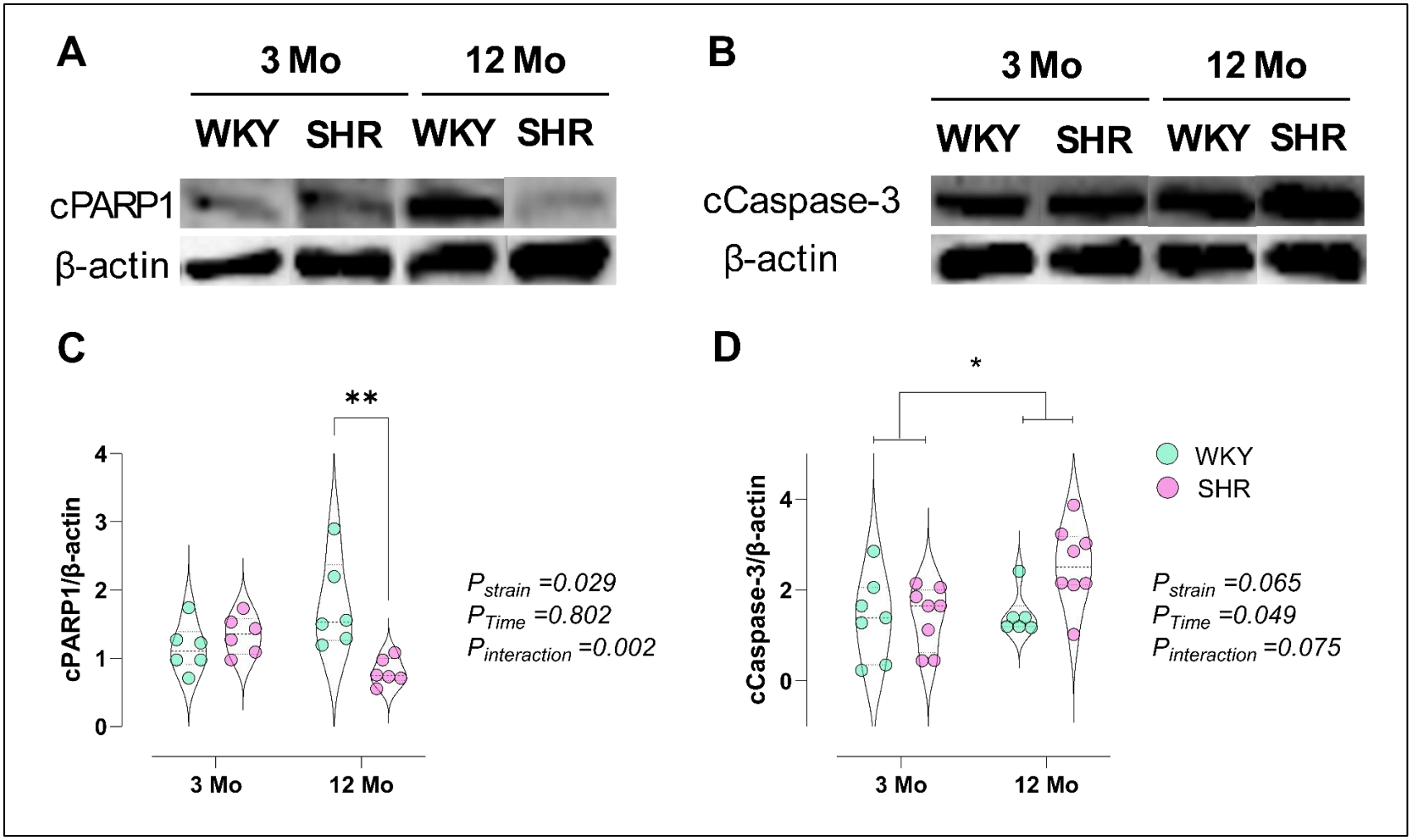

Figures 4.3A-D: Protein expression of the apoptotic markers including cleaved poly(ADP-Ribose) polymerase 1 (cPARP1, 43kDa), and cleaved caspase-3 (cCaspase-3, 17kDa) in LV tissue of 3- and 12-month-old normotensive WKYs and SHRs. In each immunoblot, β-actin (42kDa) was used as the loading control. Data expressed as mean ± SD. 2-way ANOVA with Tukey post hoc test. **P<0.0001 WKY vs SHR. *P=0.049 3 Mo vs 12 Mo.

4.3.8 Associations between mRNA expression of RUNX-1 with indices of LV remodelling, systolic and diastolic function, and gene expression in LV tissue

Figures 4.4: A volcano plot illustrating the associations between mRNA expression of runt-related transcription factor 1 *(RUNX-1)* with all cardiovascular indices including systolic and diastolic function, left ventricular geometry, gene and protein expression, and histological assessment of the LV. *RUNX-1* expression was not significantly associated with indices of diastolic (all $P > 0.05$) or systolic function including endFS (r=-0.24, P=0.206) and midFS (r=-0.31, P=0.096). However, *RUNX-1* expression demonstrated significant negative correlations with LVIDd (r=-0.57, P=0.001), LVIDs (r =-0.36, P=0.045), and with MMP9 expression (r=-0.48, P=0.013). Conversely, positive correlations were observed between *RUNX-1* and normalised heart mass (r=0.54, P=0.0009), liver mass (r=0.44, P=0.009), and LV mass (r=0.54, P<0.0001), as well as with LVPWTd (r=0.43, P=0.015), RWT (r=0.54, P=0.002), and the Bax/Bcl2 ratio (r=0.44, P=0.010). No significant associations were found between *RUNX-1* and cPARP1 (r=-0.331, P=0.123) or cCaspase-3 protein expression (r=-0.003, P=0.989).

In multivariable analyses adjusting for the confounding effect of SBP, *RUNX-1* expression remained positively associated with normalised heart mass (β [95% CI]: 4.983 [2.532 to 7.434]), LV mass: 7.442 [4.351 to 10.530], liver mass: 0.811 [0.487 to 1.135], and the Bax/Bcl2 ratio: 0.801 [0.060 to 1.541]. Additionally, *RUNX1* showed significant negative associations with LVIDd: -0.260 [-0.459 to -0.061] and MMP9 expression: -0.446 [-0.921 to 0.028], while maintaining a positive association with RWT: 0.912 [0.091 to 1.733]. After adjusting for SBP, associations with LVIDs: -0.166 [-0.420 to 0.088] and LVPWTd: 0.439 [-0.012 to 0.889] were no longer statistically significant.

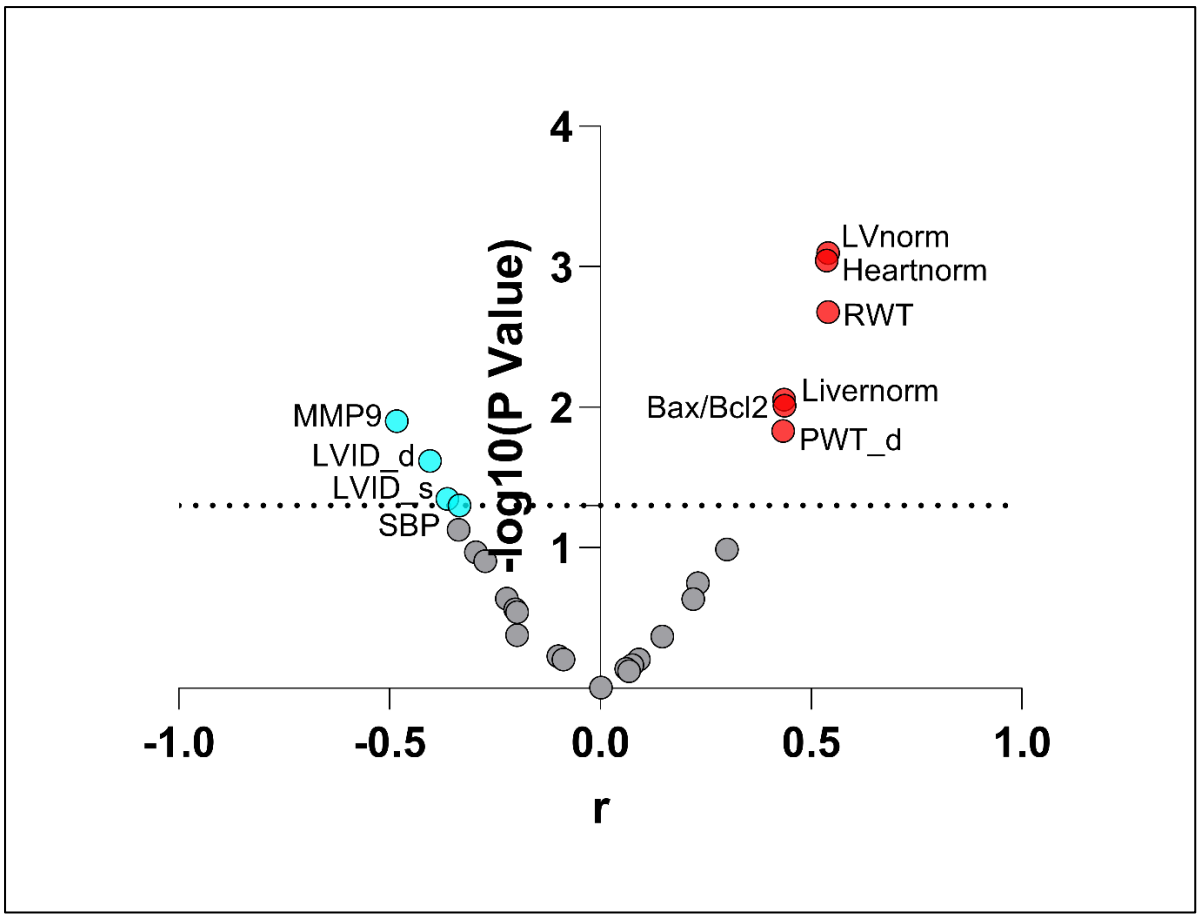

Figure 4.4: A volcano plot illustrating the associations between mRNA expression of runt-related transcription factor 1 with cardiovascular parameters, and gene expression in left ventricular tissue. The *x*-axis displays Pearson's correlation coefficient (*r*), whereas the *y*-axis shows the −log10(*P* value). Points above the horizontal dashed line [$-\log_{10}(P \text{ value}) = 1.30$, equivalent to $P = 0.05$] indicate statistically significant correlations. Red markers highlight variables with significant positive correlations with RUNX1. The turquoise markers represent variables with significant negative correlations with RUNX1. All variables exhibiting non-statistically significant associations with RUNX1 fall below the horizontal dashed line.

4.4 Discussion

In the present study, we determined the involvement of RUNX-1 in the transition to cardiac dilation in an animal model of hypertensive heart disease. SHRs exhibited significantly elevated systolic and diastolic BP at both 3 and 12 months, with SBP increasing over time. In SHRs, the greater normalised heart and LV mass, greater number of cardiomyocyte nuclei at 3-months-old, lower posterior wall thickness in diastole (PWTd), lower relative wall thickness (RWT), and the greater left ventricular internal diameter in diastole (LVIDd) at 12-months-old suggest the progression to eccentric remodeling or early cardiac dilation in aging SHRs, reflecting maladaptive structural changes in response to sustained hypertension. Functionally, diastolic performance was impaired in 12-month-old SHRs, as evidenced by the increased filling pressures (E/e'), decreased late peak tissue lengthening velocity at the lateral mitral annulus (a'), and the decreased early to late peak tissue lengthening velocity (e'/a'). Systolic function (endFS and midFS) was also impaired in hypertensive rats. At the molecular level, the gene expression of fibrotic markers was elevated in 12-month-old SHRs. The combination of reduced Bax, reduced cleaved PARP-1 and a trend toward a reduced Bax/Bcl-2 ratio and toward an elevated cleaved caspase-3 in 12-month-old SHRs represented a complex apoptotic signaling in the hypertensive heart. Taken together, 12-month-old SHRs exhibited ongoing maladaptive remodeling, predominantly fibrotic in nature, leading to a stiffer and less compliant left ventricle. This may have contributed to early dilation accompanied by diastolic dysfunction. RUNX-1 gene expression was downregulated with age and upregulated with hypertension, suggesting a hypertension-induced reactivation of the foetal gene program. Furthermore, RUNX-1 gene expression exhibited significant associations with cardiac structural parameters and apoptotic markers, including positive correlations with normalised LV mass, RWT, and Bax/Bcl-2 ratio, and negative correlations with LVID dimensions, and matrix

metalloproteinase-9 (MMP-9) expression. The associations remained after adjustment for SBP, suggesting that RUNX-1 is involved in structural changes independently of elevated blood pressure. The effect of RUNX-1 in cardiac remodeling in SHRs may extend beyond the haemodynamic impact of elevated blood pressure on the left ventricular wall. Taken together, these findings highlight the importance of RUNX-1 in structural, but not functional, changes in hypertensive heart disease progression.

SHRs are characterised by an early onset of hypertension and an increase in both systolic and diastolic BP with age (Rassler et al., 2022). Previous studies have consistently shown that hypertension begins between 7 and 15 weeks of age, and progresses over time in SHRs (Hawlitschek et al., 2022a, 2022b). At 3 months, SHRs already exhibit moderate-to-severe hypertension (Choisy et al., 2007), aligning with our findings. However, most prior studies have not examined these effects at the 12-month time point. Therefore, the present study demonstrated a continued rise in SBP from 3 to 12 months in SHRs, thereby highlighting the progressive nature of hypertension in SHRs. This longitudinal perspective may provide a more precise picture of disease development.

Between 3 and 7 months of age, SHRs exhibit a progressive and well-defined pattern of compensated LVH, driven by the sustained pressure overload (Slama et al., 2004). This response is mechanistically underpinned by La Place's law, which states that myocardial wall stress is directly proportional to intraventricular pressure and chamber size, but inversely proportional to wall thickness. Therefore, to normalise wall stress in response to elevated haemodynamic pressure overload, the myocardium increases wall thickness (Garvin et al., 2021), leading to concentric hypertrophy characterised by increased RWT and preserved or reduced chamber dimensions. Previous studies showed that 3-month-old SHRs already present with hypertension-induced

increases in myocardial wall thickness, particularly of the interventricular septum and posterior wall (Choisy et al., 2007; Slama et al., 2004), indicative of an adaptive hypertrophic response. In the present study, 3-month-old SHRs exhibited an increase in cardiomyocyte nuclei number, which may result from nuclear enlargement or polyploidy (Akins et al., 2024). These features are recognised as early indicators of cardiomyocyte hypertrophy and may reflect the onset of the hypertension-induced hypertrophic process. By 7 months of age, the hypertrophic phenotype becomes more pronounced, with further increases in left ventricular mass and wall thickness (Mkhize et al., 2024; Mkhize et al., 2025). This stage reflects a structural remodeling that serves to maintain cardiac output despite chronic haemodynamic stress.

Between 7 and 12 months of age, untreated chronic hypertension in SHRs causes the hypertrophic myocardium to undergo a pathological transition from compensated concentric LVH to eccentric remodeling, marking the onset of the maladaptive cardiac changes (Magubane et al., 2017). In the present study, we show that at 12 months of age, the SHRs exhibited LV structural changes consistent with early eccentric remodeling. Along with an age-related decline in normalised LV mass, SHRs maintained a greater normalised LV mass than WKY rats. With respect to the echocardiographic measurements, SHRs had thinner LVPWTd and a reduced RWT. With a larger sample size, the thinner LVPWTd and the reduction in RWT may prove to be specific to 12-month-old SHRs. Additionally, the increased LVIDd suggests an enlarged chamber. These findings may indicate a shift from hypertrophic growth to wall thinning and chamber dilation. In the literature, eccentric remodeling in SHRs has been consistently produced either with ageing, typically manifesting by 18 to 22 months (Badenhorst et al., 2003; Chan et al., 2011; Pfeffer et al., 1982), or via chronic β-adrenergic stimulation, which accelerates this phenotype to emerge as early as 12 to 15 months (Badenhorst et al., 2003; Magubane et al., 2017). In our 12-month-old SHRs, we

observed early signs of cardiac dilation, including increased LV cavity size and reduced RWT, placing our model at a transitional stage. This is consistent with previous work (Tamura et al., 1999), which identified reduced hypertrophic reserve by 6 months of age, suggesting that susceptibility to maladaptive remodeling may be present by 12 months of age.

Functionally, impairement in diastolic function typically begins in SHRs around 3 to 6 months of age (Cingolani et al., 2003; Nguyen et al., 2016), coinciding with the development of LVH. In the present study, Tissue Doppler imaging revealed lower atrial inflow velocities (A wave) with hypertension but no other differences were observed in 3-month-old SHRs, supporting the notion that diastolic dysfunction develops later in the disease course (Zile & Brutsaert, 2002). Indeed, diastolic dysfunction progresses with age in SHRs. The present data are consistent with what has been shown in the literature. The increase in late diastolic myocardial velocity (a') in 12-month-old SHRs suggests an enhanced atrial contribution to ventricular filling. The reduced e'/a' ratio in 12-month-old SHRs reflects impaired early diastolic relaxation, and the elevated E/e' ratio suggests increased LV filling pressures. The present study therefore demonstrates several alterations in diastolic function indicative of impaired ventricular relaxation, elevated filling pressures in 12-month-old SHRs, and a shift toward a less compliant or stiffer LV with greater reliance on atrial contraction for ventricular filling (Galderisi, 2011).

While diastolic dysfunction in SHRs is thought to precede the onset of overt systolic dysfunction or heart failure (Cingolani et al., 2003), the present study showed reduced systolic function with hypertension as indexed by the lower endFS and midFS. In addition, age results in an increased stroke volume but a decline in ejection fraction, suggesting that while the heart's output increased, its overall contractile efficiency diminished with age. These findings point to early systolic impairment in SHRs and age-related decline in global systolic performance. The observed age-

dependent changes in cardiac performance, characterised by higher stroke volume and lower ejection fraction in 12-month-old rats, may be attributed to an increase in chamber dimensions and reductions in contractile mass. An enlarged LV chamber allows the heart to produce a greater stroke volume although with reduced contractile efficiency, leading to a lower ejection fraction (Vakka et al., 2023). Indeed, similar to our observations at 12-months, cardiac dilation in SHRs was typically accompanied by progressive systolic dysfunction (Badenhorst et al., 2003; Chan et al., 2011; Magubane et al., 2017; Tamura et al., 1999).

In addition to the structural and functional changes, SHRs exhibited molecular changes suggestive of extracellular matrix (ECM) remodeling and altered apoptotic signaling at 12 months. In 12-month-old SHRs, elevated MMP-9 expression and a trend toward an increased Col1a1/Col3a1 ratio indicate active ECM remodeling with a shift toward a stiffer fibrotic matrix. The absence of changes in lysyl oxidase-1 (LOX1) expression suggests limited collagen cross-linking (Tjin et al., 2017), implying that the fibrotic response may be structurally immature. Correspondingly, the study did not show any changes in collagen content. Together, these findings reflect ongoing maladaptive remodeling that may have contributed to the established ventricular stiffness and dysfunction. Although total myocardial collagen content, as assessed histologically, was comparable across experimental groups, and the proportions of collagen phenotypes (Type I vs. Type III) and their ratio remained unchanged, previous work shows that these parameters do not appear to significantly contribute to myocardial stiffness or diastolic dysfunction in our model (Norton et al., 1997). Instead, collagen cross-linking mediated by LOX1 may play a more critical role in determining myocardial stiffness. However, in our study, LOX1 expression was evaluated only at the transcript level, which may not accurately reflect the extent of cross-linked, stiffer Type I collagen at the protein level. In this context, a collagen solubility assay, which is capable of

distinguishing between soluble and insoluble (cross-linked) collagen fractions may have provided a more direct and functional measure of collagen maturation and stiffness, thereby enhancing the interpretation of our findings. In 12-month-old SHRs, the downregulation of Bax and cleaved PARP-1, along with a reduced Bax/Bcl-2 ratio, suggests suppression of intrinsic apoptotic signaling. However, the trend toward increased cleaved caspase-3 indicates partial or alternative pathway activation. This mismatch implies dysregulated or incomplete apoptosis, potentially reflecting a chronic remodeling phase where cell survival mechanisms are favoured despite persistent stress signals. Apoptosis has been implicated as a central mechanism in the progression to eccentric remodeling; however, these observations may not be palpable during the pre-decompensatory phase at 12 months.

To better understand the mechanisms driving the structural and functional deterioration observed in SHRs at 12 months, we examined RUNX-1 expression as a potential molecular contributor to this cardiac remodeling. We surmise that this may provide a mechanistic link between the phenotypic changes with underlying transcriptional regulation. Our findings showed that RUNX-1 expression was elevated with hypertension, and the expression declined with age. In aged Wistar (7 months) rats, the production of RUNX-1 transcripts was significantly reduced compared to that in younger rats (2 months) (Song et al., 2023). This age-related reduction in transcript levels was accompanied by a corresponding age-related decrease in the overall RUNX-1 protein expression (Song et al., 2023). In our study, we extended this observation to 12 month-old normotensive and hypertensive rats, showing that cardiac-specific RUNX-1 downregulation is maintained with age in both strains. In Song et al. (2023), the older rats exhibited increased DNA methylation within the promoter regions of the RUNX-1 gene, suggesting that epigenetic regulation may contribute to the observed age-related decline in RUNX-1 expression. Notably, the pattern of promoter usage

shifted with age, as evidenced by changes in the ratio of mRNA derived from promoter 1 to promoter 2 (P1:P2), indicating that alternative promoter activation becomes more prominent in the aging heart. However, epigenetic influences on RUNX-1 expression that could explain the age-related decline in RUNX-1 expression in our study were beyond the scope of the present investigation.

For the first time in SHRs, our findings provide novel insights into the temporal dynamics of RUNX-1 expression in the hypertensive heart. Elevated expression of RUNX-1 in young SHRs may reflect an early compensatory or stress-responsive mechanism. Our study in SHRs confirms the pressure overload-induced upregulation of RUNX-1. Previous studies showed that RUNX-1 expression was upregulated in a rodent model of pressure overload achieved via transverse aortic constriction (TAC) (Ikeda et al., 2019; Zhang et al., 2021), and in neonatal rat cardiomyocytes in response to Ang II stimulation (Zhang et al., 2021). Beyond pressure overload, RUNX-1 is also increased in animal models of experimental myocardial infarction (MI) (Ikeda et al., 2019; McCarroll et al., 2018; Riddell et al., 2020), diabetic cardiomyopathy (Zhang et al., 2016), and dilated cardiomyopathy (Burke et al., 2016). These data and ours all point to an upregulation of RUNX-1 upon cardiac injury. However, the functional role that RUNX-1 may play in these pathological contexts has not been adequately described.

In addition to the observed patterns of RUNX-1 expression, we next explored its potential implications in cardiac remodeling and function. We showed that RUNX-1 expression was not significantly associated with direct measures of systolic or diastolic function. However, RUNX-1 showed strong correlations with structural parameters. Specifically, decreased RUNX-1 levels were associated with greater LVIDd and LVIDs, suggesting a link to dilated chamber geometry. RUNX-1 also correlated positively with normalised heart and liver mass, LV mass, PWTd, and

RWT, indicating a role in promoting hypertrophic growth. Additionally, RUNX-1 was positively associated with the Bax/Bcl-2 ratio, suggesting a potential influence on apoptotic signaling (Condorelli et al., 1999), and negatively associated with MMP-9 expression, implicating it in the regulation of ECM turnover (Bertrand-Philippe et al., 2004). Importantly, these associations largely persisted after adjusting for SBP, reinforcing the idea that RUNX-1 may contribute to cardiac remodeling independently of the haemodynamic load as previously shown (Ikeda et al., 2019; McCarroll et al., 2018; Riddell et al., 2020). The lack of associations between RUNX-1 expression and indices of myocardial function suggests that while RUNX-1 may influence structural remodeling, it does not directly affect cardiac performance. This raises the need for further research to explore how RUNX-1 interacts with other factors influencing heart function and to determine whether its effects are consistent across different stages of cardiac disease. Overall, these findings position RUNX-1 as a potential modulator of hypertrophic and fibrotic remodeling, rather than a direct determinant of contractile function, and highlight its relevance in the early compensatory phase of hypertensive heart disease.

4.5 Limitations

The present study was not without limitations. While histological assessment of collagen content is useful for visualising fibrosis, it does not accurately differentiate between phenotypes of collagen or stages of fibrosis, limiting its utility for detailed characterisation. Therefore, interpretation based on a combination of protein and gene expression measurements, two different levels of regulation, may give a misleading impression of the actual biological processes. Lastly, while our study provides valuable insights into the role of RUNX-1 in male SHRs, future investigations should include female SHRs to evaluate sex-specific differences and the influence of hormonal regulation on RUNX-1 expression and cardiac remodeling. This would enhance the

generalisability of our findings and provide a more comprehensive understanding of the role of RUNX-1 in hypertensive heart disease across sexes.

4.6 Conclusions

Our study positions RUNX-1 as a potential novel marker in hypertensive rats, revealing its significant role in hypertension-induced cardiac remodeling. RUNX-1 expression was positively associated with markers of concentric cardiac remodeling. Over time, RUNX-1 expression progressively declined, coinciding with a transition from concentric to eccentric remodeling in SHR. This temporal decrease in RUNX-1 expression appears to be linked to the shift in remodeling phenotype observed in SHR. Mechanistically, if chronic pressure overload or a genetic predisposition initiates a cellular repair response that leads to apoptosis, and if the heart's capacity to repair itself is surpassed, the positive correlation between RUNX-1 and Bax/Bcl-2 ratio, and negative associations with MMP-9 expression, may highlight a potential compensatory mechanism. Enhancing these protective mechanisms or inhibiting apoptosis could be a promising strategy to prevent the progression from compensated LVH to decompensated heart failure, where myocardial function declines irreversibly. Thus, targeting RUNX-1 could offer novel therapeutic opportunities in managing heart failure. In conclusion, our findings underscore a putative role of RUNX-1 as a therapeutic target for modulating structural changes in hypertensive heart disease, though further mechanistic studies are warranted to confirm its clinical relevance and explore its interactions with other determinants of cardiac function.

Chapter 5

5.1 Summary of findings, limitations, and future research directions

According to the NIH Biomarkers Definitions Working Group, a biomarker is defined as a characteristic that is objectively measured and evaluated as an indicator of normal biological processes, pathogenic processes, or pharmacologic responses to a therapeutic intervention (Ahmad et al., 2023; Strimbu & Tavel, 2010). In the context of heart disease, previous work has yielded substantial insights into disease pathophysiology (Frak et al., 2022). However, these advances have not translated into a proportional expansion of therapeutic options, largely due to persistent challenges in identifying novel molecular targets (Sharma et al., 2024). This therapeutic stagnation is compounded by the considerable phenotypic heterogeneity of heart failure (Udelson & Stevenson, 2016), which may obscure mechanistic clarity. In the setting of pressure overload-induced myocardial remodelling and dysfunction, a valuable biomarker is generally expected to possess the following critical attributes (Navanandan et al., 2023); (1) high sensitivity and specificity to detect early and subtle alterations in cardiac structure and function; (2) temporal relevance, whereby its expression precedes or coincides with the onset of pathological changes; and (3) biological plausibility, meaning the biomarker is mechanistically linked to the underlying pathophysiology. Lastly, (4) to demonstrate its translational potential, a valuable biomarker should exhibit reproducibility across experimental replicates and, where feasible, across different animal models (Singh & Bisserier, 2025).

As such, when a biomarker satisfies criteria 1 through 4, its relevance to human pathophysiology may become more compelling. Accordingly, this chapter examines the contribution of the potential novel biomarkers identified in the empirical chapters, by evaluating their alignment with the proposed criteria for translational relevance in cardiac pathophysiology.

5.2 Pentraxin-3

5.2.1 Summary of findings

In the present thesis, PTX3 was selected for evaluation due to its role in cardiovascular inflammation and tissue remodelling (Carrizzo et al., 2015), making it a promising candidate biomarker in pressure-overload cardiac pathology. In **chapter 2,** our data showed that circulating concentrations of PTX-3 were increased in SHRs and were positively correlated with SBP, indicating a link to the hypertensive state. Mechanistically, we showed that PTX-3 may act as a locally produced inflammatory mediator released during tissue injury and repair. The association between PTX-3 and VCAM-1, alongside the lack of changes in PTX-3 cardiac gene expression and lack of associations with indices of LVH suggest that PTX-3 serves more as a marker of systemic vascular inflammation and endothelial activation rather than as a direct mediator of myocardial hypertrophy. Indeed, the absence of an association between PTX-3 and systolic wall stress further indicates that PTX-3 may not influence the mechanical adaptation of the myocardium to pressure overload. Interestingly, antihypertensive treatment modulated PTX-3 concentrations. In this respect, both captopril and hydralazine reduced circulating PTX-3 concentrations, demonstrating that PTX-3 responds to changes in blood pressure.

PTX-3 demonstrated several attributes consistent with a valuable biomarker in pressure-overload cardiac pathology. PTX-3 showed sensitivity by reliably increasing in response to hypertensive stress in our SHR model similar to what has been shown in other models of pressure overload (Alp et al., 2019; Parlak, Aydogan, et al., 2012), though its specificity may be limited due to its broader role in systemic inflammation (Magrini et al., 2016). The temporal relevance of PTX-3 was evident through the sustained elevation in 7-month-old SHRs, a stage of accelerated disease progression (Li et al., 2024; Ristagno et al., 2019), aligning with findings in cardiac events in

human studies (Jenny et al., 2009). The biological plausibility of PTX-3 is supported by its mechanistic involvement in inflammation (Kunes et al., 2012), vascular dysfunction (Presta et al., 2007), and tissue remodelling (Napoleone et al., 2002). In summary, PTX-3 satisfied three out of four attributes for a valuable biomarker in pressure-overload cardiac pathology; namely, sensitivity, temporal relevance, and biological plausibility, while showing limitations in specificity. We surmise that these features, observed across both experimental and clinical contexts, may highlight the translational potential of PTX-3, particularly when interpreted within a defined pathological framework or used alongside complementary markers.

5.3 MicroRNAs

5.3.1 Summary of findings

In **chapter 3**, our study identified distinct patterns of miRNA regulation associated with hypertensive cardiac pathology in SHRs. MiRNAs were assessed due to their emerging role as key post-transcriptional regulators of gene expression involved in cardiovascular development, homeostasis, and disease (Liu & Olson, 2010). To this end, the expression patterns and relative contributions of miR-146a-5p, -29b-5p, and -155-5p in hypertensive cardiac pathology remained underexplored, particularly in the SHR model which closely mimics human essential hypertension. While other miRNAs exist, these were prioritised due to their novelty and translational potential. In the context of hypertensive heart disease, miRNAs have been shown to modulate critical processes such as inflammation (Sufianov et al., 2025), fibrosis (Melman et al., 2014), hypertrophy (Da Costa Martins & De Windt, 2012), and endothelial dysfunction (Nemecz et al., 2016). In concert with these studies, our data showed that cardiomyocyte expression of miR-146a-5p was upregulated in response to pressure-overload, correlating with markers of endothelial activation (VCAM-1), concentric LVH, diastolic dysfunction, and reactive fibrosis. In contrast, miR-155-5p

expression was reduced in female rats regardless of strain, and positively associated with heart and kidney mass, as well as stroke volume, suggesting a potential role in cardiac growth and function. Moderation analysis indicated that miR-146a-5p may modulate the relationship between VCAM-1 and macrophage infiltration independently of elevations in systolic blood pressure. No changes in miR-29b-5p were observed. Taken together, these findings highlight the regulatory role of miRNAs in cardiac remodelling and inflammation, offering mechanistic insight into their potential as biomarkers in hypertensive heart disease.

In this study, miR-146a-5p demonstrated several key attributes of a promising biomarker in pressure-overload induced cardiac pathology. MiR-146a-5p showed sensitivity, with consistent upregulation in SHRs and strong associations with pathological features such as concentric LVH, diastolic dysfunction, myocardial fibrosis, endothelial activation (VCAM-1), oxidative stress (SOD2), and inflammation (NFKBIA, macrophage infiltration). These associations remained significant even after adjusting for systolic blood pressure, suggesting that miR-146a-5p reflects underlying disease mechanisms beyond haemodynamic stress. Additionally, the biological plausibility of miR-146a-5p is supported by its known regulatory role in the NF-κB pathway (Lei et al., 2021) and redox balance (Cui et al., 2016) which are both central to cardiac remodelling. However, in terms of specificity, miR-146a-5p may be less clear-cut. In this regard, the pleiotropic nature of miR-146a-5p, with expression across multiple cardiac and immune cell types and involvement in diverse cellular processes (Shimada et al., 2020), complicates its interpretation as a disease-specific marker. Our inability to localise its expression to a specific cardiac cell type in this study further limits conclusions about tissue specificity. Despite this, the temporal relevance of miR-146a-5p is implied by its association with both structural and functional indices of remodelling in 7-month-old SHRs, a stage when LV concentric hypertrophy is established,

suggesting it coincides with the development of cardiac remodelling (Ntelios et al., 2021). Taken together, these features support its translational potential, particularly as a mechanistic biomarker of maladaptive remodelling, though its utility may be enhanced when used in combination with more specific markers. In contrast, despite evidence in other animal models (Heymans et al., 2013; Seok et al., 2014) and human studies (Sassi et al., 2017; Zhang et al., 2025), miR-155-5p and -29b-5p showed a more limited profile. MiR-155-5p expression did not differ significantly between hypertensive and normotensive rats and lacked consistent associations with structural indices of cardiac remodelling. In the present study, while miR-155-5p was linked to stroke volume and some inflammatory and fibrotic markers, these findings were context-dependent and did not meet the criteria for sensitivity, reproducibility, or broad applicability. In summary, among the miRNAs evaluated, miR-146a-5p emerged as the most promising biomarker in pressure-overload induced cardiac pathology, satisfying three out of four attributes. In contrast, miR-155-5p and miR-29b-5p exhibited a more limited biomarker profile in this model. This may be due to weaker or context-dependent associations with key pathological features of cardiac remodelling. While these miRNAs may still hold context-specific or cell-type–dependent relevance, their current performance in our SHR model does not support their use as robust standalone biomarkers for pressure-overload cardiac pathology. Further investigation is warranted to determine whether their utility may emerge under different experimental conditions, disease stages, or in combination with other molecular markers. Given the vast diversity of miRNAs and their context-dependent expression, their regulatory roles are highly dynamic and complex. MiRNAs can target multiple genes and often act together in networks, making it challenging to isolate the effects of individual miRNAs. This highlights the need for integrative approaches to fully understand their collective impact in specific biological settings.

5.4 RUNX-1

5.4.1 Summary of findings

In **chapter 4**, we investigated the role of RUNX-1 in the progression to cardiac dilation in SHRs with sustained hypertension measured at 3 and 12 months of age. RUNX-1 is a transcription factor traditionally associated with haematopoiesis (Lam & Zhang, 2012) and oncogenesis (X. Chen et al., 2024), but emerging evidence suggests its involvement in cardiovascular biology (Suzuki et al., 2023), particularly in stress-induced gene regulation and fibrosis (Qi et al., 2023). In our study, structural and functional assessments revealed signs of maladaptive remodelling, including increased LV mass, reduced wall thickness, and impaired systolic and diastolic function, particularly at 12 months. Molecular analysis showed elevated fibrotic markers and complex apoptotic signalling. RUNX-1 expression was downregulated with age but upregulated in response to hypertension, suggesting reactivation of the foetal gene program. Importantly, its expression correlated with structural parameters and apoptotic markers independently of blood pressure, indicating a role in remodelling beyond haemodynamic stress. Overall, in our study RUNX-1 appears to contribute to structural changes, but we lacked evidence linking it to functional impairments. One possible explanation for this observation is that the effects of RUNX-1 may be confined to cellular architecture and ECM turnover, without directly influencing global myocardial function. Indeed, by corollary, recent evidence suggests that while RUNX-1 can activate cardiomyocyte cell cycling, it is not essential for this process, indicating a modulatory rather than a central role in myocardial regeneration or dysfunction (Akins et al., 2024).

In the present thesis, RUNX-1 demonstrated several attributes of a valuable biomarker in the context of hypertensive cardiac remodelling. The biological plausibility of RUNX-1 is supported by its known role in gene regulation (Bertran et al., 2022), hypertrophic signalling (Zhang et al.,

2021), apoptosis (Ma et al., 2024), and ECM turnover (Bertrand-Philippe et al., 2004; Guo et al., 2023; Koth et al., 2020), processes central to structural cardiac adaptation. RUNX-1 expression was sensitive to pressure overload, being elevated in SHRs compared to normotensive controls, and showed temporal relevance by declining with age, consistent with a transient reactivation of the foetal gene program during early cardiac dilation. Importantly, RUNX-1 expression correlated positively with structural indices such as normalised LV mass, relative wall thickness, and the Bax/Bcl-2 ratio, and negatively with LVIDd and MMP-9 expression. These associations remained significant after adjusting for systolic blood pressure, suggesting that RUNX-1 contributes to structural remodelling independently of haemodynamic load. While these findings support its mechanistic relevance, once again, specificity remains a limitation. For example, because RUNX-1 is upregulated in various cardiac injury models, including myocardial infarction (Li et al., 2019; Martin et al., 2022; McCarroll et al., 2018) and diabetic cardiomyopathy (Zhang et al., 2016), indicating that its expression may reflect a generalised cardiac stress response rather than a hypertensive-specific signature. Nonetheless, its consistent association with structural, but not functional, deterioration in SHRs highlights its potential as a translational biomarker of early maladaptive remodelling. In summary, RUNX-1 satisfied three out of four attributes for a valuable biomarker in the context of hypertensive cardiac remodelling. We believe that when interpreted alongside functional and inflammatory markers, RUNX-1 may serve as a complementary indicator of disease progression in hypertensive heart disease.

5.5 Limitations

In the present thesis, there are several limitations that should be acknowledged. While circulating PTX-3 levels were associated with systolic blood pressure, causality could not be established, and PTX-3 protein expression within cardiac tissue was not assessed. Additionally, the absence of

tissue and pulsed doppler imaging limited the evaluation of diastolic function, and renal structural changes were not characterised beyond eGFR, which may have provided further insight into PTX-3 expression in chapter 2. Our investigation also focused on a select group of miRNAs including miR-146a-5p, miR-155-5p, and miR-29b-5p potentially overlooking other relevant miRNAs. Moreover, to overcome the technical limitations of RT-PCR in miRNA discovery, advanced techniques such as small RNA sequencing (Wake et al., 2016) or digital droplet PCR (Cirillo et al., 2020) could improve detection accuracy and broaden biomarker discovery. The mechanisms driving the altered expression of these miRNAs remain unclear, and our studies did not experimentally confirm whether they directly bind to and regulate their predicted target genes based on sequence matching. This means that while our web-based computational tools suggested potential gene targets through base-pair complementarity, these interactions were not validated in this study. Moreover, the oestrous cycle was not monitored in female rats, which may have clarified the observed sex-specific differences in miR-155-5p expression. It is also possible that miR-155-5p and hormonal fluctuations across the oestrous cycle interact, rather than act independently. With the use of advanced bioinformatic tools, such as integrative multi-omics and network-based analyses, future studies may uncover regulatory links between sex hormones and miRNA expression, offering deeper insight into sex-specific cardiac remodelling mechanisms. For RUNX-1, while histological assessment of fibrosis was informative, it lacks the resolution to distinguish collagen phenotypes or stages of fibrosis, and interpretation based on gene expression alone did not fully capture the biological complexity of its involvement in early-stage cardiac dilation. Additionally, RUNX-1 expression was evaluated in the present thesis only in male SHRs, limiting the generalisability of our findings across sexes. Finally, as with all preclinical studies, the translational relevance of the studied novel biomarkers requires validation in human cohorts.

5.6 Future research directions

Future research should aim to refine and validate the identified biomarkers by explicitly assessing their performance against established criteria. In this study, miR-146a-5p, RUNX-1, and PTX-3 each satisfied three out of four attributes for sensitivity, temporal relevance, and biological plausibility, though all showed limitations in specificity. These biomarkers may be considered promising, particularly when used in combination with more specific indicators. In contrast, miR-155-5p and miR-29b-5p satisfied only temporal relevance and biological plausibility and therefore may not be suitable as standalone biomarkers. Future studies should validate these findings in human cohorts, clarify tissue and cellular specificity, and explore mechanistic roles through functional studies. Expanding the biomarker panel and employing high-throughput approaches may enhance diagnostic precision and deepen our understanding of hypertensive heart disease.

5.7 Conclusions

In conclusion, this thesis provides novel insights into the molecular and structural mechanisms underlying hypertensive heart disease, with a particular focus on the biomarker potential of PTX-3, miRNAs, and RUNX-1. While PTX-3 was associated with systolic blood pressure, it did not independently predict the development of concentric LVH, highlighting a dissociation between systemic inflammation and structural cardiac remodelling. This finding challenges the specificity of PTX-3 as a biomarker for hypertensive LVH and underscores the complexity of its pathogenesis. Of the three miRNAs studied, only miR-146a-5p showed promise, satisfying 3 out of 4 biomarker attributes, while miR-155-5p and miR-29b-5p demonstrated limited and inconsistent profiles. Overall, the findings suggest that the selected miRNAs are unreliable as biomarkers in this model, and the resource-intensive nature of miRNA screening makes broad exploratory approaches impractical for biomarker development in hypertensive heart disease. Additionally, RUNX-1 was

identified as a novel marker of structural remodelling, with expression patterns linked to early cardiac dilation and apoptotic signalling, independent of haemodynamic load. Although RUNX-1 did not correlate with functional impairment, its mechanistic relevance and consistent structural associations position it as a potential therapeutic target. Collectively, these findings advance our understanding of the molecular drivers of hypertensive cardiac remodelling and highlight the importance of integrating inflammatory, genetic, and structural markers to improve the diagnosis and management of hypertensive heart disease.

References

Adamo, L., Rocha-Resende, C., Prabhu, S. D., & Mann, D. L. (2020). Reappraising the role of inflammation in heart failure. *Nat Rev Cardiol*, *17*(5), 269-285. https://doi.org/10.1038/s41569-019-0315-x

Ahmad, A., Imran, M., & Ahsan, H. (2023). Biomarkers as Biomedical Bioindicators: Approaches and Techniques for the Detection, Analysis, and Validation of Novel Biomarkers of Diseases. *Pharmaceutics*, *15*(6). https://doi.org/10.3390/pharmaceutics15061630

Akins, K. A., Flinn, M. A., Swift, S. K., Chanjeevaram, S. V., Purdy, A. L., Buddell, T., Kolell, M. E., Andresen, K. G., Paddock, S., Buday, S. L., Veldman, M. B., O'Meara, C. C., & Patterson, M. (2024). Runx1 is sufficient but not required for cardiomyocyte cell-cycle activation. *Am J Physiol Heart Circ Physiol*, *327*(2), H377-H389. https://doi.org/10.1152/ajpheart.00782.2023

Al-Gburi, S., Deussen, A. J., Galli, R., Muders, M. H., Zatschler, B., Neisser, A., Muller, B., & Kopaliani, I. (2017). Sex-specific differences in age-dependent progression of aortic dysfunction and related cardiac remodeling in spontaneously hypertensive rats. *Am J Physiol Regul Integr Comp Physiol*, *312*(5), R835-R849. https://doi.org/10.1152/ajpregu.00231.2016

Alowais, S. A., Alghamdi, S. S., Alsuhebany, N., Alqahtani, T., Alshaya, A. I., Almohareb, S. N., Aldairem, A., Alrashed, M., Bin Saleh, K., Badreldin, H. A., Al Yami, M. S., Al Harbi, S., & Albekairy, A. M. (2023). Revolutionizing healthcare: the role of artificial intelligence in clinical practice. *BMC Med Educ*, *23*(1), 689. https://doi.org/10.1186/s12909-023-04698-z

Alp, C., Dogru, M. T., Karadeniz, M., Sarak, T., Demir, V., Celik, Y., Kandemir, H., & Kisa, U. (2019). Serum pentraxin-3 levels and flow-mediated dilation in dipper and non-dipper hypertension. *J Clin Lab Anal*, *33*(3), e22718. https://doi.org/10.1002/jcla.22718

Amara, V. R., Surapaneni, S. K., & Tikoo, K. (2019). Metformin attenuates cardiovascular and renal injury in uninephrectomized rats on DOCA-salt: Involvement of AMPK and miRNAs in cardioprotection. *Toxicol Appl Pharmacol*, *362*, 95-104. https://doi.org/10.1016/j.taap.2018.10.004

An, R., Feng, J., Xi, C., Xu, J., & Sun, L. (2018). miR-146a Attenuates Sepsis-Induced Myocardial Dysfunction by Suppressing IRAK1 and TRAF6 via Targeting ErbB4 Expression. *Oxid Med Cell Longev*, *2018*, 7163057. https://doi.org/10.1155/2018/7163057

Anderson, C. E., Hamm, L. L., Batuman, G., Kumbala, D. R., Chen, C. S., Kallu, S. G., Siriki, R., Gadde, S., Kleinpeter, M. A., Krane, N. K., Simon, E. E., He, J., & Chen, J. (2018). The association of angiogenic factors and chronic kidney disease. *BMC Nephrol*, *19*(1), 117. https://doi.org/10.1186/s12882-018-0909-2

Andronic AA, M. S., Cinteza M. (2016). Heart Failure with Mid-Range Ejection Fraction – a New Category of Heart Failure or Still a Gray Zone. *Maedica (Bucur)*, *11*(4), 320-324.

Azevedo, P. S., Polegato, B. F., Minicucci, M. F., Paiva, S. A., & Zornoff, L. A. (2016). Cardiac Remodeling: Concepts, Clinical Impact, Pathophysiological Mechanisms and Pharmacologic Treatment. *Arq Bras Cardiol*, *106*(1), 62-69. https://doi.org/10.5935/abc.20160005

Badenhorst, D., Veliotes, D., Maseko, M., Tsotetsi, O. J., Brooksbank, R., Naidoo, A., Woodiwiss, A. J., & Norton, G. R. (2003). Beta-adrenergic activation initiates chamber dilatation in concentric hypertrophy. *Hypertension*, *41*(3), 499-504. https://doi.org/10.1161/01.HYP.0000056601.29613.DD

Barringhaus, K. G., & Zamore, P. D. (2009). MicroRNAs: regulating a change of heart. *Circulation*, *119*(16), 2217–2224. https://doi.org/https://doi.org/10.1161/CIRCULATIONAHA.107.715839

Beaumont, J., Lopez, B., Ravassa, S., Hermida, N., San Jose, G., Gallego, I., Valencia, F., Gomez-Doblas, J. J., de Teresa, E., Diez, J., & Gonzalez, A. (2017). MicroRNA-19b is a potential biomarker of increased myocardial collagen cross-linking in patients with aortic stenosis and heart failure. *Sci Rep*, *7*, 40696. https://doi.org/10.1038/srep40696

Bennett, M. R. (2002). Apoptosis in the cardiovascular system. *Heart (British Cardiac Society)*, *87*(5), 480–487. https://doi.org/https://doi.org/10.1136/heart.87.5.480

Bernardo, B. C., Ooi, J. Y. Y., & McMullen, J. R. (2012). The yin and yang of adaptive and maladaptive processes in heart failure. *Drug Discovery Today: Therapeutic Strategies*, *9*(4), e163-e172. https://doi.org/10.1016/j.ddstr.2013.10.001

Bertran, L., Eigbefoh-Addeh, A., Portillo-Carrasquer, M., Barrientos-Riosalido, A., Binetti, J., Aguilar, C., Ugarte Chicote, J., Bartra, H., Artigas, L., Coma, M., Richart, C., & Auguet, T. (2022). Identification of the Potential Molecular Mechanisms Linking RUNX1 Activity with Nonalcoholic Fatty Liver Disease, by Means of Systems Biology. *Biomedicines*, *10*(6). https://doi.org/10.3390/biomedicines10061315

Bertrand-Philippe, M., Ruddell, R. G., Arthur, M. J., Thomas, J., Mungalsingh, N., & Mann, D. A. (2004). Regulation of tissue inhibitor of metalloproteinase 1 gene transcription by RUNX1 and RUNX2. *J Biol Chem*, *279*(23), 24530-24539. https://doi.org/10.1074/jbc.M311804200

Bhupathy, P., Haines, D., & Leinwand, L. (2010). Influence of sex hormones and phytoestrogens on heart disease in men and women. *Women's Health*, *6*(1), 77-95. https://doi.org/https://doi.org/10.2217/WHE.0

Bidani, A. K., & Griffin, K. A. (2004). Pathophysiology of hypertensive renal damage: implications for therapy. *Hypertension*, *44*(5), 595-601. https://doi.org/10.1161/01.HYP.0000145180.38707.84

Bodaghi, A., Fattahi, N., & Ramazani, A. (2023). Biomarkers: Promising and valuable tools towards diagnosis, prognosis and treatment of Covid-19 and other diseases. *Heliyon*, *9*(2), e13323. https://doi.org/10.1016/j.heliyon.2023.e13323

Bottazzi, B., Inforzato, A., Messa, M., Barbagallo, M., Magrini, E., Garlanda, C., & Mantovani, A. (2016). The pentraxins PTX3 and SAP in innate immunity, regulation of inflammation and tissue remodelling. *J Hepatol*, *64*(6), 1416-1427. https://doi.org/10.1016/j.jhep.2016.02.029

Braunwald, E. (2015). The war against heart failure: the Lancet lecture. *Lancet*, *385*(9970), 812-824. https://doi.org/10.1016/S0140-6736(14)61889-4

Buda, V., Andor, M., Cristescu, C., Voicu, M., Cochera, F., Tuduce, P., Petrescu, L., & Tomescu, M. C. (2017). The effect of candesartan on pentraxin-3 plasma levels as marker of

endothelial dysfunction in patients with essential arterial hypertension. *Ir J Med Sci*, *186*(3), 621-629. https://doi.org/10.1007/s11845-017-1580-5

Burke, M. A., Chang, S., Wakimoto, H., Gorham, J. M., Conner, D. A., Christodoulou, D. C., Parfenov, M. G., DePalma, S. R., Eminaga, S., Konno, T., Seidman, J. G., & Seidman, C. E. (2016). Molecular profiling of dilated cardiomyopathy that progresses to heart failure. *JCI Insight*, *1*(6). https://doi.org/10.1172/jci.insight.86898

Bytyci, I., & Bajraktari, G. (2015). Mortality in heart failure patients. *Anatol J Cardiol*, *15*(1), 63-68. https://doi.org/10.5152/akd.2014.5731

Camozzi, M., Rusnati, M., Bugatti, A., Bottazzi, B., Mantovani, A., Bastone, A., Inforzato, A., Vincenti, S., Bracci, L., Mastroianni, D., & Presta, M. (2006). Identification of an antiangiogenic FGF2-binding site in the N terminus of the soluble pattern recognition receptor PTX3. *J Biol Chem*, *281*(32), 22605-22613. https://doi.org/10.1074/jbc.M601023200

Cappuccio, F. P., & Miller, M. A. (2016). Cardiovascular disease and hypertension in sub-Saharan Africa: burden, risk and interventions. *Intern Emerg Med*, *11*(3), 299-305. https://doi.org/10.1007/s11739-016-1423-9

Carrizzo, A., Lenzi, P., Procaccini, C., Damato, A., Biagioni, F., Ambrosio, M., Amodio, G., Remondelli, P., Del Giudice, C., Izzo, R., Malovini, A., Formisano, L., Gigantino, V., Madonna, M., Puca, A. A., Trimarco, B., Matarese, G., Fornai, F., & Vecchione, C. (2015). Pentraxin 3 Induces Vascular Endothelial Dysfunction Through a P-

selectin/Matrix Metalloproteinase-1 Pathway. *Circulation*, *131*(17), 1495-1505; discussion 1505. https://doi.org/10.1161/CIRCULATIONAHA.114.014822

Carthew, R. W., & Sontheimer, E. J. (2009). Origins and Mechanisms of miRNAs and siRNAs. *Cell*, *136*(4), 642-655. https://doi.org/10.1016/j.cell.2009.01.035

Chan, V., Fenning, A., Levick, S. P., Loch, D., Chunduri, P., Iyer, A., Teo, Y. L., Hoey, A., Wilson, K., Burstow, D., & Brown, L. (2011). Cardiovascular changes during maturation and ageing in male and female spontaneously hypertensive rats. *Journal of Cardiovascular Pharmacology*, *57*(4), 469–478. https://doi.org/https://doi.org/10.1097/FJC.0b013e3182102c3b

Chan, V., Fenning, A., Hoey, A., & Brown, L. (2011). Chronic β-adrenoceptor antagonist treatment controls cardiovascular remodeling in heart failure in the aging spontaneously hypertensive rat. *Journal of Cardiovascular Pharmacology*, *58*(4), 424–431. https://doi.org/https://doi.org/10.1097/FJC.0b013e3182283c78

Charan, J., & Biswas, T. (2013). How to calculate sample size for different study designs in medical research? *Indian J Psychol Med*, *35*(2), 121-126. https://doi.org/10.4103/0253-7176.116232

Charkoudian, N., & Rabbitts, J. A. (2009). Sympathetic neural mechanisms in human cardiovascular health and disease. *Mayo Clinic proceedings*, *84*(9), 822–830. https://doi.org/https://doi.org/10.4065/84.9.822

Chen, H., Wang, S., Zhang, X., Hua, X., Liu, M., Wang, Y., Wu, S., & He, W. (2024). Pharmacological inhibition of RUNX1 reduces infarct size after acute myocardial

infarction in rats and underlying mechanism revealed by proteomics implicates repressed cathepsin levels. *Funct Integr Genomics*, *24*(3), 113. https://doi.org/10.1007/s10142-024-01391-2

Chen, J. S., Pei, Y., Li, C. E., Li, Y. N., Wang, Q. Y., & Yu, J. (2020). Comparative efficacy of different types of antihypertensive drugs in reversing left ventricular hypertrophy as determined with echocardiography in hypertensive patients: A network meta-analysis of randomized controlled trials. *J Clin Hypertens (Greenwich)*, *22*(12), 2175-2183. https://doi.org/10.1111/jch.14047

Chen, R., Zhang, H., Tang, B., Luo, Y., Yang, Y., Zhong, X., Chen, S., Xu, X., Huang, S., & Liu, C. (2024). Macrophages in cardiovascular diseases: molecular mechanisms and therapeutic targets. *Signal Transduct Target Ther*, *9*(1), 130. https://doi.org/10.1038/s41392-024-01840-1

Chen, S. X., Song, T., Zhou, S. H., Liu, Y. H., Wu, S. J., & Liu, L. Y. (2008). Protective effects of ACE inhibitors on vascular endothelial dysfunction induced by exogenous advanced oxidation protein products in rats. *Eur J Pharmacol*, *584*(2-3), 368-375. https://doi.org/10.1016/j.ejphar.2008.02.020

Chen, W., Liu, Y., Pan, H., Jiang, J., Xiang, H., & Peng, L. (2021). Correlation between single nucleotide polymorphisms in the 3 primer untranslated region of PTX3 and the risk of essential hypertension: A case-control study. *Medicine (Baltimore)*, *100*(24), e25937. https://doi.org/10.1097/MD.0000000000025937

Chen, W., Zhuang, Y. S., Yang, C. X., Fang, Z. C., Liu, B. Y., Zheng, X., & Liao, Y. Y. (2021). The Protective Role of the Long Pentraxin PTX3 in Spontaneously Hypertensive Rats with Heart Failure. *Cardiovasc Toxicol*, *21*(10), 808-819. https://doi.org/10.1007/s12012-021-09671-0

Chen, X., Wang, L., Yang, M., Zhao, W., Tu, J., Liu, B., & Yuan, X. (2024). RUNX transcription factors: biological functions and implications in cancer. *Clin Exp Med*, *24*(1), 50. https://doi.org/10.1007/s10238-023-01281-0

Choisy, S. C., Arberry, L. A., Hancox, J. C., & James, A. F. (2007). Increased susceptibility to atrial tachyarrhythmia in spontaneously hypertensive rat hearts. *Hypertension*, *49*(3), 498-505. https://doi.org/10.1161/01.HYP.0000257123.95372.ab

Cingolani, O. H., Yang, X. P., Cavasin, M. A., & Carretero, O. A. (2003). Increased systolic performance with diastolic dysfunction in adult spontaneously hypertensive rats. *Hypertension*, *41*(2), 249-254. https://doi.org/10.1161/01.hyp.0000052832.96564.0b

Cirillo, P. D. R., Margiotti, K., Mesoraca, A., & Giorlandino, C. (2020). Quantification of circulating microRNAs by droplet digital PCR for cancer detection. *BMC Res Notes*, *13*(1), 351. https://doi.org/10.1186/s13104-020-05190-3

Condorelli, G., Morisco, C., Stassi, S., Notte, A., Farina, F., Sgaramella, G., de Rienzo, A., Roncarati, R., Trimarco, B., & Lembo, G. (1999). Increased Cardiomyocyte Apoptosis and Changes in Proapoptotic and Antiapoptotic Genes bax and bcl-2 During Left Ventricular Adaptations to Chronic Pressure Overload in the Rat. *Circulation*, *99*(23), 3071-3078. https://doi.org/https://doi.org/10.1161/01.CIR.99.23.3071

Constantin, A., Comarita, I. K., Alexandru, N., Filippi, A., Bojin, F., Gherghiceanu, M., Vilcu, A., Nemecz, M., Niculescu, L. S., Paunescu, V., & Georgescu, A. (2022). Stem cell-derived extracellular vesicles reduce the expression of molecules involved in cardiac hypertrophy-In a model of human-induced pluripotent stem cell-derived cardiomyocytes. *Front Pharmacol*, *13*, 1003684. https://doi.org/10.3389/fphar.2022.1003684

Crooke, S. T., Witztum, J. L., Bennett, C. F., & Baker, B. F. (2018). RNA-Targeted Therapeutics. *Cell Metab*, *27*(4), 714-739. https://doi.org/10.1016/j.cmet.2018.03.004

Cuenca-Zamora, E. J., Guijarro-Carrillo, P. J., Lopez-Poveda, M. J., Morales, M. L., Lozano, M. L., Gonzalez-Conejero, R., Martinez, C., Teruel-Montoya, R., & Ferrer-Marin, F. (2024). miR-146a(-/-) mice model reveals that NF-kappaB inhibition reverts inflammation-driven myelofibrosis-like phenotype. *Am J Hematol*, *99*(7), 1326-1337. https://doi.org/10.1002/ajh.27322

Cui, Y., She, K., Tian, D., Zhang, P., & Xin, X. (2016). miR-146a Inhibits Proliferation and Enhances Chemosensitivity in Epithelial Ovarian Cancer via Reduction of SOD2. *Oncol Res*, *23*(6), 275-282. https://doi.org/10.3727/096504016X14562725373798

Da Costa Martins, P. A., & De Windt, L. J. (2012). MicroRNAs in control of cardiac hypertrophy. *Cardiovasc Res*, *93*(4), 563-572. https://doi.org/10.1093/cvr/cvs013

Damase, T. R., Sukhovershin, R., Boada, C., Taraballi, F., Pettigrew, R. I., & Cooke, J. P. (2021). The Limitless Future of RNA Therapeutics. *Front Bioeng Biotechnol*, *9*, 628137. https://doi.org/10.3389/fbioe.2021.628137

Damiani, M. F., Zito, A., Carratu, P., Falcone, V. A., Bega, E., Scicchitano, P., Ciccone, M. M., & Resta, O. (2015). Obstructive Sleep Apnea, Hypertension, and Their Additive Effects on Atherosclerosis. *Biochem Res Int*, *2015*, 984193. https://doi.org/10.1155/2015/984193

Dasgupta, N., Peng, Y., Tan, Z., Ciraolo, G., Wang, D., & Li, R. (2015). miRNAs in mtDNA-less cell mitochondria. *Cell Death Discov*, *1*, 15004. https://doi.org/10.1038/cddiscovery.2015.4

DeGroat, W., Abdelhalim, H., Patel, K., Mendhe, D., Zeeshan, S., & Ahmed, Z. (2024). Discovering biomarkers associated and predicting cardiovascular disease with high accuracy using a novel nexus of machine learning techniques for precision medicine. *Sci Rep*, *14*(1), 1. https://doi.org/10.1038/s41598-023-50600-8

Dela Justina, V., Miguez, J. S. G., Priviero, F., Sullivan, J. C., Giachini, F. R., & Webb, R. C. (2021). Sex Differences in Molecular Mechanisms of Cardiovascular Aging. *Front Aging*, *2*, 725884. https://doi.org/10.3389/fragi.2021.725884

Diez, J., Gonzalez, A., & Kovacic, J. C. (2020). Myocardial Interstitial Fibrosis in Nonischemic Heart Disease, Part 3/4: JACC Focus Seminar. *J Am Coll Cardiol*, *75*(17), 2204-2218. https://doi.org/10.1016/j.jacc.2020.03.019

Dinh, Q. N., Drummond, G. R., Sobey, C. G., & Chrissobolis, S. (2014). Roles of inflammation, oxidative stress, and vascular dysfunction in hypertension. *Biomed Res Int*, *2014*, 406960. https://doi.org/10.1155/2014/406960

Doni, A., Garlanda, C., & Mantovani, A. (2015). PTX3 orchestrates tissue repair. *Oncotarget*, *6*(31), 30435–30436. https://doi.org/10.18632/oncotarget.5453

Doni, A., Stravalaci, M., Inforzato, A., Magrini, E., Mantovani, A., Garlanda, C., & Bottazzi, B. (2019). The Long Pentraxin PTX3 as a Link Between Innate Immunity, Tissue Remodeling, and Cancer. *Front Immunol*, *10*, 712. https://doi.org/10.3389/fimmu.2019.00712

Douglas, P. S., Katz, S. E., Weinberg, E. O., Chen, M. H., Bishop, S. P., & Lorell, B. H. (1998). Hypertrophic remodeling: gender differences in the early response to left ventricular pressure overload. *J Am Coll Cardiol*, *32*(4), 1118-1125. https://doi.org/10.1016/s0735-1097(98)00347-7

Drazner, M. H., Rame, J. E., & Marino, E. K. (2004). Increased left ventricular mass is a risk factor for the development of a depressed left ventricular ejection fraction within five years. The Cardiovascular Health Study. *ACC Current Journal Review*, *13*(12), 27-28. https://doi.org/10.1016/j.accreview.2004.11.064

Drazner, M. H., Rame, J. E., Marino, E. K., Gottdiener, J. S., Kitzman, D. W., Gardin, J. M., Manolio, T. A., Dries, D. L., & Siscovick, D. S. (2004). Increased left ventricular mass is a risk factor for the development of a depressed left ventricular ejection fraction within five years: the Cardiovascular Health Study. *J Am Coll Cardiol*, *43*(12), 2207-2215. https://doi.org/10.1016/j.jacc.2003.11.064

En-Wei Wang, X.-S. J., Chang-Wu Ruan and Zhi-Ru Ge. (2017). miR-487b mitigates chronic heart failure through inhibition of the IL-33/ST2 signaling pathway. *Oncotarget*, *7*(8(31)), 51688-51702. https://doi.org/10.18632/oncotarget.18393

Ernsberger, P., Johnson, J. L., Rosenthal, T., Mirelman, D., & Koletsky, R. J. (2007). Therapeutic actions of allylmercaptocaptopril and captopril in a rat model of metabolic syndrome. *Am J Hypertens*, *20*(8), 866-874. https://doi.org/10.1016/j.amjhyper.2007.02.015

Ertl, G., & Frantz, S. (2012). Adverse cardiac remodeling: phosphoinositide 3-kinase, another unique factor in a multifactorial condition. *Circulation*, *126*(18), 2175-2176. https://doi.org/10.1161/CIRCULATIONAHA.112.138313

Feng, B., Chen, S., Gordon, A. D., & Chakrabarti, S. (2017). miR-146a mediates inflammatory changes and fibrosis in the heart in diabetes. *J Mol Cell Cardiol*, *105*, 70-76. https://doi.org/10.1016/j.yjmcc.2017.03.002

Fina Lubaki, J.-P., Mabuza, L., Malete, N., Maduna, P., & Ndimande, J. V. (2009). Reasons for non-compliance among patients with hypertension at Vanga Hospital, Bandundu Province, Democratic Republic of Congo: A qualitative study. *African Journal of Primary Health Care & Family Medicine*, *1*(1). https://doi.org/10.4102/phcfm.v1i1.68

Florijn, B. W., Bijkerk, R., van der Veer, E. P., & van Zonneveld, A. J. (2018). Gender and cardiovascular disease: are sex-biased microRNA networks a driving force behind heart failure with preserved ejection fraction in women? *Cardiovasc Res*, *114*(2), 210-225. https://doi.org/10.1093/cvr/cvx223

Fouad-Tarazi, F. M., & Liebson, P. R. (1987). Echocardiographic studies of regression of left ventricular hypertrophy in hypertension. *Hypertension*, *9*(2), 1165-1168. https://doi.org/https://doi.org/10.1161/01.HYP.9.2_Pt_2.II65

Frak, W., Wojtasinska, A., Lisinska, W., Mlynarska, E., Franczyk, B., & Rysz, J. (2022). Pathophysiology of Cardiovascular Diseases: New Insights into Molecular Mechanisms of Atherosclerosis, Arterial Hypertension, and Coronary Artery Disease. *Biomedicines*, *10*(8). https://doi.org/10.3390/biomedicines10081938

Galderisi, M. (2011). Diagnosis and management of left ventricular diastolic dysfunction in the hypertensive patient. *Am J Hypertens*, *24*(5), 507-517. https://doi.org/10.1038/ajh.2010.235

García, R., Salido-Medina, A. B., Gil, A., Merino, D., Gómez, J., Villar, A. V., González-Vílchez, F., Hurlé, M. A., & Nistal, J. F. (2020). Sex-Specific Regulation of miR-29b in the Myocardium Under Pressure Overload is Associated with Differential Molecular, Structural and Functional Remodeling Patterns in Mice and Patients with Aortic Stenosis. *Cells*, *9*(4), 833. https://doi.org/10.3390/cells9040833

Garvin, A. M., De Both, M. D., Talboom, J. S., Lindsey, M. L., Huentelman, M. J., & Hale, T. M. (2021). Transient ACE (Angiotensin-Converting Enzyme) Inhibition Suppresses Future Fibrogenic Capacity and Heterogeneity of Cardiac Fibroblast Subpopulations. *Hypertension*, *77*(3), 904-918. https://doi.org/10.1161/HYPERTENSIONAHA.120.16352

Gerdts, E., Zabalgoitia, M., Björnstad, H., Svendsen, T. L., & Devereux, R. B. (2001). Gender differences in systolic left ventricular function in hypertensive patients with electrocardiographic left ventricular hypertrophy (the LIFE study). *The American Journal of Cardiology*, *87*(8), 980–A984. https://doi.org/https://doi.org/10.1016/s0002-9149(01)01433-3

Gilyazova, I., Asadullina, D., Kagirova, E., Sikka, R., Mustafin, A., Ivanova, E., Bakhtiyarova, K., Gilyazova, G., Gupta, S., Khusnutdinova, E., Gupta, H., & Pavlov, V. (2023). MiRNA-146a-A Key Player in Immunity and Diseases. *Int J Mol Sci*, *24*(16). https://doi.org/10.3390/ijms241612767

Guo, Z., Liu, X., Zhao, S., Sun, F., Ren, W., & Ma, M. (2023). RUNX1 promotes liver fibrosis progression through regulating TGF-beta signalling. *Int J Exp Pathol*, *104*(4), 188-198. https://doi.org/10.1111/iep.12474

Gustin, C., Delaive, E., Dieu, M., Calay, D., & Raes, M. (2008). Upregulation of pentraxin-3 in human endothelial cells after lysophosphatidic acid exposure. *Arterioscler Thromb Vasc Biol*, *28*(3), 491-497. https://doi.org/10.1161/ATVBAHA.107.158642

Halkein, J., Tabruyn, S. P., Ricke-Hoch, M., Haghikia, A., Nguyen, N. Q., Scherr, M., Castermans, K., Malvaux, L., Lambert, V., Thiry, M., Sliwa, K., Noel, A., Martial, J. A., Hilfiker-Kleiner, D., & Struman, I. (2013). MicroRNA-146a is a therapeutic target and biomarker for peripartum cardiomyopathy. *J Clin Invest*, *123*(5), 2143-2154. https://doi.org/10.1172/JCI64365

Harrison, D. G., Coffman, T. M., & Wilcox, C. S. (2021). Pathophysiology of Hypertension: The Mosaic Theory and Beyond. *Circ Res*, *128*(7), 847-863. https://doi.org/10.1161/CIRCRESAHA.121.318082

Hartupee, J., & Mann, D. L. (2017). Neurohormonal activation in heart failure with reduced ejection fraction. *Nat Rev Cardiol*, *14*(1), 30-38. https://doi.org/10.1038/nrcardio.2016.163

Hawlitschek, C., Brendel, J., Gabriel, P., Schierle, K., Salameh, A., Zimmer, H. G., & Rassler, B. (2022a). Antihypertensive and cardioprotective effects of different monotherapies and combination therapies in young spontaneously hypertensive rats - A pilot study. *Saudi J Biol Sci*, *29*(1), 339-345. https://doi.org/10.1016/j.sjbs.2021.08.093

Hawlitschek, C., Brendel, J., Gabriel, P., Schierle, K., Salameh, A., Zimmer, H. G., & Rassler, B. (2022b). How Effective Is a Late-Onset Antihypertensive Treatment? Studies with Captopril as Monotherapy and in Combination with Nifedipine in Old Spontaneously Hypertensive Rats. *Biomedicines*, *10*(8). https://doi.org/10.3390/biomedicines10081964

Heggermont, W. A., Papageorgiou, A. P., Quaegebeur, A., Deckx, S., Carai, P., Verhesen, W., Eelen, G., Schoors, S., van Leeuwen, R., Alekseev, S., Elzenaar, I., Vinckier, S., Pokreisz, P., Walravens, A. S., Gijsbers, R., Van Den Haute, C., Nickel, A., Schroen, B., van Bilsen, M., . . . Heymans, S. (2017). Inhibition of MicroRNA-146a and Overexpression of Its Target Dihydrolipoyl Succinyltransferase Protect Against Pressure Overload-Induced Cardiac Hypertrophy and Dysfunction. *Circulation*, *136*(8), 747-761. https://doi.org/10.1161/CIRCULATIONAHA.116.024171

Hengel, F. E., Benitah, J. P., & Wenzel, U. O. (2022). Mosaic theory revised: inflammation and salt play central roles in arterial hypertension. *Cell Mol Immunol*, *19*(5), 561-576. https://doi.org/10.1038/s41423-022-00851-8

Heymans, S., Corsten, M. F., Verhesen, W., Carai, P., van Leeuwen, R. E., Custers, K., Peters, T., Hazebroek, M., Stoger, L., Wijnands, E., Janssen, B. J., Creemers, E. E., Pinto, Y. M., Grimm, D., Schurmann, N., Vigorito, E., Thum, T., Stassen, F., Yin, X., . . . Schroen, B. (2013). Macrophage microRNA-155 promotes cardiac hypertrophy and failure.

Circulation, *128*(13), 1420-1432. https://doi.org/10.1161/CIRCULATIONAHA.112.001357

Hitzeroth, J., Mpe, M., Klug, E., Ranjith, N., Sliwa, K., Steingo, L., Lachman, L., Tsabedze, N., Ntusi, N. A. B., & Society Of South Africa, H. F. (2020). 2020 Heart Failure Society of South Africa perspective on the 2016 European Society of Cardiology Chronic Heart Failure Guidelines. *South African Medican Journal*, *110*(19b), 938-951. https://doi.org/10.7196/SAMJ.2020.v110i8.14681

Hu, J., Huang, S., Liu, X., Zhang, Y., Wei, S., & Hu, X. (2022). miR-155: An Important Role in Inflammation Response. *J Immunol Res*, *2022*, 7437281. https://doi.org/10.1155/2022/7437281

Hueso, M., Mallen, A., Sune-Pou, M., Aran, J. M., Sune-Negre, J. M., & Navarro, E. (2021). ncRNAs in Therapeutics: Challenges and Limitations in Nucleic Acid-Based Drug Delivery. *Int J Mol Sci*, *22*(21). https://doi.org/10.3390/ijms222111596

Ibrahim, N. E., Gaggin, H. K., Konstam, M. A., & Januzzi, J. L., Jr. (2016). Established and Emerging Roles of Biomarkers in Heart Failure Clinical Trials. *Circ Heart Fail*, *9*(9). https://doi.org/10.1161/CIRCHEARTFAILURE.115.002528

Ibrahim, N. E., & Januzzi, J. L., Jr. (2018). Established and Emerging Roles of Biomarkers in Heart Failure. *Circ Res*, *123*(5), 614-629. https://doi.org/10.1161/CIRCRESAHA.118.312706

Ikeda, S., Mizushima, W., Sciarretta, S., Abdellatif, M., Zhai, P., Mukai, R., Fefelova, N., Oka, S. I., Nakamura, M., Del Re, D. P., Farrance, I., Park, J. Y., Tian, B., Xie, L. H., Kumar, M.,

Hsu, C. P., Sadayappan, S., Shimokawa, H., Lim, D. S., & Sadoshima, J. (2019). Hippo Deficiency Leads to Cardiac Dysfunction Accompanied by Cardiomyocyte Dedifferentiation During Pressure Overload. *Circ Res*, *124*(2), 292-305. https://doi.org/10.1161/CIRCRESAHA.118.314048

Ikitimur, B., Cakmak, H. A., Coskunpinar, E., Barman, H. A., & Vural, V. A. (2015). The relationship between circulating microRNAs and left ventricular mass in symptomatic heart failure patients with systolic dysfunction. *Kardiol Pol*, *73*(9), 740-746. https://doi.org/10.5603/KP.a2015.0082

Inoue, K., Kodama, T., & Daida, H. (2012). Pentraxin 3: a novel biomarker for inflammatory cardiovascular disease. *Int J Vasc Med*, *2012*, 657025. https://doi.org/10.1155/2012/657025

Iyer, A. S., Ahmed, M. I., Filippatos, G. S., Ekundayo, O. J., Aban, I. B., Love, T. E., Nanda, N. C., Bakris, G. L., Fonarow, G. C., Aronow, W. S., & Ahmed, A. (2010). Uncontrolled hypertension and increased risk for incident heart failure in older adults with hypertension: findings from a propensity-matched prospective population study. *J Am Soc Hypertens*, *4*(1), 22-31. https://doi.org/10.1016/j.jash.2010.02.002

Jenny, N. S., Arnold, A. M., Kuller, L. H., Tracy, R. P., & Psaty, B. M. (2009). Associations of pentraxin 3 with cardiovascular disease and all-cause death: the Cardiovascular Health Study. *Arterioscler Thromb Vasc Biol*, *29*(4), 594-599. https://doi.org/10.1161/ATVBAHA.108.178947

Jessen, N., Mocumbi, A. O., & Sliwa, K. (2023). Heart failure in Africa: challenges of dealing with a heterogeneous syndrome in a heterogeneous continent. *Eur Heart J*, *44*(48), 5015-5017. https://doi.org/10.1093/eurheartj/ehad742

Jin, W., Wang, J., Liu, C. P., Wang, H. W., & Xu, R. M. (2020). Structural Basis for pri-miRNA Recognition by Drosha. *Mol Cell*, *78*(3), 423-433 e425. https://doi.org/10.1016/j.molcel.2020.02.024

Johanson, T. M., Lew, A. M., & Chong, M. M. (2013). MicroRNA-independent roles of the RNase III enzymes Drosha and Dicer. *Open Biol*, *3*(10), 130144. https://doi.org/10.1098/rsob.130144

Johnson, G., Nour, A. A., Nolan, T., Huggett, J., & Bustin, S. (2014). Minimum information necessary for quantitative real-time PCR experiments. *Methods Mol Biol*, *1160*, 5-17. https://doi.org/10.1007/978-1-4939-0733-5_2

Kanbay, A., Kaya, E., Buyukoglan, H., Kaya, M. G., Simsek, Z. O., Tutar, N., & Demir, R. (2015). Correlation between pentraxin-3 and endothelial dysfunction in obstructive sleep apnea syndrome. *Ann Thorac Med*, *10*(3), 199-203. https://doi.org/10.4103/1817-1737.160840

Kandala, N. B., Nnanatu, C. C., Dukhi, N., Sewpaul, R., Davids, A., & Reddy, S. P. (2021). Mapping the Burden of Hypertension in South Africa: A Comparative Analysis of the National 2012 SANHANES and the 2016 Demographic and Health Survey. *Int J Environ Res Public Health*, *18*(10). https://doi.org/10.3390/ijerph18105445

Kaneko, M., Satomi, T., Fujiwara, S., Uchiyama, H., Kusumoto, K., & Nishimoto, T. (2017). AT1 receptor blocker azilsartan medoxomil normalizes plasma miR-146a and miR-342-3p in a murine heart failure model. *Biomarkers*, *22*(3-4), 253-260. https://doi.org/10.1080/1354750X.2016.1204001

Karamfilova, V., Assyov, Y., Nedeva, I., Gateva, A., Ivanova, I., Cherkezov, N., Mateva, L., & Kamenov, Z. (2022). Increased Serum Pentraxin 3 Is Associated with Prediabetes and Type 2 Diabetes in Obese Patients with Nonalcoholic Fatty Liver Disease. *Metab Syndr Relat Disord*, *20*(2), 132-136. https://doi.org/10.1089/met.2021.0086

Katholi, R. E., & Couri, D. M. (2011). Left ventricular hypertrophy: major risk factor in patients with hypertension: update and practical clinical applications. *Int J Hypertens*, *2011*, 495349. https://doi.org/10.4061/2011/495349

Kemp, J. R., Unal, H., Desnoyer, R., Yue, H., Bhatnagar, A., & Karnik, S. S. (2014). Angiotensin II-regulated microRNA 483-3p directly targets multiple components of the renin-angiotensin system. *J Mol Cell Cardiol*, *75*, 25-39. https://doi.org/10.1016/j.yjmcc.2014.06.008

Kenta Hirai, Daiki Ousaka, Yosuke Fukushima, Maiko Kondo, Takahiro Eitoku, Yusuke Shigemitsu, Mayuko Hara, Kenji Baba, Tatsuo Iwasaki, Shingo Kasahara, Shinichi Ohtsuki, & Oh, H. (2020). Cardiosphere-derived exosomal microRNAs for myocardial repair in pediatric dilated cardiomyopathy. *SCIENCE TRANSLATIONAL MEDICINE*, *12*(573), eabb3336. https://doi.org/10.1126/scitranslmed.abb3336

Kizilgul, M., Beysel, S., Ozcelik, O., Kan, S., Apaydin, M., Caliskan, M., Ucan, B., Sencar, E., Ozdemir, S., & Cakal, E. (2017). Pentraxin 3 as a New Cardiovascular Marker in Adrenal Adenomas. *Endocr Pract*, *23*(6), 662-668. https://doi.org/10.4158/EP161713.OR

Knoflach, M., Kiechl, S., Mantovani, A., Cuccovillo, I., Bottazzi, B., Xu, Q., Xiao, Q., Gasperi, A., Mayr, A., Kehrer, M., Willeit, J., & Wick, G. (2012). Pentraxin-3 as a marker of advanced atherosclerosis results from the Bruneck, ARMY and ARFY Studies. *PLoS One*, *7*(2), e31474. https://doi.org/10.1371/journal.pone.0031474

Knowles, H. J., Tian, Y.-M., Mole, D. R., & Harris, A. L. (2004). Novel Mechanism of Action for Hydralazine. *Circulation Research*, *95*(2), 162-169. https://doi.org/10.1161/01.Res.0000134924.89412.70

Kocyigit, I., Eroglu, E., Orscelik, O., Unal, A., Gungor, O., Ozturk, F., Karakukcu, C., Imamoglu, H., Sipahioglu, M. H., Tokgoz, B., & Oymak, O. (2014). Pentraxin 3 as a novel bio-marker of inflammation and endothelial dysfunction in autosomal dominant polycystic kidney disease. *J Nephrol*, *27*(2), 181-186. https://doi.org/10.1007/s40620-014-0045-4

Koth, J., Wang, X., Killen, A. C., Stockdale, W. T., Potts, H. G., Jefferson, A., Bonkhofer, F., Riley, P. R., Patient, R. K., Göttgens, B., & Mommersteeg, M. T. M. (2020). Runx1 promotes scar deposition and inhibits myocardial proliferation and survival during zebrafish heart regeneration. *Development*, *147*(8). https://doi.org/10.1242/dev.186569

Kunes, P., Holubcova, Z., Kolackova, M., & Krejsek, J. (2012). Pentraxin 3(PTX 3): an endogenous modulator of the inflammatory response. *Mediators Inflamm*, *2012*, 920517. https://doi.org/10.1155/2012/920517

Lam, K., & Zhang, D. E. (2012). RUNX1 and RUNX1-ETO: roles in hematopoiesis and leukemogenesis. *Frontiers in bioscience (Landmark edition)*, *17*(3), 1120–1139. https://doi.org/https://doi.org/10.2741/3977

Lang, R. M., Badano, L. P., Mor-Avi, V., Afilalo, J., Armstrong, A., Ernande, L., Flachskampf, F. A., Foster, E., Goldstein, S. A., Kuznetsova, T., Lancellotti, P., Muraru, D., Picard, M. H., Rietzschel, E. R., Rudski, L., Spencer, K. T., Tsang, W., & Voigt, J. U. (2015). Recommendations for cardiac chamber quantification by echocardiography in adults: an update from the American Society of Echocardiography and the European Association of Cardiovascular Imaging. *J Am Soc Echocardiogr*, *28*(1), 1-39 e14. https://doi.org/10.1016/j.echo.2014.10.003

Leali, D., Inforzato, A., Ronca, R., Bianchi, R., Belleri, M., Coltrini, D., Di Salle, E., Sironi, M., Norata, G. D., Bottazzi, B., Garlanda, C., Day, A. J., & Presta, M. (2012). Long pentraxin 3/tumor necrosis factor-stimulated gene-6 interaction: a biological rheostat for fibroblast growth factor 2-mediated angiogenesis. *Arterioscler Thromb Vasc Biol*, *32*(3), 696-703. https://doi.org/10.1161/ATVBAHA.111.243998

Lee, L. C., Zhihong, Z., Hinson, A., & Guccione, J. M. (2013). Reduction in left ventricular wall stress and improvement in function in failing hearts using Algisyl-LVR. *J Vis Exp*(74). https://doi.org/10.3791/50096

Lei, B., Liu, J., Yao, Z., Xiao, Y., Zhang, X., Zhang, Y., & Xu, J. (2021). NF-kappaB-Induced Upregulation of miR-146a-5p Promoted Hippocampal Neuronal Oxidative Stress and Pyroptosis via TIGAR in a Model of Alzheimer's Disease. *Front Cell Neurosci*, *15*, 653881. https://doi.org/10.3389/fncel.2021.653881

Lerman, L. O., Kurtz, T. W., Touyz, R. M., Ellison, D. H., Chade, A. R., Crowley, S. D., Mattson, D. L., Mullins, J. J., Osborn, J., Eirin, A., Reckelhoff, J. F., Iadecola, C., & Coffman, T. M. (2019). Animal Models of Hypertension: A Scientific Statement From the American Heart Association. *Hypertension*, *73*(6), e87-e120. https://doi.org/10.1161/HYP.0000000000000090

Levick, S. P., Murray, D. B., Janicki, J. S., & Brower, G. L. (2010). Sympathetic Nervous System Modulation of Inflammation and Remodeling in the Hypertensive Heart. *Hypertension*, *55*(2), 270-276. https://doi.org/10.1161/hypertensionaha.109.142042

Li, L., Liu, H., Zhang, Q., Jin, H., Tao, H., Chen, H., & Zhou, Z. (2024). Pentraxin-3 and Outcomes in CKD: A Systematic Review and Meta-analysis. *Kidney Med*, *6*(4), 100800. https://doi.org/10.1016/j.xkme.2024.100800

Li, L., Yi-Ming, W., Li, Z. Z., Zhao, L., Yu, Y. S., Li, D. J., Xia, C. Y., Liu, J. G., & Su, D. F. (2008). Local RAS and inflammatory factors are involved in cardiovascular hypertrophy in spontaneously hypertensive rats. *Pharmacol Res*, *58*(3-4), 196-201. https://doi.org/10.1016/j.phrs.2008.06.009

Li, P., & Jia, X. Y. (2022). MicroRNA-18-5p inhibits the oxidative stress and apoptosis of myocardium induced by hypoxia by targeting RUNX1. *Eur Rev Med Pharmacol Sci*, *26*(2), 432-439. https://doi.org/10.26355/eurrev_202201_27867

Li, X., Zhang, S., Wa, M., Liu, Z., & Hu, S. (2019). MicroRNA-101 Protects Against Cardiac Remodeling Following Myocardial Infarction via Downregulation of Runt-Related Transcription Factor 1. *J Am Heart Assoc*, *8*(23), e013112. https://doi.org/10.1161/jaha.119.013112

Li, Z., Bing, O. H., Long, X., Robinson, K. G., & Lakatta, E. G. (1997). Increased cardiomyocyte apoptosis during the transition to heart failure in the spontaneously hypertensive rat. *American Journal of Physiology-Heart and Circulatory Physiology*, *272*(5), H2313–H2319. https://doi.org/https://doi.org/10.1152/ajpheart.1997.272.5.H2313

Li, Z., Lindner, D. P., Bishop, N. M., & Cipolla, M. J. (2020). ACE (Angiotensin-Converting Enzyme) Inhibition Reverses Vasoconstriction and Impaired Dilation of Pial Collaterals in Chronic Hypertension. *Hypertension*, *76*(1), 226-235. https://doi.org/10.1161/HYPERTENSIONAHA.119.14315

Liu, J. I. A., Wang, F., Yuan, B. O., & Luo, F. (2023). Transcriptional factor RUNX1: A potential therapeutic target for fibrotic pulmonary disease. *Biocell*, *47*(4), 697-705. https://doi.org/10.32604/biocell.2023.026148

Liu, M., Cao, Y., Hu, Y., Zhang, Z., Ji, S., Shi, L., & Tao, G. (2022). MiR-199a-3p Restrains Foaming and Inflammation by Regulating RUNX1 in Macrophages. *Mol Biotechnol*, *64*(10), 1130-1142. https://doi.org/10.1007/s12033-022-00484-2

Liu, N., & Olson, E. N. (2010). MicroRNA regulatory networks in cardiovascular development. *Dev Cell*, *18*(4), 510-525. https://doi.org/10.1016/j.devcel.2010.03.010

Liu, W., Jiang, J., Yan, D., Li, D., Li, W., Ma, Y., Yang, L., Qu, Z., & Ruan, Q. (2014). Pentraxin 3 promotes oxLDL uptake and inhibits cholesterol efflux from macrophage-derived foam cells. *Exp Mol Pathol*, *96*(3), 292-299. https://doi.org/10.1016/j.yexmp.2014.03.007

Livak, K. J., & Schmittgen, T. D. (2001). Analysis of relative gene expression data using real-time quantitative PCR and the 2(-Delta Delta C(T)) Method. *Methods*, *25*(4), 402-408. https://doi.org/10.1006/meth.2001.1262

Loda, A., Collombet, S., & Heard, E. (2022). Gene regulation in time and space during X-chromosome inactivation. *Nat Rev Mol Cell Biol*, *23*(4), 231-249. https://doi.org/10.1038/s41580-021-00438-7

Lorell, B., & Carabello, B. (2000). Left Ventricular Hypertrophy: Pathogenesis, Detection, and Prognosis. *Circulation*, *102*(4), 470-479. https://doi.org/https://doi.org/10.1161/01.CIR.102.4.470

Lu, P., Ding, F., Xiang, Y. K., Hao, L., & Zhao, M. (2022). Noncoding RNAs in Cardiac Hypertrophy and Heart Failure. *Cells*, *11*(5). https://doi.org/10.3390/cells11050777

Luo, M., Zhao, F., Cheng, H., Su, M., & Wang, Y. (2024). Macrophage polarization: an important role in inflammatory diseases. *Front Immunol*, *15*, 1352946. https://doi.org/10.3389/fimmu.2024.1352946

Luo, P., Zhang, H., Liang, Y., Li, X., Wen, Z., Xia, C., Lan, X., Yang, Y., Xiong, Y., Huang, J., Ling, X., Zhou, S., Miao, J., Shen, W., Hou, F. F., Liu, Y., Zhou, L., & Liang, M. (2023). Pentraxin 3 plays a key role in tubular cell senescence and renal fibrosis through inducing beta-catenin signaling. *Biochim Biophys Acta Mol Basis Dis*, *1869*(7), 166807. https://doi.org/10.1016/j.bbadis.2023.166807

Lymperopoulos, A., Rengo, G., & Koch, W. J. (2013). Adrenergic nervous system in heart failure: pathophysiology and therapy. *Circ Res*, *113*(6), 739-753. https://doi.org/10.1161/CIRCRESAHA.113.300308

Ma, X., Cao, Y., Yang, D., Dong, Z., & Wang, X. (2024). Inhibition of RUNX1 slows the progression of pulmonary hypertension by targeting CBX5. *Biomol Biomed*. https://doi.org/10.17305/bb.2024.10720

Magder, S. (2018). The meaning of blood pressure. *Crit Care*, *22*(1), 257. https://doi.org/10.1186/s13054-018-2171-1

Magrini, E., Mantovani, A., & Garlanda, C. (2016). The Dual Complexity of PTX3 in Health and Disease: A Balancing Act? *Trends Mol Med*, *22*(6), 497-510. https://doi.org/10.1016/j.molmed.2016.04.007

Magubane, M., Michel, F. S., Erlwanger, K. H., Norton, G. R., & Woodiwiss, A. J. (2017). Prevention of βeta-adrenergic-induced Adverse Cardiac Remodeling by Gonadectomy in Male but Not Female Spontaneously Hypertensive Rats. *Journal of Cardiovascular Pharmacology*, *70*(3), 202–209. https://doi.org/https://doi.org/10.1097/FJC.0000000000000506

Malgie, J., Clephas, P. R. D., Brunner-La Rocca, H. P., de Boer, R. A., & Brugts, J. J. (2023). Guideline-directed medical therapy for HFrEF: sequencing strategies and barriers for life-saving drug therapy. *Heart Fail Rev*, *28*(5), 1221-1234. https://doi.org/10.1007/s10741-023-10325-2

Malmhall, C., Weidner, J., & Radinger, M. (2020). MicroRNA-155 expression suggests a sex disparity in innate lymphoid cells at the single-cell level. *Cell Mol Immunol*, *17*(5), 544-546. https://doi.org/10.1038/s41423-019-0303-4

Manilall, A., Mokotedi, L., Gunter, S., Le Roux, R., Fourie, S., Flanagan, C. A., & Millen, A. M. E. (2021). Inflammation-induced left ventricular fibrosis is partially mediated by tumor necrosis factor-alpha. *Physiol Rep*, *9*(21), e15062. https://doi.org/10.14814/phy2.15062

Mann, D. L., & Bristow, M. R. (2005). Mechanisms and models in heart failure: the biomechanical model and beyond. *Circulation*, *111*(21), 2837-2849. https://doi.org/10.1161/CIRCULATIONAHA.104.500546

Mann, M., Mehta, A., Zhao, J. L., Lee, K., Marinov, G. K., Garcia-Flores, Y., Lu, L. F., Rudensky, A. Y., & Baltimore, D. (2017). An NF-kappaB-microRNA regulatory network tunes macrophage inflammatory responses. *Nat Commun*, *8*(1), 851. https://doi.org/10.1038/s41467-017-00972-z

Manolis, A. A., Manolis, T. A., & Manolis, A. S. (2023). Neurohumoral Activation in Heart Failure. *Int J Mol Sci*, *24*(20). https://doi.org/10.3390/ijms242015472

Martin, T. P., MacDonald, E. A., Bradley, A., Watson, H., Saxena, P., Rog-Zielinska, E. A., Fisher, S., Elbassioni, A. M., Almuzaini, O., Booth, C., Campbell, M., Herzyk, P., Blyth,

K., Nixon, C., Zentilin, L., Berry, C., Braun, T., Giacca, M., McBride, M. W., . . . Loughrey, C. M. (2022). Inhibiting Runx1 protects heart function after myocardial infarction. *bioRxiv*. https://doi.org/https://doi.org/10.1101/2022.02.17.480749

Martin, T. P., MacDonald, E. A., Bradley, A., Watson, H., Saxena, P., Rog-Zielinska, E. A., Raheem, A., Fisher, S., Elbassioni, A. A. M., Almuzaini, O., Booth, C., Campbell, M., Riddell, A., Herzyk, P., Blyth, K., Nixon, C., Zentilin, L., Berry, C., Braun, T., . . . Loughrey, C. M. (2023). Ribonucleicacid interference or small molecule inhibition of Runx1 in the border zone prevents cardiac contractile dysfunction following myocardial infarction. *Cardiovasc Res*, *119*(16), 2663-2671. https://doi.org/10.1093/cvr/cvad107

Masenga, S. K., & Kirabo, A. (2023). Hypertensive heart disease: risk factors, complications and mechanisms. *Front Cardiovasc Med*, *10*, 1205475. https://doi.org/10.3389/fcvm.2023.1205475

Masiha, S., Sundstrom, J., & Lind, L. (2013). Inflammatory markers are associated with left ventricular hypertrophy and diastolic dysfunction in a population-based sample of elderly men and women. *J Hum Hypertens*, *27*(1), 13-17. https://doi.org/10.1038/jhh.2011.113

McCarroll, C. S., He, W., Foote, K., Bradley, A., McGlynn, K., Vidler, F., Nixon, C., Nather, K., Fattah, C., Riddell, A., Bowman, P., Elliott, E. B., Bell, M., Hawksby, C., MacKenzie, S. M., Morrison, L. J., Terry, A., Blyth, K., Smith, G. L., . . . Loughrey, C. M. (2018). Runx1 Deficiency Protects Against Adverse Cardiac Remodeling After Myocardial Infarction. *Circulation*, *137*(1), 57-70. https://doi.org/10.1161/circulationaha.117.028911

McCarron, R. M., Wang, L., Siren, A. L., Spatz, M., & Hallenbeck, J. M. (1994). Monocyte adhesion to cerebromicrovascular endothelial cells derived from hypertensive and normotensive rats. *American Journal of Physiology-Heart and Circulatory Physiology*, *267*(6), H2491-H2497. https://doi.org/https://doi.org/10.1152/ajpheart.1994.267.6.H2491

McDermott, J. E., Wang, J., Mitchell, H., Webb-Robertson, B. J., Hafen, R., Ramey, J., & Rodland, K. D. (2013). Challenges in Biomarker Discovery: Combining Expert Insights with Statistical Analysis of Complex Omics Data. *Expert Opin Med Diagn*, *7*(1), 37-51. https://doi.org/10.1517/17530059.2012.718329

McNamara, P. J., Jain, A., El-Khuffash, A., Giesinger, R., Weisz, D., Freud, L., Levy, P. T., Bhombal, S., de Boode, W., Leone, T., Richards, B., Singh, Y., Acevedo, J. M., Simpson, J., Noori, S., & Lai, W. W. (2024). Guidelines and Recommendations for Targeted Neonatal Echocardiography and Cardiac Point-of-Care Ultrasound in the Neonatal Intensive Care Unit: An Update from the American Society of Echocardiography. *J Am Soc Echocardiogr*, *37*(2), 171-215. https://doi.org/10.1016/j.echo.2023.11.016

Medrano-Bosch, M., Simon-Codina, B., Jimenez, W., Edelman, E. R., & Melgar-Lesmes, P. (2023). Monocyte-endothelial cell interactions in vascular and tissue remodeling. *Front Immunol*, *14*, 1196033. https://doi.org/10.3389/fimmu.2023.1196033

Melman, Y. F., Shah, R., & Das, S. (2014). MicroRNAs in heart failure: is the picture becoming less miRky? *Circ Heart Fail*, *7*(1), 203-214. https://doi.org/10.1161/CIRCHEARTFAILURE.113.000266

Metra, M., & Teerlink, J. R. (2017). Heart failure. *Lancet*, *390*(10106), 1981-1995. https://doi.org/10.1016/S0140-6736(17)31071-1

Mihl C, D. W., Kuipers H. (2008). Cardiac remodelling: concentric versus eccentric hypertrophy in strength and endurance athletes. *Neth Heart J*, *16*(4), 129-133. https://doi.org/10.1007/BF03086131

Millen, A. M. E., Woodiwiss, A. J., Gomes, M., Michel, F., & Norton, G. R. (2018). Systemic Angiotensinogen Concentrations Are Independently Associated With Left Ventricular Diastolic Function in a Community Sample. *Am J Hypertens*, *31*(2), 212-219. https://doi.org/10.1093/ajh/hpx156

Mitsis, T., Efthimiadou, A., Bacopoulou, F., Vlachakis, D., Chrousos, G., & Eliopoulos, E. (2020). Transcription factors and evolution: An integral part of gene expression (Review). *World Academy of Sciences Journal*. https://doi.org/10.3892/wasj.2020.32

Mkhize, S., Manilall, A., Mokotedi, L., Gunter, S., & Michel, F. S. (2024). Involvement of pentraxin-3 in the development of hypertension but not left ventricular hypertrophy in male spontaneously hypertensive rats. *Physiological reports*, *12*(20), e70086. https://doi.org/10.14814/phy2.70086

Mkhize, S. A., Gunter, S., Manilall, A., Mokotedi, L., Mosoma, K. L., Nthlane, R., Millen, A. M. E., & Michel, F. S. (2025). Involvement of microRNA-146a-5p, but not -155-5p and -29b-5p, in left ventricular remodeling and dysfunction in spontaneously hypertensive rats. *Am J Physiol Heart Circ Physiol*, *328*(4), H885-H899. https://doi.org/10.1152/ajpheart.00696.2024

Mokotedi, L., Michel, F. S., Mogane, C., Gomes, M., Woodiwiss, A. J., Norton, G. R., & Millen, A. M. E. (2020). Associations of inflammatory markers with impaired left ventricular diastolic and systolic function in collagen-induced arthritis. *PLoS One*, *15*(3), e0230657. https://doi.org/10.1371/journal.pone.0230657

Mokotedi, L., Millen, A. M. E., Mogane, C., Gomes, M., Woodiwiss, A. J., Norton, G. R., & Michel, F. S. (2019). Associations of inflammatory markers and vascular cell adhesion molecule-1 with endothelial dysfunction in collagen-induced arthritis. *Eur J Pharmacol*, *865*, 172786. https://doi.org/10.1016/j.ejphar.2019.172786

Morii, J., Miura, S., Shiga, Y., Sugihara, M., Arimura, T., Sako, H., Zhang, B., Uehara, Y., & Saku, K. (2012). Comparison of the efficacy and safety of irbesartan and olmesartan in patients with hypertension (EARTH study). *Clin Exp Hypertens*, *34*(5), 342-349. https://doi.org/10.3109/10641963.2012.683912

Mosterd, A., Cost, B., Hoes, A. W., de Bruijne, M. C., Deckers, J. W., Hofman, A., & Grobbee, D. E. (2001). The prognosis of heart failure in the general population: The Rotterdam Study. *Eur Heart J*, *22*(15), 1318-1327. https://doi.org/10.1053/euhj.2000.2533

Nabeebaccus, A., Zheng, S., & Shah, A. M. (2016). Heart failure-potential new targets for therapy. *Br Med Bull*, *119*(1), 99-110. https://doi.org/10.1093/bmb/ldw025

Napoleone, E., Di Santo, A., Bastone, A., Peri, G., Mantovani, A., de Gaetano, G., Donati, M. B., & Lorenzet, R. (2002). Long pentraxin PTX3 upregulates tissue factor expression in human endothelial cells: a novel link between vascular inflammation and clotting

activation. *Arterioscler Thromb Vasc Biol*, *22*(5), 782-787. https://doi.org/10.1161/01.atv.0000012282.39306.64

Narayan, S. I., Terre, G. V., Amin, R., Shanghavi, K. V., Chandrashekar, G., Ghouse, F., Ahmad, B. A., S, G. N., Satram, C., Majid, H. A., & Bayoro, D. K. (2023). The Pathophysiology and New Advancements in the Pharmacologic and Exercise-Based Management of Heart Failure With Reduced Ejection Fraction: A Narrative Review. *Cureus*, *15*(9), e45719. https://doi.org/10.7759/cureus.45719

Nauta, A. J., de Haij, S., Bottazzi, B., Mantovani, A., Borrias, M. C., Aten, J., Rastaldi, M. P., Daha, M. R., van Kooten, C., & Roos, A. (2005). Human renal epithelial cells produce the long pentraxin PTX3. *Kidney Int*, *67*(2), 543-553. https://doi.org/10.1111/j.1523-1755.2005.67111.x

Navanandan, N., Searns, J., & Ambroggio, L. (2023). Method/ology of Phases of Biomarker Discovery. *Hosp Pediatr*, *13*(7), e181-e185. https://doi.org/10.1542/hpeds.2022-007012

Nemecz, M., Alexandru, N., Tanko, G., & Georgescu, A. (2016). Role of MicroRNA in Endothelial Dysfunction and Hypertension. *Curr Hypertens Rep*, *18*(12), 87. https://doi.org/10.1007/s11906-016-0696-8

Nguyen, T. P., Sovari, A. A., Pezhouman, A., Iyer, S., Cao, H., Ko, C. Y., Bapat, A., Vahdani, N., Ghanim, M., Fishbein, M. C., & Karagueuzian, H. S. (2016). Increased susceptibility of spontaneously hypertensive rats to ventricular tachyarrhythmias in early hypertension. *J Physiol*, *594*(6), 1689-1707. https://doi.org/10.1113/JP271318

Ni, T., Huang, X., Pan, S., & Lu, Z. (2021). Dihydrolycorine Attenuates Cardiac Fibrosis and Dysfunction by Downregulating Runx1 following Myocardial Infarction. *Oxid Med Cell Longev*, *2021*, 8528239. https://doi.org/10.1155/2021/8528239

Norton, G. R., Tsotetsi, J., Trifunovic, B., Hartford, C., Candy, G. P., & Woodiwiss, A. J. (1997). Myocardial Stiffness Is Attributed to Alterations in Cross-Linked Collagen Rather Than Total Collagen or Phenotypes in Spontaneously Hypertensive Rats. *Circulation*, *96*(6), 1991-1998. https://doi.org/10.1161/01.CIR.96.6.1991

Nouaille, S., Mondeil, S., Finoux, A. L., Moulis, C., Girbal, L., & Cocaign-Bousquet, M. (2017). The stability of an mRNA is influenced by its concentration: a potential physical mechanism to regulate gene expression. *Nucleic Acids Res*, *45*(20), 11711-11724. https://doi.org/10.1093/nar/gkx781

Novak, J., Kruzliak, P., Bienertova-Vasku, J., Slaby, O., & Novak, M. (2014). MicroRNA-206: a promising theranostic marker. *Theranostics*, *4*(2), 119-133. https://doi.org/10.7150/thno.7552

Ntelios, D., Efthimiadis, G., Zegkos, T., Didagelos, M., Katopodi, T., Meditskou, S., Parcharidou, D., Karvounis, H., & Tzimagiorgis, G. (2021). Correlation of miR-146a-5p plasma levels and rs2910164 polymorphism with left ventricle outflow tract obstruction in hypertrophic cardiomyopathy. *Hellenic J Cardiol*, *62*(5), 349-354. https://doi.org/10.1016/j.hjc.2020.04.015

O'Brien, J., Hayder, H., Zayed, Y., & Peng, C. (2018). Overview of MicroRNA Biogenesis, Mechanisms of Actions, and Circulation. *Front Endocrinol (Lausanne)*, *9*, 402. https://doi.org/10.3389/fendo.2018.00402

O'Neill, C. L., Guduric-Fuchs, J., Chambers, S. E., O'Doherty, M., Bottazzi, B., Stitt, A. W., & Medina, R. J. (2016). Endothelial cell-derived pentraxin 3 limits the vasoreparative therapeutic potential of circulating angiogenic cells. *Cardiovasc Res*, *112*(3), 677-688. https://doi.org/10.1093/cvr/cvw209

Oh, J. G., Watanabe, S., Lee, A., Gorski, P. A., Lee, P., Jeong, D., Liang, L., Liang, Y., Baccarini, A., Sahoo, S., Brown, B. D., Hajjar, R. J., & Kho, C. (2018). miR-146a Suppresses SUMO1 Expression and Induces Cardiac Dysfunction in Maladaptive Hypertrophy. *Circ Res*, *123*(6), 673-685. https://doi.org/10.1161/CIRCRESAHA.118.312751

Pacinella, G., Ciaccio, A. M., & Tuttolomondo, A. (2022). Endothelial Dysfunction and Chronic Inflammation: The Cornerstones of Vascular Alterations in Age-Related Diseases. *Int J Mol Sci*, *23*(24). https://doi.org/10.3390/ijms232415722

Parlak, A., Aydogan, U., Iyisoy, A., Dikililer, M. A., Kut, A., Cakir, E., & Saglam, K. (2012). Elevated pentraxin-3 levels are related to blood pressure levels in hypertensive patients: an observational study. *Anadolu Kardiyol Derg*, *12*(4), 298-304. https://doi.org/10.5152/akd.2012.092

Parlak, A., Iyisoy, A., Aydogan, U., Cakir, E., & Saglam, K. (2012). The effect of valsartan and nebivolol treatment on ADMA and pentraxin-3 levels in hypertensive patients. *Med Hypotheses*, *79*(3), 294-298. https://doi.org/10.1016/j.mehy.2012.05.011

Percie du Sert, N., Ahluwalia, A., Alam, S., Avey, M. T., Baker, M., Browne, W. J., Clark, A., Cuthill, I. C., Dirnagl, U., Emerson, M., Garner, P., Holgate, S. T., Howells, D. W., Hurst, V., Karp, N. A., Lazic, S. E., Lidster, K., MacCallum, C. J., Macleod, M., . . . Wurbel, H. (2020). Reporting animal research: Explanation and elaboration for the ARRIVE guidelines 2.0. *PLoS Biol*, *18*(7), e3000411. https://doi.org/10.1371/journal.pbio.3000411

Percie du Sert, N., Hurst, V., Ahluwalia, A., Alam, S., Avey, M. T., Baker, M., Browne, W. J., Clark, A., Cuthill, I. C., Dirnagl, U., Emerson, M., Garner, P., Holgate, S. T., Howells, D. W., Karp, N. A., Lazic, S. E., Lidster, K., MacCallum, C. J., Macleod, M., . . . Wurbel, H. (2020). The ARRIVE guidelines 2.0: Updated guidelines for reporting animal research. *PLoS Biol*, *18*(7), e3000410. https://doi.org/10.1371/journal.pbio.3000410

Perez, D. M. (2021). Targeting Adrenergic Receptors in Metabolic Therapies for Heart Failure. *Int J Mol Sci*, *22*(11). https://doi.org/10.3390/ijms22115783

Peterlin, A., Pocivavsek, K., Petrovic, D., & Peterlin, B. (2020). The Role of microRNAs in Heart Failure: A Systematic Review. *Front Cardiovasc Med*, *7*, 161. https://doi.org/10.3389/fcvm.2020.00161

Pfeffer, J., Pfeffer, M., Fletcher, P., & Braunwald, E. (1979). Alterations of cardiac performance in rats with established spontaneous hypertension. *The American Journal of Cardiology*, *44*(5), 994–998. https://doi.org/https://doi.org/10.1016/0002-9149(79)90234-0

Pfeffer, J. M., Pfeffer, M. A., Fletcher, P., Fishbein, M. C., & Braunwald, E. (1982). Favorable effects of therapy on cardiac performance in spontaneously hypertensive rats. *American*

Journal of Physiology-Heart and Circulatory Physiology, *242*(5), H776–H784. https://doi.org/https://doi.org/10.1152/ajpheart.1982.242.5.H776

Pfeffer, T. J., Mueller, J. H., Haebel, L., Erschow, S., Yalman, K. C., Talbot, S. R., Koenig, T., Berliner, D., Zwadlo, C., Scherr, M., Hilfiker-Kleiner, D., Bauersachs, J., & Ricke-Hoch, M. (2023). Cabergoline treatment promotes myocardial recovery in peripartum cardiomyopathy. *ESC Heart Fail*, *10*(1), 465-477. https://doi.org/10.1002/ehf2.14210

Philippe, G. (2005). Left ventricular hypertrophy as a predictor of cardiovascular risk. *Journal of hypertension*, *23*, S27-S33. https://doi.org/10.1097/01.hjh.0000165625.79933.9a

Piek, A., Du, W., de Boer, R. A., & Sillje, H. H. W. (2018). Novel heart failure biomarkers: why do we fail to exploit their potential? *Crit Rev Clin Lab Sci*, *55*(4), 246-263. https://doi.org/10.1080/10408363.2018.1460576

Prescott, J. A., Mitchell, J. P., & Cook, S. J. (2021). Inhibitory feedback control of NF-kappaB signalling in health and disease. *Biochem J*, *478*(13), 2619-2664. https://doi.org/10.1042/BCJ20210139

Presta, M., Camozzi, M., Salvatori, G., & Rusnati, M. (2007). Role of the soluble pattern recognition receptor PTX3 in vascular biology. *J Cell Mol Med*, *11*(4), 723-738. https://doi.org/10.1111/j.1582-4934.2007.00061.x

Presta, M., Foglio, E., Churruca Schuind, A., & Ronca, R. (2018). Long Pentraxin-3 Modulates the Angiogenic Activity of Fibroblast Growth Factor-2. *Front Immunol*, *9*, 2327. https://doi.org/10.3389/fimmu.2018.02327

Qi, P., Zhai, Q., & Zhang, X. (2023). RUNX1 facilitates heart failure progression through regulating TGF-β-induced cardiac remodeling. *PeerJ*, *11*, e16202. https://doi.org/10.7717/peerj.16202

Qiu, S., Cai, Y., Yao, H., Lin, C., Xie, Y., Tang, S., & Zhang, A. (2023). Small molecule metabolites: discovery of biomarkers and therapeutic targets. *Signal Transduct Target Ther*, *8*(1), 132. https://doi.org/10.1038/s41392-023-01399-3

Rababa'h, A. M., Guillory, A. N., Mustafa, R., & Hijjawi, T. (2018). Oxidative Stress and Cardiac Remodeling: An Updated Edge. *Curr Cardiol Rev*, *14*(1), 53-59. https://doi.org/10.2174/1573403X14666180111145207

Rapp, J. P. (2000). Genetic Analysis of Inherited Hypertension in the Rat. *Physiological Reviews*, *80*(1), 135-172. https://doi.org/https://doi.org/10.1152/physrev.2000.80.1.135

Rasoulinejad, S. A., Akbari, A., & Nasiri, K. (2021). Interaction of miR-146a-5p with oxidative stress and inflammation in complications of type 2 diabetes mellitus in male rats: Anti-oxidant and anti-inflammatory protection strategies in type 2 diabetic retinopathy. *Iran J Basic Med Sci*, *24*(8), 1078-1086. https://doi.org/10.22038/IJBMS.2021.56958.12706

Rassler, B., Hawlitschek, C., Brendel, J., & Zimmer, H. G. (2022). How Do Young and Old Spontaneously Hypertensive Rats Respond to Antihypertensive Therapy? Comparative Studies on the Effects of Combined Captopril and Nifedipine Treatment. *Biomedicines*, *10*(12). https://doi.org/10.3390/biomedicines10123059

Ratti, M., Lampis, A., Ghidini, M., Salati, M., Mirchev, M. B., Valeri, N., & Hahne, J. C. (2020). MicroRNAs (miRNAs) and Long Non-Coding RNAs (lncRNAs) as New Tools for

Cancer Therapy: First Steps from Bench to Bedside. *Target Oncol*, *15*(3), 261-278. https://doi.org/10.1007/s11523-020-00717-x

Reckelhoff, J. F. (2001). Gender Differences in the Regulation of Blood Pressure. *Hypertension*, *37*, 1199-1208. https://doi.org/https://doi.org/10.1161/01.HYP.37.5.1199

Reckelhoff, J. F., Zhang, H., & Granger, J. P. (1998). Testosterone Exacerbates Hypertension and Reduces Pressure-Natriuresis in Male Spontaneously Hypertensive Rats. *Hypertension*, *31*(1), 435-439. https://doi.org/https://doi.org/10.1161/01.HYP.31.1.435

Reckelhoff, J. F., Zhang, H., & Srivastava, K. (2000). Gender Differences in Development of Hypertension in Spontaneously Hypertensive Rats: Role of the Renin-Angiotensin System. *Hypertension*, *35*(1), 480-483. https://doi.org/https://doi.org/10.1161/01.HYP.35.1.480

Reckelhoff, J. F., Zhang, H., Srivastava, K., & Granger, J. P. (1999). Gender Differences in Hypertension in Spontaneously Hypertensive Rats:

Role of Androgens and Androgen Receptor. *Hypertension*, *34*(4), 920-923. https://doi.org/https://doi.org/10.1161/01.HYP.34.4.920

Reddy, D. S., Singh, M., Ghosh, S., & Ganguly, N. K. (1996). Role of cardiac renin-angiotensin system in the development of pressure-overload left ventricular hypertrophy in rats with abdominal aortic constriction. *Molecular and Cellular Biochemistr*, *155*, 1-11.

Riddell, A., McBride, M., Braun, T., Nicklin, S. A., Cameron, E., Loughrey, C. M., & Martin, T. P. (2020). RUNX1: an emerging therapeutic target for cardiovascular disease. *Cardiovasc Res*, *116*(8), 1410-1423. https://doi.org/10.1093/cvr/cvaa034

Ristagno, G., Fumagalli, F., Bottazzi, B., Mantovani, A., Olivari, D., Novelli, D., & Latini, R. (2019). Pentraxin 3 in Cardiovascular Disease. *Front Immunol*, *10*, 823. https://doi.org/10.3389/fimmu.2019.00823

Roostalu, U., Thisted, L., Skytte, J. L., Salinas, C. G., Pedersen, P. J., Hecksher-Sorensen, J., Rolin, B., Hansen, H. H., MacKrell, J. G., Christie, R. M., Vrang, N., Jelsing, J., & Zois, N. E. (2021). Effect of captopril on post-infarction remodelling visualized by light sheet microscopy and echocardiography. *Sci Rep*, *11*(1), 5241. https://doi.org/10.1038/s41598-021-84812-7

Rusnati, M., Camozzi, M., Moroni, E., Bottazzi, B., Peri, G., Indraccolo, S., Amadori, A., Mantovani, A., & Presta, M. (2004). Selective recognition of fibroblast growth factor-2 by the long pentraxin PTX3 inhibits angiogenesis. *Blood*, *104*(1), 92-99. https://doi.org/10.1182/blood-2003-10-3433

Sahn, D. J., DeMaria, A., Kisslo, J., & Weyman, A. (1978). Recommendations Regarding Quantitation in M-Mode Echocardiography:

Results of a Survey of Echocardiographic Measurements. *Circulation*, *58*, 1072–1083. https://doi.org/https://doi.org/10.1161/01.CIR.58.6.1072

Salles, G. F., Fiszman, R., Cardoso, C. R., & Muxfeldt, E. S. (2007). Relation of left ventricular hypertrophy with systemic inflammation and endothelial damage in resistant hypertension. *Hypertension*, *50*(4), 723-728. https://doi.org/10.1161/HYPERTENSIONAHA.107.093120

Sam, F., Kerstetter, D. L., Pimental, D. R., Mulukutla, S., Tabaee, A., Bristow, M. R., Colucci, W. S., & Sawyer, D. B. (2005). Increased reactive oxygen species production and functional alterations in antioxidant enzymes in human failing myocardium. *J Card Fail*, *11*(6), 473-480. https://doi.org/10.1016/j.cardfail.2005.01.007

Samak, M., Fatullayev, J., Sabashnikov, A., Zeriouh, M., Schmack, B., Farag, M., Popov, A. F., Dohmen, P. M., Choi, Y. H., Wahlers, T., & Weymann, A. (2016). Cardiac Hypertrophy: An Introduction to Molecular and Cellular Basis. *Med Sci Monit Basic Res*, *22*, 75-79. https://doi.org/10.12659/MSMBR.900437

Sanchis-Gomar, F., Arnau-Moyano, M., Daimiel, L., Lippi, G., Leischik, R., Vallecillo, N., Yvert, T., Jiménez, S. L., Santiago, C., & Pareja-Galeano, H. (2021). Circulating microRNAs fluctuations in exercise-induced cardiac remodeling: A systematic review. *American journal of translational research*, *13*(12), 13298–13309.

Sandoo, A., van Zanten, J. J., Metsios, G. S., Carroll, D., & Kitas, G. D. (2010). The endothelium and its role in regulating vascular tone. *The open cardiovascular medicine journal*, *4*, 302–312. https://doi.org/https://doi.org/10.2174/1874192401004010302

Sassi, Y., Avramopoulos, P., Ramanujam, D., Gruter, L., Werfel, S., Giosele, S., Brunner, A. D., Esfandyari, D., Papadopoulou, A. S., De Strooper, B., Hubner, N., Kumarswamy, R., Thum, T., Yin, X., Mayr, M., Laggerbauer, B., & Engelhardt, S. (2017). Cardiac myocyte miR-29 promotes pathological remodeling of the heart by activating Wnt signaling. *Nat Commun*, *8*(1), 1614. https://doi.org/10.1038/s41467-017-01737-4

Schipke, J., Brandenberger, C., Rajces, A., Manninger, M., Alogna, A., Post, H., & Muhlfeld, C. (2017). Assessment of cardiac fibrosis: a morphometric method comparison for collagen quantification. *J Appl Physiol (1985)*, *122*(4), 1019-1030. https://doi.org/10.1152/japplphysiol.00987.2016

Schirone, L., Forte, M., Palmerio, S., Yee, D., Nocella, C., Angelini, F., Pagano, F., Schiavon, S., Bordin, A., Carrizzo, A., Vecchione, C., Valenti, V., Chimenti, I., De Falco, E., Sciarretta, S., & Frati, G. (2017). A Review of the Molecular Mechanisms Underlying the Development and Progression of Cardiac Remodeling. *Oxid Med Cell Longev*, *2017*, 3920195. https://doi.org/10.1155/2017/3920195

Schmitz, B., Vischer, P., Brand, E., Schmidt-Petersen, K., Korb-Pap, A., Guske, K., Nedele, J., Schelleckes, M., Hillen, J., Rotrige, A., Simmet, T., Paul, M., Cambien, F., & Brand, S. M. (2013). Increased monocyte adhesion by endothelial expression of VCAM-1 missense variation in vitro. *Atherosclerosis*, *230*(2), 185-190. https://doi.org/10.1016/j.atherosclerosis.2013.07.039

Schwinger, R. H. G. (2021). Pathophysiology of heart failure. *Cardiovasc Diagn Ther*, *11*(1), 263-276. https://doi.org/10.21037/cdt-20-302

Seok, H. Y., Chen, J., Kataoka, M., Huang, Z. P., Ding, J., Yan, J., Hu, X., & Wang, D. Z. (2014). Loss of MicroRNA-155 protects the heart from pathological cardiac hypertrophy. *Circ Res*, *114*(10), 1585-1595. https://doi.org/10.1161/CIRCRESAHA.114.303784

Sharma, K. R., Malik, A., Roof, R. A., Boyce, J. P., & Verma, S. K. (2024). New approaches for challenging therapeutic targets. *Drug Discov Today*, *29*(4), 103942. https://doi.org/10.1016/j.drudis.2024.103942

Shimada, B. K., Yang, Y., Zhu, J., Wang, S., Suen, A., Kronstadt, S. M., Jeyaram, A., Jay, S. M., Zou, L., & Chao, W. (2020). Extracellular miR-146a-5p Induces Cardiac Innate Immune Response and Cardiomyocyte Dysfunction. *Immunohorizons*, *4*(9), 561-572. https://doi.org/10.4049/immunohorizons.2000075

Silva, J., & da Costa Martins, P. A. (2022). Non-Coding RNAs in the Therapeutic Landscape of Pathological Cardiac Hypertrophy. *Cells*, *11*(11). https://doi.org/10.3390/cells11111805

Singh, D. D., Kim, Y., Choi, S. A., Han, I., & Yadav, D. K. (2023). Clinical Significance of MicroRNAs, Long Non-Coding RNAs, and CircRNAs in Cardiovascular Diseases. *Cells*, *12*(12). https://doi.org/10.3390/cells12121629

Singh, E., & Bisserier, M. (2025). Experimental animal models and patient-derived platforms to bridge preclinical discovery and translational therapeutics in pulmonary arterial hypertension. *J Transl Med*, *23*(1), 665. https://doi.org/10.1186/s12967-025-06709-7

Slama, M., Ahn, J., Varagic, J., Susic, D., & Frohlich, E. D. (2004). Long-term left ventricular echocardiographic follow-up of SHR and WKY rats: effects of hypertension and age. *American journal of physiology. Heart and circulatory physiology*, *286*(1), H181–H185. https://doi.org/https://doi.org/10.1152/ajpheart.00642.2003

Sliwa, K., Wilkinson, D., Hansen, C., Ntyintyane, L., Tibazarwa, K., Becker, A., & Stewart, S. (2008). Spectrum of heart disease and risk factors in a black urban population in South

Africa (the Heart of Soweto Study): a cohort study. *Lancet*, *371*(9616), 915-922. https://doi.org/10.1016/S0140-6736(08)60417-1

Soller, K. J., Yang, J., Veglia, G., & Bowser, M. T. (2016). Reversal of Phospholamban Inhibition of the Sarco(endo)plasmic Reticulum Ca2+-ATPase (SERCA) Using Short, Protein-interacting RNAs and Oligonucleotide Analogs. *J Biol Chem*, *291*(41), 21510-21518. https://doi.org/10.1074/jbc.M116.738807

Song, J., Zhang, X., Lv, S., Liu, M., Hua, X., Yue, L., Wang, S., & He, W. (2023). Age-related promoter-switch regulates Runx1 expression in adult rat hearts. *BMC Cardiovasc Disord*, *23*(1), 541. https://doi.org/10.1186/s12872-023-03583-3

Song, R., & Zhang, L. (2024). MicroRNAs and therapeutic potentials in acute and chronic cardiac disease. *Drug Discov Today*, 104179. https://doi.org/10.1016/j.drudis.2024.104179

St Pierre, S. R., Peirlinck, M., & Kuhl, E. (2022). Sex Matters: A Comprehensive Comparison of Female and Male Hearts. *Front Physiol*, *13*, 831179. https://doi.org/10.3389/fphys.2022.831179

Strimbu, K., & Tavel, J. A. (2010). What are biomarkers? *Curr Opin HIV AIDS*, *5*(6), 463-466. https://doi.org/10.1097/COH.0b013e32833ed177

Sufianov, A., Agaverdiev, M., Mashkin, A., & Ilyasova, T. (2025). The functions of immune system-derived miRNAs in cardiovascular diseases. *Noncoding RNA Res*, *11*, 91-103. https://doi.org/10.1016/j.ncrna.2024.11.004

Sullivan, J. C., Pardieck, J. L., Doran, D., Zhang, Y., She, J. X., & Pollock, J. S. (2009). Greater fractalkine expression in mesenteric arteries of female spontaneously hypertensive rats compared with males. *Am J Physiol Heart Circ Physiol*, *296*(4), H1080-1088. https://doi.org/10.1152/ajpheart.01093.2008

Sun, H. X., Zeng, D. Y., Li, R. T., Pang, R. P., Yang, H., Hu, Y. L., Zhang, Q., Jiang, Y., Huang, L. Y., Tang, Y. B., Yan, G. J., & Zhou, J. G. (2012). Essential role of microRNA-155 in regulating endothelium-dependent vasorelaxation by targeting endothelial nitric oxide synthase. *Hypertension*, *60*(6), 1407-1414. https://doi.org/10.1161/HYPERTENSIONAHA.112.197301

Suzuki, S., Shishido, T., Funayama, A., Netsu, S., Ishino, M., Kitahara, T., Sasaki, T., Katoh, S., Otaki, Y., Watanabe, T., Shibata, Y., Mantovani, A., Takeishi, Y., & Kubota, I. (2013). Long pentraxin PTX3 exacerbates pressure overload-induced left ventricular dysfunction. *PLoS One*, *8*(1), e53133. https://doi.org/10.1371/journal.pone.0053133

Suzuki, S., Tanaka, S., Kametani, Y., Umeda, A., Nishinaka, K., Egawa, K., Okada, Y., Obana, M., & Fujio, Y. (2023). Runx1 is upregulated by STAT3 and promotes proliferation of neonatal rat cardiomyocytes. *Physiol Rep*, *11*(23), e15872. https://doi.org/10.14814/phy2.15872

Szczerba, E., Zajkowska, A., Bochowicz, A., Pankiewicz, K., Szewczyk, G., Opolski, G., Maciejewski, T., Malecki, M., & Fijalkowska, A. (2020). Downregulated expression of microRNAs associated with cardiac hypertrophy and fibrosis in physiological pregnancy and the association with echocardiographically-evaluated myocardial function. *Biomed Rep*, *13*(5), 41. https://doi.org/10.3892/br.2020.1348

Tamura, T., Said, S., & Gerdes, A. M. (1999). Gender-related differences in myocyte remodeling in progression to heart failure. *Hypertension*, *33*(2), 676–680. https://doi.org/https://doi.org/10.1161/01.hyp.33.2.676

Tan, S. C., Carr, C. A., Yeoh, K. K., Schofield, C. J., Davies, K. E., & Clarke, K. (2012). Identification of valid housekeeping genes for quantitative RT-PCR analysis of cardiosphere-derived cells preconditioned under hypoxia or with prolyl-4-hydroxylase inhibitors. *Mol Biol Rep*, *39*(4), 4857-4867. https://doi.org/10.1007/s11033-011-1281-5

Taubel, J., Hauke, W., Rump, S., Viereck, J., Batkai, S., Poetzsch, J., Rode, L., Weigt, H., Genschel, C., Lorch, U., Theek, C., Levin, A. A., Bauersachs, J., Solomon, S. D., & Thum, T. (2021). Novel antisense therapy targeting microRNA-132 in patients with heart failure: results of a first-in-human Phase 1b randomized, double-blind, placebo-controlled study. *Eur Heart J*, *42*(2), 178-188. https://doi.org/10.1093/eurheartj/ehaa898

Theall, B., & Alcaide, P. (2022). The heart under pressure: immune cells in fibrotic remodeling. *Curr Opin Physiol*, *25*. https://doi.org/10.1016/j.cophys.2022.100484

Thornburg, K. L., Drake, R., & Valent, A. M. (2020). Maternal Hypertension Affects Heart Growth in Offspring. *J Am Heart Assoc*, *9*(9), e016538. https://doi.org/10.1161/JAHA.120.016538

Thum, T., Gross, C., Fiedler, J., Fischer, T., Kissler, S., Bussen, M., Galuppo, P., Just, S., Rottbauer, W., Frantz, S., Castoldi, M., Soutschek, J., Koteliansky, V., Rosenwald, A., Basson, M. A., Licht, J. D., Pena, J. T., Rouhanifard, S. H., Muckenthaler, M. U., . . . Engelhardt, S. (2008). MicroRNA-21 contributes to myocardial disease by stimulating

MAP kinase signalling in fibroblasts. *Nature*, *456*(7224), 980-984. https://doi.org/10.1038/nature07511

Tipton, A. J., Baban, B., & Sullivan, J. C. (2014). Female spontaneously hypertensive rats have a compensatory increase in renal regulatory T cells in response to elevations in blood pressure. *Hypertension*, *64*(3), 557-564. https://doi.org/10.1161/HYPERTENSIONAHA.114.03512

Tjin, G., White, E. S., Faiz, A., Sicard, D., Tschumperlin, D. J., Mahar, A., Kable, E. P. W., & Burgess, J. K. (2017). Correction: Lysyl oxidases regulate fibrillar collagen remodelling in idiopathic pulmonary fibrosis (doi: 10.1242/dmm.030114). *Dis Model Mech*, *10*(12), 1545. https://doi.org/10.1242/dmm.033191

Tomek, J., & Bub, G. (2017). Hypertension-induced remodelling: on the interactions of cardiac risk factors. *J Physiol*, *595*(12), 4027-4036. https://doi.org/10.1113/JP273043

Torimoto, K., Elliott, K., Nakayama, Y., Yanagisawa, H., & Eguchi, S. (2024). Cardiac and perivascular myofibroblasts, matrifibrocytes, and immune fibrocytes in hypertension; commonalities and differences with other cardiovascular diseases. *Cardiovasc Res*, *120*(6), 567-580. https://doi.org/10.1093/cvr/cvae044

Tuller, T., Waldman, Y. Y., Kupiec, M., & Ruppin, E. (2010). Translation efficiency is determined by both codon bias and folding energy. *Proc Natl Acad Sci U S A*, *107*(8), 3645-3650. https://doi.org/10.1073/pnas.0909910107

Udelson, J. E., & Stevenson, L. W. (2016). The Future of Heart Failure Diagnosis, Therapy, and Management. *Circulation*, *133*(25), 2671-2686. https://doi.org/10.1161/CIRCULATIONAHA.116.023518

Unlu, M., Karaman, M., Ay, S. A., Balta, S., Cakar, M., Demirkol, S., Celik, T., Arslan, E., Demirbas, S., Turker, T., Yaman, H., Bulucu, F., & Saglam, K. (2013). The comparative effects of valsartan and amlodipine on vascular microinflammation in newly diagnosed hypertensive patients. *Clin Exp Hypertens*, *35*(6), 418-423. https://doi.org/10.3109/10641963.2012.739237

Usui, T., Okada, M., Hara, Y., & Yamawaki, H. (2012). Death-associated protein kinase 3 mediates vascular inflammation and development of hypertension in spontaneously hypertensive rats. *Hypertension*, *60*(4), 1031-1039. https://doi.org/10.1161/HYPERTENSIONAHA.112.200337

Vakka, A., Warren, J. S., & Drosatos, K. (2023). Cardiovascular aging: from cellular and molecular changes to therapeutic interventions. *J Cardiovasc Aging*, *3*(3). https://doi.org/10.20517/jca.2023.09

Valentova, M., von Haehling, S., Bauditz, J., Doehner, W., Ebner, N., Bekfani, T., Elsner, S., Sliziuk, V., Scherbakov, N., Murin, J., Anker, S. D., & Sandek, A. (2016). Intestinal congestion and right ventricular dysfunction: a link with appetite loss, inflammation, and cachexia in chronic heart failure. *Eur Heart J*, *37*(21), 1684-1691. https://doi.org/10.1093/eurheartj/ehw008

Van Assche, E., Van Puyvelde, S., Vanderleyden, J., & Steenackers, H. P. (2015). RNA-binding proteins involved in post-transcriptional regulation in bacteria. *Front Microbiol*, *6*, 141. https://doi.org/10.3389/fmicb.2015.00141

Vigil-Garcia, M., Demkes, C. J., Eding, J. E. C., Versteeg, D., de Ruiter, H., Perini, I., Kooijman, L., Gladka, M. M., Asselbergs, F. W., Vink, A., Harakalova, M., Bossu, A., van Veen, T. A. B., Boogerd, C. J., & van Rooij, E. (2021). Gene expression profiling of hypertrophic cardiomyocytes identifies new players in pathological remodelling. *Cardiovasc Res*, *117*(6), 1532-1545. https://doi.org/10.1093/cvr/cvaa233

Vlachopoulos, C., Xaplanteris, P., Aboyans, V., Brodmann, M., Cifkova, R., Cosentino, F., De Carlo, M., Gallino, A., Landmesser, U., Laurent, S., Lekakis, J., Mikhailidis, D. P., Naka, K. K., Protogerou, A. D., Rizzoni, D., Schmidt-Trucksass, A., Van Bortel, L., Weber, T., Yamashina, A., . . . Townsend, R. R. (2015). The role of vascular biomarkers for primary and secondary prevention. A position paper from the European Society of Cardiology Working Group on peripheral circulation: Endorsed by the Association for Research into Arterial Structure and Physiology (ARTERY) Society. *Atherosclerosis*, *241*(2), 507-532. https://doi.org/10.1016/j.atherosclerosis.2015.05.007

Wake, C., Labadorf, A., Dumitriu, A., Hoss, A. G., Bregu, J., Albrecht, K. H., DeStefano, A. L., & Myers, R. H. (2016). Novel microRNA discovery using small RNA sequencing in post-mortem human brain. *BMC Genomics*, *17*(1), 776. https://doi.org/10.1186/s12864-016-3114-3

Wallace, E., Morrell, N. W., Yang, X. D., Long, L., Stevens, H., Nilsen, M., Loughlin, L., Mair, K. M., Baker, A. H., & MacLean, M. R. (2015). A Sex-Specific MicroRNA-96/5-

Hydroxytryptamine 1B Axis Influences Development of Pulmonary Hypertension. *Am J Respir Crit Care Med*, *191*(12), 1432-1442. https://doi.org/10.1164/rccm.201412-2148OC

Wang, X., Xu, X., Ma, Z., Huo, Y., Xiao, Z., Li, Y., & Wang, Y. (2011). Dynamic mechanisms for pre-miRNA binding and export by Exportin-5. *RNA*, *17*(8), 1511-1528. https://doi.org/10.1261/rna.2732611

Wang, X. Y., Zhang, F., Zhang, C., Zheng, L. R., & Yang, J. (2020). The Biomarkers for Acute Myocardial Infarction and Heart Failure. *Biomed Res Int*, *2020*, 2018035. https://doi.org/10.1155/2020/2018035

Wei, C., Henderson, H., Spradley, C., Li, L., Kim, I. K., Kumar, S., Hong, N., Arroliga, A. C., & Gupta, S. (2013). Circulating miRNAs as potential marker for pulmonary hypertension. *PLoS One*, *8*(5), e64396. https://doi.org/10.1371/journal.pone.0064396

Weinberg, E. O., Thienelt, C. D., Katz, S. E., Bartunek, J., Tajima, M., Rohrbach, S., Douglas, P. S., & Lorell, B. H. (1999). Gender differences in molecular remodeling in pressure overload hypertrophy. *J Am Coll Cardiol*, *34*(1), 264-273. https://doi.org/10.1016/s0735-1097(99)00165-5

Wilson, A. J., Wang, V. Y., Sands, G. B., Young, A. A., Nash, M. P., & LeGrice, I. J. (2017). Increased cardiac work provides a link between systemic hypertension and heart failure. *Physiol Rep*, *5*(1). https://doi.org/10.14814/phy2.13104

Winter, J., Bishop, M. J., Wilder, C. D. E., O'Shea, C., Pavlovic, D., & Shattock, M. J. (2018). Sympathetic Nervous Regulation of Calcium and Action Potential Alternans in the Intact Heart. *Front Physiol*, *9*, 16. https://doi.org/10.3389/fphys.2018.00016

Wu, T., Zhu, B., Zhu, Q., Tursun, D., Liu, S., Liu, S., Hu, J., & Li, N. (2019). Study on Serum Pentraxin-3 Levels in Vasculitis with Hypertension. *J Interferon Cytokine Res*, *39*(9), 522-530. https://doi.org/10.1089/jir.2018.0150

Wu, Y., Zhang, Z., Chen, Z., Fu, C., Huang, L., Wang, J., Li, J., Barszczyk, A., & Yang, D. (2022). MicroRNA-29b suppresses TGF-beta-induced epithelial-mesenchymal transition in renal interstitium of spontaneously hypertensive rats. *Chin Med J (Engl)*, *135*(7), 857-859. https://doi.org/10.1097/CM9.0000000000001922

Xu, L., Su, Y., Yang, X., Bai, X., Wang, Y., Zhuo, C., & Meng, Z. (2023). Gramine protects against pressure overload-induced pathological cardiac hypertrophy through Runx1-TGFBR1 signaling. *Phytomedicine*, *114*, 154779. https://doi.org/10.1016/j.phymed.2023.154779

Y. Liu, T. Liu, R. M. McCarron, M. Spatz, G. Feuerstein, J. M. Hallenbeck, & Siren, A. L. (1996). Evidence for activation of endothelium and monocytes in hypertensive rats. *American Journal of Physiology-Heart and Circulatory Physiology*, *270*(6), H2125-H2131. https://doi.org/https://doi.org/10.1152/ajpheart.1996.270.6.H2125

Yano, Y., Matsuda, S., Hatakeyama, K., Sato, Y., Imamura, T., Shimada, K., Kodama, T., Kario, K., & Asada, Y. (2010). Plasma Pentraxin 3, but not high-sensitivity C-reactive protein, is a useful inflammatory biomarker for predicting cognitive impairment in elderly

hypertensive patients. *J Gerontol A Biol Sci Med Sci*, *65*(5), 547-552. https://doi.org/10.1093/gerona/glq030

Yavuzer, H., Cengiz, M., Yavuzer, S., Riza Altiparmak, M., Korkmazer, B., Balci, H., Yaldiran, A. L., & Uzun, H. (2016). Procalcitonin and Pentraxin-3: Current biomarkers in inflammation in white coat hypertension. *J Hum Hypertens*, *30*(7), 424-429. https://doi.org/10.1038/jhh.2015.59

Zhang, D., Liang, C., Li, P., Yang, L., Hao, Z., Kong, L., Tian, X., Guo, C., Dong, J., Zhang, Y., & Du, B. (2021). Runt-related transcription factor 1 (Runx1) aggravates pathological cardiac hypertrophy by promoting p53 expression. *J Cell Mol Med*, *25*(16), 7867-7877. https://doi.org/10.1111/jcmm.16704

Zhang, R. L., Wang, W. M., Li, J. Q., Li, R. W., Zhang, J., Wu, Y., & Liu, Y. (2025). The role of miR-155 in cardiovascular diseases: Potential diagnostic and therapeutic targets. *Int J Cardiol Cardiovasc Risk Prev*, *24*, 200355. https://doi.org/10.1016/j.ijcrp.2024.200355

Zhang, X., Ma, S., Zhang, R., Li, S., Zhu, D., Han, D., Li, X., Li, C., Yan, W., Sun, D., Xu, B., Wang, Y., & Cao, F. (2016). Oncostatin M-induced cardiomyocyte dedifferentiation regulates the progression of diabetic cardiomyopathy through B-Raf/Mek/Erk signaling pathway. *Acta Biochim Biophys Sin (Shanghai)*, *48*(3), 257-265. https://doi.org/10.1093/abbs/gmv137

Zhang, X., McLendon, J. M., Peck, B. D., Chen, B., Song, L. S., & Boudreau, R. L. (2023). Modulation of miR-29 influences myocardial compliance likely through coordinated

regulation of calcium handling and extracellular matrix. *Mol Ther Nucleic Acids*, *34*, 102081. https://doi.org/10.1016/j.omtn.2023.102081

Zhang, Y., Huang, X. R., Wei, L. H., Chung, A. C., Yu, C. M., & Lan, H. Y. (2014). miR-29b as a therapeutic agent for angiotensin II-induced cardiac fibrosis by targeting TGF-beta/Smad3 signaling. *Mol Ther*, *22*(5), 974-985. https://doi.org/10.1038/mt.2014.25

Zile, M. R., & Brutsaert, D. L. (2002). New concepts in diastolic dysfunction and diastolic heart failure: Part I: diagnosis, prognosis, and measurements of diastolic function. *Circulation*, *105*(11), 1387-1393. https://doi.org/10.1161/hc1102.105289

Zlibut, A., Bocsan, I. C., & Agoston-Coldea, L. (2019). Pentraxin-3 and endothelial dysfunction. *Adv Clin Chem*, *91*, 163-179. https://doi.org/10.1016/bs.acc.2019.03.005

Zong, Y., Li, H., Liao, P., Chen, L., Pan, Y., Zheng, Y., Zhang, C., Liu, D., Zheng, M., & Gao, J. (2024). Mitochondrial dysfunction: mechanisms and advances in therapy. *Signal Transduct Target Ther*, *9*(1), 124. https://doi.org/10.1038/s41392-024-01839-8

Zorov, D. B., Juhaszova, M., & Sollott, S. J. (2014). Mitochondrial reactive oxygen species (ROS) and ROS-induced ROS release. *Physiol Rev*, *94*(3), 909-950. https://doi.org/10.1152/physrev.00026.2013

Appendix 1: Ethics application for 3- and 12-month-old male WKYs and SHRs

ANIMALS RESEARCH ETHICS COMMITTEE (AREC)

UNIVERSITY OF THE WITWATERSRAND, JOHANNESBURG

STRICTLY CONFIDENTIAL

CLEARANCE CERTIFICATE NUMBER: AREC22-08-009B

APPLICANT: Mr S Mkhize
School: School of Physiology; Department: IMPRI; Location: WRAF

PROJECT TITLE: The expression of microRNAs in the early development of hypertension in spontaneously hypertensive rats
Category: B; Species and Numbers involved: 12X, 2 Month old, Male, Spontaneously Hypertensive Rats (SHR)

Approval is hereby given for the use of animals for the research project named above and described in the application reviewed by a quorate meeting of the AREC held on 28 Mar 2023. This approval remains valid until 14 May 2025 and is conditional to the following (if blank there are no special conditions):

Condition 1	Condition 2	Condition 3	Condition 4

All material changes to the approved research must be reported to the AREC before they are implemented. Failure to do so will invalidate this clearance certificate.

An annual progress report must be provided to the AREC.

The use of these animals is subject to AREC guidelines on the use and care of laboratory animals, is limited to the procedures described in the application and is subject to additional conditions listed below:

I, the Chair of the AREC (or my designated representative) am satisfied that the proposed research is ethical as judged by local law, international standards and University policy.

Signed: _____ Date: 15 May 2023
(Deputy Chairperson of the AREC)

I am satisfied that the persons listed in this application are competent to perform the procedures described in the application, in the context of Section 23 (1) (c) of the veterinary and Para-veterinary Professions Act (19 of 1982).

Signed: _____ Date: _15 May 2023_____
(Registered Veterinarian)

CC: Student supervisor: «Title1» «Initials1» «Supervisor_surname»
Director Wits Research Animal Facility (WRAF): Dr Kim Jardine

Appendix 2: Ethics application for 7-month-old male and female WKY and SHR

ANIMALS RESEARCH ETHICS COMMITTEE (AREC)

UNIVERSITY OF THE WITWATERSRAND, JOHANNESBURG

STRICTLY CONFIDENTIAL

CLEARANCE CERTIFICATE NUMBER: 2021/03/03/C

APPLICANT: Prof F Michel
School: School of Physiology; Department: N/A; Location: WRAF

PROJECT TITLE: The involvement of intrarenal renin angiotensin system (RAS) in the sexual dimorphism associated with the development of hypertension in Spontaneously Hypertensive Rat (SHR)
Category: C; Species and Numbers involved: *28X each of male and female, 1 month old Spontaneously Hypertensive Rats (SHR) and 7X each of male and female, 1 month old Wistar Kyoto Rats (WKY)*

Approval is hereby given for the use of animals for the research project named above and described in the application reviewed by a quorate meeting of the AREC held on 30 Mar 2021. This approval remains valid until 27 Apr 2023 and is conditional to the following (if blank there are no special conditions):

Condition 1	Condition 2	Condition 3	Condition 4

All material changes to the approved research must be reported to the AREC before they are implemented. Failure to do so will invalidate this clearance certificate.

An annual progress report must be provided to the AREC.

The use of these animals is subject to AREC guidelines on the use and care of laboratory animals, is limited to the procedures described in the application and is subject to additional conditions listed below:

I, the Chair of the AREC (or my designated representative) am satisfied that the proposed research is ethical as judged by local law, international standards and University policy.

Signed: _____ Date: 28 April 2021

(Deputy Chairperson of the AREC)

I am satisfied that the persons listed in this application are competent to perform the procedures described in the application, in the context of Section 23 (1) (c) of the veterinary and Para-veterinary Professions Act (19 of 1982).

CC: Student supervisor: «Title1» «Initials1» «Supervisor_surname»
Director Wits Research Animal Facility (WRAF): Dr Kim Jardine

Appendix 3: Turnitin Report



Turnitin PhD thesis_Siluleko Mkhize.docx

ORIGINALITY REPORT

13%	13%	8%	3%
SIMILARITY INDEX	INTERNET SOURCES	PUBLICATIONS	STUDENT PAPERS

PRIMARY SOURCES

1	www.ncbi.nlm.nih.gov Internet Source	8%
2	journals.lww.com Internet Source	2%
3	cvja.co.za Internet Source	1%
4	wiredspace.wits.ac.za Internet Source	1%
5	Pinto, Vanda Carina Ribeiro. "O Papel do Stress Oxidativo na Regulação dos Transportadores de Aminoácidos Renais na Hipertensão e no Envelhecimento", Universidade do Porto (Portugal), 2024 Publication	1%
6	Tshiamo T. Maluleke, Aletta M.E. Millen, Frédéric S. Michel. "The effects of estrogen deficiency and aging on myocardial deformation and motion in normotensive female rats", Menopause, 2022 Publication	1%